

# **Damage in Polyethylene and its Pressure Pipe - Characterization and Detection Methods**

by

Yi Zhang

A thesis submitted in partial fulfillment of the requirements for the degree of

Doctor of Philosophy

Department of Mechanical Engineering  
University of Alberta

© Yi Zhang, 2017

## Abstract

Approaches for accurate prediction of ductile failure of polyethylene (PE) pipe have been explored using the experimentally determined, material-specific damage parameter  $D$ . Although many methods are available for quantifying the  $D$  values, they are mainly suitable for metallic materials. For PE, damage characterization using these existing methods is difficult because of the insignificant effects of damage on the short-term mechanical properties for PE. In addition, deformation of PE is a nonlinear viscous behavior that further increases the challenge for the damage characterization. The main objective of this thesis is through characterizing the deformation-induced damage in PE to find a reliable method for its damage characterization. Initially, mechanical properties of PE pipe materials under various strain rates were systematically studied. It was observed that mechanical behavior of PE is strongly dependent on strain rate. In addition, it was found that strain rate can serve as an additional factor for time-temperature superposition principle to predict long-term properties of PE. Based on the above findings, time-strain rate superposition principle is proposed to construct relaxation master curve for PE pipe. Furthermore, damage evolution in PE pipe materials under tensile loading condition was investigated, using the proposed two-stage test method and phenomenological finite element (FE) modelling. Mechanical properties of two most popular PE pipe materials (PE80 and PE100) were also investigated and compared.

The above two-stage test method was then applied to examine the influence of squeeze-off on the degradation of mechanical properties for PE pipe. Three squeezing speeds of 0.01, 1 and 50mm/min were used to cover the possible scenarios that may be encountered during the pipe repair or maintenance. Results show that squeeze-off of PE pipe causes significant degradation

in elastic modulus and yield strength, with the maximum reduction of 82% for elastic modulus and 27% for yield strength. Furthermore, it was found that reducing the squeezing speed has no effect on the extent of property degradation. In view of those findings, a study was conducted using mechanical testing and FE simulation to elucidate the damage evolution in PE pipe. Results show that both tensile and compressive loading modes can cause severe degradation in elastic modulus and yield strength. The results also show that under a single loading mode, the extent of damage at a given prestrain level is indeed a function of loading rate. However, in a squeezed pipe which is subjected to both tension and compression through the pipe wall thickness, our analysis based on damage mechanics suggests that degradation of elastic modulus and yield strength can become insensitive to the loading rate.

A new methodology based on the effective stress concept in continuum damage mechanics (CDM) was developed to characterize ductile damage in PE pipe. Quasi-static stress-strain relationships as a function of strain rate and ligament width in the notched pipe ring (NPR) samples were first determined by conducting stress relaxation tests and applying a viscous model to remove viscous stress from the total true stress-strain relationships. By fitting the experimentally determined variation of quasi-static stress with strain rate which was then extrapolated to zero strain rate, an estimate was made for the effective stress at an undamaged configuration. Finally, the damage parameter was determined using the proposed method and showed good correlation with the method based on the degradation of elastic modulus.

Finally, a non-destructive ultrasonic test method was proposed to characterize damage in high-density polyethylene (HDPE). Various damage levels were first introduced to the HDPE specimens through stretching the specimens to different prestrain levels at a constant crosshead speed of 1mm/min. Ultrasonic speeds in virgin and damaged HDPE specimens were then

measured using time-of-flight in the through-transmission mode. The results show that the ultrasonic wave speed, normalized by the speed in the virgin plate of the same thickness, decreases with the increase of prestrain introduced to the specimens. The study also shows that with the correction of density change by the prestrain, the normalized ultrasonic wave speed can be used to determine the dependence of damage level on the prestrain, which for specimens with long gauge length, is consistent with the damage determined from the mechanical testing. The study concludes that ultrasonic testing can be used as a non-destructive means to quantify deformation-induced damage evolution in PE.

## Preface

This thesis is an original work by Yi Zhang under the supervision of Prof. P.-Y. Ben Jar. The main body of this thesis is composed of eight published/submitted journal papers and one published book chapter.

Chapter 2 of this thesis is mainly based on one published book chapter: Zhang, Y. and Jar, P.Y.B., 2016. Characterization of damage development in semi-crystalline polymers, In *Polymer Science: Research Advances, Practical Applications and Educational Aspects*, pp.121-130. I was responsible for the data collection and analysis as well as the manuscript composition. Dr. Jar was the supervisory author and assisted with editing the manuscript.

Chapter 3 is based on three published journal papers: (1) Zhang, Y. and Jar, P.Y.B., 2016. Quantitative assessment of deformation-induced damage in polyethylene pressure pipe. *Polymer Testing*, 47, pp.42-50; (2) Zhang, Y. and Jar, P.Y.B., 2016. Time-strain rate superposition for relaxation behavior of polyethylene pressure pipes. *Polymer Testing*, 50, pp.292-296 and (3) Zhang, Y. and Jar, P.Y.B., 2016. Comparison of Mechanical Properties between PE80 and PE100 Pipe Materials. *Journal of Materials Engineering and Performance*, 25(10), pp.4326-4332. I was responsible for the data collection and analysis and all the experimental and simulation work, as well as the manuscript composition. Dr. Jar was the supervisory author and assisted with editing the manuscript.

Chapter 4 is based on one published journal paper: Zhang, Y. and Jar, P.Y.B., 2015. Phenomenological modelling of tensile fracture in PE pipe by considering damage evolution. *Materials & Design*, 77, pp.72-82; Zhang, Y. and Jar, P.Y.B., 2015. I was responsible for the data collection and analysis and all the experimental and simulation work, as well as the

manuscript composition. Dr. Jar was the supervisory author and assisted with editing the manuscript.

Chapter 5 is based on one submitted journal paper: Zhang, Y. and Jar, P.Y.B., 2017. Effects of Squeeze-off on Mechanical Properties of Polyethylene Pipes. Submitted to *International Journal of Solids and Structures*. I was responsible for the data collection and analysis and all the experimental and simulation work, as well as the manuscript composition. Dr. Jar was the supervisory author and assisted with editing the manuscript.

Chapter 6 is based on one published journal paper: Zhang, Y. and Jar, P.Y.B., 2016. Effects of Crosshead Speed on the Quasi-Static Stress-Strain Relationship of Polyethylene (PE) Pipes. *Journal of Pressure Vessel Technology*, 139(2), pp.021402–021402-6. and one submitted journal paper: Zhang, Y. and Jar, P.Y.B., 2017. Characterization of Ductile Damage in Polyethylene based on Effective Stress Concept. Submitted to *International Journal of Mechanical Sciences*. I was responsible for the data collection and analysis and all the experimental work, as well as the manuscript composition. Dr. Jar was the supervisory author and assisted with editing the manuscript.

Chapter 7 is based on one submitted journal paper: Zhang, Y., Jar, P.Y.B., Nguyen, K.C.T. and Le, L.H., 2017. Characterization of Ductile Damage in Polyethylene Plate Using Ultrasonic Testing. Submitted to *Polymer Testing*. I was involved in formation of concept, research planning, data analysis and all of the mechanical testing, as well as the manuscript composition. Kim-Cuong T Nguyen and Dr. Lawrence H Le in the Department of Radiology and Diagnostic Imaging at the University of Alberta assisted with the ultrasonic testing and data collection. Dr. Jar was the supervisory author and involved in the experimental design and manuscript editing.

## **Acknowledgements**

I would like to express my sincere gratitude to my supervisor and mentor, Professor P.-Y. Ben Jar for his support, encouragement and guidance throughout my Ph.D. study. Thanks for providing the invaluable advice, persistent help and excellent experimental facilities, without which I would not have finished my Ph.D. study so smoothly. It has been a great experience to conduct research under his guidance. Sincere appreciation is also due to my supervisory committee members, Dr. Lawrence H. Le and Dr. Ming J. Zuo for their invaluable inputs and suggestions.

My sincere appreciation is extended to the faculty and staff in the Machine Shop, especially Bernie Faulkner for the fabrication of extensometers used in the experiments and invaluable suggestions, Daniel Mooney and Tuula Hilvo for help in specimen preparation and Rick Conrad for design of the data collection system.

I would like to thank Prof. Lawrence H. Le for the amazing collaboration. Special thanks go to Dr. Le's student, Kim-Cuong T Nguyen for her kindness and help in the ultrasonic testing.

Many thanks go to the China Scholarship Council (CSC) and Natural Sciences and Engineering Research Council of Canada (NSERC) for the financial support.

Lastly, and most importantly, I would like to thank my family for their unconditional love, presence and support, especially my beloved wife Lin, our parents and lovely daughter Zihui. You have always been my great source of power and support, without which I could not overcome difficulties during the course of this research.

# Table of Contents

Abstract .....	ii
Preface.....	v
Acknowledgements.....	vii
Table of Contents.....	viii
List of tables.....	xi
List of figures.....	xii
List of symbols and abbreviations .....	xviii
<b>Chapter 1 Introduction .....</b>	<b>1</b>
1.1 Background and motivation.....	1
1.2 Research objectives and approach .....	9
1.3 Thesis Organization .....	11
References.....	13
<b>Chapter 2 Review of the damage characterization methods.....</b>	<b>15</b>
2.1 Introduction.....	15
2.2 Mechanics of porous media (MPM)-based approach .....	18
2.3 Continuum damage mechanics (CDM)-based approach .....	20
2.3.1 Damage variables.....	20
2.3.2 Effective stress concept.....	20
2.3.3 Damage measurement.....	21
2.3.4 A practical example .....	23
2.4 Major factors influencing damage development.....	27
2.4.1 Effects of temperature.....	28
2.4.2 Effects of strain rate.....	28
2.4.3 Effects of stress triaxiality .....	30
2.4.3 Effects of microstructure.....	32
2.5 Conclusions.....	32
References.....	33
<b>Chapter 3 Characterization of deformation damage in PE pipe .....</b>	<b>38</b>

3.1 Introduction.....	38
3.2 Materials, specimens and mechanical testing.....	43
3.3 An additional factor to time-temperature superposition for deformation of PE.....	46
3.4 Damage development under tensile loading using two-stage test method.....	53
3.4.1 Effect of strain rate on damage development.....	53
3.4.2 Effect of microstructure on damage development.....	67
3.5 Conclusions.....	73
References.....	75
<b>Chapter 4 Phenomenological modelling of tensile fracture in PE pipe with the consideration of damage evolution.....</b>	<b>80</b>
4.1 Introduction.....	81
4.2 Experimental testing.....	85
4.2.1 Specimens and test conditions.....	85
4.2.2 Test results.....	86
4.3 Finite element simulation.....	88
4.3.1 The FE model.....	88
4.3.2 The first series of FE simulation.....	90
4.3.3 The second series of FE simulation.....	94
4.3.4 Rate of damage evolution.....	99
4.4 Conclusions.....	101
References.....	102
<b>Chapter 5 Effects of squeeze-off on mechanical properties of PE pipe.....</b>	<b>108</b>
5.1 Introduction.....	109
5.2 Experimental details and test results.....	112
5.2.1 Squeeze-off-and-tensile tests.....	112
5.2.2 Tensile-and-tensile tests on NPR specimens.....	116
5.2.3 Compressive-and-compressive tests on stub specimens.....	118
5.2.4 Tensile-and-tensile and compressive-and-tensile tests on half NPR specimens.....	120
5.3 Finite element simulation.....	122
5.4 Insensitivity of the drop of elastic modulus to the squeezing speed.....	126
5.5 Conclusions.....	133

References.....	134
<b>Chapter 6 Characterization of ductile damage in polyethylene based on effective stress concept.....</b>	<b>138</b>
6.1 Introduction.....	139
6.2 Experimental details.....	143
6.2.1 Material and specimens.....	143
6.2.2 Mechanical testing.....	143
6.3 Model for determining the quasi-static stress.....	145
6.4 Results and discussion.....	146
6.4.1 Effects of strain rate.....	146
6.4.2 Effects of specimen geometry.....	151
6.4.3 Damage characterization.....	154
6.5 Conclusions.....	160
References.....	161
<b>Chapter 7 Characterization of ductile damage in polyethylene using ultrasonic technique.....</b>	<b>165</b>
7.1 Introduction.....	165
7.2 Experimental details.....	169
7.2.1 Material and specimens.....	169
7.2.2 Mechanical testing.....	170
7.2.3 Ultrasonic testing.....	172
7.3 Results and discussion.....	174
7.4 Conclusions.....	185
References.....	186
<b>Chapter 8 Summary and future work.....</b>	<b>191</b>
8.1 Summary of contributions.....	191
8.2 Future work.....	195
References.....	196
Bibliography.....	198

## List of tables

Table 3.1 Values for vertical shift used to construct the master curves at 0.01mm/min .....	51
Table 4.1 Values for parameters in Eq. (4.3) determined from the first series of FE simulation.	93
Table 4.2 Strain ranges for Eq. (4.3) used in the first series of FE simulation .....	94
Table 4.3 Values for parameters in Eq. (4.3) used in the second series of FE simulation .....	98
Table 4.4 Strain ranges used for Eq. (4.3) in the second series of FE simulation .....	99
Table 4.5 Values for parameters in Eq. (4.2) for the second series of FE simulation .....	99
Table 5.1 Values for parameters and strain range in Eq. (5.3), determined from the FE simulation .....	126
Table 5.2 Damage accumulation data for the part of cross section under tension.....	133
Table 5.3 Damage accumulation data for the part of cross section under compression.....	133
Table 6.1 Summary of values for $\sigma_r(0)$ and $\sigma_0$ in Eq. (6.7), with $\tau_r = 1.6 \times 10^4$ .....	148
Table 6.2 Values for parameters in Eq. (6.8) and quasi-static stress as crosshead speed reaches zero.....	151
Table 7.1 Material characteristics for HDPE used in this study .....	170
Table 7.2 Measurements of the longitudinal wave velocity for undamaged material .....	176

## List of figures

Fig. 1.1 Squeeze-off of PE pipe: (a) commercial squeeze-off tool [14] and (b) definition of the terms used for the squeeze-off process. ....	3
Fig. 1.2 Measurement of ductile damage on copper. [19], Copyright 2015. Reproduced with permission from Elsevier. ....	7
Fig. 1.3 Potential application of the proposed effective stress (a) and ultrasonic methods (b) for damage characterization and detection in PE pipe .....	9
Fig. 2.1 A schematic description of the stress-strain relationship for deformation of semi-crystalline polymers and the corresponding microstructural change during the tensile deformation. ....	17
Fig. 2.2 Schematic description of mechanics of porous media (MPM) theory (top), and continuum damage mechanics (CDM) theory (bottom). ....	19
Fig. 2.3 Schematic description of the linear-fitting method (a) and energy method (b) for determining the unloading stiffness. ....	24
Fig. 2.4 Information on test setup, NPR specimens and test procedure used in this study: (a) D-split tensile test setup, (b) dimensions of NPR specimens and (c) schematic description of test procedure of the first-stage test. ....	25
Fig. 2.5 Effects of prestrain applied in the first-stage test on loading stiffness determined from the second-stage test (a) and unloading stiffness measured from the first-stage test (b). ....	26
Fig. 2.6 Comparison of damage development determined based on LUS and LLS, with the prestrains generated at the crosshead speed of (a) 0.01, (b) 1, (c) 10 and (d) 100mm/min. ....	27
Fig. 2.7 Variation of volume strain at different temperatures. [14], Copyright 2002. Reproduced with permission from John Wiley and Sons. ....	28
Fig. 2.8 Changes of volume strain as a function of strain and strain rate. [10] Copyright 2008. Reproduced with permission from American Chemical Society. ....	30
Fig. 2.9 Schematic description of the dependence of damage development on factors such as strain rate ( $\dot{\epsilon}$ ), temperature ( $T$ ) and stress triaxiality ( $\eta$ ). ....	31

Fig. 3.1 Information on specimens and test set-up used in the study: (a) a pipe section (left) and a modified NPR specimen (right), (b) setup for the D-split tensile test, and (c) specimen dimensions .....	44
Fig. 3.2 Schematic illustration of test procedure used for the first test .....	45
Fig. 3.3 Variation of strain rate as a function of area strain during the tensile deformation at crosshead speeds of 0.01, 1, 10 and 100mm/min .....	47
Fig. 3.4 Plots of relaxation modulus versus time for NPR specimens, stretched to the relaxation strains at crosshead speeds of 0.01 (a), 1 (b), 10 (c), and 100mm/min (d).....	49
Fig. 3.5 Variation of relaxation modulus with time for NPR specimens at the relaxation strain of 5%: (a) original test results and (b) master curve after the shifting.....	51
Fig. 3.6 Master curves for relaxation modulus of PE specimens at different relaxation strains, with the crosshead speed of 0.01mm/min to generate the initial stretch .....	52
Fig. 3.7 Comparison of master curves for the relaxation modulus at the relaxation strain of 5%, with various crosshead speeds to generate the initial stretch.....	53
Fig. 3.8 Results from the monotonic loading of NPR specimen: (a) plots of engineering stress versus stroke at different crosshead speeds and (b) yield stress as a function of logarithmic scale of crosshead speed .....	54
Fig. 3.9 Summary of curves of engineering stress versus stroke and true stress versus area strain at various crosshead speeds: 0.01mm/min for (a) and (b), 1mm/min for (c) and (d), 10mm/min for (e) and (f), and 100mm/min for (g) and (h).....	56
Fig. 3.10 Curves of true stress versus second strain from the second test at the crosshead speed of 0.01mm/min, on NPR specimens that have been subjected to monotonic tensile loading in the first test, at the following crosshead speeds: (a) 0.01mm/min, (b) 1mm/min .....	57
Fig. 3.11 Curves of true stress versus second strain from the second test, for the NPR specimens that have been subjected to monotonic tensile loading to the prestrain level labelled for each curve. Crosshead speed used in the first test was 0.01mm/min for (a) and 1mm/min for (b).....	58
Fig. 3.12 Effect of prestrain introduced in the first test on the elastic modulus measured from the second test .....	60
Fig. 3.13 Variation of damage parameter D for NPR specimens as a function of prestrain introduced in the first test, up to the prestrain level of 80%. .....	62

Fig. 3.14 Variation of damage parameter D as a function of prestrain introduced in the first test, including the prestrains of 120% and 160%, at the crosshead speed of 0.01mm/min.....	64
Fig. 3.15 Variation of yield stress and yield area strain for NPR specimens as functions of prestrain introduced at the following crosshead speeds: (a) 0.01mm/min, (b) 1mm/min, (c) 10mm/min, and (d) 100mm/min.....	65
Fig. 3.16 Plots of true stress versus first strain from the second test at the following crosshead speeds: (a) 0.01mm/min (b) 1mm/min (c) 10mm/min and (d) 100mm/min.....	67
Fig. 3.17 Variation of yield stress (a) and elastic modulus (b) with crosshead speed for PE80 and PE100 pipe materials .....	68
Fig. 3.18 Comparison of relaxation behavior of NPR specimens made from PE80 and PE100 pipe materials, stretched to pre- strains of 20% and 40% at crosshead speeds of (a) 0.01mm/min and (b) 1mm/min.....	70
Fig. 3.19 Effects of pre-strain on elastic modulus of PE80 and PE100 pipe materials, with pre-strain introduced at the first-stage tests at the crosshead speed of (a) 0.01mm/min and (b) 1mm/min.....	71
Fig. 3.20 (a) Gaussian plots of PE80 and PE100 pipe materials with pre-strain of 0.2 and (b) strain hardening modulus ( $G_p$ ) from the second-stage tests as a function of pre-strain introduced in the first-stage tests at the crosshead speed of 0.01mm/min (open symbols) .....	72
Fig. 4.1 Schematic diagram of the D-split tensile test and dimensions of the modified NPR specimens.....	86
Fig. 4.2 Typical curves of engineering stress versus stroke at different crosshead speeds .....	87
Fig. 4.3 FE model of the modified NPR specimen: (a) mesh pattern, (b) deformation from the FE model and (c) deformation from the experimental testing.....	89
Fig. 4.4 Comparison between the first series of FE simulation and the experimental testing at all three crosshead speeds: (a) engineering stress versus stroke at 0.01 mm/min, (b) normalized ligament area versus stroke at 0.01 mm/min, (c) engineering stress versus stroke at 100mm/min .....	91
Fig. 4.5 Curves of equivalent stress versus equivalent strain established from the first series of FE simulation .....	92
Fig. 4.6 Comparison of results from the second series of FE simulation with those from the experimental testing: (a) engineering stress at 0.01 mm/min, (b) normalized ligament area at 0.01	

mm/min, (c) engineering stress at 1 mm/min, (d) normalized ligament area at 1 mm/min, (e) engineering stress at 100 mm/min, and (f) normalized ligament area at 100 mm/min .....	96
Fig. 4.7 Input for the second series of FE simulation: (a) equivalent stress versus equivalent strain, and (b) the damage evolution with the increase of the plastic strain .....	97
Fig. 4.8 (a) Damage evolution laws considered for the FE simulation, and (b) the corresponding curves of engineering stress versus stroke generated from the FE model, based on the stress-strain relationship shown in Fig. 7(a) for 0.01 mm/min .....	101
Fig. 5.1 Squeeze-off test: (a) test setup and specimen and (b) an example of displacement and force as functions of time.....	113
Fig. 5.2 Variation of squeezing force with displacement at squeezing speeds of 0.01, 1 and 50 mm/min.....	114
Fig. 5.3 D-split test and specimen preparation from a squeezed pipe section: (a) schematic description of relative positions (left) and dimensions (right) of NPR specimens, sampled from a squeezed pipe, and (b) D-split test setup .....	115
Fig. 5.4 Effects of the squeeze-off process on mechanical properties of PE pipe at the squeezing speeds of 0.01 mm/min (a), 1 mm/min (b), and 50 mm/min (c) (Note that the relative position is defined in Fig. 5.3(a)) .....	116
Fig. 5.5 Variation of the tensile elastic modulus (a), the corresponding damage evolution (b), and yield stress (c) for NPR specimens, as a function of prestrain introduced in the first test .....	117
Fig. 5.6 Dimensions for the stub specimens (left) and compressive test setup (right) .....	118
Fig. 5.7 Variation of the compressive elastic modulus (a), the corresponding damage evolution (b) and compressive yield stress (c) for stub specimens, as a function of compressive prestrain introduced in the first test .....	120
Fig. 5.8 Schematic description of the two-stage tests on half NPR specimens .....	121
Fig. 5.9 Elastic modulus (a) and yield stress (b) for half NPR specimens, as a function of prestrain applied in the first test.....	122
Fig. 5.10 Elastic modulus (a) and yield stress (b) for half NPR specimens, as a function of stroke applied in the first test.....	122
Fig. 5.11 The 2-D view of a 3-D FE model for the squeeze-off process.....	124

Fig. 5.12 Comparison between FE simulation and experimental testing at squeezing speeds of 0.01 (a), 1 (b) and 50 mm/min (c).....	125
Fig. 5.13 Strain generated across wall thickness of the PE pipe: (a) schematic description of the cross-section of the PE pipe wall between the squeeze-off bars, and (b) distribution of circumferential normal strain ( $\varepsilon_{22}$ ) on the cross-section of pipe wall directly between the squeeze-off bars .....	128
Fig. 5.14 Variation of average equivalent strain from the FE simulation as a function of displacement: (a) tension and (b) compression.....	129
Fig. 5.15 Evolution of average strain rate with deformation under tension and compression for squeezing speeds of 0.01 (a), 1 (b) and 50mm/min (c) from the FE simulation .....	130
Fig. 5.16 Relationship between damage parameter (D) and strain rate at tensile strain 0.56 (a) and compressive strain 0.27 (b), from Fig. 5.5(b) and 5.7(b), respectively .....	131
Fig. 6.1 D-split test: (a) NPR specimen dimensions and (b) test setup .....	143
Fig. 6.2 True stress-strain curves for five crosshead speeds.....	147
Fig. 6.3 Curves generated from Eq. (6.7) (open symbols) and obtained from stress relaxation tests (lines) at the relaxation strain of 10% (a) and 30% (b) with the initial stretch introduced at the crosshead speeds of 0.001, 0.01, 0.1, 1 and 10mm/min.....	148
Fig. 6.4 Viscous stress (a) and quasi-static stress (b) for crosshead speeds of 0.001, 0.01, 0.1, 1 and 10mm/min .....	149
Fig. 6.5 The relationship between quasi-static stress and crosshead speed for various strains ..	151
Fig. 6.6 Experimental curves of true stress versus area strain for PE samples with different ligament widths, at the crosshead speed of 0.001mm/min .....	152
Fig. 6.7 Viscous stress and quasi-static stress for PE samples with different widths, tested at the crosshead speed of 0.001mm/min.....	153
Fig. 6.8 Variation of quasi-static stress with the ligament width for various strains.....	154
Fig. 6.9 Schematic depiction of undamaged, damaged and fictitious undamaged configurations .....	155
Fig. 6.10 Damage variable as a function of prestrain, generated at crosshead speeds of 0.01, 1 and 10mm/min .....	157

Fig. 6.11 Comparison of damage variables based on the proposed effective stress method, the SE method and the EE method.....	159
Fig. 7.1 Dimensions for short (a) and long (b) specimens with nominal thickness ranging from 1.5 to 10mm .....	170
Fig. 7.2 Ultrasonic test: (a) schematic diagram of the test setup, (b) transducers and PE specimen used in the ultrasonic tests, and (c) three measurement locations on the specimen .....	173
Fig. 7.3 Relationship between travelling distance and time for specimens L-6 (a) and S-3 (b). .....	174
Fig. 7.4 Summary of curves of engineering stress versus stroke: (a) L-10, (b) S-10, (c) L-6, (d) S-6, (e) L-3, (f) S-3, (g) L-1.5, and (h) S-1.5. Prestrain for each curve, as indicated by the legend, is calculated using Eq. (7.1).....	175
Fig. 7.4 Top and front views of a test block used to establish the relationship between ultrasonic velocity and specimen thickness.....	177
Fig. 7.6 The dependence of ultrasonic velocity on the thickness of specimens .....	179
Fig. 7.7 Examples of longitudinal wave traces from virgin and prestrained specimens: (a) L-6 and (b) S-6.....	179
Fig. 7.8 Ultrasonic test results: (a) normalized ultrasonic velocity versus prestrain and (b) damage parameter $D_v$ based on the decrease of ultrasonic velocity, Eq. (7.2) .....	180
Fig. 7.9 Comparison of damage parameter $D_v$ based on degradation of ultrasonic velocity without considering the density change, with damage parameter $D_{SE}$ based on degradation of elastic modulus under the hypothesis of strain equivalence: (a) L-10, (b) S-10, (c) L-6, (d).....	182
Fig. 7.10 (a) Change of the density ratio ( $\rho_D/\rho_0$ ) as a function of prestrain based on experimental data given in ref. [15], and (b) variation of damage parameters $D_{SE}$ , $D_v$ and $D_{v\rho}$ as functions of prestrain for L-10.....	184

## List of symbols and abbreviations

$a, b, c, d, e, \alpha, k, N, M, \beta, A, ak$	Constants for constitutive model
AE	Acoustic emission
CDM	Continuum damage mechanics
CPD	Current potential drop
CRB	Cracked round bar
CT	Compact tension
$D$	Damage variable/parameter
$D_A$	Damage variable measured from the ratio of damaged to total cross-sectional areas
$D_c$	Critical damage value
$D_{EE}$	Damage variable based on the hypothesis of energy equivalence
$D_{eff}$	Damage variable based on the degradation of effective stress
$D_H$	Damage variable measured from the change of hardness
$D_{SE}$	Damage variable based on the hypothesis of strain equivalence
$D_v$	Damage variable measured from the change of ultrasonic velocity
$D_\rho$	Damage variable measured from the change of material density
$E_0$	Elastic modulus for undamaged materials
$E_1$	Elastic moduli for virgin specimen with the isotropic, semi-crystalline microstructure

$E_2$	Elastic moduli for virgin specimen with aligned microstructure
$E_D$	Elastic modulus for damaged materials
EEE	Elastic energy equivalence
ESE	Elastic strain equivalence
FE	Finite element
FEA	Finite element analysis
$G_p$	Strain-hardening modulus
HDPE	High density polyethylene
HDS	Hydrostatic design stress
IRT	Infrared thermography
$L$	Minimum distance between the squeeze-off bars
LLS	Loading-loading stiffness
LUS	Loading-unloading stiffness
MPM	Mechanics of porous media
MRS	Minimum required strength
NDE	Non-destructive evaluation
NPR	Notched pipe ring
PA11	Polyamide 11
PE	Polyethylene
PLA	Poly(l-lactide)
PP	Polypropylene
PVDF	Polyvinylidene fluoride

RVE	Representative volume element
$S$	Overall cross-sectional area of the representative volume element
SAXS	Small-angle X-ray scattering
SCG	Slow crack growth
SCR	Slow crack resistant
$S_D$	Effective area of micro-cracks and cavities
SEM	Scanning electron microscopy
SENB	Single edge notched bending
$SR$	Squeezing ratio
$t$	Uncompressed pipe wall thickness
TTS	Time-temperature superposition
$v_{L0}$	Longitudinal ultrasonic velocity for undamaged material
$v_{LD}$	Longitudinal ultrasonic velocity for damaged material
$WC$	Wall compression
$\epsilon_1$	Axial strain along the stretching direction
$\epsilon_2, \epsilon_3$	Transverse strains
$\epsilon_{eff}$	Effective strain in fictitious undamaged configuration
$\epsilon_n$	Critical strain for the on-set of necking
$\epsilon_t$	Strain at the beginning of the exponential hardening
$\epsilon_{true}$	True strain
$\epsilon_V$	Volume strain
$\epsilon_w$	Area strain based on the change of ligament width

$\varepsilon_y$	Transitional strain from linear to nonlinear deformation
$\dot{\varepsilon}^{cr}$	Equivalent creep strain rate
$\bar{\varepsilon}$	Average equivalent strain rate
$\lambda$	Stretch ratio
$\nu$	Poisson's ratio
$\sigma_{eff}$	Effective stress in fictitious undamaged configuration
$\sigma_r$	Viscous stress
$\tau_r, E_r, \sigma_0$	Characteristic relaxation time, relaxation modulus and reference stress
$w_0, w$	Initial and deformed width

# Chapter ***1***

## **Introduction**

### **1.1 Background and motivation**

Semi-crystalline polymers are increasingly used in a broad range of applications such as pressure tubing, pipeline systems and parts in nuclear power plant. Nowadays, majority of low-pressure natural gas pipes with a 50-year service life are made of polyethylene (PE). According to the most recent data provided by U.S. Department of Transportation, PE has surpassed steel as the most widely used material for natural gas transportation due to its good physical and mechanical properties. Furthermore, statistics shows that over 90% of the newly installed low-pressure gas pipeline systems are made of PE [1]. However, unexpected, catastrophic failures of PE pipeline were still reported in the last decade [2–4], suggesting that the current approach for characterizing PE pipes has blind spots for the performance evaluation.

The long-term performance, design stress and service lifetime of PE pipe are typically characterized by performing internal pressure tests of full-sized pipes at multiple temperatures, through standard extrapolation methods according to EN ISO 9080 or ASTM D2837. In this type of tests, a log-log diagram of hoop stress versus failure time is recorded and used to estimate the design stress at the desired temperature and lifetime. The above hoop stress curve shows that based on the stress level, three failure mechanisms are involved in the pressurized PE pipe: (I) ductile failure, (II) brittle failure and (III) degradation-controlled failure. However, these full-

sized pipe tests require a long duration (around 1.5 year) to complete. Thus, a number of accelerated laboratory test methods, including fully-notched test (FNCT) [5], the Pennsylvania edge-notched test (PENT) [6] and cracked round bar (CRB) test [7], have been developed to investigate the resistance to slow crack growth (SCG) in brittle failure region of modern PE pipe. In addition to those tests, it was found that strain hardening modulus, determined from short-term tensile test on notch-free specimens, can also be used to characterize resistance to brittle failure of PE pipe when subjected to stress in an aggressive environment, commonly known as environmental stress cracking resistance (ESCR) [8, 9]. However, results from the above tests are mainly for prediction of overall SCG resistance, not for determining the critical stress level for the SCG initiation. Since time for SCG initiation ( $t_{ini}$ ) can account for 20%-80% of total time to failure ( $t_{tot}$ ) thus playing an important role for the reliability of PE pipe, [10], it is important to develop a method that can characterize resistance to SCG initiation. In this study, damage development that is used to characterize progressive property degradation is used to characterize the critical condition for crack initiation. Since damage development can be quantified using decrease in strength, stiffness, hardness, ultrasonic wave velocity, etc., results from the damage characterization can help in predicting  $t_{ini}$ , thus improving the prediction of lifetime for PE pipe.

Furthermore, it is now also a general consensus that external loading scenarios such as squeeze-off process as shown in Fig. 1.1, can cause deterioration of mechanical properties and reduce the remaining lifetime of the pipe [11, 12]. Such process is widely used to shut off or control gas flow in gas pipes when this is required in order to perform maintenance and repair of the pipeline systems. However, evidence has led to suspect that degradation of mechanical properties caused by the squeeze-off process is responsible for some of the unexpected, catastrophic failures of PE pipe [12, 13]. Research conducted to study effects of squeeze-off on

mechanical properties of PE pipe shows that wall compression (WC) greater than 30% is typically necessary to induce damage in PE pipe. The definition of WC is given in Eq. (1.1) and depicted in Fig. 1.1(b).

$$WC = \left(1 - \frac{L}{2t}\right) \times 100\% \quad (1.1)$$

where  $L$  and  $t$  are the minimum distance between the squeeze-off bars and the uncompressed pipe wall thickness, respectively. It has been specified in ASTM F 1734 that the maximum WC value of 30% should not be exceeded. However, damage may occur with WC of less than 30% for low slow crack resistant (SCR) materials. Furthermore, if improper squeeze-off tools or procedures are applied there is a possibility to induce damage to PE pipe. Therefore, it is very important to understand the squeeze-off phenomenon.

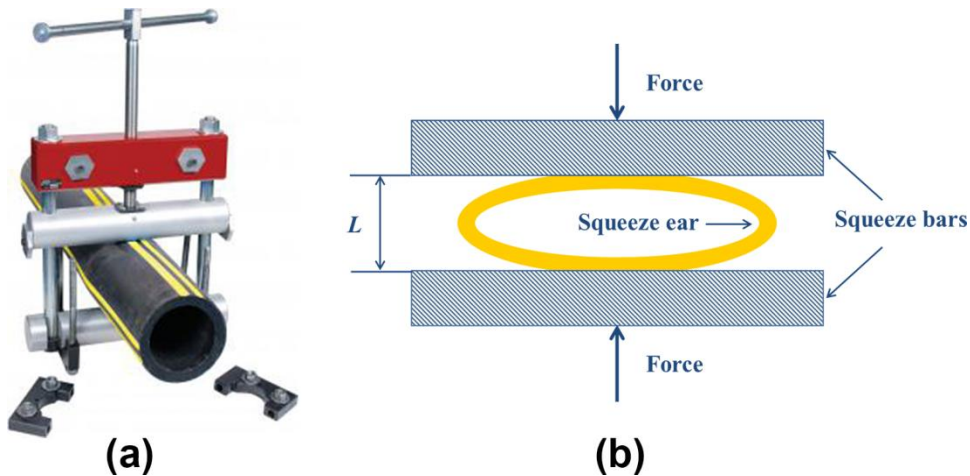


**Fig. 1.1** Squeeze-off of PE pipe: (a) commercial squeeze-off tool [14] and (b) definition of the terms used for the squeeze-off process.

On the other hand, thanks to the rapid advancement in computational power, finite element analysis (FEA) has been used as an effective tool to design complex full-scale tests and predict lifetime of engineering components. However, continuum damage models embedded in FEA

softwares require experimental determination of material-specific damage evolution model as well as the constitutive model, which can accurately predict deformation response of materials. Thus the urge for damage evolution model calls for highly accurate and reliable damage measurement and characterization methodologies. Although various damage characterization methods have been proposed, but mainly for metallic materials. The first damage measurement method is developed from the definition of damage variable  $D$ , as the ratio of damaged to total cross-sectional area. Apart from the geometry-based damage characterization method, mechanical property-based methods are also proposed that measure damage based on the degradation of mechanical properties such as elastic modulus and yield or flow stress. An example is given in Fig. 1.2 for measurement of ductile damage of copper using cyclic loading-unloading tests. It appears that the change of elastic modulus is the most convenient technique to estimate damage and has been widely used for metals [15–17]. However, for semi-crystalline polymers such as PE, its nonlinear rate-dependent deformation behaviour caused by viscous component must be taken into consideration. As a result, instead of using the traditional cyclic loading-unloading test methods, in this study a two-stage test method [18] is proposed to quantitatively characterize damage evolution in PE pipe materials. As the name suggested, the first-stage test is to introduce damage by subjecting the specimens to different damage levels and two months later the second-stage test to apply monotonic tensile loading, at a crosshead speed of 0.01mm/min, to characterize the mechanical properties for virgin and damaged specimens.

It is also well known that mechanical properties of PE are strongly dependent on its molecular structures. Driven by the advancement of polymerization technology, the performance of PE pipe has been improved significantly. For example, around 1980 high density polyethylene (HDPE) materials, characterized as PE3408 under the ASTM/PPI system or PE80 under ISO

system, were first introduced in North America and Europe. To be qualified for PE3408 or PE80 pressure rating, PE pipe must withstand a minimum hoop stress of 800 psi (5.52 MPa), named as hydrostatic design stress (HDS) for up to 11 years at 73°F (23.8°C) under ASTM/PPI pressure rating system, or the pipe must withstand a minimum hoop stress of 8 MPa, named as minimum required strength (MRS) for up to 50 years at 68°F (20°C). Later these materials were improved to PE4710 with a HDS of 1000 psi (6.9 MPa) and PE100 with a MRS of 10 MPa. This improvement is primarily driven by the introduction of Bimodal PE resins. However, in the advancement from PE80 to PE100, not all performances were improved. Experimental results show that fracture toughness of PE80 for compact tension (CT) and single edge notched bending (SENB) specimens is higher than that of PE100 at both low temperature and room temperature [13]. In addition, the performance of PE pipes made from PE80 resins is less affected by squeeze-off process than PE pipes manufactured from PE100 resins [14]. However the knowledge about the difference in relaxation behavior, damage evolution and strain hardening properties in PE80 and PE100 pipe materials is yet to be available in literature.

Thanks to the rapid advancement in computational power, quantitative prediction of deformation and fracture behaviour becomes a realistic possibility through the use of finite element analysis (FEA) software. However, continuum damage models embedded in the software require experimental determination of material-specific damage evolution model as well as the constitutive model, in order to predict accurately the deformation response of materials. Thus, the urge for damage evolution model calls for highly accurate and reliable damage measurement and characterization methodologies. Although various damage characterization methods have been proposed, they are mainly used for metallic materials. The first damage measurement method is developed from the definition of damage variable  $D$ , as the

ratio of damaged to total cross-sectional area. Apart from the geometry-based damage characterization method, mechanical-property-based methods are also proposed which measure damage based on the degradation of mechanical properties such as elastic modulus and yield or flow stress. An example is given in Fig. 1.2 for measurement of ductile damage of copper using cyclic loading-unloading tests. It appears that the change of elastic modulus is the most convenient technique to estimate damage, which has been widely used for metals [15–17]. However, for semi-crystalline polymers such as PE, its nonlinear rate-dependent deformation behaviour due to viscous component must be taken into consideration for the measurement of elastic modulus. Recently, a so called two-stage test method was proposed [18] to study effects of loading history on mechanical properties of PE, which will be used in this study. A detailed review and discussion on the damage characterization methods based on continuum damage mechanics (CDM) will be presented in the next chapter.

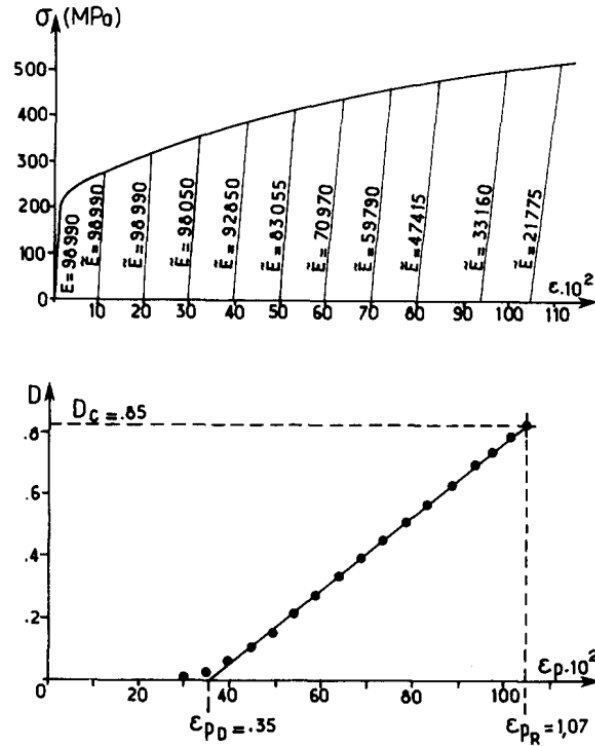


**Fig. 1.2** Measurement of ductile damage on copper. [19], Copyright 2015. Reproduced with permission from Elsevier.

In addition to the above mentioned destructive CDM-based characterization methods, a variety of non-destructive evaluation (NDE) methods such as acoustic emission (AE), infrared thermography (IRT), current potential drop (CPD) and ultrasonic techniques are also widely used to characterize mechanical properties of engineering materials. Among the above mentioned NDE methods, ultrasonic velocity approaches have proven to be an ideal and effective technique for tracking property change of materials due to damage accumulation. However, majority of these methods are designed for metallic or ceramic materials. Although some pioneering work has been conducted to investigate mechanical or physical properties in polymeric materials, none of the approaches developed are for damage characterization and quantification. In this work, feasibility of applying ultrasonic techniques to the damage characterization and detection for PE materials will be studied. The potential application of the ultrasonic method proposed as shown

in Fig. 1.3 is to monitor the state of damage, to estimate the residual service life and to provide guidance for maintenance and repair of pipeline systems.

Although the damage characterization methods based on the degradation of elastic modulus have been proved to be an effective way to quantify damage growth in various kinds of engineering materials, they are not applicable for in-situ damage characterization and detection. Moreover, the current damage variables are defined based on various transformation hypotheses describing the relationship between damaged and fictitious undamaged configurations such as strain equivalence or energy equivalence hypothesis. In this study, a novel approach is proposed to characterize damage in PE materials based on the effective stress concept without using any hypothesis. Furthermore, successful determination of effective stress in the fictitious, undamaged configuration can potentially be applied to development of an in-situ damage characterization and detection method for PE pipe materials, as shown in Fig. 1.3(a).

In addition to the above mentioned mechanical property-based damage characterization methods, a variety of non-destructive evaluation (NDE) methods such as acoustic emission (AE), infrared thermography (IRT), current potential drop (CPD) and ultrasonic techniques are also widely used to characterize mechanical properties of engineering materials. Among the above mentioned NDE methods, ultrasonic velocity approaches have proved to be an idea and effective technique used to track property change of materials due to damage accumulation. However, majority of these methods are designed for metallic or cement materials. Although some pioneering research work has been conducted to investigate mechanical or physical properties in polymeric materials, none of the approaches developed are for damage characterization and quantification. In this work the feasibility of applying ultrasonic techniques to the damage characterization and detection for PE materials will be studied. The potential application of the

ultrasonic method proposed as shown in Fig. 1.3(b) is to monitor the state of damage, to estimate the residual service life and to provide guidance for maintenance and repair of pipeline systems.

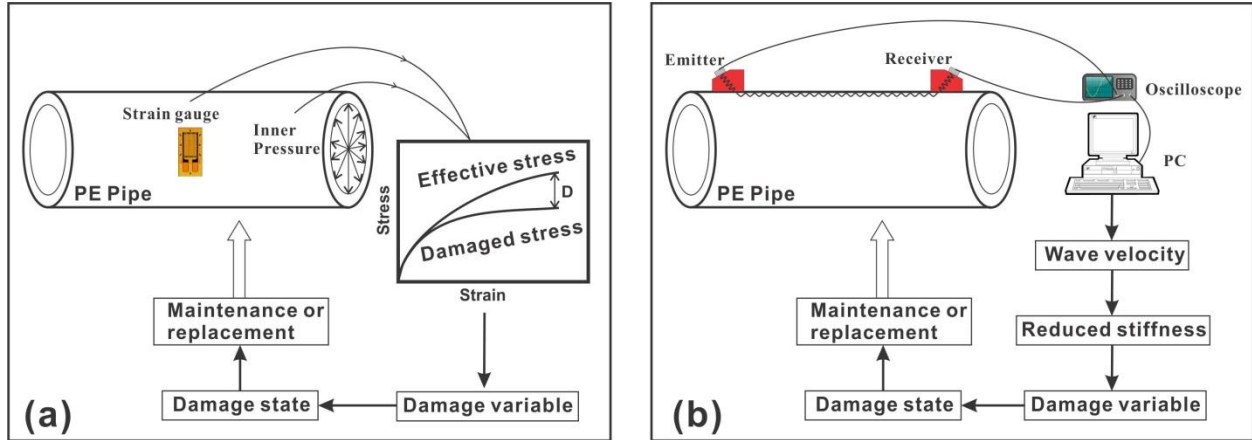


**Fig. 1.3** Potential application of the proposed effective stress (a) and ultrasonic (b) methods for damage characterization and detection in PE pipe

## 1.2 Research objectives and approach

Despite that some progress has been made in understanding the deformation-induced damage and developing damage characterization and quantification methods, there are still much room for improvement. The overall objective of this thesis is to investigate deformation-induced damage in a wide range of strain levels, from yielding to neck formation and propagation, to characterize damage initiation and growth until fracture is generated, in order to develop an effective damage characterization and detection method based on the concept of CDM. This objective will be achieved through completing the following research topics:

1. A two-stage test method is developed to evaluate effects of deformation-induced damage (or loading history) on mechanical properties of PE pipe. The damage development in PE pipe is characterized and quantified from the measurement of degradation of elastic modulus. In particular, the influence of strain rate and microstructure on damage

development in PE pipe is examined. In addition, a phenomenological modelling approach is proposed to study the damage development in PE pipe under tensile loading condition.

2. The above proposed two-stage test method is further applied to study effects of squeeze-off process on mechanical properties of PE pipe, with a special emphasis placed on the squeezing speed (loading rate). Furthermore, a study using mechanical testing and finite element (FE) simulation is conducted to elucidate the damage evolution in PE pipe in different loading modes (including tension and compression) and with different loading history (in terms of maximum pre-strain level and loading speed).
3. A novel approach combining relaxation tests and viscous model is proposed to obtain quasi-static stress-strain relationship for PE pipe by removing the viscous stress component from the experimentally measured total stress. Effects of crosshead speed and specimen geometry on quasi-static stress-strain relationship are investigated. Furthermore, the effective stress under the fictitious undamaged configuration is estimated as the quasi-static stress at zero crosshead speed. Based on the difference between stress at damaged configuration and effective stress at undamaged configuration, the damage development in PE pipe is quantified and compared with that measured from the degradation of elastic modulus.
4. A non-destructive ultrasonic method is proposed to characterize damage in PE materials through employing time-of-flight in the through-transmission mode. PE samples with different geometries are designed to study effects of stress triaxiality on damage development. Damage evolution in PE materials is determined based on the degradation of ultrasonic velocity. In addition, mechanical testing is applied to characterize damage

development in these PE samples and the results obtained are compared with those from ultrasonic tests.

Successful completion of the above studies will enable a better understanding of damage mechanisms occurring in PE pipes and provide insights into the possibility of developing new damage detection and lifetime prediction methods. The main benefits to industry are to provide useful guidelines for improving installation and maintenance procedures as well as for extending the service life of PE pipes.

### **1.3 Thesis Organization**

This thesis provides a detailed description of the proposed damage characterization and detection methods and their application to elucidating the damage process in the squeeze-off process. This thesis is composed of eight chapters as follows.

Chapter 1 describes the background of the presented research and highlights the motivation behind the current research, research objectives and the proposed methodologies. Finally, the thesis outline is provided.

Chapter 2 presents an introduction to theories including mechanics of porous media (MPM) and continuum damage mechanics (CDM), based on which damage characterization methods are developed. Summary of recent development on the characterization methods for damage development in semi-crystalline polymers is then provided. A practical example of applying two CDM-based damage characterization methods is used for better understanding the damage concept and the measurement techniques for semi-crystalline polymers.

Chapter 3 deals with the experimental characterization of deformation damage in PE pipe. Strain rate is found to be an additional factor to the time-temperature superposition principle for PE deformation and is used as an accelerating factor to construct long-term relaxation master curve for PE pipe. This chapter also includes experimental study on the damage development under tensile loading with special attention to the influence of strain rate and microstructure of PE pipe on the damage evolution.

Chapter 4 presents a phenomenon-based, hybrid approach of combining experimental testing and finite element (FE) simulation to investigate tensile fracture in PE pipe with the consideration of damage evolution. Results from the FE simulation suggest that the proposed approach enables the FE model to simulate both large deformation and stress drop in the final stage of the test. The influence of damage evolution rate on the load-stroke curve generated from the D-split test is characterized using the proposed approach.

Chapter 5 presents a study on the effects of squeeze-off process on mechanical properties of PE pipe. Three squeezing speeds are used to cover the possible scenarios that may be encountered during the pipe repair or maintenance. In order to elucidate the finding that reducing the squeezing speed has no effect on the extent of property degradation, a study is conducted using mechanical testing and FE simulation.

Chapter 6 presents a novel damage characterization method based on the concept of effective stress. Quasi-static stress-strain relationship is first determined by removing the viscous stress component through the application of relaxation test results to a viscous model. Influence of strain rate and specimen geometry on the quasi-static stress-strain relationship is emphasized. By fitting the experimentally determined quasi-static stress as a function of strain rate and

extrapolating the strain rate to zero, an estimate of the effective stress at the undamaged configuration is made. Finally, the damage development based on the degradation of stress is quantified and compared with that measured from the degradation of elastic modulus.

Chapter 7 presents a NDE approach of characterizing and detecting ductile damage in PE materials using ultrasonic techniques. Velocity of ultrasonic wave in virgin and damaged PE samples is measured using the time-of-flight method in the through transmission mode. Damage development measured from the degradation of ultrasonic velocity is compared with that based on the degradation of elastic modulus. Effects of stress triaxiality on the damage development in PE samples are also studied and included in this chapter.

Chapter 8 provides conclusions and recommendation for the future work.

## References

- [1] Kiass, N., Khelif, R., Boulanouar, L., and Chaoui, K., 2005, "Experimental Approach to Mechanical Property Variability through a High-Density Polyethylene Gas Pipe Wall," *J. Appl. Polym. Sci.*, **97**(1), pp. 272–281.
- [2] Shalaby, H. M., Riad, W. T., Alhazza, A. A., and Behbehani, M. H., 2006, "Failure Analysis of Fuel Supply Pipeline," *Engineering Failure Analysis*, **13**(5), pp. 789–796.
- [3] Azevedo, C. R. F., 2007, "Failure Analysis of a Crude Oil Pipeline," *Engineering Failure Analysis*, **14**(6), pp. 978–994.
- [4] Majid, Z. A., Mohsin, R., Yaacob, Z., and Hassan, Z., 2010, "Failure Analysis of Natural Gas Pipes," *Engineering Failure Analysis*, **17**(4), pp. 818–837.
- [5] ISO 16770., 2004, "Plastics-Determination of Environmental Stress Cracking (ESC) on Polyethylene (PE) – Full Notch Creep Test (FNCT)."
- [6] 2005, *ISO 16241, Notch Tensile Test to Measure the Resistance to Slow Crack Growth of Polyethylene Materials for Pipe and Fitting Products (PENT)*, International Organization for Standardization.
- [7] Pinter, G., Haager, M., Balika, W., and Lang, R. W., 2007, "Cyclic Crack Growth Tests with CRB Specimens for the Evaluation of the Long-Term Performance of PE Pipe Grades," *Polymer Testing*, **26**(2), pp. 180–188.

- [8] Cheng, J. J., Polak, M. A., and Penlidis, A., 2008, "A Tensile Strain Hardening Test Indicator of Environmental Stress Cracking Resistance," *Journal of Macromolecular Science®*, Part A: Pure and Applied Chemistry, **45**(8), pp. 599–611.
- [9] Kurelec, L., Teeuwen, M., Schoffeleers, H., and Deblieck, R., 2005, "Strain Hardening Modulus as a Measure of Environmental Stress Crack Resistance of High Density Polyethylene," *Polymer*, **46**(17), pp. 6369–6379.
- [10] Chudnovsky, A., Zhou, Z., Zhang, H., and Sehanobish, K., 2012, "Lifetime Assessment of Engineering Thermoplastics," *International Journal of Engineering Science*, **59**, pp. 108–139.
- [11] Krishnaswamy, R. K., 2005, "Analysis of Ductile and Brittle Failures from Creep Rupture Testing of High-Density Polyethylene (HDPE) Pipes," *Polymer*, **46**(25), pp. 11664–11672.
- [12] Palermo, G., 2004, "Correlating Aldyl 'A' and Century PE Pipe Rate Process Method Projections with Actual Field Performance," *Plastics Pipes XII Conference. Milan, Italy*.
- [13] Brown, N., and Crate, J. M., 2012, "Analysis of a Failure in a Polyethylene Gas Pipe Caused by Squeeze off Resulting in an Explosion," *J Fail. Anal. and Preven.*, **12**(1), pp. 30–36.
- [14] "PE Squeeze-Off Tools - Reed Manufacturing" [Online]. Available: <https://www.reedmfgco.com/en/products/plastic-pipe-tools/pe-squeeze-off-tools/>. [Accessed: 09-Feb-2017].
- [15] Lemaitre, J., and Dufailly, J., 1987, "Damage Measurements," *Engineering Fracture Mechanics*, **28**(5–6), pp. 643–661.
- [16] Bonora, N., Gentile, D., Pirondi, A., and Newaz, G., 2005, "Ductile Damage Evolution under Triaxial State of Stress: Theory and Experiments," *International Journal of Plasticity*, **21**(5), pp. 981–1007.
- [17] Celentano, D. J., and Chaboche, J.-L., 2007, "Experimental and Numerical Characterization of Damage Evolution in Steels," *International Journal of Plasticity*, **23**(10–11), pp. 1739–1762.
- [18] Jar, P.-Y. B., 2014, "Effect of Tensile Loading History on Mechanical Properties for Polyethylene," *Polym Eng Sci*, **55**(9), pp. 2002–2010.
- [19] Lemaitre, J., 1984, "How to Use Damage Mechanics," *Nuclear Engineering and Design*, **80**(2), pp. 233–245.

# Chapter 2

## **Review of the damage characterization methods**

This chapter gives a summary of recent developments on the characterization methods for damage development in semi-crystalline polymers. Current methods for the damage characterization are based on either mechanics of porous media (MPM) theory or continuum damage mechanics (CDM) theory. The former regards cavitation as the main mechanism for the damage generation, and uses volume strain or void volume fraction to represent the damage level. The latter, on the other hand, is to characterize the damage state based on a macroscopic damage variable, defined as the ratio of effective area of micro-cracks and cavities to the overall cross-sectional area of the representative volume element (RVE). Special attention will be given to the influence of polymer microstructure, strain rate, temperature and stress triaxiality on the damage development. Two CDM-based methods for the damage measurement will be demonstrated using pipe-grade polyethylene materials, as examples for the difference in the results from the two CDM-based methods, for better understanding the damage concept and the measurement techniques for semi-crystalline polymers.

### **2.1 Introduction**

Semi-crystalline polymers, such as polyethylene (PE) and polypropylene (PP), are widely used for engineering applications, because of their low density, relatively low cost and ease in processing. For example, polyethylene is now used for natural gas transportation. Statistics

shows that in this application, over 90% of newly installed gas pipes are made of PE. Uncertainty in the failures of such plastic pipes can cause significant financial loss and sometimes fatalities. Therefore, it is extremely important to understand the damage process that is responsible for the failure, in order to predict the service lifetime of pipes. Here, “damage development” or “damage evolution” is quantified based on a damage parameter that is also dependent on plastic strain and strain rate used to introduce the deformation. By understanding the damage development process, time for the damage-induced fracture can be predicted to allow the required repair and maintenance to be scheduled in time to prevent the unexpected failure. Although various approaches have been developed to quantify the damage development in semi-crystalline polymers, none of the current methods provides effective and economic means to distinguish the difference in damage development among the semi-crystalline polymers.

Damage development in semi-crystalline polymers can be characterized at either a microscopic or a macroscopic scale. At the microscopic scale, a series of studies have been conducted to understand mechanisms involved in the damage generation [1–8]. It is now believed that the main mechanism for the damage development in semi-crystalline polymers is cavitation in the inter-lamellar, amorphous phase [9]. Cavitation starts around the yield point, and its development depends on both external factors, such as deformation rate [10–12] and temperature [13–15], and internal factors that include molecular weight and lamella thickness [16–18]. At the macroscopic scale, the damage development can be characterized based on variation in mechanical properties such as elastic modulus [6, 19, 20]. Although a lot of efforts have been spent on quantifying the damage development in semi-crystalline polymers, important factors such as critical damage parameter for fracture, onset point for damage initiation, and influence of viscous deformation on the damage development have yet to be fully characterized.

Semi-crystalline polymers are well known for their complicated microstructure which is composed of lamellar crystals that are interconnected through tie molecules and separated by soft amorphous phase, as shown in Fig. 2.1. When subjected to tensile deformation, cavities or micro-cavities are nucleated, coalesced and then enlarged in the amorphous phase, which eventually leads to fracture. As a result, cavitation has been regarded as one of the main damage mechanisms for semi-crystalline polymers. In the following, background of damage theories is introduced, to help better understanding the complexity of mechanical behavior of semi-crystalline polymers, especially when cavitation is involved in the damage development. Approaches used here to describe the damage development are based on either mechanics of porous media (MPM) theory or continuum damage mechanics (CDM) theory.

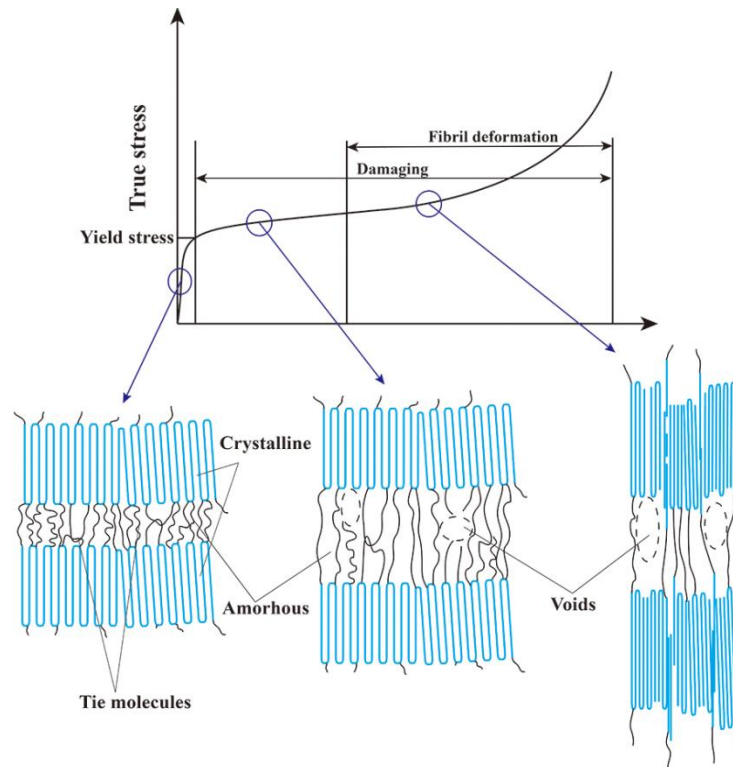


**Fig. 2.1** A schematic description of the stress-strain relationship for deformation of semi-crystalline polymers and the corresponding microstructural change during the tensile deformation.

## 2.2 Mechanics of porous media (MPM)-based approach

Mechanics of porous media (MPM) theory was developed based on the assumption that damage occurs at a microstructural level, due to void nucleation, growth and coalescence till failure takes place. Porous media theory was traditionally used for porous solids such as soil. However, voids or cavities also occur in semi-crystalline polymers during the deformation, as shown in Fig. 2.1. Therefore, porous media theory has long been adopted to describe the deformation and damage behaviour of semi-crystalline polymers. Essence of the MPM theory is to mimic the process of void nucleation, growth and coalescence, as shown in Fig. 2.2. In order to give a quantitative description of this damage process, macroscopic parameters such as porosity, void volume fraction, or volume strain has been developed. For example, total volume increase due to the occurrence of cavitation, i.e., volume strain, can serve as an indicator for the level of damage in semi-crystalline polymers. A novel video-controlled testing system was developed by G'Sell and his co-workers [21] in such a way that the volume strain  $\varepsilon_V$  can be determined from the measurement of three normal strains, using the following equation:

$$\varepsilon_V = \varepsilon_1 + \varepsilon_2 + \varepsilon_3 \quad (2.1)$$

where  $\varepsilon_1$  represents the axial strain along the stretching direction, and  $\varepsilon_2$  and  $\varepsilon_3$  the transverse strains. Another damage parameter, named void volume fraction or porosity, is commonly used in GTN damage model [22–24] which is one of the most widely used models based on the MPM theory. In addition, cavitation in semi-crystalline polymers has been studied at the microscopic level by employing the imaging methods such as X-ray scattering [25–27] and scanning electron microscopy (SEM) [28]. It is now widely accepted that cavitation in semi-crystalline polymers

occurs around the yield point and its occurrence depends on loading conditions such as strain rate, temperature and stress state.

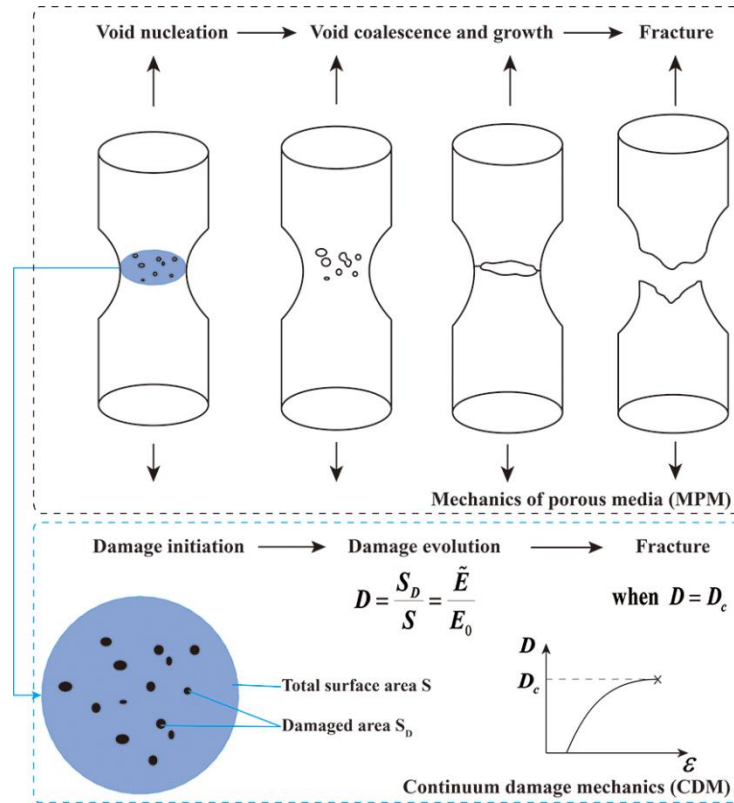


**Fig. 2.2** Schematic description of mechanics of porous media (MPM) theory (top), and continuum damage mechanics (CDM) theory (bottom).

In the GTN model, porosity or void volume fraction, defined as the ratio of void volume to total volume, is used as the damage parameter, thus with a value between 0 and 1. It is assumed that with the increase of porosity, material gradually loses its load-carrying capacity till the porosity reaches 1. The GTN-type damage models have been widely used to analyze the shear failure mode [29–31] and to evaluate ductile damage and fracture behaviour [32, 33].

## 2.3 Continuum damage mechanics (CDM)-based approach

### 2.3.1 Damage variables

Continuum damage mechanics (CDM)-based on damage quantification method is to characterize the damage state based on a macroscopic damage variable,  $D$ , defined as the ratio of effective area of micro-cracks and cavities to the overall cross-sectional area of the representative volume element (RVE). For one dimensional case of isotropic damage, damage variable  $D$  is usually described as:

$$D = \frac{S_D}{S} \quad (2.2)$$

This damage variable can reflect various types of damage at the microscopic level, such as nucleation and growth of voids. Similar to the MPM theory, CDM theory is with the assumption that once a critical damage value  $D_c$  is reached, the material can no longer carry any load, and thus failure occurs.

### 2.3.2 Effective stress concept

The concept of effective stress under uniaxial tension was first introduced by Kachanov [34, 35] and later extended to three dimensional stress state by Lemaitre [36, 37]. For the case of isotropic damage, effective stress is defined by

$$\sigma_{eff} = \frac{\sigma}{1-D} \quad (2.3)$$

Where  $\sigma$  and  $\sigma_{eff}$  are Cauchy stress tensor and the corresponding the effective stress tensor applied to a fictitious state of material which is totally undamaged. Based on the hypothesis of strain equivalence (SE) or energy equivalence (EE), the fictitious state is assumed to be mechanically equivalent to the actual damaged state of the material. For example, under the hypothesis of SE it is assumed that:

$$\varepsilon = \varepsilon_{eff} \quad (2.4)$$

The elastic constitutive equations in damage and fictitious undamaged configuration can be described as follows:

$$\sigma = E_D \varepsilon \quad (2.5)$$

$$\sigma_{eff} = E_0 \varepsilon_{eff} \quad (2.6)$$

When the hypothesis of EE is applied, the complimentary elastic energy  $\sigma^2/2E$  in both configurations is assumed to be equivalent:

$$\frac{\sigma^2}{2E_D} = \frac{\sigma_{eff}^2}{2E_0} \quad (2.7)$$

### 2.3.3 Damage measurement

A number of experimental methods have been proposed to quantify the damage process describing the deterioration of material that can be evaluated through the decrease of elastic modulus or stiffness, toughness or hardness. The pioneering work was conducted by Lemaitre and Dufailly [38] through applying the concept of effective stress to propose eight different

experimental techniques to measure the deformation-induced damage. For example, damage can be measured from the ratio of damaged area to undamaged cross-sectional area,  $D_A = A_D/A_0$ , or from the decrease of material density,  $D_\rho = (1 - \rho_D/\rho_0)^{2/3}$ . In addition to the direct experimental methods based on the change of geometry, indirect experimental methods based on the variation of mechanical property were also proposed that measure the degradation of elastic modulus,  $D_E = 1 - E_D/E_0$  or measure the degradation of micro-hardness  $D_H = 1 - H_D/H_0$  or measure the variation of ultrasonic velocity assuming the density remains constant,  $D_v \approx 1 - v_D^2/v_0^2$ . More recently, an in-depth comparison of six methodologies was made by Tasan et al. [39] and their results showed that the geometry-based damage characterization methodologies introduce significant systematic errors as they probe a very limited damage spectrum, whereas the methodologies that measure the degradation of a mechanical property suffer from low precision and high complexity, especially for high strains and material anisotropy.

Since then, these CDM-based methodologies have been widely employed for the measurement and characterization of ductile damage. For instance, ductile damage in metallic materials was measured and characterized through the degradation of elastic modulus determined from cyclic loading-unloading tensile test [40–49] or micro-indentation test [50–53]. In addition potential drop method [54, 55] and ultrasonic technique [56–59] have also been proposed to quantify and characterize ductile damage. Furthermore, influence of external factors including strain rate, stress triaxiality and temperature on ductile damage evolution has also been investigated and results show that damage develops faster under higher strain rate [47, 48] or higher stress triaxiality [44, 60, 61]. Although significant effort has been made to evaluate

ductile damage evolution in metallic materials, there has been much less work carried out on developing CDM-based damage characterization methods for semi-crystalline polymers.

#### 2.3.4 A practical example

Traditionally, especially for metallic materials [62, 63], damage evolution is determined based on the variation of unloading stiffness, through the application of cyclic loading. However, for semi-crystalline polymers, because of the highly nonlinear, viscous properties there is no widely accepted method to quantify the damage evolution. For instance, some researchers simply use the variation of unloading stiffness during the cyclic loading to determine the damage development [6, 19]. Stiffness for semi-crystalline polymers can be determined from the nonlinear curve during the unloading using two methods, namely, linear-fitting method and energy method. In the linear-fitting method, three points, A, B and C need to be defined during the unloading part of the curve, in which Point A is denoted as the first data point for the reversal strain, points B and C are defined with  $\varepsilon_A - \varepsilon_B = 0.0005$  and  $\varepsilon_A - \varepsilon_C = 0.0025$  respectively, as shown in Fig. 2.3(a). The unloading modulus is calculated as the slope of line BC. The energy method is based on the energy dissipation in the entire unloading stage, which is equivalent to the triangular area SACD shown in Fig. 2.3(b) in which point A is same as that defined in the linear-fitting method. Point C is determined by equating the triangular area  $S_{ACD}$  to the area under the unloading curve,  $S_{ABD}$ . Sloped of the straight line AC is defined as the unloading stiffness.

Damage development can also be determined based on the variation of volume strain. Experimental results show that the volume damage is much smaller than stiffness damage, for which the possible reason is that void growth and the corresponding dilatation contribute to only

part of the total damage in materials. Results in the literature also suggest that damage calculated based on the linear-fitting method is smaller than that calculated based on the energy method [64].

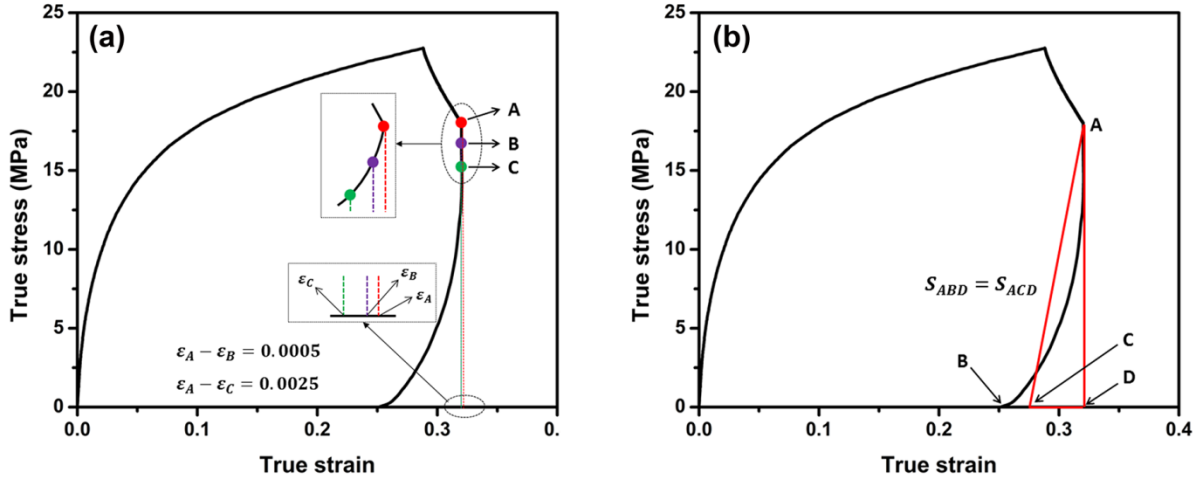


**Fig. 2.3** Schematic description of the linear-fitting method (a) and energy method (b) for determining the unloading stiffness.

A two-stage test method, recently proposed by Jar [65, 66], has also been used to determine the damage development in polyethylene, based on variation of stiffness during the loading phase in the second test, instead of the unloading phase in the first test [67–69]. Work presented here is to apply this two-stage test method to notched pipe ring (NPR) specimens, to investigate the damage development in the pipe-grade polyethylene (PE). Damage characterization using the two-stage test, based on the difference between the loading stiffness of virgin specimen and damaged specimen, are named loading-loading stiffness (LLS), in contrast to the damage characterization based on the difference between loading and unloading stiffness from the first-stage test, named loading-unloading stiffness (LUS). In this study, the stiffness is measured using D-split tensile test, first proposed for characterizing the mechanical properties of composite materials [70]. Set-up for the D-split tensile test is illustrated in Fig. 2.4(a). In this study, all

specimens were prepared from commercial PE4710, Cell classification 445576C HDPE pipe that has inner diameter and nominal wall thickness of 52.5 mm and 5.84 mm, respectively. Dimensions of the NPR specimens are shown in Fig. 2.4(b). It should be noted that due to the short gauge length, strain introduced to the NPR specimens is represented by area strain which is the logarithmic ratio of the ligament width before and after the deformation, as given below, under the assumption that with the aspect ratio of the ligament cross section remains close to 1 during the test [71].

$$\varepsilon_w = 2 \times \ln(w_0/w) \quad (2.8)$$

Where  $w_0$  and  $w$  are the initial and deformed width, respectively, in the ligament section of NPR specimens. As shown in Fig. 2.4(c), in the first stage test the NPR specimens were first stretched to predetermined prestrain values at crosshead speeds of 0.01, 1, 10 and 100mm/min, relaxed for 10,000s (around 3 hours) by keeping the displacement constant, and then unloaded at the crosshead speed of 0.1mm/min. The unloading curve from the first-stage test was used to determine the unloading stiffness based on the energy method.

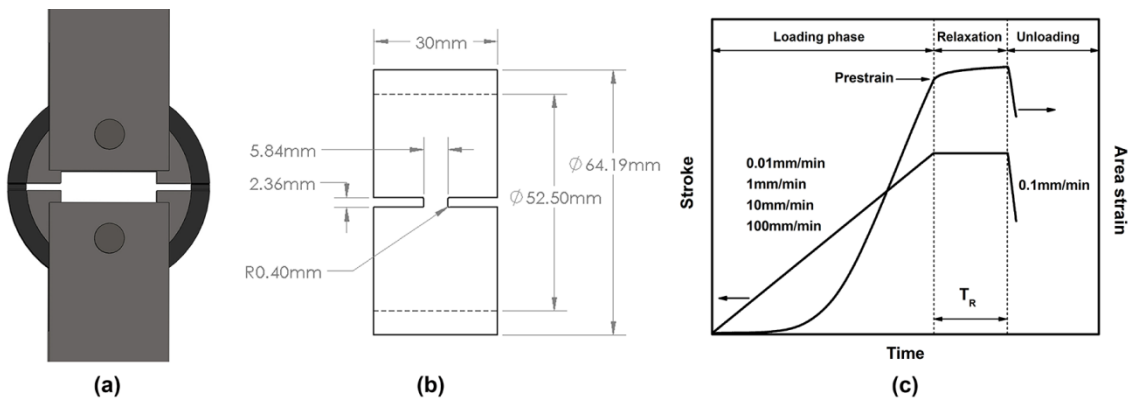


**Fig. 2.4** Information on test setup, NPR specimens and test procedure used in this study: (a) D-split tensile test setup, (b) dimensions of NPR specimens and (c) schematic description of test procedure of the first-stage test.

Fig. 2.5(a) shows the relationship between the loading stiffness measured from the second-stage test and the prestrain applied in the first-stage test. Variation of the unloading stiffness determined from the first-stage test, using the energy method, is presented in Fig. 2.5(b) as a function of prestrain. Results in Fig. 2.5 suggest that both loading stiffness and unloading stiffness decrease with the increase of prestrain applied to the specimens. In addition, the rate of stiffness decrease with the increase of prestrain is dependent on the crosshead speed used to introduce the prestrain levels.

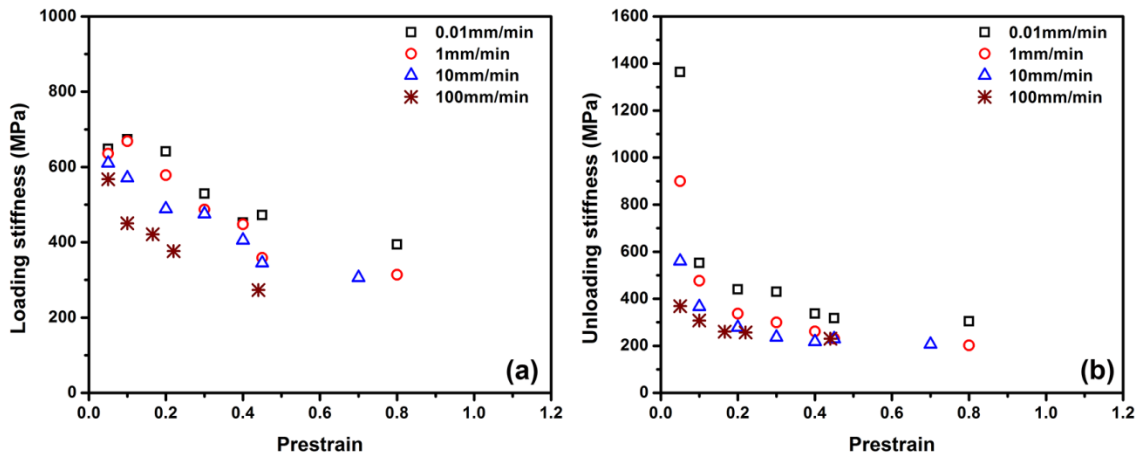


**Fig. 2.5** Effects of prestrain applied in the first-stage test on loading stiffness determined from the second-stage test (a) and unloading stiffness measured from the first-stage test (b).

Damage developments determined using LUS and LLS are compared in Fig. 2.6 which also includes fitting curves based on the following equation to depict the trend of change of the damage parameter  $D$  with the increase of prestrain.

$$D = A[1 - \exp(-B\varepsilon)] \quad (2.9)$$

Fig. 2.6 clearly shows that damage calculated based on LUS is much larger than that calculated from LLS. Difference in the damage characterization suggests that further study is

needed in order to develop a characterization approach that can reflect the true damage development in semi-crystalline polymers.

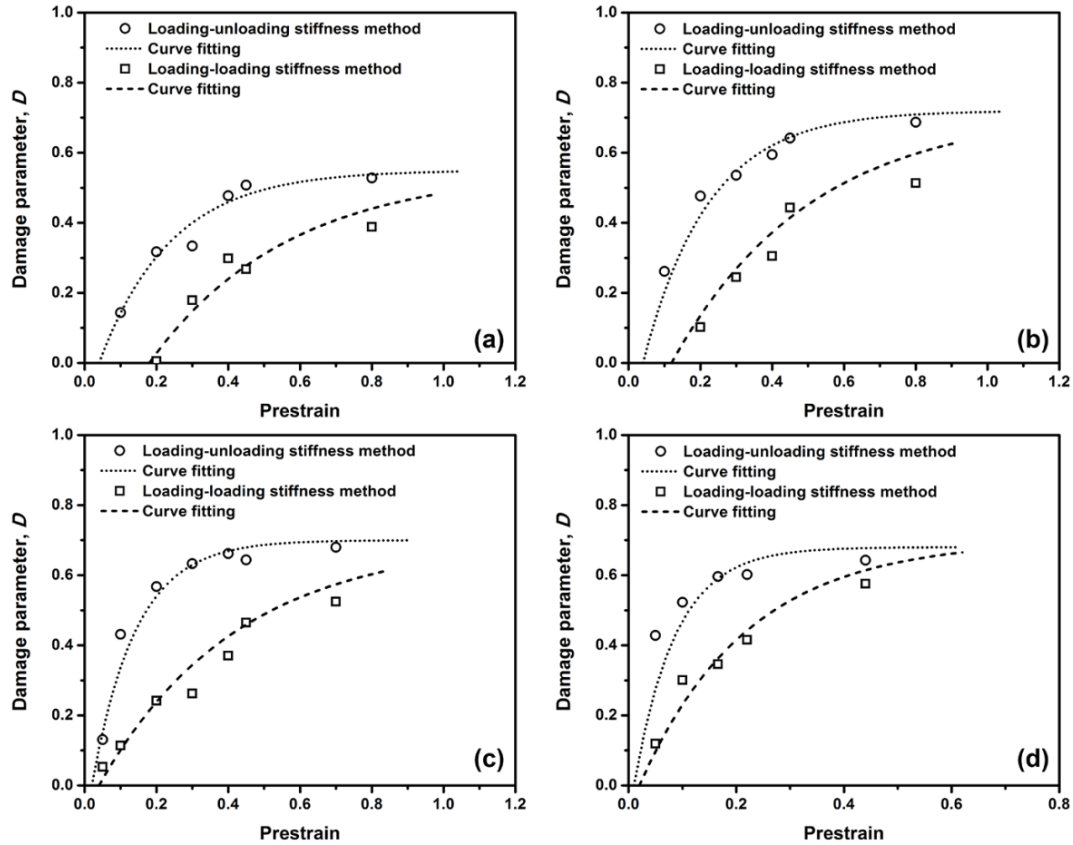


**Fig. 2.6** Comparison of damage development determined based on LUS and LLS, with the prestrains generated at the crosshead speed of (a) 0.01, (b) 1, (c) 10 and (d) 100mm/min.

## 2.4 Major factors influencing damage development

Damage development in semi-crystalline polymers is affected by several factors, including temperature, strain rate, stress triaxiality (defined as the ratio of mean normal stress to von Mises stress), and microstructure. In this section, influence of each factor on the damage development is discussed.

### 2.4.1 Effects of temperature

Influence of temperature on the damage development in various semi-crystalline polymers, such as polyvinylidene fluoride (PVDF) [14, 15], poly(l-lactide) (PLA) [13] and polypropylene (PP) [72, 73] has been extensively studied. Variation of volume strain during the monotonic tensile test at various temperatures was characterized using strain gauge [15], X-ray scattering [72], or a novel video-controlled testing system [14] to determine the level of deformation. The change of volume strain with the increase of the applied strain at different temperatures was obtained. The results show that lower the temperature larger the volume strain, as shown in Fig. 2.7.

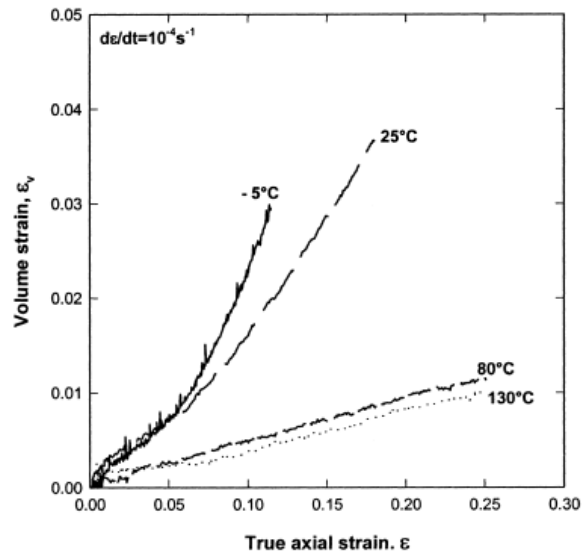


**Fig. 2.7** Variation of volume strain at different temperatures. [14], Copyright 2002. Reproduced with permission from John Wiley and Sons.

### 2.4.2 Effects of strain rate

Influence of strain rate on deformation and damage development in semi-crystalline polymers has been an area of intensive investigation. For example, volume strain under large deformation

of high-density polyethylene (HDPE) was studied by means of video extensometer and wide-angle X-ray diffraction analysis [11]. It was observed that the increase of volume strain depends on strain rate. The onset of volume dilatation occurs earlier at a higher strain rate. Possible explanation for this phenomenon is that the increase of the deformation rate results in the decrease in the chain mobility of the amorphous phase and the increase of the yield stress for the crystalline phase [11], which promotes the cavitation process in the amorphous region. Another interesting study using small-angle X-ray scattering (SAXS) [10] show that under tensile deformation, volume strain for polypropylene increases rapidly after the yield point, due to the cavity development in the amorphous phase, as shown in Fig. 2.8. Furthermore, high strain rate is found to favour void growth due to the increase in the involvement of the crystalline phase in the response to loading. Their results show that volume strain increases with the increase of the deformation rate. A recent study, based on continuum damage mechanics (CDM), was applied to characterization of damage development in PE based on a novel two-stage test method [20, 74]. Conclusion from this study is consistent with those in the literature, that is, higher the strain rate, bigger the damage development at a given strain level.

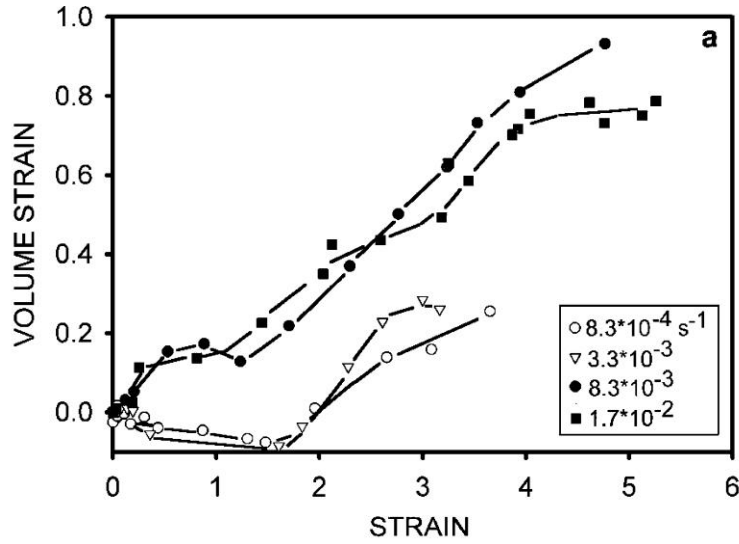


**Fig. 2.8** Changes of volume strain as a function of strain and strain rate. [10] Copyright 2008. Reproduced with permission from American Chemical Society.

### 2.4.3 Effects of stress triaxiality

Another important factor that influences damage development in semi-crystalline polymers is the local stress state, represented by stress triaxiality. Stress triaxiality  $\eta$  is defined as the ratio of mean normal stress  $\sigma_m$  to the von Mises stress  $\sigma_{eq}$ :

$$\eta = \frac{\sigma_m}{\sigma_{eq}} \quad (2.10)$$

which can be determined for a round-notched specimen using the expression below

$$\eta = \frac{1}{3} + \log\left(\frac{1+a}{2R}\right) \quad (2.11)$$

where  $a$  and  $R$  are minimum cross section radius and notch radius of cylindrical specimens [75]. Equation (6) suggests that the stress triaxiality is bigger when the notch radius is smaller. Effects of stress triaxiality on cavitation in semi-crystalline polymers, e.g. PVDF, was studied

using round-notched specimens with different notch radii, such as diabolo specimens with a small radius of curvature for high stress triaxiality and dumbbell specimens or diabolo specimens with a large radius of curvature for low stress triaxiality [76]. Later, Laiarinandrasana and his co-workers [77] studied the influence of stress triaxiality on the cavitation and damage in polyamide 11 (PA11) under tension, through microscopic observations of microtomed specimens with four different notch radii. Experimental results clearly show that smaller the notch radius (i.e., higher the stress triaxiality), larger the amount of voids. Cavitation damage in PVC and HDPE, represented by the increase of volume strain, under different levels of stress triaxiality was investigated [78], which reaches the same conclusion as that based on the X-ray microtomography analysis [79].

In summary, when the temperature increases, strain rate decreases or stress triaxiality decreases. As a result, the onset of cavitation is delayed and the total amount of voids (thus damage) at a given strain level is reduced, as depicted in Fig. 2.9.

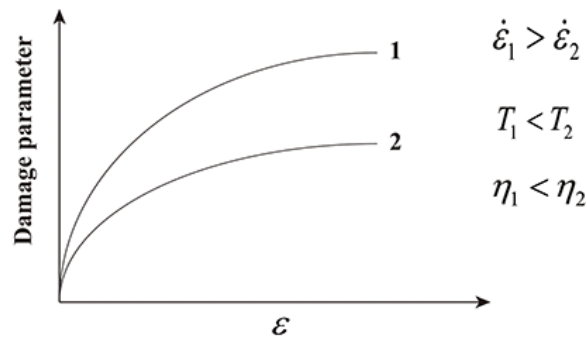


**Fig. 2.9** Schematic description of the dependence of damage development on factors such as strain rate ( $\dot{\epsilon}$ ), temperature ( $T$ ) and stress triaxiality ( $\eta$ ).

### **2.4.3 Effects of microstructure**

Mechanical properties of semi-crystalline polymers are strongly dependent on microstructure, molecular weight, degree of crystallinity, etc. In particular, cavitation damage in semi-crystalline polymers is directly related to the relationship between strength of amorphous and crystalline phases [9]. Influence of molecular weight on the cavitation in linear polyethylene was studied [18] and the results show that lower the weight averaged molecular weight, bigger the volume strain and fewer the entanglements in the amorphous region, thus promoting the development of cavities. It was also found that lower the chain mobility in the amorphous phase, larger the amount of cavities [76]. Moreover, the influence of other microstructural parameters such as tie molecules, entanglement density and lamella thickness are highlighted for HDPE [17]. Pawlak and Galeski [80] also pointed out that volume strain is increased with the increase of lamella thickness and degree of crystallinity. Furthermore, a critical lamella thickness was determined for a given deformation temperature, below which cavitation does not occur [16]. This is because below the critical lamella thickness, plastic deformation of the crystalline phase occurs before cavitation can be generated in the amorphous phase.

## **2.5 Conclusions**

This chapter presented an overview of mechanics of porous media (MPM) theory and continuum damage mechanics (CDM) theory and specially towards the recent development on the damage characterization methods. Special emphasis was given to the definition of damage variables and effective stress concept in CDM, as well as various damage measurement methods. A case study applying two CDM-based methods to characterize damage in semi-crystalline polymers was demonstrated for better understanding of damage concept and measurement

strategies. Furthermore, the influence of deformation conditions (strain rate, temperature and stress triaxiality) and microstructure on the damage development in semi-crystalline polymers has been reviewed and discussed.

## References

- [1] Pawlak, A., Galeski, A., and Rozanski, A., 2014, “Cavitation during deformation of semicrystalline polymers,” *Progress in polymer science*, **39**(5), pp. 921–958.
- [2] Alvarado-Contreras, J. A., Polak, M. A., and Penlidis, A., 2010, “Constitutive modeling of damage evolution in semicrystalline polyethylene,” *Journal of Engineering Materials and Technology*, **132**(4), p. 041009.
- [3] Rozanski, A., Galeski, A., and Debowska, M., 2010, “Initiation of cavitation of polypropylene during tensile drawing,” *Macromolecules*, **44**(1), pp. 20–28.
- [4] Alvarado-Contreras, J., Polak, M. A., and Penlidis, A., 2007, “Micromechanical approach to modeling damage in crystalline polyethylene,” *Polymer Engineering & Science*, **47**(4), pp. 410–420.
- [5] Humbert, S., Lame, O., Chenal, J. M., Rochas, C., and Vigier, G., 2010, “New insight on initiation of cavitation in semicrystalline polymers: in-situ SAXS measurements,” *Macromolecules*, **43**(17), pp. 7212–7221.
- [6] Detrez, F., Cantournet, S., and Seguela, R., 2011, “Plasticity/damage coupling in semi-crystalline polymers prior to yielding: Micromechanisms and damage law identification,” *Polymer*, **52**(9), pp. 1998–2008.
- [7] Patlazhan, S., and Remond, Y., 2012, “Structural mechanics of semicrystalline polymers prior to the yield point: a review,” *Journal of Materials Science*, **47**(19), pp. 6749–6767.
- [8] Addiego, F., Patlazhan, S., Wang, K., André, S., Bernstorff, S., and Ruch, D., 2015, “Time-resolved small-angle X-ray scattering study of void fraction evolution in high-density polyethylene during stress unloading and strain recovery,” *Polymer International*, **64**(11), pp. 1513–1521.
- [9] Pawlak, A., Galeski, A., and Rozanski, A., 2014, “Cavitation during deformation of semicrystalline polymers,” *Progress in polymer science*, **39**(5), pp. 921–958.
- [10] Pawlak, A., and Galeski, A., 2008, “Cavitation during tensile deformation of polypropylene,” *Macromolecules*, **41**(8), pp. 2839–2851.
- [11] Addiego, F., Dahoun, A., G’Sell, C., and Hiver, J.-M., 2006, “Characterization of volume strain at large deformation under uniaxial tension in high-density polyethylene,” *Polymer*, **47**(12), pp. 4387–4399.
- [12] Mohanraj, J., Barton, D. C., Ward, I. M., Dahoun, A., Hiver, J. M., and G’Sell, C., 2006, “Plastic deformation and damage of polyoxymethylene in the large strain range at elevated temperatures,” *Polymer*, **47**(16), pp. 5852–5861.

- [13] Zhang, X., Schneider, K., Liu, G., Chen, J., Brüning, K., Wang, D., and Stamm, M., 2012, “Deformation-mediated superstructures and cavitation of poly (L-lactide): In-situ small-angle X-ray scattering study,” *Polymer*, **53**(2), pp. 648–656.
- [14] Quatravaux, T., Elkoun, S., G’sell, C., Cangemi, L., and Meimon, Y., 2002, “Experimental characterization of the volume strain of poly (vinylidene fluoride) in the region of homogeneous plastic deformation,” *Journal of Polymer Science Part B: Polymer Physics*, **40**(22), pp. 2516–2522.
- [15] Laiarinandrasana, L., Besson, J., Lafarge, M., and Hochstetter, G., 2009, “Temperature dependent mechanical behaviour of PVDF: experiments and numerical modelling,” *International Journal of Plasticity*, **25**(7), pp. 1301–1324.
- [16] Xiong, B., Lame, O., Chenal, J. M., Rochas, C., Seguela, R., and Vigier, G., 2013, “In-situ SAXS study and modeling of the cavitation/crystal-shear competition in semi-crystalline polymers: Influence of temperature and microstructure in polyethylene,” *Polymer*, **54**(20), pp. 5408–5418.
- [17] Humbert, S., Lame, O., Chenal, J. M., Rochas, C., and Vigier, G., 2010, “New insight on initiation of cavitation in semicrystalline polymers: in-situ SAXS measurements,” *Macromolecules*, **43**(17), pp. 7212–7221.
- [18] Butler, M. F., Donald, A. M., and Ryan, A. J., 1998, “Time resolved simultaneous small- and wide-angle X-ray scattering during polyethylene deformation—II. Cold drawing of linear polyethylene,” *Polymer*, **39**(1), pp. 39–52.
- [19] Gu, G., Xia, Y., Lin, C., Lin, S., Meng, Y., and Zhou, Q., 2013, “Experimental study on characterizing damage behavior of thermoplastics,” *Materials & Design*, **44**, pp. 199–207.
- [20] Zhang, Y., and Jar, P.-Y. B., 2015, “Quantitative assessment of deformation-induced damage in polyethylene pressure pipe,” *Polymer Testing*, **47**, pp. 42–50.
- [21] G’sell, C., Hiver, J. M., Dahoun, A., and Souahi, A., 1992, “Video-controlled tensile testing of polymers and metals beyond the necking point,” *J Mater Sci*, **27**(18), pp. 5031–5039.
- [22] Needleman, A., 1972, “A numerical study of necking in circular cylindrical bar,” *Journal of the Mechanics and Physics of Solids*, **20**(2), pp. 111–127.
- [23] Gurson, A. L., 1977, “Continuum Theory of Ductile Rupture by Void Nucleation and Growth: Part I—Yield Criteria and Flow Rules for Porous Ductile Media,” *J. Eng. Mater. Technol.*, **99**(1), pp. 2–15.
- [24] Tvergaard, V., 1982, “On localization in ductile materials containing spherical voids,” *Int J Fract*, **18**(4), pp. 237–252.
- [25] Hughes, D. J., Mahendrasingam, A., Oatway, W. B., Heeley, E. L., Martin, C., and Fuller, W., 1997, “A simultaneous SAXS/WAXS and stress-strain study of polyethylene deformation at high strain rates,” *Polymer*, **38**(26), pp. 6427–6430.
- [26] Pawlak, A., and Galeski, A., 2010, “Cavitation during tensile drawing of annealed high density polyethylene,” *Polymer*, **51**(24), pp. 5771–5779.
- [27] Humbert, S., Lame, O., Chenal, J. M., Rochas, C., and Vigier, G., 2010, “New insight on initiation of cavitation in semicrystalline polymers: in-situ SAXS measurements,” *Macromolecules*, **43**(17), pp. 7212–7221.
- [28] Pawlak, A., and Galeski, A., 2010, “Cavitation and morphological changes in polypropylene deformed at elevated temperatures,” *Journal of Polymer Science Part B: Polymer Physics*, **48**(12), pp. 1271–1280.

- [29] Benseddiq, N., and Imad, A., 2008, "A ductile fracture analysis using a local damage model," *International Journal of Pressure Vessels and Piping*, **85**(4), pp. 219–227.
- [30] Nahshon, K., and Xue, Z., 2009, "A modified Gurson model and its application to punch-out experiments," *Engineering fracture mechanics*, **76**(8), pp. 997–1009.
- [31] Nahshon, K., and Hutchinson, J. W., 2008, "Modification of the Gurson model for shear failure," *European Journal of Mechanics-A/Solids*, **27**(1), pp. 1–17.
- [32] Acharyya, S., and Dhar, S., 2008, "A complete GTN model for prediction of ductile failure of pipe," *Journal of Materials Science*, **43**(6), pp. 1897–1909.
- [33] Oh, C.-K., Kim, Y.-J., Baek, J.-H., Kim, Y.-P., and Kim, W., 2007, "A phenomenological model of ductile fracture for API X65 steel," *International Journal of Mechanical Sciences*, **49**(12), pp. 1399–1412.
- [34] Kachanov, L. M., 1958, "Time of the rupture process under creep conditions," *Isv. Akad. Nauk. SSR. Otd Tekh. Nauk*, **8**, pp. 26–31.
- [35] Kachanov, L., 2013, *Introduction to continuum damage mechanics*, Springer Science & Business Media.
- [36] Lemaitre, J., 1972, "Evaluation of dissipation and damage in metals submitted to dynamic loading," *Mechanical behavior of materials*, pp. 540–549.
- [37] Lemaitre, J., 1985, "A continuous damage mechanics model for ductile fracture," *Journal of engineering materials and technology*, **107**(1), pp. 83–89.
- [38] Lemaitre, J., and Dufailly, J., 1987, "Damage measurements," *Engineering Fracture Mechanics*, **28**(5–6), pp. 643–661.
- [39] Tasan, C. C., Hoefnagels, J. P. M., and Geers, M. G. D., 2012, "Identification of the continuum damage parameter: An experimental challenge in modeling damage evolution," *Acta Materialia*, **60**(8), pp. 3581–3589.
- [40] Chow, C. L., and Wang, J., 1987, "An anisotropic theory of continuum damage mechanics for ductile fracture," *Engineering Fracture Mechanics*, **27**(5), pp. 547–558.
- [41] Tai, W. H., 1990, "Plastic damage and ductile fracture in mild steels," *Engineering Fracture Mechanics*, **37**(4), pp. 853–880.
- [42] Alves, M., Yu, J., and Jones, N., 2000, "On the elastic modulus degradation in continuum damage mechanics," *Computers & Structures*, **76**(6), pp. 703–712.
- [43] Straffelini, G., and Molinari, A., 2002, "Evolution of tensile damage in porous iron," *Materials Science and Engineering: A*, **334**(1), pp. 96–103.
- [44] Bonora, N., Gentile, D., Pironi, A., and Newaz, G., 2005, "Ductile damage evolution under triaxial state of stress: theory and experiments," *International Journal of Plasticity*, **21**(5), pp. 981–1007.
- [45] Celentano, D. J., and Chaboche, J.-L., 2007, "Experimental and numerical characterization of damage evolution in steels," *International Journal of Plasticity*, **23**(10), pp. 1739–1762.
- [46] Wu, T., Coret, M., and Combescure, A., 2011, "Strain Localisation and Damage Measurement by Full 3D Digital Image Correlation: Application to 15-5PH Stainless Steel," *Strain*, **47**(1), pp. 49–61.
- [47] Abed, F. H., Al-Tamimi, A. K., and Al-Himairee, R. M., 2012, "Characterization and modeling of ductile damage in structural steel at low and intermediate strain rates," *Journal of Engineering Mechanics*, **138**(9), pp. 1186–1194.
- [48] Darras, B. M., Abed, F. H., Pervaiz, S., and Abdu-Latif, A., 2013, "Analysis of damage in 5083 aluminum alloy deformed at different strainrates," *Materials Science and Engineering: A*, **568**, pp. 143–149.

- [49] Chiantoni, G., Comi, C., Mariani, S., and Bonora, N., 2014, “Experimental assessment of ductile damage in P91 steel at high temperature,” *International Journal of Damage Mechanics*, **23**(4), pp. 567–587.
- [50] Guelorget, B., François, M., and Lu, J., 2007, “Microindentation as a local damage measurement technique,” *Materials letters*, **61**(1), pp. 34–36.
- [51] Tasan, C. C., Hoefnagels, J. P. M., and Geers, M. G. D., 2009, “A critical assessment of indentation-based ductile damage quantification,” *Acta materialia*, **57**(17), pp. 4957–4966.
- [52] Li, J., Li, F., Xue, F., Cai, J., and Chen, B., 2012, “Micromechanical behavior study of forged 7050 aluminum alloy by microindentation,” *Materials & Design*, **37**, pp. 491–499.
- [53] Li, J., Li, F., Ma, X., Wang, Q., Dong, J., and Yuan, Z., 2015, “A strain-dependent ductile damage model and its application in the derivation of fracture toughness by micro-indentation,” *Materials & Design*, **67**, pp. 623–630.
- [54] Padma, S., Srivathsa, B., Rao, N. V., and Kumar, V., 2009, “Evolution of Damage in Near IMI-834 Titanium Alloy Under Monotonic Loading Condition: A Continuum Damage Mechanics Approach,” *Journal of Engineering Materials and Technology*, **131**, pp. 031012–1.
- [55] Zhang, S. J., Zhou, C., Xia, Q. X., and Chen, S. M., 2015, “Quantification and Characterization of Full Field Ductile Damage Evolution for Sheet Metals Using an Improved Direct Current Potential Drop Method,” *Experimental Mechanics*, **55**(3), pp. 611–621.
- [56] Yeh, H.-Y., and Cheng, J.-H., 2003, “NDE of metal damage: ultrasonics with a damage mechanics model,” *International journal of solids and structures*, **40**(26), pp. 7285–7298.
- [57] Kim, J.-Y., Jacobs, L. J., Qu, J., and Littles, J. W., 2006, “Experimental characterization of fatigue damage in a nickel-base superalloy using nonlinear ultrasonic waves,” *The Journal of the Acoustical Society of America*, **120**(3), pp. 1266–1273.
- [58] Antonaci, P., Bruno, C. L. E., Gliozzi, A. S., and Scalerandi, M., 2010, “Monitoring evolution of compressive damage in concrete with linear and nonlinear ultrasonic methods,” *Cement and Concrete Research*, **40**(7), pp. 1106–1113.
- [59] Chen, J., Xu, Z., Yu, Y., and Yao, Y., 2014, “Experimental characterization of granite damage using nonlinear ultrasonic techniques,” *NDT & E International*, **67**, pp. 10–16.
- [60] Chandrakanth, S., and Pandey, P. C., 1995, “An isotropic damage model for ductile material,” *Engineering fracture mechanics*, **50**(4), pp. 457–465.
- [61] La Rosa, G., Mirone, G., and Risitano, A., 2001, “Effect of stress triaxiality corrected plastic flow on ductile damage evolution in the framework of continuum damage mechanics,” *Engineering Fracture Mechanics*, **68**(4), pp. 417–434.
- [62] Chaboche, J.-L., 1988, “Continuum damage mechanics: Part II—Damage growth, crack initiation, and crack growth,” *Journal of applied mechanics*, **55**(1), pp. 65–72.
- [63] Celentano, D. J., and Chaboche, J.-L., 2007, “Experimental and numerical characterization of damage evolution in steels,” *International Journal of Plasticity*, **23**(10), pp. 1739–1762.
- [64] Gu, G., Xia, Y., Lin, C., Lin, S., Meng, Y., and Zhou, Q., 2013, “Experimental study on characterizing damage behavior of thermoplastics,” *Materials & Design*, **44**, pp. 199–207.
- [65] Jar, P.-Y., 2014, “Transition of neck appearance in polyethylene and effect of the associated strain rate on the damage generation,” *Polymer Engineering & Science*, **54**(8), pp. 1871–1878.

- [66] Jar, P. B., 2014, “Degradation of mechanical properties for polyethylene by small-deformation damage,” ASME 2014 Pressure Vessels and Piping Conference, American Society of Mechanical Engineers, p. V06BT06A040–V06BT06A040.
- [67] Jar, P.-Y. B., 2015, “Effect of Loading History on Elastic Modulus of HDPE,” ASME 2015 Pressure Vessels and Piping Conference, American Society of Mechanical Engineers, p. V06BT06A045–V06BT06A045.
- [68] Jar, P.-Y. B., 2015, “Effect of tensile loading history on mechanical properties for polyethylene,” *Polymer Engineering & Science*, **55**(9), pp. 2002–2010.
- [69] Zhang, Y., and Jar, P.-Y. B., 2015, “Quantitative assessment of deformation-induced damage in polyethylene pressure pipe,” *Polymer Testing*, **47**, pp. 42–50.
- [70] Chen, J. F., Li, S. Q., Bisby, L. A., and Ai, J., 2011, “FRP rupture strains in the split-disk test,” *Composites Part B: Engineering*, **42**(4), pp. 962–972.
- [71] Muhammad, S., and Jar, P.-Y. B., 2011, “Effect of aspect ratio on large deformation and necking of polyethylene,” *J Mater Sci*, **46**(4), pp. 1110–1123.
- [72] Pawlak, A., and Galeski, A., 2010, “Cavitation and morphological changes in polypropylene deformed at elevated temperatures,” *Journal of Polymer Science Part B: Polymer Physics*, **48**(12), pp. 1271–1280.
- [73] Zhang, C., Liu, G., Song, Y., Zhao, Y., and Wang, D., 2014, “Structural evolution of  $\beta$ -iPP during uniaxial stretching studied by in-situ WAXS and SAXS,” *Polymer*, **55**(26), pp. 6915–6923.
- [74] Jar, P.-Y., 2014, “Transition of neck appearance in polyethylene and effect of the associated strain rate on the damage generation,” *Polymer Engineering & Science*, **54**(8), pp. 1871–1878.
- [75] Laiarinandrasana, L., Morgeneuer, T. F., Proudhon, H., N’guyen, F., and Maire, E., 2012, “Effect of multiaxial stress state on morphology and spatial distribution of voids in deformed semicrystalline polymer assessed by x-ray tomography,” *Macromolecules*, **45**(11), pp. 4658–4668.
- [76] Castagnet, S., and Deburck, Y., 2007, “Relative influence of microstructure and macroscopic triaxiality on cavitation damage in a semi-crystalline polymer,” *Materials Science and Engineering: A*, **448**(1), pp. 56–66.
- [77] Boisot, G., Laiarinandrasana, L., Besson, J., Fond, C., and Hochstetter, G., 2011, “Experimental investigations and modeling of volume change induced by void growth in polyamide 11,” *International Journal of Solids and Structures*, **48**(19), pp. 2642–2654.
- [78] Ognedal, A. S., Clausen, A. H., Dahlen, A., and Hopperstad, O. S., 2014, “Behavior of PVC and HDPE under highly triaxial stress states: An experimental and numerical study,” *Mechanics of Materials*, **72**, pp. 94–108.
- [79] Rosenberg, E., Brusselle-Dupend, N., and Epsztein, T., 2011, “A mesoscale quantification method of cavitation in semicrystalline polymers using X-ray microtomography,” *Materials Science and Engineering: A*, **528**(21), pp. 6535–6544.
- [80] Pawlak, A., and Galeski, A., 2010, “Cavitation during tensile drawing of annealed high density polyethylene,” *Polymer*, **51**(24), pp. 5771–5779.

# Chapter 3

## **Characterization of deformation damage in PE pipe**

The deformation damage in polyethylene (PE) pressure pipe is investigated through the application of a novel two-stage approach to the D-split test of notched pipe ring (NPR) specimens. The first stage test consisting of monotonic tension, relaxation and unloading phases is to introduce damage by subjecting the specimens to different levels of tensile strain at crosshead speeds of 0.01, 1, 10 or 100mm/min. Using results from relaxation tests a new superposition principle based on time and strain rate is suggested as an alternative approach to construct a master curve of relaxation modulus versus time for PE pipe. Experimental results suggest that elastic modulus and yield stress decrease and yield strain increases with the increase of the strain introduced in the first test. Variation of experimentally measured elastic modulus is used to establish influence of crosshead speed on the damage evolution in the PE pressure pipe. In addition, mechanical properties, including yield stress, relaxation behavior, and moduli (elastic modulus at the strain of 0.5% and strain hardening modulus at strains above 70%), are compared between PE pipes that are made of PE80 and PE100 resins.

### **3.1 Introduction**

Polyethylene (PE) pressure pipe has been widely used for gas transportation for more than four decades. Because of its good mechanical and physical properties and low cost for installation and maintenance, over 90% of the newly installed gas pipeline systems are now

made of PE [1]. However, unexpected, catastrophic failures of PE pipeline were still reported in the last decade [2–5], suggesting that the current approach for characterizing PE pipes has blind spots for the performance evaluation. For example, third-party damages, such as dig-in, rock impingement, excessive bending, improper squeeze-off operation, and poor fusion joint, are known to accelerate the slow crack growth (SCG) to cause PE pipe failure [6–8], but proper criteria for those damages in order to prevent the SCG occurrence are yet to be established. For the squeeze-off process, even in the normal operation conditions, damage may still be introduced to the PE pipes to affect their short- and long-term performance [8], most seriously at the location of squeeze-off ears where yield stress was found to decrease with the increase of the squeeze-off ratio. In view that squeeze-off is the only feasible process currently available for maintenance and repair of gas pipes, it is important to understand how the excessive deformation introduced in the squeeze-off process affects mechanical properties for PE pipes.

Several studies have been conducted to analyze the effects of loading history on the mechanical behaviours of metallic and polymeric materials. Most of the studies used the maximum applied strain to represent the loading history, referred to as the “prestrain” henceforth. The effects of prestrain introduced by monotonic [9], fatigue [10], and creep loading [11] on the tensile properties for metals, such as stainless steel, have been successfully characterized. Similar studies were performed on polymers. For example, Zhang and Moore [12] conducted a series of experiments to analyze the stress relaxation behaviour of high-density PE (HDPE) immediately following a specific loading history. That study also examined the effects of prestrain and strain rate used to introduce the loading history on the permanent strain and strain recovery. Another study [13] investigated the effects of loading history on creep and relaxation behaviour of thermoplastics. Those studies were based on the approach that uses one

continuous test to introduce the loading history and to characterize the creep or relaxation behaviour. That is, the loading history was introduced during the loading phase, and creep and relaxation behaviours characterized during the unloading phase. As a result of characterizing the mechanical properties immediately after introducing the loading history, the creep and relaxation behaviours were found to be complicated by the rate-reversal phenomenon, that is, increase and then decrease of stress in the relaxation test and decrease and then increase of strain in the creep test. Such an approach of one test with multiple phases was also used to investigate the effects of loading history and manufacturing techniques on the mechanical behaviour of HDPE [14], from which it was confirmed that the uniaxial tensile behaviour of HDPE shows clear dependence on the manufacturing techniques.

Alternatively, a so-called two-test method [15–17] was used to study the influence of loading history on the mechanical properties of PE. As the name suggests, the two-test method contains two separate tests. The first test is to introduce the loading history and the second test to characterize the mechanical properties. Difference of this method from the continuous, multiphase test is that the second test in the former is conducted a long time after the first test, two months for the current study, in order to minimize the influence of the viscous deformation recovery after the first test on the results obtained from the second test. Work presented in this chapter is to apply the two-test method to notched pipe ring (NPR) specimens, to investigate the influence of the deformation-induced damage on the mechanical properties of PE pipe. Parameters used to vary the deformation-induced damage in the first test are strain rate, via the change of crosshead speed, and prestrain level.

Several studies have been conducted to investigate the effects of strain rate on the mechanical properties for semi-crystalline polymers. For example, Dasari and Misra [18] investigated the

sensitivity of mechanical properties for HDPE and polypropylene on the strain rate, and showed the increase of yield stress with the increase of strain rate. This phenomenon was also reported on the recycled HDPE [19–21]. Such a dependence is further observed for the whole true stress-strain curve [22] in which the stress at a given strain increases with the increase of strain rate. However, the effect of strain rate on the damage evolution has attracted much less attention. Xu and Wang [23] and Wang et al. [24] investigated the dynamics of damage evolution and its dependence on the strain rate, by combining the split Hopkinson pressure bar test and back propagation neural network analysis. They concluded that damage evolution is dependent on both strain and strain rate. The strain threshold, at which damage is initiated, decreases with the increase of the strain rate for Nylon in the range of high strain rate (from  $4 \times 10^2 \text{ s}^{-1}$  to  $2 \times 10^3 \text{ s}^{-1}$ ). However, this range of strain rate is too high compared to the strain rate encountered by PE pressure pipes in service. As a result, current knowledge on the damage evolution in semi-crystalline polymers is far from sufficient to provide the full understanding of the influence of strain rate on the pipe-grade PE.

PE pipes are expected to have a lifetime of at least 50 years. Because of such a long service time, assurance of mechanical performance of the PE pipes has been a major challenge for pipe design, especially when the short-term mechanical properties are considered for characterizing the long-term behavior of PE, due to the complication caused by the significant viscous deformation. Various test methods have been developed to overcome this problem. Those test methods are often based on creep deformation or load relaxation mode [25–30]. Currently, time-temperature superposition (TTS) is a popular approach to construct a master curve for the long-term behavior for polymers [31–33], of which the majority is concerned with creep deformation, e.g. [34–38]. Much less work is about the load relaxation counterpart, e.g. [39]. Nevertheless,

none of the previous work has considered the strain rate used to reach the targeted creep stress or relaxation strain as a variable for constructing the master curve for the creep deformation or load relaxation, respectively.

It is well recognized that short-term and long-term mechanical behavior of PE materials is strongly influenced by its microstructure, such as molecular weight (MW), molecular weight distribution (MWD), crystallinity and short chain branch (SCB) content. Many investigations have been conducted to reveal the relationship between the molecular structure of PE and its failure mechanisms. For example, results presented in [38] showed that the resistance to long-term brittle failure increases by incorporating short chain branches in PE materials. In addition, the physical chain entanglements that connect crystalline lamellae are known to have positive effect on the SCG resistance [39]. Currently, two types of pipes are used for the gas transportation. One was first introduced to North America and Europe around 1980s, categorized as PE80 under ISO system which certifies the pipe to be able to withstand a hoop stress, known as minimum required strength (MRS), of 8MPa at 20°C for 50 years. For PE100, the MRS is raised to 10MPa, primarily due to the bimodal molecular weight distribution of the PE resin. In spite of the popularity of PE80 and PE100 in the gas pipe industry, difference in their mechanical performance is yet to be fully characterized. In general, PE100 is known to have higher crack growth resistance [39], yield strength and elastic modulus [40] than PE80. Furthermore, results from cyclic loading on cracked round bar (CRB) specimens suggest that PE100 should have a much longer service life than PE80 [40, 41]. However, not all properties for PE100 are better than PE80. For example, compact tension (CT) and single-edge-notched bending (SENB) tests suggest that PE80 has higher fracture toughness than PE100 at both low and room temperatures [40]. In addition, experience from the field indicates that performance of

PE80 pipes is less affected by the squeeze-off process than PE100 pipes [8]. Such mixed conclusions suggest that further testing is needed in order to fully characterize the difference between PE80 and PE100 in their performance for the gas pipe applications.

### 3.2 Materials, specimens and mechanical testing

Specimens used in this study were prepared from two kinds of commercial HDPE pipe manufactured by Endot Industries. The first, PE3408 of Cell classification 445574C, is made of PE80 resin, and the second, PE4710 of Cell classification 445576C, is made of PE100 resin. Dimensions of the modified notched pipe ring (NPR) specimens follow those recommended in ASTM D2290-12, except that the notch profile is flat, instead of round, in order to have a relatively uniform stress distribution in the ligament region. The ligament length is selected to be equal to the nominal pipe wall thickness, 5.84 mm, in order to have the aspect ratio for the ligament cross section to be close to 1 so that during the test, contractions in the width and thickness directions are similar.

Fig. 3.1 shows a pipe section, a modified NPR specimen, setup for the D-split test, and dimensions of the NPR specimens used in this study. Damage level is represented by the prestrain  $\varepsilon_w$  applied to the NPR specimens in the first test, with  $\varepsilon_w$  calculated using the following expression, based on the assumption that contraction in the width direction is equivalent to that in the ligament length direction.

$$\varepsilon_w = 2 \times \ln(w_0/w) \quad (3.1)$$

where  $w_0$  and  $w$  are original and deformed ligament lengths, respectively. Variation of  $w$  during the test was determined using an extensometer.

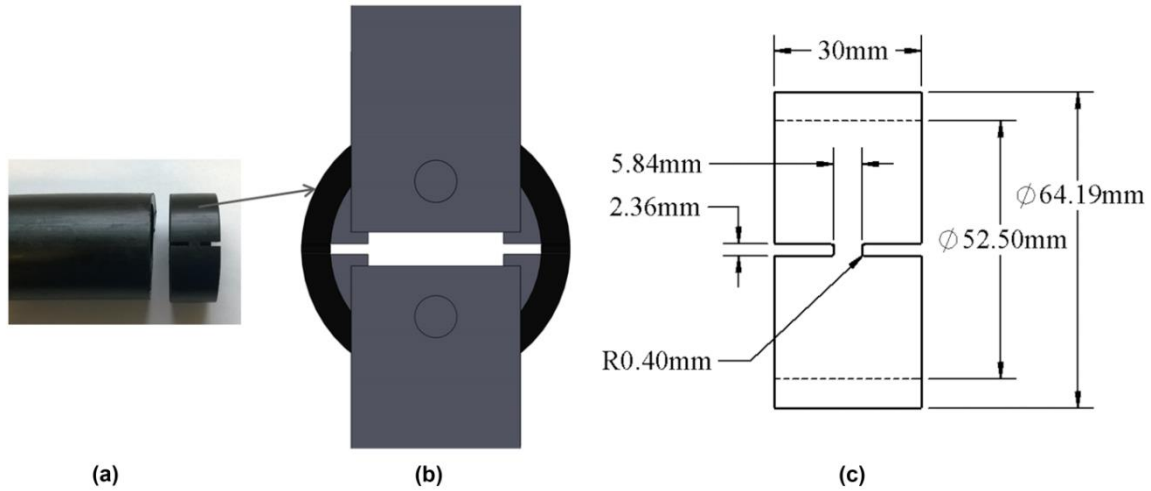


**Fig. 3.1** Information on specimens and test set-up used in the study: (a) a pipe section (left) and a modified NPR specimen (right), (b) setup for the D-split tensile test, and (c) specimen dimensions

The D-split tensile test, first proposed for characterizing mechanical properties of composite materials [44–47], was adopted for the experimental testing, for which the setup is illustrated in Fig. 3.1(b). All tests were conducted using a universal test machine (QUASAR 100) at room temperature. A two-stage test procedure, proposed by Jar [15–17, 48], was adopted for the mechanical testing in which the first test was to generate damage in the NPR specimens and the second test to determine the mechanical properties of damaged specimens. Procedure for the first test is depicted schematically in Fig. 3.2, which is to stretch the NPR specimens first to various, preselected area strains, followed by 3 hours of relaxation and then unloading. Six crosshead speeds were considered in the preliminary study, among which four crosshead speeds of 0.01, 1, 10 and 100mm/min were used to vary the strain rate to examine its influence on the damage generation in the first test. Unloading for all first tests was kept at the same crosshead speed 0.1mm/min. It should be pointed out that our preliminary study has suggested that area strains for tensile fracture of the NPR specimens is around 200% at the crosshead speeds of 0.01

and 1mm/min, 100% at 10mm/min, and 70% at 100mm/min. Therefore, the range of area strain introduced in the first test was from 5% to 160% at the crosshead speeds of 0.01 and 1mm/min, 5% to 70% at 10mm/min, and 5% to 45% at 100mm/min.

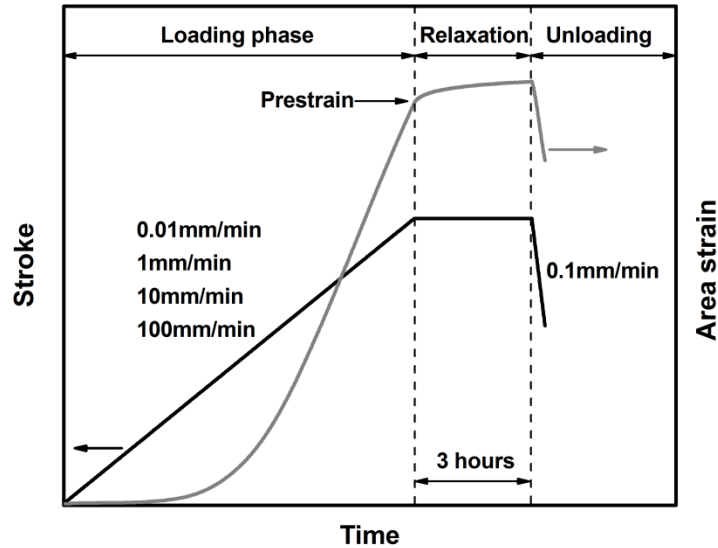


**Fig. 3.2** Schematic illustration of test procedure used for the first test

The choice of two-test method over one continuous, multi-phase test for this study is because PE is known to take a long time to recover from the viscous deformation. A study has shown that deformation recovery for HDPE is still detectable several months after the test [31], though majority of the recovery occurs within several hours after the unloading [32-34]. In order to avoid the significant deformation recovery during the second test, all specimens used in this study were stored for at least two months after the first tests, to allow majority of the viscoelastic deformation to be recovered, before they were used in the second tests. Furthermore, all second tests were conducted at a low crosshead speed of 0.01mm/min which corresponds to an initial strain rate of  $7 \times 10^{-5} \text{ s}^{-1}$ , in order to minimize the possibility of introducing additional damage to the specimens in the second tests.

Since the cross sectional dimension for the ligament region of the NPR specimens after the first test depends on the residual strain generated from the first test, engineering stress and area strain from the second test can be calculated based on the specimen dimensions either before the first test or at the beginning of the second test. In this chapter, area strains based on dimensions before the first test are referred to as “first strains” and those based on dimensions at the beginning of the second test “second strains”. Relaxation strain is defined as the prestrain at the beginning of relaxation phase in the first stage tests.

### **3.3 An additional factor to time-temperature superposition for deformation of PE**

This section is to summarize the discovery from a preliminary study, to show the trend of change of the relaxation modulus with time by varying the strain rate used to reach the relaxation strain. Based on the test results, this section describes a new approach to construct a master curve of the relaxation modulus versus time, for a period that is comparable to or longer than the service time required for the PE pipe.

Four crosshead speeds of 0.01, 1, 10 and 100mm/min were selected to vary the strain rate. A series of finite element (FE) simulation, following the procedure in [49], was performed to determine the strain rates generated at a given crosshead speed. The results are presented in Fig. 3.3, which suggests that the maximum strain rates are  $7 \times 10^{-5}$ ,  $7 \times 10^{-3}$ ,  $7 \times 10^{-2}$ , and  $7 \times 10^{-1} \text{ s}^{-1}$  for the above four crosshead speeds, respectively. Fig. 3.3 also suggests that the strain rate did not remain constant during the initial stretch of the relaxation test. Rather, the above maximum strain rates are about 20 to 30 times of the initial strain rates generated at a given crosshead speed. Nevertheless, in view that the maximum strain rates show a linear relationship with the

crosshead speed used, and the ranges of strain rate variation for the four crosshead speeds are clearly distinguishable, crosshead speed is used to represent the rate of deformation experienced by each specimen, based on which the amount of horizontal shift is determined for constructing the master curve, as will be shown later.

Five relaxation strain levels, namely, 5%, 10%, 20%, 30%, and 40%, were used to monitor the load relaxation at the crosshead speeds of 0.01, 1 and 10mm/min. However, at the crosshead speed of 100mm/min, the relaxation strains considered were only 5% and 10%, due to difficulties encountered in manual control of the test machine to generate the desired relaxation strains at such a high crosshead speed, and sensitivity of the specimens to the presence of foreign particles [50].

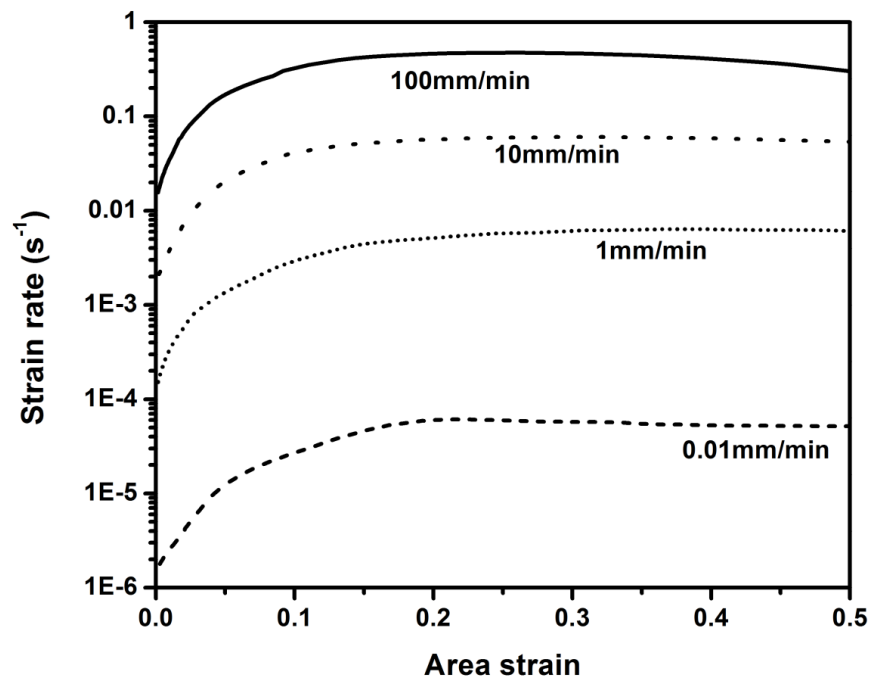


**Fig. 3.3** Variation of strain rate as a function of area strain during the tensile deformation at crosshead speeds of 0.01, 1, 10 and 100mm/min

Relaxation modulus is defined here as the ratio of engineering stress to the relaxation strain, similar to the definition in the literature [39] except that strain is expressed in terms of area strain, due to the short gauge length of the NPR specimens. Each of the plots in Fig. 3.4 summarizes variation of relaxation modulus as a function of time for NPR specimens that were stretched to the targeted relaxation strains at the same crosshead speed, that is 0.01, 1, 10 or 100mm/min. The figure clearly shows that, at a given time, the relaxation modulus decreases with the increase of the relaxation strain, consistent with that reported before [39].

Fig. 3.4 also suggests that curve profile from the relaxation test is affected by the crosshead speed used to reach the relaxation strain. That is, by increasing the crosshead speed from 0.01 to 100mm/min, the curve profile changes from concave downward to concave upward. The latter has been reported many times in the literature [39, 51, 52] but the former, to the best of our knowledge, has never been observed before, possibly because a very low crosshead speed, i.e., at or below the strain rate of  $7 \times 10^{-3} \text{ s}^{-1}$ , is needed to introduce the initial stretch in order to generate such a concave-downward curve profile.

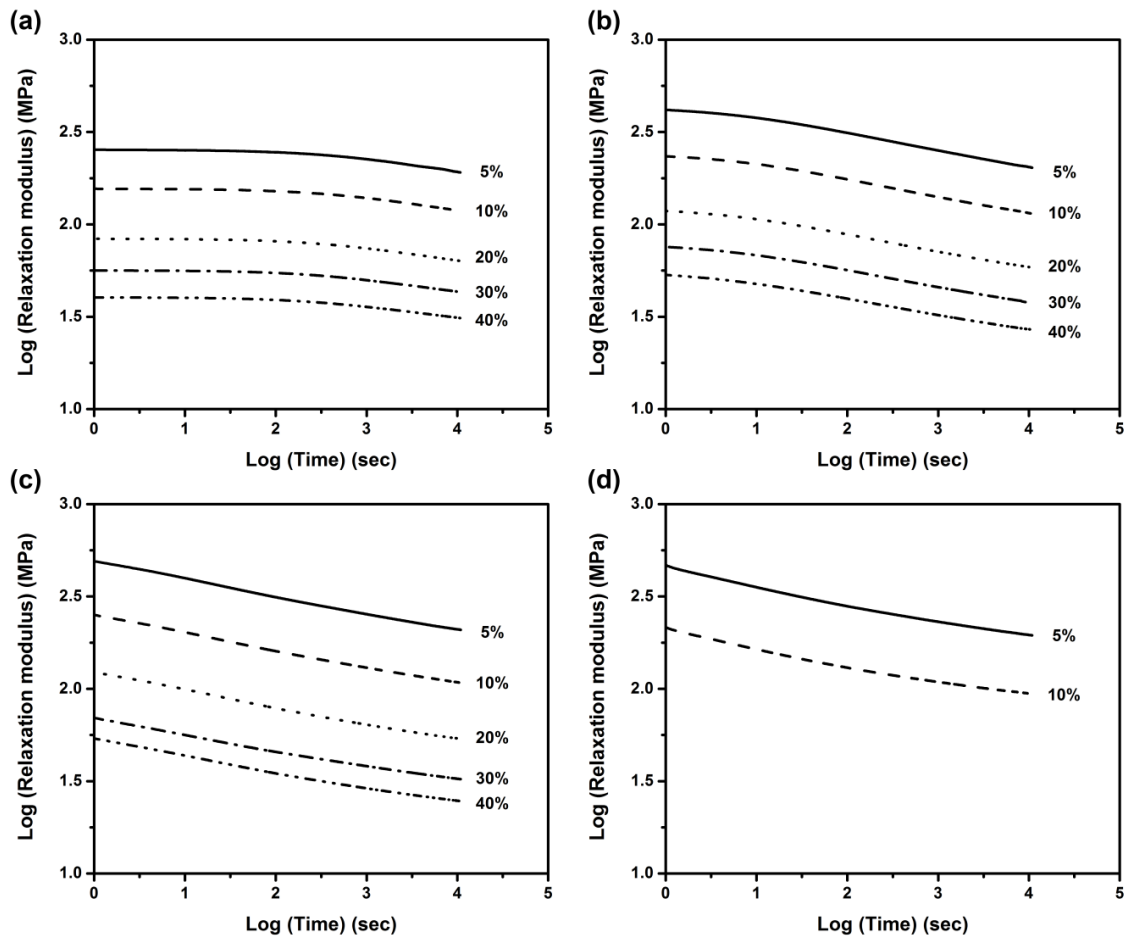


**Fig. 3.4** Plots of relaxation modulus versus time for NPR specimens, stretched to the relaxation strains at crosshead speeds of 0.01 (a), 1 (b), 10 (c), and 100mm/min (d)

Fig. 3.5(a) gives an example of the curves of relaxation modulus from the experimental testing, and Fig. 3.5(b) the corresponding master curve constructed using the superposition principle. All curves in Fig. 3.5(a) are with the relaxation strain of 5%, but using different crosshead speeds to generate the initial stretch. The master curve in Fig. 3.5(b) is also for the relaxation strain of 5%, with the initial stretch generated at the crosshead speed of 0.01mm/min.

The master curve in Fig. 3.5(b) is constructed by first horizontally shifting each curve in Fig. 3.5(a) by a time duration  $a_{\dot{\epsilon}}$ , calculated using an expression similar to the WLF equations [53] except that the governing variable is changed from temperature to crosshead speed. That is,

$$\log a_{\dot{\epsilon}} = \frac{C_1(v - v_0)}{(C_2 + v - v_0)} \quad (3.2)$$

where  $C_1$  and  $C_2$  are adjusting factors for which the values are 6.4 and 1.7, respectively, for all crosshead speeds and relaxation strains considered in this study,  $v_0$  the reference crosshead speed which is 0.01mm/min for Fig. 3.5(b), and  $v$  is the crosshead speed for the curve to be shifted.

After the above horizontal shift, vertical shift is applied to the curves to generate a coherent, continuous master curve. The vertical shift values required for Fig. 3.5(b) are summarized in the first row of Table 3.1. The table also provides the vertical shift values required to generate the master curves at other relaxation strains, with the same crosshead speed of 0.01mm/min to generate the initial stretch.

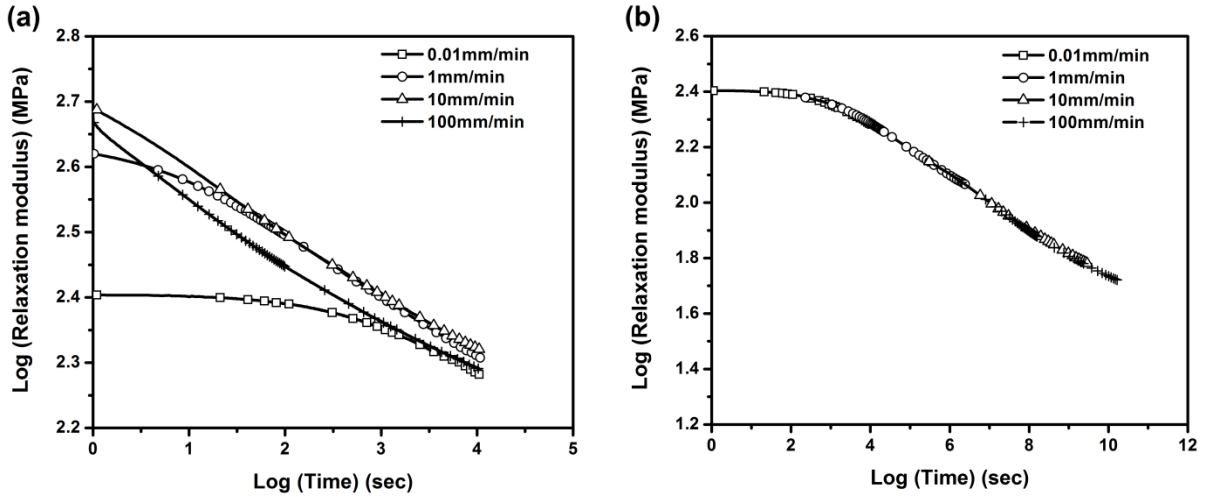


**Fig. 3.5** Variation of relaxation modulus with time for NPR specimens at the relaxation strain of 5%: (a) original test results and (b) master curve after the shifting

**Table 3.1** Values for vertical shift used to construct the master curves at 0.01mm/min

Relaxation strain	1mm/min	10mm/min	100mm/min
5%	-0.241	-0.539	-0.573
10%	-0.204	-0.462	-0.447
20%	-0.175	-0.423	—
30%	-0.153	-0.340	—
40%	-0.142	-0.365	—

Fig. 3.6 summarizes all relaxation master curves obtained from the study, with the crosshead speed of 0.01mm/min for the initial stretch. Note that only curves with relaxation strains of 5% and 10% contain test data that were obtained at the crosshead speed of 100mm/min. As mentioned earlier, this is because accurate manual control of the initial stretch is difficult when the desired relaxation strain is above 10%.

Fig. 3.6 indicates clearly two transitions for the drop rate of the relaxation modulus, the first at around  $10^3$  seconds, causing the increase of the drop rate, and the second after  $10^8$  seconds (over 3 years), for the reverse change of the drop rate. Note that the master curves reported in the literature, such as in ref. [39], only show the second transition.

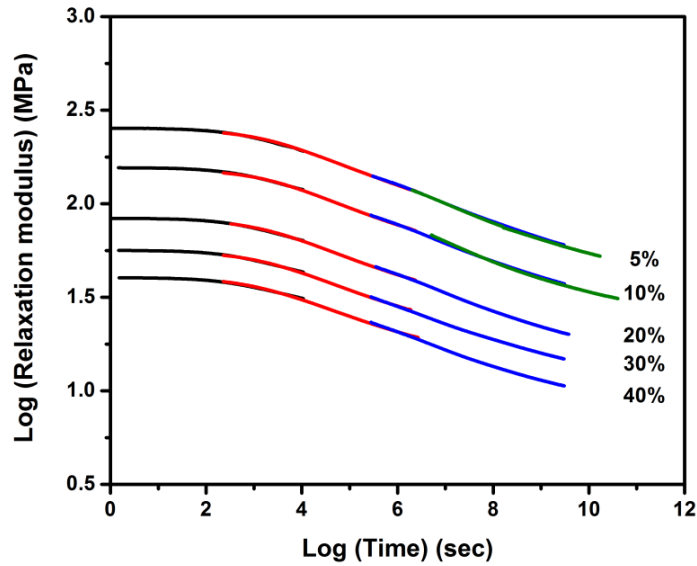


**Fig. 3.6** Master curves for relaxation modulus of PE specimens at different relaxation strains, with the crosshead speed of 0.01mm/min to generate the initial stretch

The above approach can also be applied to construction of master curves for relaxation modulus with the initial stretch at other crosshead speeds. Fig. 3.7 summarizes master curves at the relaxation strain of 5%, for which the initial stretch was generated at all crosshead speeds considered in this study. Fig. 3.7 also includes a master curve from ref. [39], generated at a strain rate of  $1 \times 10^{-2} \text{ s}^{-1}$ , which corresponds to the crosshead speed of around 30mm/min for our specimens. As mentioned earlier, the curve from ref. [39] shows only the second transition, that is, for the decrease of the drop rate for the relaxation modulus.

Fig. 3.7 suggests that with the increase of the crosshead speed used to generate the relaxation strain, time for the appearance of the first transition in the relaxation test decreases. Therefore, it

is possible that, due to the high strain rate used for the initial stretch in the previous work, only the second transition could be observed. Further study needs to be conducted to understand mechanisms that are responsible for the first transition of the drop of the relaxation modulus shown in Fig. 3.7, and whether a relationship exists between the time for the occurrence of the first transition and the long-term properties for PE.

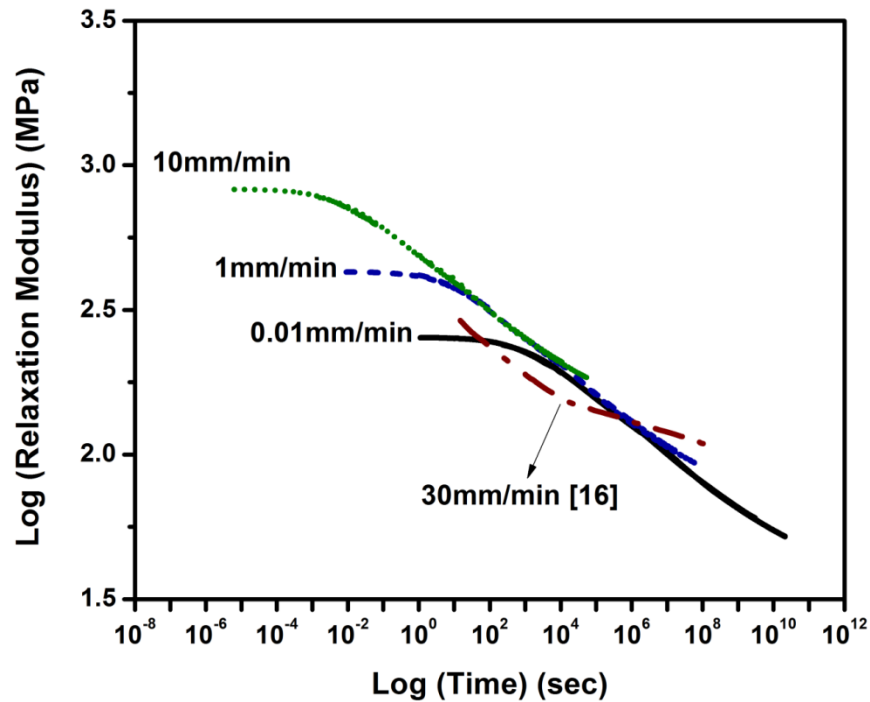


**Fig. 3.7** Comparison of master curves for the relaxation modulus at the relaxation strain of 5%, with various crosshead speeds to generate the initial stretch

### 3.4 Damage development under tensile loading using two-stage test method

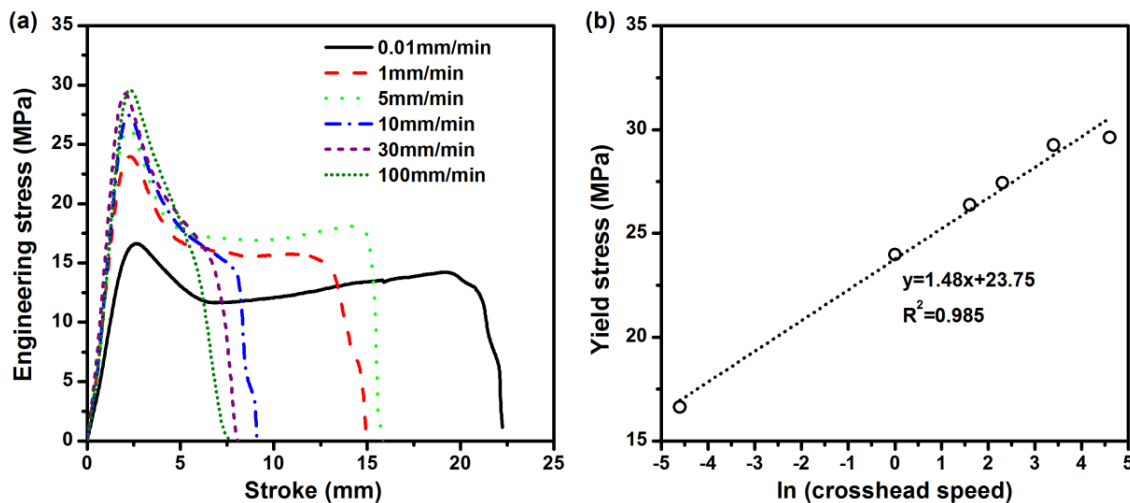
#### 3.4.1 Effect of strain rate on damage development

This section presents a study to investigate the influence of strain rate in the range that is encountered during the installation, repair and maintenance of the PE pressure pipe on the damage evolution. The study applies the two-test method to the D-split tensile specimens

prepared from a PE pressure pipe. Elastic modulus measured from the second test is then used to establish a phenomenological damage evolution law to depict the influence of strain rate on the damage evolution.

### 3.4.1.1 The first stage test

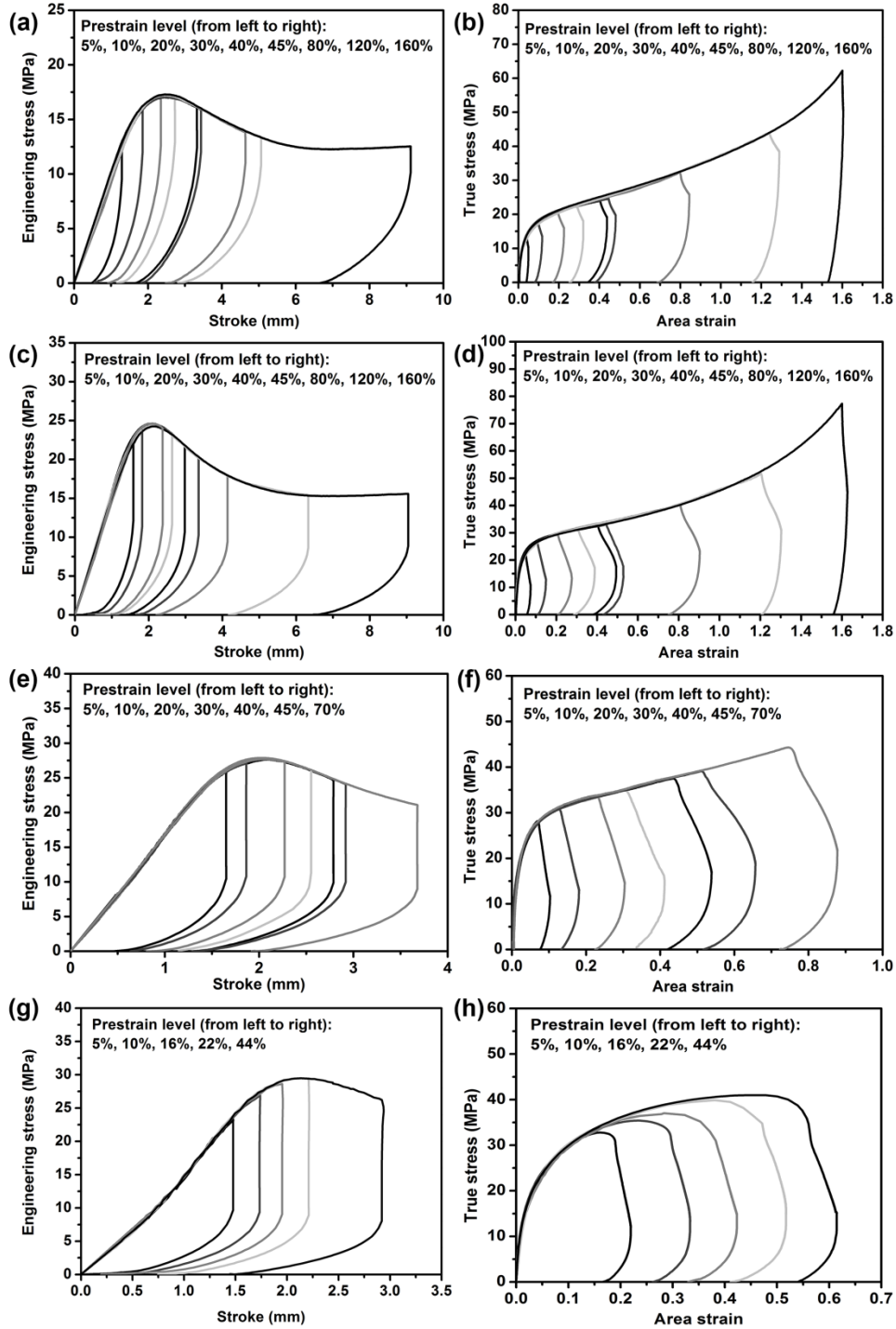
Engineering stress-stroke curves from the NPR specimens at six crosshead speeds of 0.01, 1, 5, 10, 30 and 100mm/min are presented in Fig. 3.8. The figure indicates that yield stress increases linearly with the increase of the logarithmic scale of crosshead speed at the rate of 1.48, which is very close to the value of 1.64 reported previously [18].



**Fig. 3.8** Results from the monotonic loading of NPR specimen: (a) plots of engineering stress versus stroke at different crosshead speeds and (b) yield stress as a function of logarithmic scale of crosshead speed

Fig. 3.9 summaries results from the first tests, conducted at crosshead speeds of 0.01, 1, 10 and 100mm/min. For example, Figs. 3.9(a) and 4(b), from the crosshead speed of 0.01mm/min, present curves of engineering stress versus stroke and true stress versus area strain, respectively, with the prestrain in the range from 5% (the very left curve) to 160% (the very right curve) . It

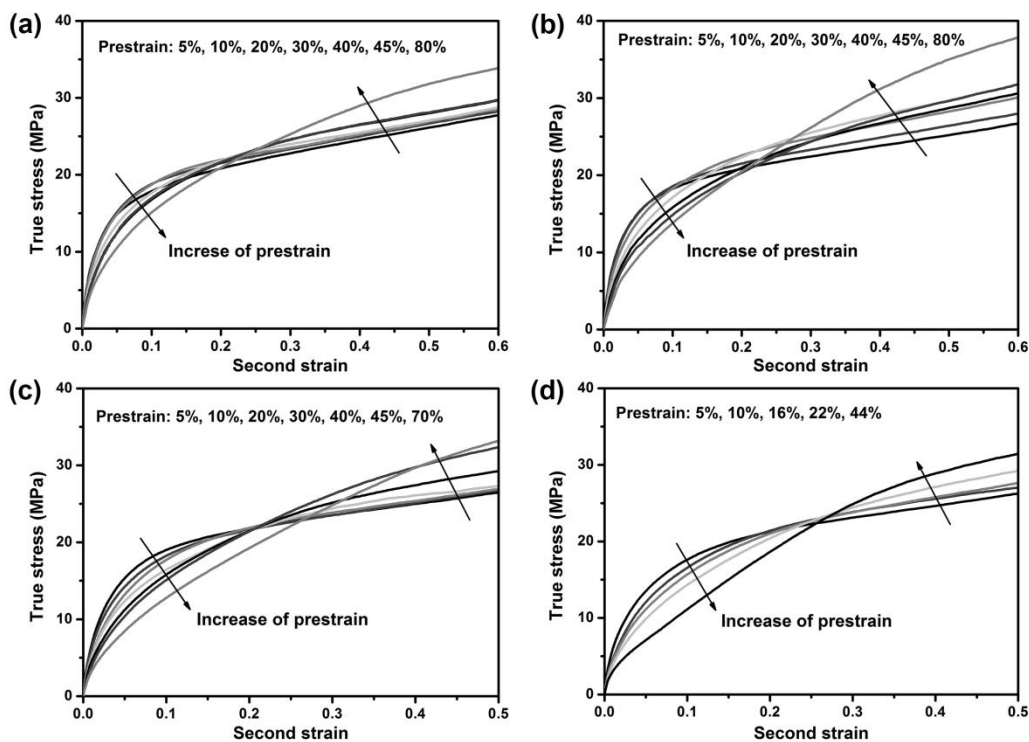
should be noted that at the crosshead speed of 100mm/min, Figs. 3.9(g) and 4(h), the number of specimens actually used for the testing is larger than the number of curves presented here. This is because at this crosshead speed, deformation and fracture behaviour has been strongly affected by the presence of foreign particles in the ligament region of the specimens. Therefore, quite a few tests had to be conducted to obtain curves that show little influence by the presence of foreign particles, which are presented in Figs. 3.9(g) and (h).



**Fig. 3.9** Summary of curves of engineering stress versus stroke and true stress versus area strain at various crosshead speeds: 0.01mm/min for (a) and (b), 1mm/min for (c) and (d), 10mm/min for (e) and (f), and 100mm/min for (g) and (h)

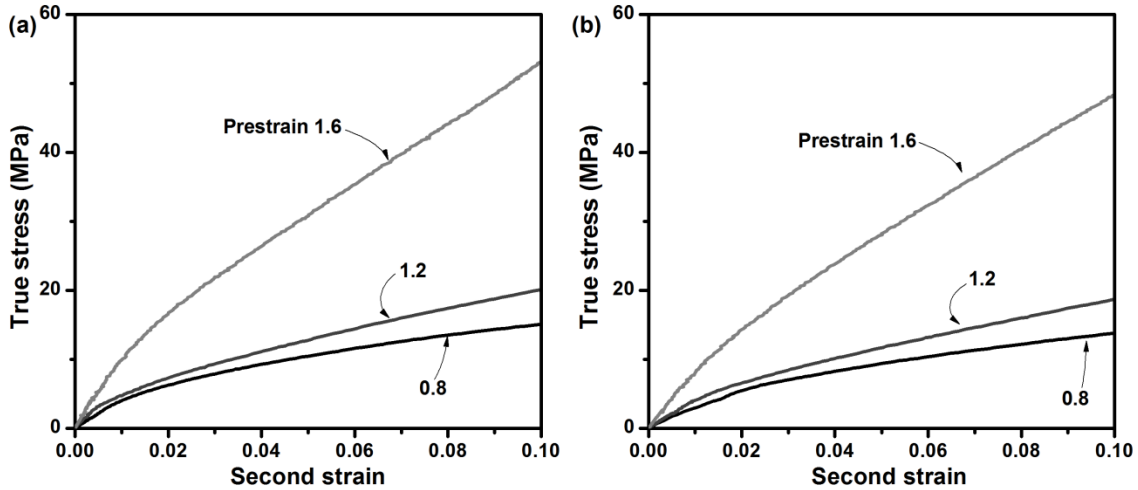
### 3.4.1.2 The second stage test

Curves of true stress versus second strain from the second tests, for prestrains of up to 80%, are presented in Fig. 3.10. Note that since calculation of the second strain does not consider the residual deformation from the first test, all curves in Fig. 3.10 starts from the origin. An obvious trend in Fig. 3.10 is that below the second strain of 10%, stress at a given second strain decreases with the increase of the prestrain applied in the first test. However, this trend is reversed for the second strain above a critical value which lies between 20% and 30% in Fig. 3.10. This phenomenon is consistent with that reported previously, from coupon specimens that were prepared from compression-molded plaques [15, 48].



**Fig. 3.10** Curves of true stress versus second strain from the second test at the crosshead speed of 0.01mm/min, on NPR specimens that have been subjected to monotonic tensile loading in the first test, at the following crosshead speeds: (a) 0.01mm/min, (b) 1mm/min

Curves with the prestrains of 120% and 160%, from specimens that have been subjected to the crosshead speeds of 0.01 and 1mm/min in the first test, are presented in Fig. 3.11. Note that Fig. 3.11 also includes curves for the prestrain of 80% at the same crosshead speeds, to serve as a reference for the comparison. Fig. 3.11 suggests that at a prestrain level above 80%, increase of the prestrain always causes increase of the stress response in the second test, even at the second strain level below 10%. This is different from the trend shown in Fig. 3.10 in which the curves are from specimens with the prestrain below 80%.



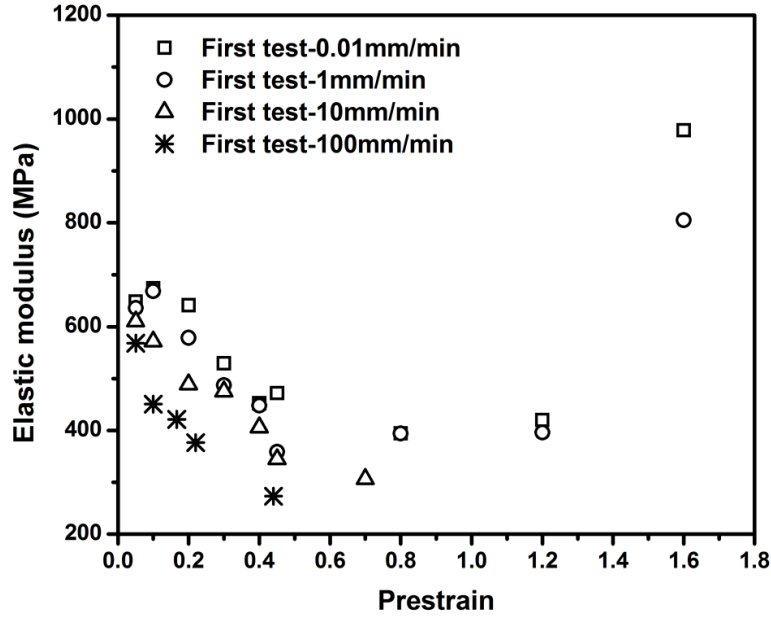
**Fig. 3.11** Curves of true stress versus second strain from the second test, for the NPR specimens that have been subjected to monotonic tensile loading to the prestrain level labelled for each curve. Crosshead speed used in the first test was 0.01mm/min for (a) and 1mm/min for (b)

Fig. 3.12 shows the relationship between the elastic modulus measured from the second test and the prestrain applied in the first test, in which the elastic modulus is defined as the slope for the straight line tangent to the curve of true stress versus second strain at the second strain of 0.5%. Fig. 3.12 suggests that for the specimens that have been subjected to the crosshead speeds of 0.01 and 1mm/min in the first test, the elastic modulus decreases first with the increase of the prestrain up to 80%. However, the trend of change for the elastic modulus is reversed with the

further increase of the prestrain. Such a phenomenon has been observed before [22], except that in the previous work, the test applied cyclic loading to the specimens and the elastic modulus was measured during the unloading phase.

Fig. 3.12 also shows that at the crosshead speeds of 10 and 100mm/min, the elastic modulus changes with the increase of prestrain introduced in the first test. However, since the maximum prestrain before fracture at those crosshead speeds is below 80%, the V-shaped trend shown by the specimens tested at the crosshead speeds of 0.01 and 1mm/min could not be observed. In addition, Fig. 3.12 indicates that at a given prestrain level, increase of the crosshead speed used in the first test causes decrease of the elastic modulus measured from the second test.

One possible explanation for the V-shaped trend for the elastic modulus in Fig. 3.12 is that at a high prestrain level, i.e., above 80%, PE molecules become increasingly aligned in the loading direction, resulting in a microstructure that yields a higher elastic modulus in the loading direction than that for a virgin specimen [54–56].



**Fig. 3.12** Effect of prestrain introduced in the first test on the elastic modulus measured from the second test.

The following equation has been suggested, based on the concept of continuum damage mechanics (CDM) [57], to calculate damage parameter  $D$  :

$$D = 1 - \frac{E_D}{E_0} \quad (3.3)$$

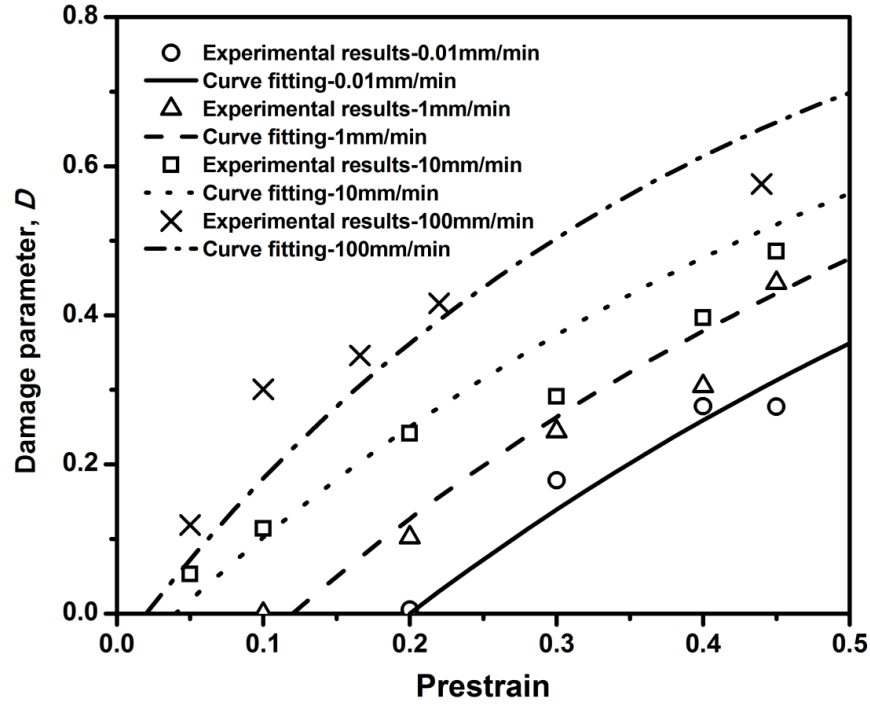
where  $D$  represents the ratio of damaged surface area to the total surface area, and  $E_D$  and  $E_0$  are elastic moduli of the damaged and virgin specimens, respectively.

Fig. 3.13 presents variation of  $D$ , based on Eq. (3.2), as a function of prestrain introduced in the first test. The figure includes curves based on the following one-term exponential function, to fit the trend of change of the  $D$  values with the increase of prestrain.

$$D = A[1 - \exp(-B\varepsilon)] \quad (3.4)$$

Fig. 3.13 indicates that damage starts at a critical prestrain level that is lowered by the increase of the crosshead speed used in the first test. In other words, at a given prestrain level damage is more severe by using a higher crosshead speed to generate the prestrain. The figure also indicates that both crosshead speed and prestrain level have a significant effect on the damage generation.

It should be noted that Fig. 3.13 does not include  $D$  values for specimens with the prestrain levels above 80%, generated at the crosshead speeds of 0.01 and 1mm/min in the first test. This is because at such high prestrain levels, micro-structure of PE should have been significantly altered from that of the virgin NPR specimen, due to the improved alignment of molecular chains in the loading direction. Therefore,  $D$  for those highly-deformed specimens should be calculated using  $E_0$  for a virgin specimen that has already had the microstructure of aligned molecular chains. It should be pointed out that  $D$  for the specimens with the prestrain of 160% would have been a negative value if  $E_0$  for a virgin NPR specimens had been used to calculate the  $D$  value.



**Fig. 3.13** Variation of damage parameter  $D$  for NPR specimens as a function of prestrain introduced in the first test, up to the prestrain level of 80%.

To take into account the difference of  $E_0$  due to the microstructure change in PE, the following expressions are used to calculate  $D$  for the entire prestrain range considered in this study:

$$D = \begin{cases} 1 - \frac{E_D}{E_1} & \varepsilon \leq 0.8 \\ 1 - \frac{E_D}{E_2} & \varepsilon > 0.8 \end{cases} \quad (3.5)$$

where  $E_D$  is the elastic modulus for the damaged specimen, and  $E_1$  and  $E_2$  the elastic moduli for virgin specimen with the isotropic, semi-crystalline microstructure and virgin specimen with aligned microstructure, respectively. The critical strain for the change from the former to the latter microstructure in PE has been suggested to be around 60% [58]. Our results suggest that

such a change becomes permanent and shows a significant influence on the elastic modulus at a strain level around 80%.

Fig. 3.14 presents an example for the above concept, showing variation of damage parameter  $D$  as a function of prestrain for specimens subjected to a crosshead speed of 0.01mm/min in the first test. Values for  $D$  in Fig. 3.14 were determined based on Eq. (3.4), with  $E_1$  being the elastic modulus for a virgin NPR specimen and  $E_2$  determined using results published in the literature [55], as detailed in the following. In [55], Bigg summarizes elastic modulus for PE with different molecular weight characteristics and subjected to a wide range of thermal treatments and processing techniques [59–64], to show that after the transverse compression, the elastic modulus values for PEs depict a unique trend line with the draw ratio ( $L$ ) in the axial direction. The trend line seems to be independent of the above variations in molecular weight and thermal and processing history. As a result,  $E_2$  in Eq. (3.4) for  $D$  in Fig. 3.14 was determined based on the plot of elastic modulus versus  $L$  proposed by Bigg, at the values of  $L$  that are equivalent to the area strains of 120% and 160%, determined from the following equation with the assumption of volume conservation during the deformation process.

$$L = \exp(\varepsilon) \quad (3.6)$$

Using the above equation, area strains  $\varepsilon$  of 120% and 160% correspond to  $L$  of 3.32 and 4.95, respectively.

Variation of  $D$  with prestrain shown in Fig. 3.14 suggests that damage evolution in PE may be a two-stage process. The  $D$  value may increase initially at a decreasing rate to a plateau value at the prestrain of around 80%. Further increase of the prestrain, however, may cause the increase

of  $D$  in an accelerating manner. Such a trend has also been observed in another study using coupon specimens of HDPE from compression moulded plaques [65]. Note that the two trend lines in Fig. 3.14 are drawn based on the expressions modified from Eq. (3.3), as given in the figure, to depict the change of  $D$  with the increase of prestrain. Further investigation is planned to confirm the  $D$  evolution at large prestrains.

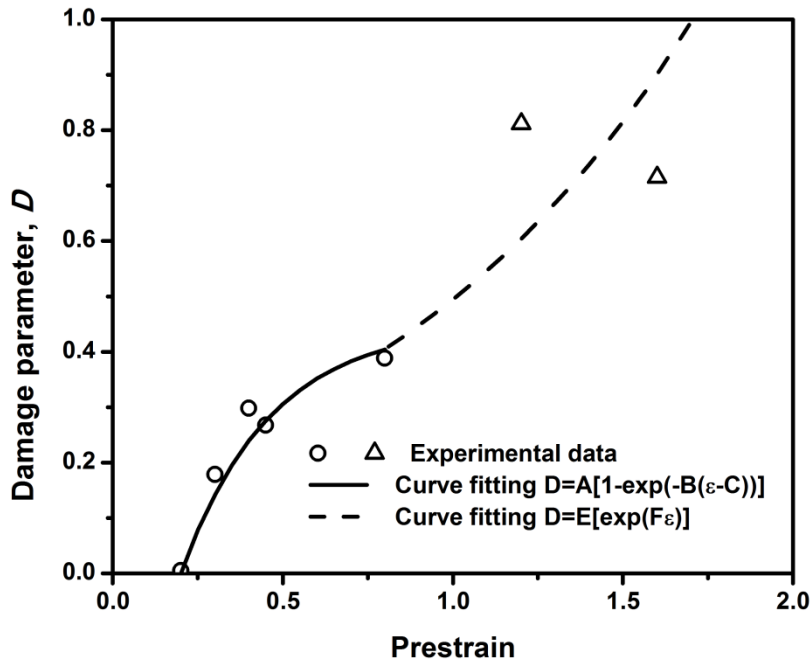


**Fig. 3.14** Variation of damage parameter  $D$  as a function of prestrain introduced in the first test, including the prestrains of 120% and 160%, at the crosshead speed of 0.01 mm/min.

Fig. 3.15 presents yield stress and the corresponding area strain (named yield area strain) as functions of prestrain applied in the first test, at all four crosshead speeds considered in this study. Note that yield stress here is the engineering stress calculated using the cross sectional area before the first test as the reference, and the yield area strain is the “first strain” at the yield point of the second test. Fig. 3.15 suggests that yield stress from the second test decreases but yield area strain increases with the increase of prestrain applied in the first test. Values for the slope of the linear trend lines shown in Fig. 3.15 suggest that increase of the crosshead speed

used in the first test causes increase of the change rate, with respect to the increase of prestrain, of the yield stress and yield area strain from the second test.

The increase of the yield area strain with the increase of prestrain, as shown in Fig. 3.15, can be understood from the viewpoint of microstructure evolution of PE under tensile deformation. Degree of crystallinity for PE is known to decrease by the tensile deformation, due to the damage generation, which leads to the eventual destruction of the original lamellar structure [66] and causes the increase of the tensile yield strain [67].

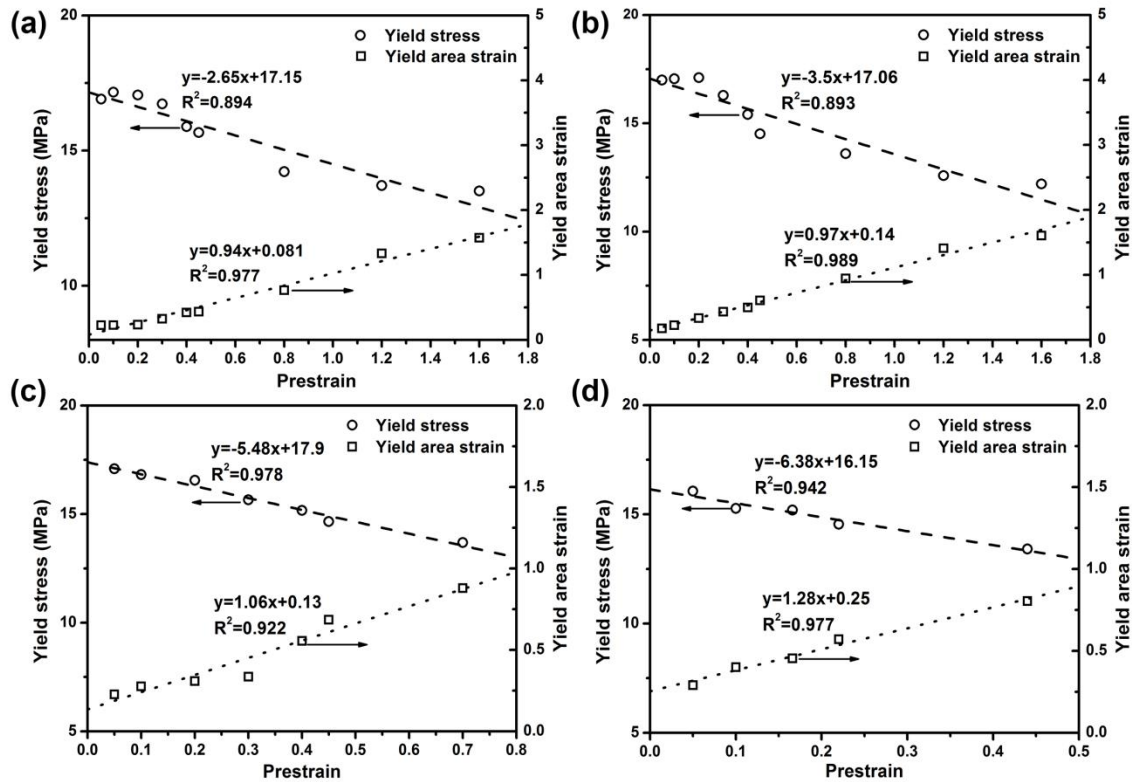


**Fig. 3.15** Variation of yield stress and yield area strain for NPR specimens as functions of prestrain introduced at the following crosshead speeds: (a) 0.01mm/min, (b) 1mm/min, (c) 10mm/min, and (d) 100mm/min

Fig. 3.16 summaries plots of true stress versus first strain from the second tests, for specimens subjected to different crosshead speeds in the first test. Each plot in Fig. 3.16 contains a curve from a virgin specimen, to serve as a reference for the comparison. Apart from the reference curve, each curve in Fig. 3.16 starts from a non-zero first strain due to the residual plastic deformation generated from the first test. Larger the prestrain applied in the first test, larger the residual plastic stain measured before the second test. In view that in the continuum damage mechanics, plastic strain has been adopted to reflect the damage level [68], residual plastic strain may serve as an indicator to characterize the damage in PE pipe. Such a possibility is being investigated when this manuscript is prepared.

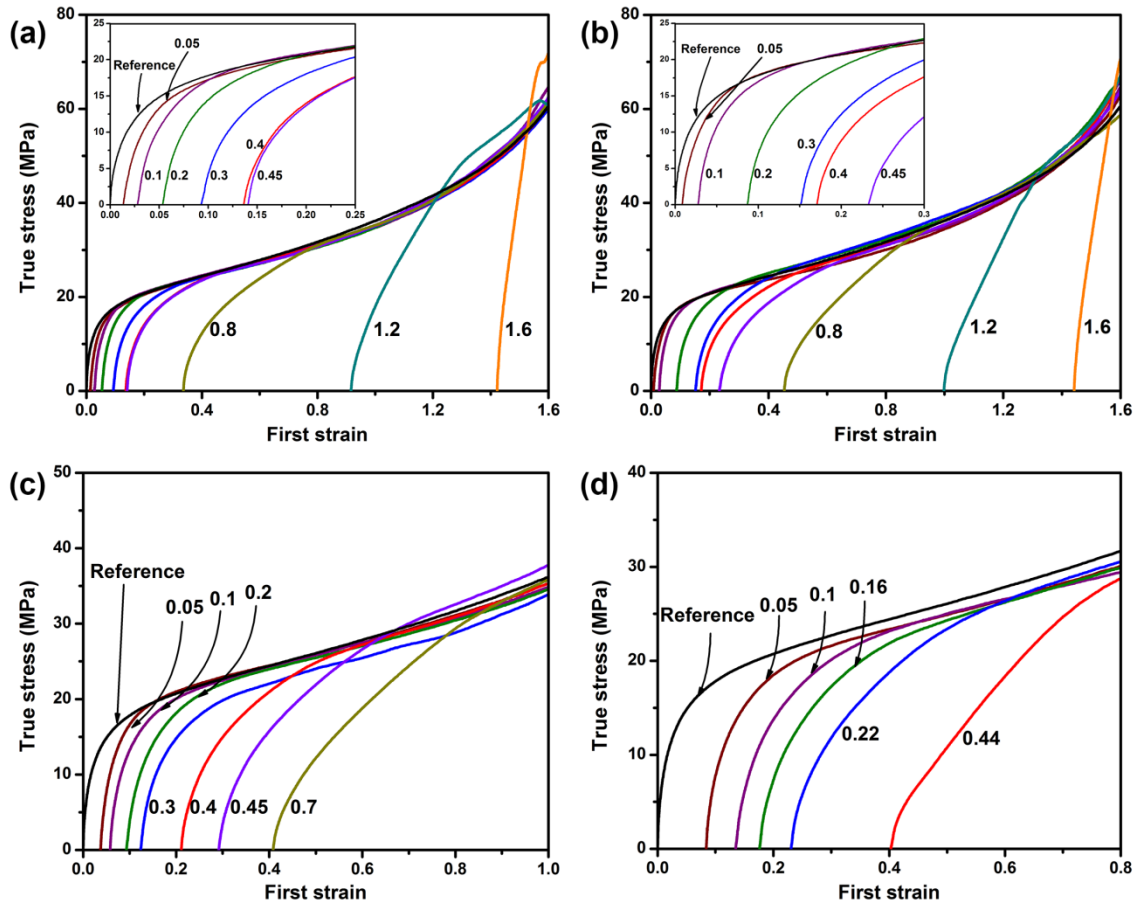


**Fig. 3.16** Plots of true stress versus first strain from the second test at the following crosshead speeds: (a) 0.01mm/min (b) 1mm/min (c) 10mm/min and (d) 100mm/min

### 3.4.2 Effect of microstructure on damage development

In this section, influence of loading conditions on the fundamental mechanical behaviour of PE80 and PE100 pipe materials is compared. In view of PE's significantly non-linear, time-dependent deformation behavior, the comparison is focused on two aspects. The first is the influence of strain rate (through the change of test crosshead speed) on the short-term mechanical properties such as tensile modulus, yield strength and relaxation resistance, and the second is the influence of loading history (in terms of the maximum strain in the loading history, to be named pre-strain hereafter) on elastic modulus at a strain of 0.5% and strain hardening modulus at post-

yield strains above 70%. In spite that both PE80 and PE100 pipe materials are now widely used for gas transportation, systematic comparison for the above properties are yet to be available in the literature. Note that for PE100 pipe material, results for the influence of pre-strain on the change of elastic modulus at a low strain level have been reported in our previous publication [69].

Yield stress is defined based on engineering stress, i.e., calculated using the cross-sectional area of the virgin specimen, before the first-stage test. Yield stress and elastic modulus at the strain of 0.5%, measured from tests at the first-stage, are presented in Fig. 3.17(a) and (b), respectively, as functions of the logarithmic scale of the crosshead speed. The results indicate that both yield stress and elastic modulus increase linearly with the increase of the logarithmic scale of the crosshead speed, which is consistent with that reported in ref. [70]. Furthermore, Fig. 3.17 suggests that both yield stress and elastic modulus of PE100 are larger than those of PE80, also consistent with results in the literature [41, 71], due to higher density of PE100 [72–74].

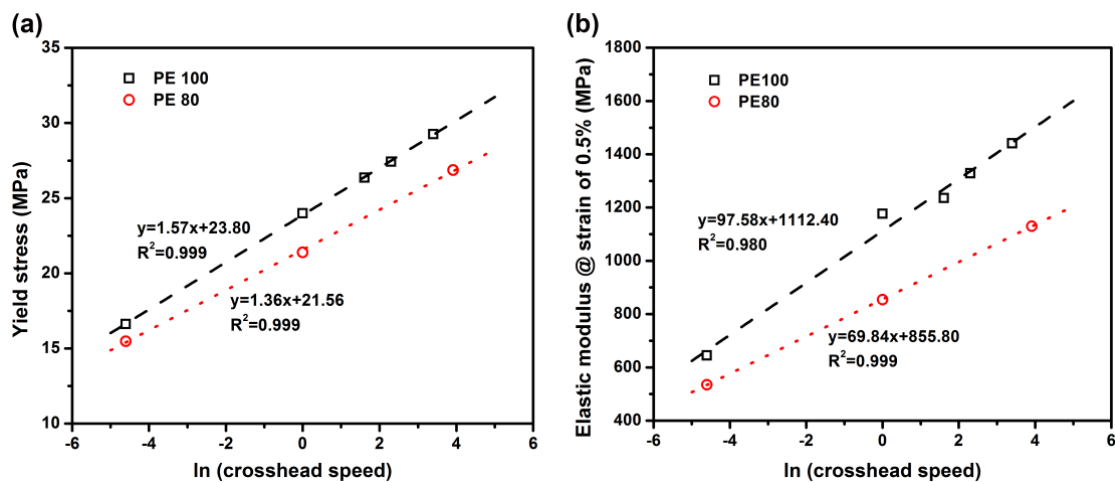


**Fig. 3.17** Variation of yield stress (a) and elastic modulus (b) with crosshead speed for PE80 and PE100 pipe materials

Fig. 3.18 presents examples of relaxation behavior for PE80 and PE100 pipe materials, measured from the first-stage tests after reaching the specified pre-strain levels at the crosshead speed of either 0.01mm/min (a) or 1mm/min (b). Load drop in the figure is normalized by the load at the beginning of the relaxation. The plots in Fig. 3.18 are only for two pre-strain levels, 20% and 40%, but the phenomenon and the trend of change are applicable to all other strain levels. Fig. 3.18 suggests that at a given crosshead speed for the pre-loading and the same pre-strain level, the percentage of load drop for PE80 pipe material is lower than that for PE100, suggesting that the former has a better relaxation resistance than the latter. Fig. 3.18 also suggests that the relaxation resistance increases with the increase of the pre-strain level, or with the decrease of the crosshead speed used for the pre-loading.

The above difference in the relaxation resistance has been suggested to be due to the difference in the molecular chain mobility between PE80 and PE100 pipe materials [75]. Based on the results in Fig. 3.18, molecular chain mobility for PE100 should be bigger than that for PE80. However, further study is required to determine the mechanisms that are responsible for the relaxation behavior, in order to fully understand the implication of the difference in relaxation resistance on the PE pipe performance.

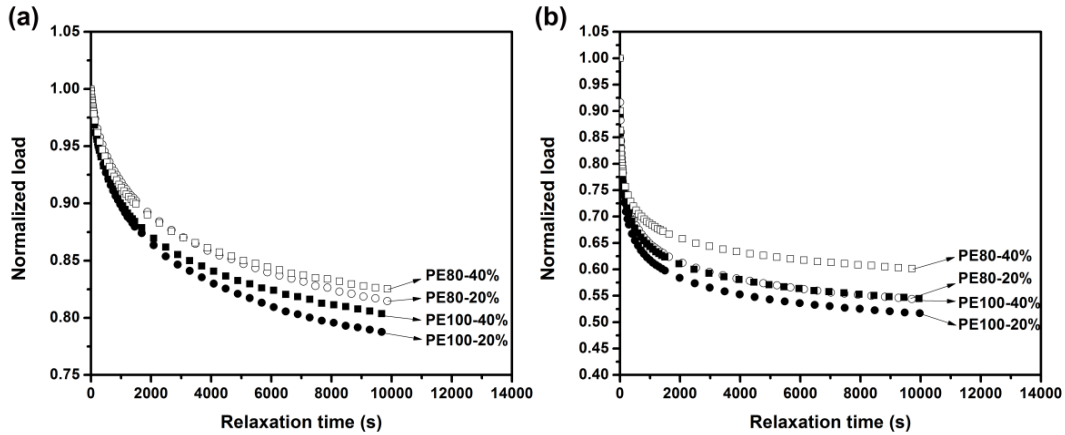


**Fig. 3.18** Comparison of relaxation behavior of NPR specimens made from PE80 and PE100 pipe materials, stretched to pre- strains of 20% and 40% at crosshead speeds of (a) 0.01mm/min and (b) 1mm/min

As mentioned earlier, elastic modulus was determined using true stress-strain curves from the second-stage tests, at the strain level of 0.5%. Fig. 3.19 summarizes results of the elastic modulus, from specimens which have been subjected to the first-stage tests at the crosshead speed of 0.01mm/min for (a) and 1mm/min for (b). As shown in Fig. 3.19, both PE80 and PE100 show decrease of the elastic modulus with the increase of the pre-strain levels. Based on the classical damage mechanics concept [68], in which damage parameter  $D$  is defined using the following Eq. (3.3), Fig. 3.19 suggests that damage can be introduced to both pipe materials at an early stage of deformation, especially using a high crosshead speed.

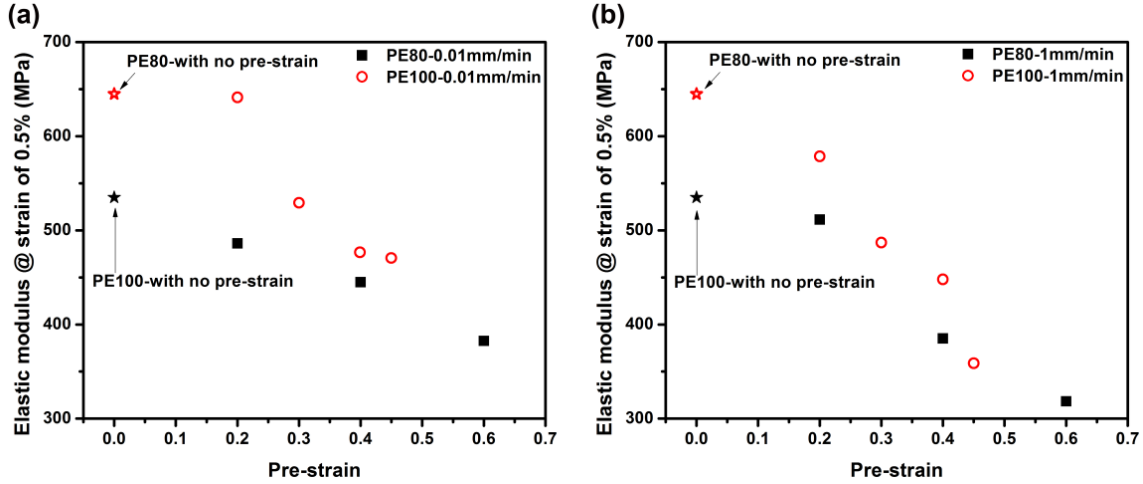


**Fig. 3.19** Effects of pre-strain on elastic modulus of PE80 and PE100 pipe materials, with pre-strain introduced at the first-stage tests at the crosshead speed of (a) 0.01mm/min and (b) 1mm/min

Strain hardening after the yield point [76, 77] has been characterized using the plot of true stress versus neo-Hookean (NH) strain which is defined as  $\lambda^2 - \frac{1}{\lambda}$ , where  $\lambda$  is the stretch ratio. Two examples of true stress versus NH strain from the second-stage tests, one for PE80 and the other PE100, are shown in Fig. 3.20(a). The figure suggests that a section of the curves, with NH strain above 3.75 or  $\varepsilon_w$  defined by Eq. (3.1) larger than 70%, shows an approximately linear relationship between stress and strain, of which the slope is defined as the strain-hardening modulus ( $G_p$ ). In this study, value for  $G_p$  was determined from the curve section with NH strain between 12 and 18, as shown in Fig. 3.20(a), or  $\varepsilon_w$  from 125% to 145%.

Fig. 3.20(b) summarizes  $G_p$  values for PE80 and PE100 with different pre-strain levels. The figure suggests that pre-strains ( $\varepsilon$ ) up to 45% have little influence on the  $G_p$  values. This is different from the trend shown in Fig. 3.19 in which elastic modulus measured at the strain of 0.5% is strongly affected by the  $\varepsilon_w$  values. Since  $G_p$  is measured at a high strain level, above

70% for  $\varepsilon_w$ , at which the deformation should have caused some disintegration of the crystalline lamellae, the relatively constant  $G_p$  values in Fig. 3.20 indicate that pre-strain of up to 45%, introduced in the first-stage tests, does not affect the crystalline lamellae in their resistance to deformation. On the other hand, deformation introduced for the measurement of elastic modulus, at  $\varepsilon_w$  of 0.5%, is expected to occur mainly in the inter-lamellar amorphous region. Therefore, the change in elastic modulus with the pre-strain level, as shown in Fig. 3.19, indicates that the pre-strain introduced in the first-stage tests should have affected the inter-lamellar amorphous region in its resistance to deformation.

Fig. 3.20 also suggests that  $G_p$  for PE100 has a larger value than that for PE80, possibly due to the stronger crystalline phase in PE100 than that in PE80, consistent with the higher degree of crystallinity for PE100 [40, 41].

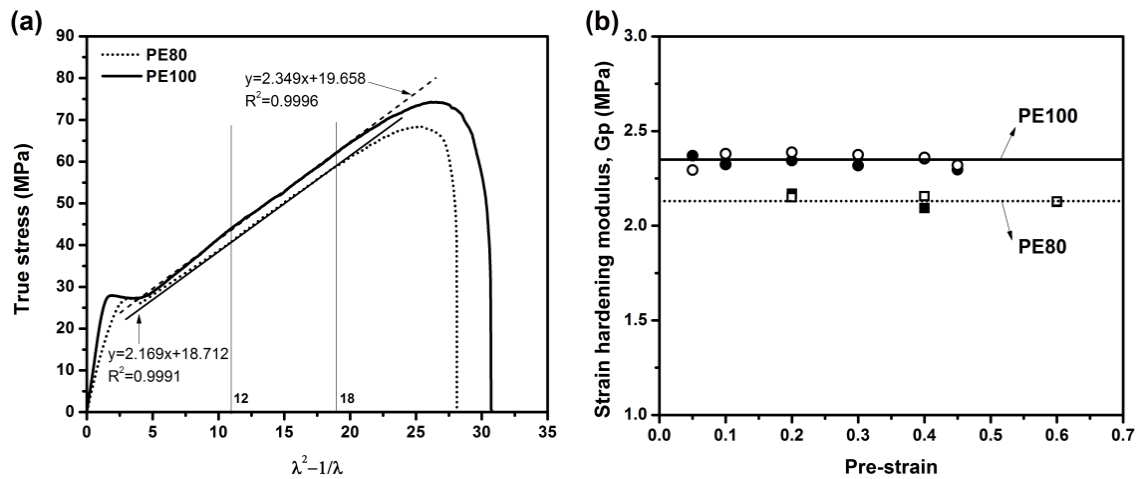


**Fig. 3.20** (a) Gaussian plots of PE80 and PE100 pipe materials with pre-strain of 0.2 and (b) strain hardening modulus ( $G_p$ ) from the second-stage tests as a function of pre-strain introduced in the first-stage tests at the crosshead speed of 0.01 mm/min (open symbols)

### 3.5 Conclusions

Effects of deformation-induced damage on mechanical properties of PE pipe have been assessed using the two-test method, on NPR specimens from the pipe. Results from the second tests were compared with those for virgin specimens at the same crosshead speed. The results show that mechanical properties of PE are strongly affected by the loading conditions used in the first test. In particular, elastic modulus from the second test, measured at the second strain of 0.5%, decreases significantly with the increase of prestrain applied in the first test, up to the prestrain level of 80%. At higher prestrain levels of 120% and 160%, subjected to the crosshead speeds of 0.01 and 1 mm/min, the trend of change for the elastic modulus is reversed. Yield stress and yield area strain, on the other hand, show the monotonic, linear change with the increase of prestrain, i.e., decrease in yield stress and increase in yield strain with the increase of the prestrain level.

Damage evolution in the first test is established based on a phenomenological damage law using the elastic modulus measured from the second test. The results suggest that prestrain for the damage initiation decreases with the increase of the crosshead speed used to generate the damage. Therefore, increase of the crosshead speed, i.e., increase of the strain rate, causes acceleration of the damage evolution, thus increasing the extent of damage in the PE pipe.

The study concludes that the change of mechanical properties for PE pipe shows a strong dependence on the loading history. In particular, variation of the tensile strain rate in the loading history, introduced by varying the crosshead speed, can result in a significantly different trend of change in the mechanical properties for PE pipe. The maximum strain introduced in the loading history (i.e., the prestrain level) also affects the mechanical properties.

In addition, mechanical properties, including yield stress, relaxation behavior, and elastic and strain hardening moduli, were compared between PE80 and PE100 pipe. The results show that yield stress and elastic modulus of PE100 are larger than those of PE80. PE100 also has a higher strain hardening modulus than PE80, suggesting that the former is better in the resistance to deformation. However, PE80 has a better resistance to relaxation. Results from the study also show a different dependence of elastic modulus (at  $\varepsilon$  of 0.5%) and strain hardening modulus (at strains above 70%) on the prestrain level introduced in the first-stage test, suggesting that the prestrain levels used in the study, with  $\varepsilon$  up to 45%, affect mainly the deformation resistance in the inter-lamellar, amorphous region, not in the crystalline phase.

The study also examines the influence of two parameters, relaxation strain and crosshead speed used to generate the relaxation strain, on the relaxation behavior of PE pressure pipes. An approach based on superposition of time and strain rate (represented by the crosshead speed here) is proposed to construct master curves for the relaxation modulus based on short-term test results. The results show that two transitions exist for the drop of relaxation modulus with time. One occurs after a long relaxation period, and the other within a short period after the relaxation strain is reached. The latter causes increase of the drop rate for the relaxation modulus, and has not been observed before. The study shows the possibility of constructing a master curve for the relaxation modulus using short-term test results based on the time-strain rate superposition principle. This approach can serve as an alternative means to evaluate the long-term behavior of PE and semi-crystalline polymers in general.

## References

- [1] Kiass, N., Khelif, R., Boulanouar, L., and Chaoui, K., 2005, "Experimental Approach to Mechanical Property Variability through a High-Density Polyethylene Gas Pipe Wall," *J. Appl. Polym. Sci.*, **97**(1), pp. 272–281.
- [2] Azevedo, C. R. F., 2007, "Failure Analysis of a Crude Oil Pipeline," *Engineering Failure Analysis*, **14**(6), pp. 978–994.
- [3] Shalaby, H. M., Riad, W. T., Alhazza, A. A., and Behbehani, M. H., 2006, "Failure Analysis of Fuel Supply Pipeline," *Engineering Failure Analysis*, **13**(5), pp. 789–796.
- [4] Majid, Z. A., Mohsin, R., Yaacob, Z., and Hassan, Z., 2010, "Failure Analysis of Natural Gas Pipes," *Engineering Failure Analysis*, **17**(4), pp. 818–837.
- [5] Hasan, F., Iqbal, J., and Ahmed, F., 2007, "Stress Corrosion Failure of High-Pressure Gas Pipeline," *Engineering Failure Analysis*, **14**(5), pp. 801–809.
- [6] Krishnaswamy, R. K., 2005, "Analysis of Ductile and Brittle Failures from Creep Rupture Testing of High-Density Polyethylene (HDPE) Pipes," *Polymer*, **46**(25), pp. 11664–11672.
- [7] Palermo, G., 2004, "Correlating Aldyl 'A' and Century PE Pipe Rate Process Method Projections with Actual Field Performance," *Plastics Pipes XII Conference. Milan, Italy*.
- [8] Yayla, P., and Bilgin, Y., 2007, "Squeeze-off of Polyethylene Pressure Pipes: Experimental Analysis," *Polymer Testing*, **26**(1), pp. 132–141.
- [9] Kim, J.-H., Park, W.-S., Chun, M.-S., Kim, J.-J., Bae, J.-H., Kim, M.-H., and Lee, J.-M., 2012, "Effect of Pre-Straining on Low-Temperature Mechanical Behavior of AISI 304L," *Materials Science and Engineering: A*, **543**, pp. 50–57.
- [10] Nakajima, M., Akita, M., Uematsu, Y., and Tokaji, K., 2010, "Effect of Strain-Induced Martensitic Transformation on Fatigue Behavior of Type 304 Stainless Steel," *Procedia Engineering*, **2**(1), pp. 323–330.
- [11] Kikuchi, S., and Ilschner, B., 1986, "Effects of a Small Prestrain at High Temperatures on the Creep Behaviour of AISI 304 Stainless Steel," *Scripta Metallurgica*, **20**(2), pp. 159–162.
- [12] Zhang, C., and Moore, I. D., 1997, "Nonlinear Mechanical Response of High Density Polyethylene. Part I: Experimental Investigation and Model Evaluation," *Polym Eng Sci*, **37**(2), pp. 404–413.
- [13] Khan, F., 2006, "Loading History Effects on the Creep and Relaxation Behavior of Thermoplastics," *Journal of Engineering Materials and Technology*, **128**(4), pp. 564–571.
- [14] Dusunceli, N., and Aydemir, B., 2011, "The Effects of Loading History and Manufacturing Methods on the Mechanical Behavior of High-Density Polyethylene," *Journal of Elastomers and Plastics*, **43**(5), pp. 451–468.
- [15] Jar, P.-Y. B., 2014, "Effect of Tensile Loading History on Mechanical Properties for Polyethylene," *Polym Eng Sci*, **55**(9), pp. 2002–2010.
- [16] Ben Jar, P.-Y., 2014, "Transition of Neck Appearance in Polyethylene and Effect of the Associated Strain Rate on the Damage Generation," *Polym Eng Sci*, **54**(8), pp. 1871–1878.
- [17] Jar, P. B., 2013, "Assessment of Damage and Long-Term Strength of Polyethylene," *ICF13*.
- [18] Dasari, A., and Misra, R. D. K., 2003, "On the Strain Rate Sensitivity of High Density Polyethylene and Polypropylenes," *Materials Science and Engineering: A*, **358**(1–2), pp. 356–371.

- [19] Reis, J. M. L., Pacheco, L. J., and da Costa Mattos, H. S., 2014, “Temperature and Variable Strain Rate Sensitivity in Recycled HDPE,” *Polymer Testing*, **39**, pp. 30–35.
- [20] Reis, J. M. L., Pacheco, L. J., and da Costa Mattos, H. S., 2013, “Tensile Behavior of Post-Consumer Recycled High-Density Polyethylene at Different Strain Rates,” *Polymer Testing*, **32**(2), pp. 338–342.
- [21] Reis, J. M. L., Pacheco, L. J., and da Costa Mattos, H. S., 2013, “Influence of the Temperature and Strain Rate on the Tensile Behavior of Post-Consumer Recycled High-Density Polyethylene,” *Polymer Testing*, **32**(8), pp. 1576–1581.
- [22] Ayoub, G., Zaïri, F., Naït-Abdelaziz, M., and Gloaguen, J. M., 2010, “Modelling Large Deformation Behaviour under Loading–unloading of Semicrystalline Polymers: Application to a High Density Polyethylene,” *International Journal of Plasticity*, **26**(3), pp. 329–347.
- [23] Xu, M., and Wang, L., 2006, “A New Method for Studying the Dynamic Response and Damage Evolution of Polymers at High Strain Rates,” *Mechanics of Materials*, **38**(1–2), pp. 68–75.
- [24] Wang, L.-L., Zhou, F.-H., Sun, Z.-J., Wang, Y.-Z., and Shi, S.-Q., 2010, “Studies on Rate-Dependent Macro-Damage Evolution of Materials at High Strain Rates,” *International Journal of Damage Mechanics*, **19**(7), pp. 805–820.
- [25] Drozdov, A. D., and Yuan, Q., 2003, “The Viscoelastic and Viscoplastic Behavior of Low-Density Polyethylene,” *International Journal of Solids and Structures*, **40**(10), pp. 2321–2342.
- [26] Hong, K., Rastogi, A., and Strobl, G., 2004, “A Model Treating Tensile Deformation of Semicrystalline Polymers: Quasi-Static Stress–Strain Relationship and Viscous Stress Determined for a Sample of Polyethylene,” *Macromolecules*, **37**(26), pp. 10165–10173.
- [27] Dusunceli, N., and Colak, O. U., 2006, “High Density Polyethylene (HDPE): Experiments and Modeling,” *Mech Time-Depend Mater*, **10**(4), pp. 331–345.
- [28] Lu, Y., Yang, W., Zhang, K., and Yang, M., 2010, “Stress Relaxation Behavior of High Density Polyethylene (HDPE) Articles Molded by Gas-Assisted Injection Molding,” *Polymer Testing*, **29**(7), pp. 866–871.
- [29] *ASTM D5262 Standard Test Method for Evaluating the Unconfined Tension Creep and Creep Rupture Behavior of Geosynthetics*, ASTM International.
- [30] *ASTM D6048 Standard Practice for Stress Relaxation Testing of Raw Rubber, Unvulcanized Rubber Compounds, and Thermoplastic Elastomers*, ASTM International.
- [31] *ASTM F1473 Standard Test Method for Notch Tensile Test to Measure the Resistance to Slow Crack Growth of Polyethylene Pipes and Resins*, ASTM International.
- [32] Struik, L. C. E., 1989, “Mechanical Behaviour and Physical Ageing of Semi-Crystalline Polymers: 3. Prediction of Long Term Creep from Short Time Tests,” *Polymer*, **30**(5), pp. 799–814.
- [33] Lai, J., and Bakker, A., 1995, “Analysis of the Non-Linear Creep of High-Density Polyethylene,” *Polymer*, **36**(1), pp. 93–99.
- [34] Bozorg-Haddad, A., and Iskander, M., 2008, “Compressive Creep Behavior of HDPE Using Time Temperature Superposition,” *GeoCongress 2008@ sGeosustainability and Geohazard Mitigation*, ASCE, pp. 915–922.
- [35] Nitta, K., and Maeda, H., 2010, “Creep Behavior of High Density Polyethylene under a Constant True Stress,” *Polymer Testing*, **29**(1), pp. 60–65.

- [36] Bozorg-Haddad, A., and Iskander, M., 2011, “Comparison of Accelerated Compressive Creep Behavior of Virgin HDPE Using Thermal and Energy Approaches,” *Journal of materials engineering and performance*, **20**(7), pp. 1219–1229.
- [37] Popelar, C. F., Popelar, C. H., and Kenner, V. H., 1990, “Viscoelastic Material Characterization and Modeling for Polyethylene,” *Polym Eng Sci*, **30**(10), pp. 577–586.
- [38] Cheng, J. J., 2008, “Mechanical and Chemical Properties of High Density Polyethylene: Effects of Microstructure on Creep Characteristics.”
- [39] Adib, A., Domínguez, C., Rodríguez, J., Martín, C., and García, R. A., 2014, “The Effect of Microstructure on the Slow Crack Growth Resistance in Polyethylene Resins,” *Polym Eng Sci*, **55**(5), pp. 1018–1023.
- [40] Graice, L. M., Younan, M. Y. A., and Naga, S. A. R., 2004, “Experimental Investigation into the Fracture Toughness of Polyethylene Pipe Material,” *Journal of pressure vessel technology*, **127**(1), pp. 70–75.
- [41] Frank, A., Pinter, G., and Lang, R. W., 2010, “Fracture Mechanics Lifetime Prediction of PE 80 and PE 100 Pipes under Complex Loading Conditions,” *Proceedings Pipes XV*, Vancouver, Canada.
- [42] Frank, A., Hutař, P., and Pinter, G., 2012, “Numerical Assessment of PE 80 and PE 100 Pipe Lifetime Based on Paris-Erdogan Equation,” *Macromolecular Symposia*, Wiley Online Library, pp. 112–121.
- [43] Rafiee, R., 2012, “Apparent Hoop Tensile Strength Prediction of Glass Fiber-Reinforced Polyester Pipes,” *Journal of Composite Materials*, p. 0021998312447209.
- [44] Shlitsa, R. P., and Novikova, E. A., 1983, “Characteristics of the Use of the Split-Disk Method for Investigating Modern Winding Composites,” *Mech Compos Mater*, **18**(4), pp. 502–508.
- [45] Jiang, L., Jonas, J. J., Boyle, K., and Martin, P., 2008, “Deformation Behavior of Two Mg Alloys during Ring Hoop Tension Testing,” *Materials Science and Engineering: A*, **492**(1–2), pp. 68–73.
- [46] Chen, J. F., Li, S. Q., Bisby, L. A., and Ai, J., 2011, “FRP Rupture Strains in the Split-Disk Test,” *Composites Part B: Engineering*, **42**(4), pp. 962–972.
- [47] Jar, P. B., 2014, “Degradation of Mechanical Properties for Polyethylene by Small-Deformation Damage,” *ASME 2014 Pressure Vessels and Piping Conference*, American Society of Mechanical Engineers, p. V06BT06A040–V06BT06A040.
- [48] Fotheringham, D. G., and Cherry, B. W., 1978, “Strain Rate Effects on the Ratio of Recoverable to Non-Recoverable Strain in Linear Polyethylene,” *J Mater Sci*, **13**(2), pp. 231–238.
- [49] Addiego, F., Patlazhan, S., Wang, K., André, S., Bernstorff, S., and Ruch, D., 2015, “Time-Resolved Small-Angle X-Ray Scattering Study of Void Fraction Evolution in High-Density Polyethylene during Stress Unloading and Strain Recovery,” *Polym. Int.*, **64**(11), pp. 1513–1521.
- [50] Lai, J., and Bakker, A., 1995, “An Integral Constitutive Equation for Nonlinear Plasto-Viscoelastic Behavior of High-Density Polyethylene,” *Polym Eng Sci*, **35**(17), pp. 1339–1347.
- [51] Dusunceli, N., and Colak, O. U., 2008, “The Effects of Manufacturing Techniques on Viscoelastic and Viscoplastic Behavior of High Density Polyethylene (HDPE),” *Materials & Design*, **29**(6), pp. 1117–1124.

- [52] Muhammad, S., 2014, “Deformation and Fracture of Polymers with Work Hardening Behavior,” Ph.D., University of Alberta.
- [53] Zhang, Y., and Jar, P.-Y. B., 2015, “Phenomenological Modelling of Tensile Fracture in PE Pipe by Considering Damage Evolution,” *Materials & Design*, **77**, pp. 72–82.
- [54] Popelar, C. H., Kenner, V. H., and Wooster, J. P., 1991, “An Accelerated Method for Establishing the Long Term Performance of Polyethylene Gas Pipe Materials,” *Polymer Engineering & Science*, **31**(24), pp. 1693–1700.
- [55] Djoković, V., Kostoski, D., and Dramićanin, M. D., 2000, “Viscoelastic Behavior of Semicrystalline Polymers at Elevated Temperatures on the Basis of a Two-Process Model for Stress Relaxation,” *Journal of Polymer Science Part B: Polymer Physics*, **38**(24), pp. 3239–3246.
- [56] Ferry, J. D., 1980, *Viscoelastic Properties of Polymers*, John Wiley & Sons.
- [57] Andrews, J. M., and Ward, I. M., 1970, “The Cold-Drawing of High Density Polyethylene,” *J Mater Sci*, **5**(5), pp. 411–417.
- [58] Bigg, D. M., 1976, “A Review of Techniques for Processing Ultra-High Modulus Polymers,” *Polym Eng Sci*, **16**(11), pp. 725–734.
- [59] Barham, P. J., and Keller, A., 1976, “A Study on the Achievement of High-Modulus Polyethylene Fibres by Drawing,” *J Mater Sci*, **11**(1), pp. 27–35.
- [60] Lemaitre, J., 2012, *A Course on Damage Mechanics*, Springer Science & Business Media.
- [61] Hobeika, S., Men, Y., and Strobl, G., 2000, “Temperature and Strain Rate Independence of Critical Strains in Polyethylene and Poly(ethylene-Co-Vinyl Acetate),” *Macromolecules*, **33**(5), pp. 1827–1833.
- [62] Imada, K., Yamamoto, T., Shigematsu, K., and Takayanagi, M., 1971, “Crystal Orientation and Some Properties of Solid-State Extrudate of Linear Polyethylene,” *J Mater Sci*, **6**(6), pp. 537–546.
- [63] Gibson, A. G., Ward, I. M., Cole, B. N., and Parsons, B., 1974, “Hydrostatic Extrusion of Linear Polyethylene,” *J Mater Sci*, **9**(7), pp. 1193–1196.
- [64] Weeks, N., and Porter, R., 1974, “Mechanical-Properties of Ultra-Oriented Polyethylene,” *J. Polym. Sci. Pt. B-Polym. Phys.*, **12**(4), pp. 635–643.
- [65] Capaccio, G., and Ward, I. M., 1974, “Preparation of Ultra-High Modulus Linear Polyethylenes; Effect of Molecular Weight and Molecular Weight Distribution on Drawing Behaviour and Mechanical Properties,” *Polymer*, **15**(4), pp. 233–238.
- [66] Capiati, N., and Porter, R., 1975, “Tensile Properties of Ultradrawn Polyethylene,” *J. Polym. Sci. Pt. B-Polym. Phys.*, **13**(6), pp. 1177–1186.
- [67] Capaccio, G., and Ward, I., 1973, “Properties of Ultrahigh Modulus Linear Polyethylenes,” *Nature-Physical Science*, **243**(130), pp. 143–143.
- [68] Jar, P.-Y. B., 2015, “Deformation-Induced Change in Long-Term Mechanical Properties of Polyethylene (PE),” Lille, France.
- [69] Jiang, Z., Tang, Y., Rieger, J., Enderle, H.-F., Lilge, D., Roth, S. V., Gehrke, R., Heckmann, W., and Men, Y., 2010, “Two Lamellar to Fibrillar Transitions in the Tensile Deformation of High-Density Polyethylene,” *Macromolecules*, **43**(10), pp. 4727–4732.
- [70] Brooks, N. W. J., Duckett, R. A., and Ward, I. M., 1999, “Effects of Crystallinity and Stress State on the Yield Strain of Polyethylene,” *Polymer*, **40**(26), pp. 7367–7372.
- [71] Lemaitre, J., 1996, *A Course on Damage Mechanics*, Springer.
- [72] Zhang, Y., and Jar, P.-Y. B., 2015, “Quantitative Assessment of Deformation-Induced Damage in Polyethylene Pressure Pipe,” *Polymer Testing*, **47**, pp. 42–50.

- [73] DesLauriers, P. J., McDaniel, M. P., Rohlfing, D. C., Krishnaswamy, R. K., Secora, S. J., Benham, E. A., Maeger, P. L., Wolfe, A. r., Sukhadia, A. M., and Beaulieu, B. B., 2005, "A Comparative Study of Multimodal vs. Bimodal Polyethylene Pipe Resins for PE-100 Applications," *Polym Eng Sci*, **45**(9), pp. 1203–1213.
- [74] Popli, R., and Mandelkern, L., 1987, "Influence of Structural and Morphological Factors on the Mechanical Properties of the Polyethylenes," *Journal of Polymer Science Part B: Polymer Physics*, **25**(3), pp. 441–483.
- [75] Lu, X., Qian, R., and Brown, N., 1995, "The Effect of Crystallinity on Fracture and Yielding of Polyethylenes," *Polymer*, **36**(22), pp. 4239–4244.
- [76] Humbert, S., Lame, O., and Vigier, G., 2009, "Polyethylene Yielding Behaviour: What Is behind the Correlation between Yield Stress and Crystallinity?," *Polymer*, **50**(15), pp. 3755–3761.
- [77] Haward, R. N., 1993, "Strain Hardening of Thermoplastics," *Macromolecules*, **26**(22), pp. 5860–5869.
- [78] Haward, R. N., 2007, "Strain Hardening of High Density Polyethylene," *J. Polym. Sci. B Polym. Phys.*, **45**(9), pp. 1090–1099.

# Chapter 4

## **Phenomenological modelling of tensile fracture in PE pipe with the consideration of damage evolution**

Tensile fracture of polyethylene (PE) pipe in the hoop direction has been investigated using a phenomenon-based, hybrid approach of combining experimental testing and FE simulation. A modified D-split test was used for the experimental testing, at three crosshead speeds of 0.01, 1, and 100 mm/min. The test results were then used to establish the governing equation for the specimen deformation so that the FE model can regenerate the data obtained from the experimental testing. Two approaches were considered for the FE simulation, one with separate expressions for deformation and damage evolution, and the other without. Results from the FE simulation suggest that the former approach enables the FE model to simulate both large deformation and ductile fracture of the test, while the latter can only mimic the large deformation before the final stress drop. Although the expression established in this study is unlikely to be unique for the damage evolution, it provides a qualitative means to depict the damage evolution during the test. Using parameters in the expression for damage evolution as variables, with the stress-strain relationship fixed, the FE simulation provides results to characterize the influence of damage evolution rate on the load-stroke curve generated from the D-split test.

## 4.1 Introduction

Polyethylene (PE) has been widely used to replace steel, concrete and clay as pipe material for fluid transportation, due to PE's durability, reliability, relative low cost, and ease for construction and maintenance. Statistics suggests that PE pipe is now the main component for over 90% of newly installed natural gas systems [1,2]. In spite of the above advantages and popularity, however, unexpected, catastrophic failure of PE pipeline has been reported in Pakistan [3], Mexico [4], Kuwait [5], Brazil [6] and Malaysia [7], suggesting that blind spots still exist for characterizing the PE pipe. Moreover, experimental results have shown that degradation of mechanical properties can be caused by small deformation which may happen during installation and maintenance process, such as squeeze-off [8,9] which has been reported to lead to failure of PE pipe [10].

It is well established that majority of the PE pipe failures are attributed to a quasi-brittle fracture behavior known as slow crack growth (SCG) [11–13]. Current method to characterize resistance of PE pipe to SCG is based on a time-consuming hydrostatic rupture test that should be conducted using full-sized specimens at different temperatures and stress levels to collect data for extrapolation, as specified in EN ISO 9080:2012 [14]. To avoid the long duration involved in the hydrostatic rupture test various laboratory test methods, such as fully-notched creep test (FNCT) [15,16], the Pennsylvania edge-notched test (PENT) [17], notched pipe test (NPT) [18] and cracked round bar (CRB) test [19], have been developed to characterize the transition to the SCG development within a reasonable timeframe. However, because of the artificial notches that are required for the specimens used in the above laboratory test methods [9], the results cannot be used to determine the critical stress level for the SCG initiation and propagation. Therefore, new methods are desired which do not require any notch in the specimen, in order to

generate data for identifying mechanisms responsible for the pipe failure. Finite element (FE) method has been used to model pipe failure in the hydrostatic rupture test to estimate the failure time [20–22]. As a result, the main objective of this chapter is to establish constitutive equations and damage evolution laws that are needed to input into the FE model in order to accurately mimic the pipe failure behavior. It should be noted that environmental stress cracking resistance (ESCR) is another important pipe failure mechanism but is not considered in this chapter.

Many studies for developing new test methods have taken the approach of establishing constitutive models that consider nonlinear viscoelastic and viscoplastic properties of PE. These constitutive models can be grouped in two categories, i.e., phenomenological and physical models. One of the popular models in the former group, known as the BP model [23], was used to represent the elastic-viscoplastic strain hardening behaviour by separating the total deformation rate into elastic and plastic components. The BP model has been adopted by Frank and Brockman [24] to describe the mechanical behavior of glassy polymers, and modified by Zaïri et al. [25] for the nonlinear viscoplastic behavior of glassy polymers under isothermal loading.

Rheological models that are composed of springs and dashpots are usually adopted in modelling viscous behavior of semi-crystalline polymers, such as the extended Khan, Huang and Liang (KHL) model [26, 27] to include the standard linear solid spring-dashpot elements to mimic the deformation responses of polymeric materials [28]. Nonlinear mechanical behavior of high-density PE (HDPE) was modelled by Zhang and Moore [29] using the combination of a viscoelastic model of one independent spring and six Kelvin elements in series and a viscoplastic model based on Bodner's theory [23]. Viscoplasticity based on overstress (VBO) model, derived

from a unified state variable theory [30, 31], has been widely used to predict cyclic deformation behaviour of polymeric materials [32–34].

The physical models are based on the relationship between microstructure and mechanical properties. A one-dimensional model consisting of one Eyring dashpot to represent the intermolecular resistance and a Langevin spring to represent the entropic resistance was proposed to describe the stress-strain relationship of glassy thermoplastics [35]. This model was later expanded by Parks et al. [36] to represent the three-dimensional deformation, and further by Boyce et al. [37] to include the effect of deformation rate on the resistance to plastic deformation. A constitutive model to analyze the strain-induced crystallization in polymers has been proposed by Boyce et al. [38], and later extended by Ahzi et al. [39]. This model was recently used by Ayoub et al. [40] to simulate a large cyclic deformation behaviour of HDPE. A different approach for the physical models, based on chain network structure, has been developed to study deformation of rubbery polymers. Several examples, including 3-chain model by James and Guth [41], 4-chain model by Flory and Rehner [42], 8-chain model by Arruda and Boyce [43] and full-network model by Wu and van der Giessen [44], have been successfully used to simulate mechanical behavior of rubbery polymers. Among these models, the one by Arruda and Boyce was found to be most computationally efficient as it requires only two material constants for the model calibration.

For semi-crystalline polymers, modelling of damage and ductile fracture is usually based on the assumption that inter-lamellar micro-voids are responsible for the initiation of fracture [45, 46]. Most of the models for such fracture behavior adopt one of the following two approaches to develop the constitutive equation, i.e., continuum damage mechanics (CDM) or porous solid plasticity. CDM models originate from the work in [47], of which the basic assumption is to

treat damage as an internal variable that is embedded in the thermodynamics of an irreversible process. Various CDM models have been proposed, including ductile damage models [48–58], creep damage models [59–63] and damage models for fatigue fracture [64–68]. The models based on porous solid plasticity, also known as GTN models [69–72], are mainly used to analyze the damage phenomena in porous solids. Yield functions for the GTN models were originally developed by Gurson [69], and later modified and applied to void nucleation in pressure sensitive materials [73]. Application of the GTN models has been extended to void growth and coalescence in elasto-plastic deformation [74–76], in which variation of void shape is allowed to enhance the modelling capability.

The above damage models and their constitutive equations have been implemented in finite element (FE) simulation to allow the change in mechanical properties so that the deformation behavior observed from the mechanical testing can be regenerated using the FE simulation. It is worth mentioning that both CDM and GTN models have been successfully used to evaluate ductile fracture [77–81], but mainly for metallic materials. For polymeric materials, much fewer studies have been conducted. Sample works that we could find in literature that applied CDM or GTN models to fracture of polymeric materials are given in [82–84].

This chapter summarizes results from a hybrid, phenomenological approach, based on experimental testing and FE simulation, to model large deformation and ductile fracture of ring specimens prepared from a commercial PE pipe. The experimental testing adopted a modified D-split test method, from which data were applied to FE simulation to establish the governing equation for the deformation. In this study, two series of FE simulation were conducted, one with separate expressions for damage evolution and for the stress-strain relationship, and the other without. In this work, after verifying the feasibility of using the former series to mimic the

deformation and fracture behaviour obtained from the experimental testing, the FE model was then used as a virtual tool to investigate the effect of damage evolution rate on the deformation and fracture behavior of PE pipe specimen.

## **4.2 Experimental testing**

### **4.2.1 Specimens and test conditions**

Notched pipe ring (NPR) specimens modified from ASTM: D2290-12 [85] were used for the experimental testing, prepared from a commercial PE4710 Cell classification 445576C HDPE pipe, manufactured by Endot Industries. The resin used to manufacture the PE pipe is PE-100 and therefore the PE pipe meets the minimum required strength (MRS) of 10MPa specified in EN ISO standard 12162:2009 [86]. Inner diameter and nominal wall thickness of the PE pipe are 52.5mm and 5.84mm, respectively. The D-split tensile test, first proposed for characterizing the mechanical properties of composite materials [87–90], was adopted for the testing. For this study, notch tip of the NPR specimens was modified to have a flat profile, instead of round, so that stress distribution in the ligament region is relatively uniform. Schematic diagram of the D-split tensile test and dimensions of the modified NPR specimens are shown in Fig. 4.1. Note that ligament length for the modified NPR specimens was chosen to be 5.84 mm so that the aspect ratio of width to thickness in the ligament region is close to 1, in order to generate the same contraction rate in the width and thickness directions during the test.

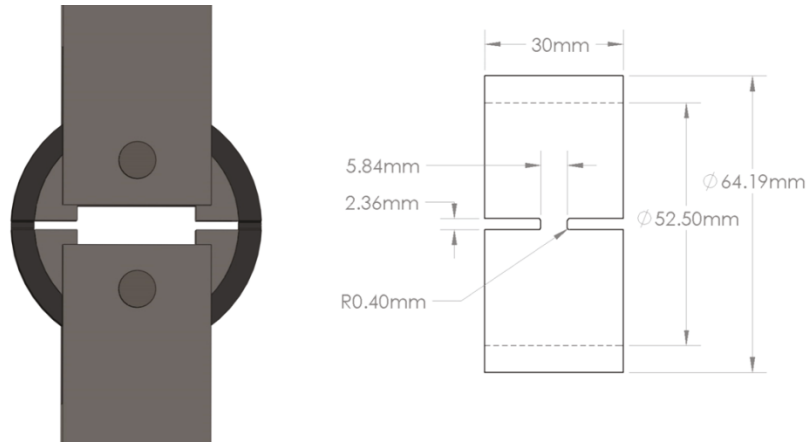


**Fig. 4.1** Schematic diagram of the D-split tensile test and dimensions of the modified NPR specimens

The experimental testing was conducted using a universal testing machine (QUASAR 100) at three crosshead speeds, 0.01, 1 and 100 mm/min, until one of the ligaments broke. Changes in load, stroke, and ligament length were recorded as functions of time. The test results showed excellent repeatability, except the stroke at break for which the scattering was possibly caused by defects (voids, foreign particles, etc.) that happened to be in the ligament region in some specimens. The scattering, however, did not affect the trend of change with the increase of crosshead speed from 0.01 to 100 mm/min.

A preliminary study has confirmed that the aspect ratio of the ligament cross section remained nearly constant during the test. Therefore, ligament length measured during the test was used to determine the change of ligament cross sectional area during the test, which was then used to verify the input to a finite element model for the simulation of the deformation behavior.

#### **4.2.2 Test results**

Typical curves of engineering stress versus stroke at the three crosshead speeds are presented in Fig. 4.2. The trend is similar to that reported in the literature [91], that is, yield stress

increases, but stroke at break decreases, with the increase of the crosshead speed. Note that localised deformation (necking) did not occur in any of the specimens, possibly due to the short ligament height of 2.36 mm (Fig. 4.1) that was insufficient to accommodate the neck development.

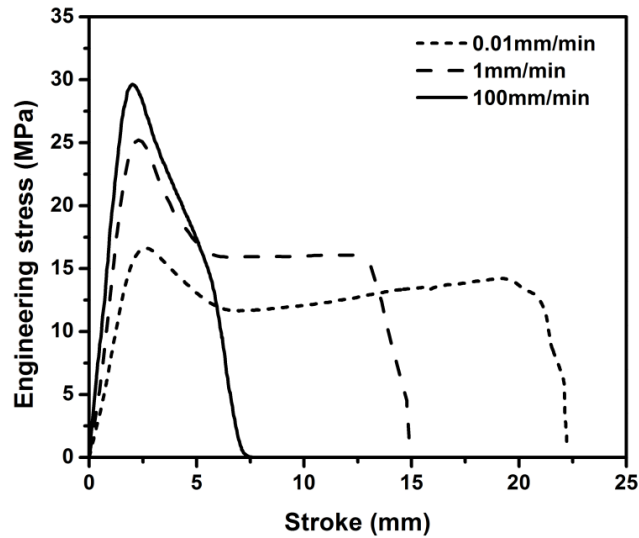


**Fig. 4.2** Typical curves of engineering stress versus stroke at different crosshead speeds

Damage evolution during the deformation was characterized using damage variable  $D$  which based on the concept of continuum damage mechanics (CDM), is defined as:

$$D = 1 - \frac{E_D}{E_0} \quad (4.1)$$

where  $E_D$  is the elastic modulus for the damaged specimen and  $E_0$  the elastic modulus for the virgin specimen. Some studies have measured the change of  $E_D$  by introducing unloading periodically during the test [92–94]. However, HDPE is known to have a strong viscous component in the stress-strain relationship, which results in a significant load drop immediately at the end of the loading phase [40, 97]. The preliminary results from our experimental testing

showed that the unloading curve for the modified NPR specimens is highly nonlinear and the amount of load drop at the end of the loading phase affects the unloading curve profile. Therefore, value for  $E_D$  determined from the unloading curve is strongly dependent on the crosshead speed used for the testing and location selected in the unloading curve for the calculation. Because of these factors, decrease of the  $E_D$  value from the unloading curve may not reflect the damage development. As a result, rather than choosing an arbitrarily condition to determine  $E_D$  from the unloading curve, we decided to treat  $D$  as an intrinsic variable which is governed by a phenomenological damage law based on a one-term exponential function [93], as given below.

$$D = A \left[ 1 - \exp(-B\varepsilon_p) \right] \quad (4.2)$$

where  $\varepsilon_p$  is the plastic strain, and  $A$  and  $B$  the user-defined constants. In this study, values for  $A$  and  $B$  were determined through the FE simulation so that data from the experimental testing can be regenerated by the FE model. Details of the simulation procedure are given in the next section.

### 4.3 Finite element simulation

#### 4.3.1 The FE model

A three-dimensional FE model of the modified NPR specimen was developed using ABAQUS/Explicit (Version 6.12-2). The model consists of half of the NPR specimen and the corresponding D-shaped loading blocks inside the NPR. The former, as shown in Fig. 4.3(a), has 34860 elements (C3D8R) of the first-order, following the suggestion given in [96]. The D-shaped loading block, not shown in Fig. 4.3(a), are modelled as analytical rigid body. Fig. 4.3(b)

depicts a deformation behavior generated from the FE simulation, and Fig. 4.3(c) a typical deformed specimen from the experiment.

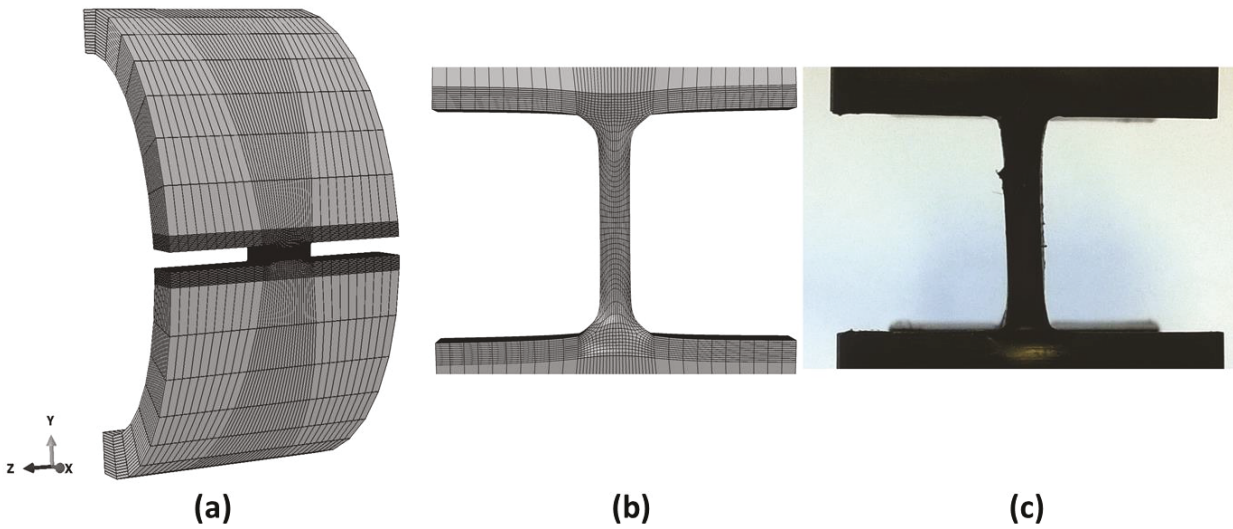


**Fig. 4.3** FE model of the modified NPR specimen: (a) mesh pattern, (b) deformation from the FE model and (c) deformation from the experimental testing

Two series of FE simulation were conducted in the study. In the first series, deformation of the FE model was governed only by the input stress-strain relationship, but in the second series, the deformation was also governed by an explicit expression for the damage evolution. Both series used a tabular format for the material input, which consisted of more than two thousands discrete points.

It should be noted that the version of ABAQUS used in this study does not allow the FE simulation to consider both creep deformation and damage evolution. Therefore, time involved in the simulation was set to be very short (around 1s), in order to avoid any requirement of considering the viscous properties of PE for the model deformation.

### 4.3.2 The first series of FE simulation

The first series of FE simulation followed the framework described in [97–99], that is, based on the following constitutive equation for the stress-strain relationship and without any explicit expression for the damage evolution.

$$\sigma(\varepsilon) = \begin{cases} \frac{3}{2(1+\nu)} E\varepsilon & \varepsilon \leq \varepsilon_y \quad (\text{a}) \\ d \left\{ [a(\varepsilon+b)]^{(c-1)} - [a(\varepsilon+b)]^{(-c)} \right\} + e & \varepsilon_y \leq \varepsilon \leq \varepsilon_n \quad (\text{b}) \\ \alpha k \varepsilon^N & \varepsilon_n \leq \varepsilon \leq \varepsilon_t \quad (\text{c}) \\ k \exp(M\varepsilon^\beta) & \varepsilon \geq \varepsilon_t \quad (\text{d}) \end{cases} \quad (4.3)$$

where  $\sigma$  and  $\varepsilon$  are equivalent stress and equivalent strain, respectively,  $\varepsilon_y$  the transitional strain from linear to nonlinear deformation,  $\varepsilon_n$  the critical strain for the on-set of necking, and  $\varepsilon_t$  the strain at the beginning of the exponential hardening. The other parameters (a, b, c, d, e,  $\alpha k$ , N and M) are user-defined variables for which the values were determined in an iterative process until variations of engineering stress and ligament cross sectional area as functions of stroke from the FE simulation matched those from the experimental testing. Details of the iterative process are described in [98].

It should be noted that although damage evolution was not explicitly considered in the first series of FE simulation, values determined for parameters in Eq. (4.3) have actually included the influence from the damage evolution.

Fig. 4.4 presents results from the first series of FE simulation (open circles), compared with data from the experimental testing (solid line) at all three crosshead speeds used in the study.

The figure clearly shows that good match can be achieved using Eq. (4.3) alone, without any explicit consideration of the damage evolution, except for the stress drop before the final fracture, as illustrated in Fig. 4.4(c) at the crosshead speed of 1 mm/min. Similar phenomena were also observed for the other two crosshead speeds.

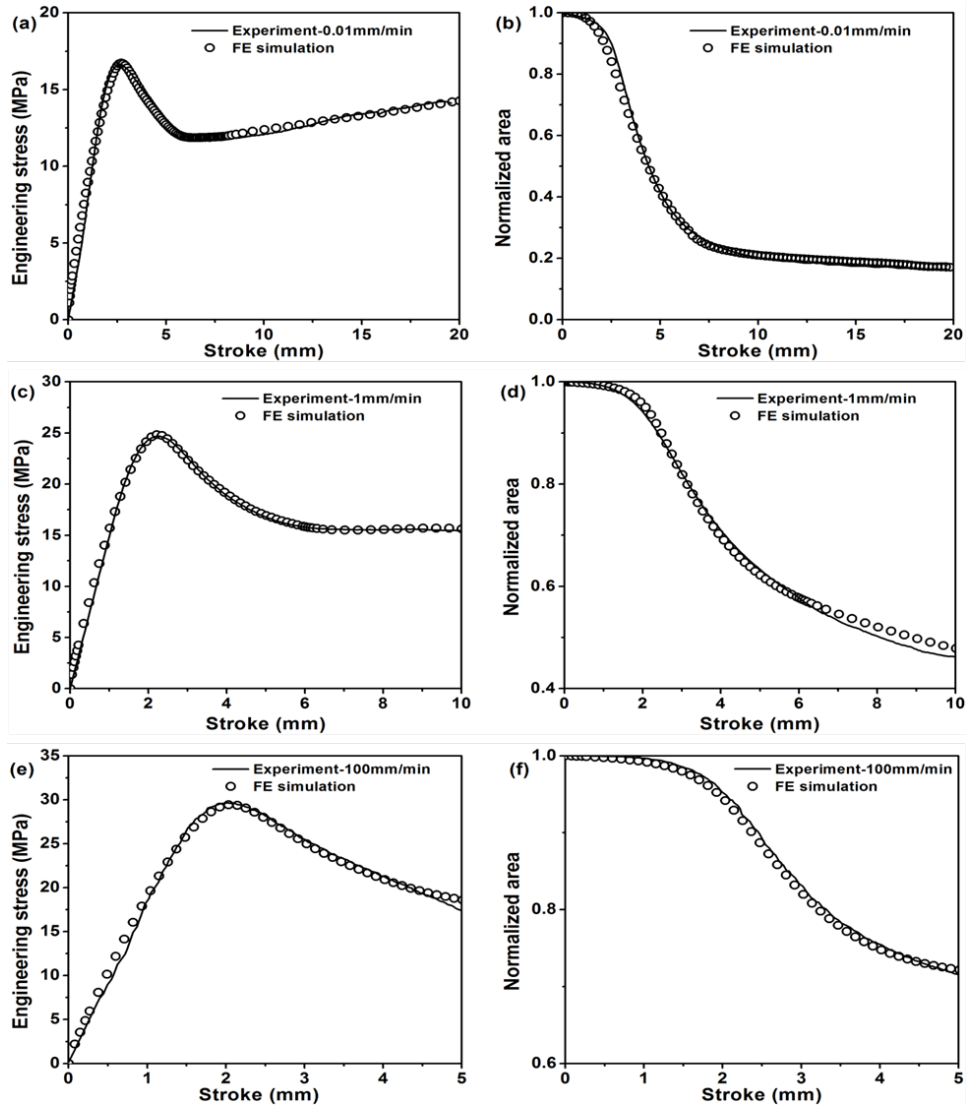


**Fig. 4.4** Comparison between the first series of FE simulation and the experimental testing at all three crosshead speeds: (a) engineering stress versus stroke at 0.01 mm/min, (b) normalized ligament area versus stroke at 0.01 mm/min, (c) engineering stress versus stroke at 100mm/min

Fig. 4.5 summarizes the stress-strain relationship used for the FE model in the first series of FE simulation, in order to produce the data shown in Fig. 4.4. Values for the parameters in Eq. (4.3) and the corresponding strain ranges for each of the three crosshead speeds are given in Tables 4.1 and 4.2, respectively. Fig. 4.5 indicates that the initial yielding stress increases with the increase of the crosshead speed, but the trend for the strain hardening rate at the strain level above 1.5 is opposite.

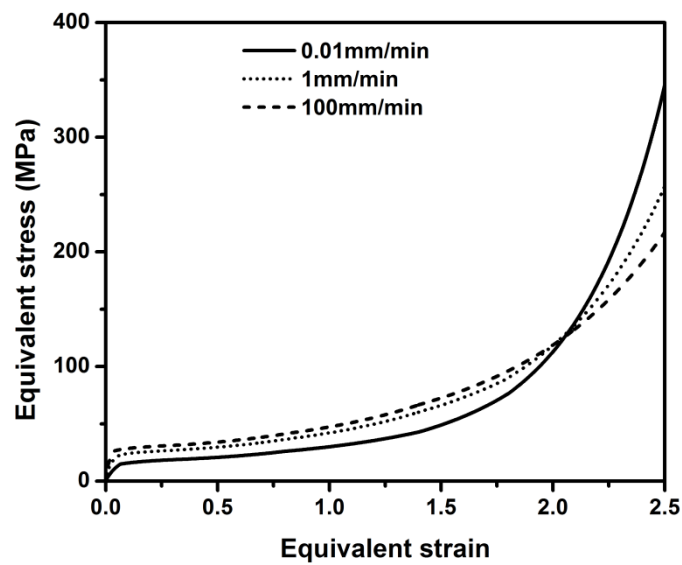


**Fig. 4.5** Curves of equivalent stress versus equivalent strain established from the first series of FE simulation

**Table 4.1** Values for parameters in Eq. (4.3) determined from the first series of FE simulation

FE model		Notched pipe ring specimen			
		Crosshead speed			
		0.01mm/min	1mm/min	100mm/min	
Equation (4.3a)	E	864	880	885	
	v	0.35	0.35	0.35	
Equation (4.3b)	a	6.3	20	32	
	b	0.0889	0.0260	0.0186	
	c	0.09	0.141	0.002	
	d	-23.8	-23.8	-23.8	
	e	15.5	15.5	15.5	
Equation (4.3c)	$\alpha k$	22.4	30.4	34.3	
	N	0.15	0.1	0.08	
Equation (4.3d)	Section 1	$K_1$	17.5	25.4	29.5
		$M_1$	0.59	0.54	0.50
		$\beta_1$	1.8	1.8	1.8
	Section 2	$K_2$	19.5	27.4	31.4
		$M_2$	0.43	0.43	0.41
		$\beta_2$	1.8	1.8	1.8
	Section 3	$K_3$	15.7	30.1	35.1
		$M_3$	0.55	0.38	0.35
		$\beta_3$	1.8	1.8	1.8
	Section 4	$K_4$	11.7	24.7	27.1
		$M_4$	0.65	0.45	0.45
		$\beta_4$	1.8	1.8	1.8
	Section 5	$K_5$	13.0	24.7	27.1
		$M_5$	0.6	0.45	0.45
		$\beta_5$	1.8	1.8	1.8

**Table 4.2** Strain ranges for Eq. (4.3) used in the first series of FE simulation

FE model		Notched pipe ring specimen		
Crosshead speed		0.01mm/min	1mm/min	100mm/min
Equation (4.3a)		0-0.0005	0-0.0005	0-0.0005
Equation (4.3b)		0.0005-0.065	0.0005-0.065	0.0005-0.04
Equation (4.3c)		0.065-0.3	0.065-0.3	0.04-0.3
Equation (4.3d)	Section 1	0.3-0.8	0.3-0.8	0.3-0.8
	Section 2	0.8-1.4	0.8-1.4	0.8-1.4
	Section 3	1.4-1.8	1.4-1.8	1.4-1.8
	Section 4	1.8-2.0	1.8-2.0	1.8-2.0
	Section 5	2.0-2.5	2.0-2.5	2.0-2.5

#### 4.3.3 The second series of FE simulation

For the second series of FE simulation, in addition to the use of Eq. (4.3) to govern the stress-strain relationship, Eq. (4.2) was used for the damage evolution. Ideally, Eq. (4.3) is to represent the damage-free stress-strain relationship and Eq. (4.2) for all changes in mechanical properties due to the presence of damage. However, at this stage no data are available to quantify the change in mechanical properties purely due to the damage. Therefore, the second series of FE simulation was simply to ensure that the FE model based on Eq. (4.2) and (4.3) can regenerate the results obtained experimentally. For this purpose, two additional pieces of information are needed to mimic the deformation and fracture behavior of the modified NRP specimens: (a) criterion for the onset of damage, and (b) critical damage level ( $D_C$ ) for the element failure. Following the suggestion given in [100, 101], damage was assumed to start at the yield point during the loading phase, that is, when the equivalent strain reached  $\varepsilon_n$ . For the  $D_C$  value, Lemaitre's damage model [48] has suggested that material is fully damaged when  $D$  reaches 1.

However, experimental studies [49, 102, 103] have suggested that the final fracture may occur before  $D$  reaches 1. After several attempts in our preliminary study to mimic the experimental results, it was decided that  $D_C$  value can be fixed at 0.8 for all crosshead speeds to mimic the onset of fracture observed in the study.

The iterative process to determine the values for the user-defined parameters in Eq. (4.2) and (4.3) in the second series was similar to that used in the first series of FE simulation, i.e., until variations of engineering stress and normalized cross sectional area generated from the FE model matched those from the experimental testing. However, in the second series of FE simulation, the iterative process used to match the engineering stress-stroke curve included the consideration of the curve section during the final stage of the test, i.e., the final load drop with the increase of the stroke before the specimen fracture.

Fig. 4.6 compares results from the second series of FE simulation (open circles) with those from the experimental testing (solid line). The figure suggests that with the consideration of damage evolution, even based on a simple one-term exponential function to express the variation of  $D$  during the test, the curve profile for the engineering stress drop in the final stage of the D-split test can be regenerated by the FE model.

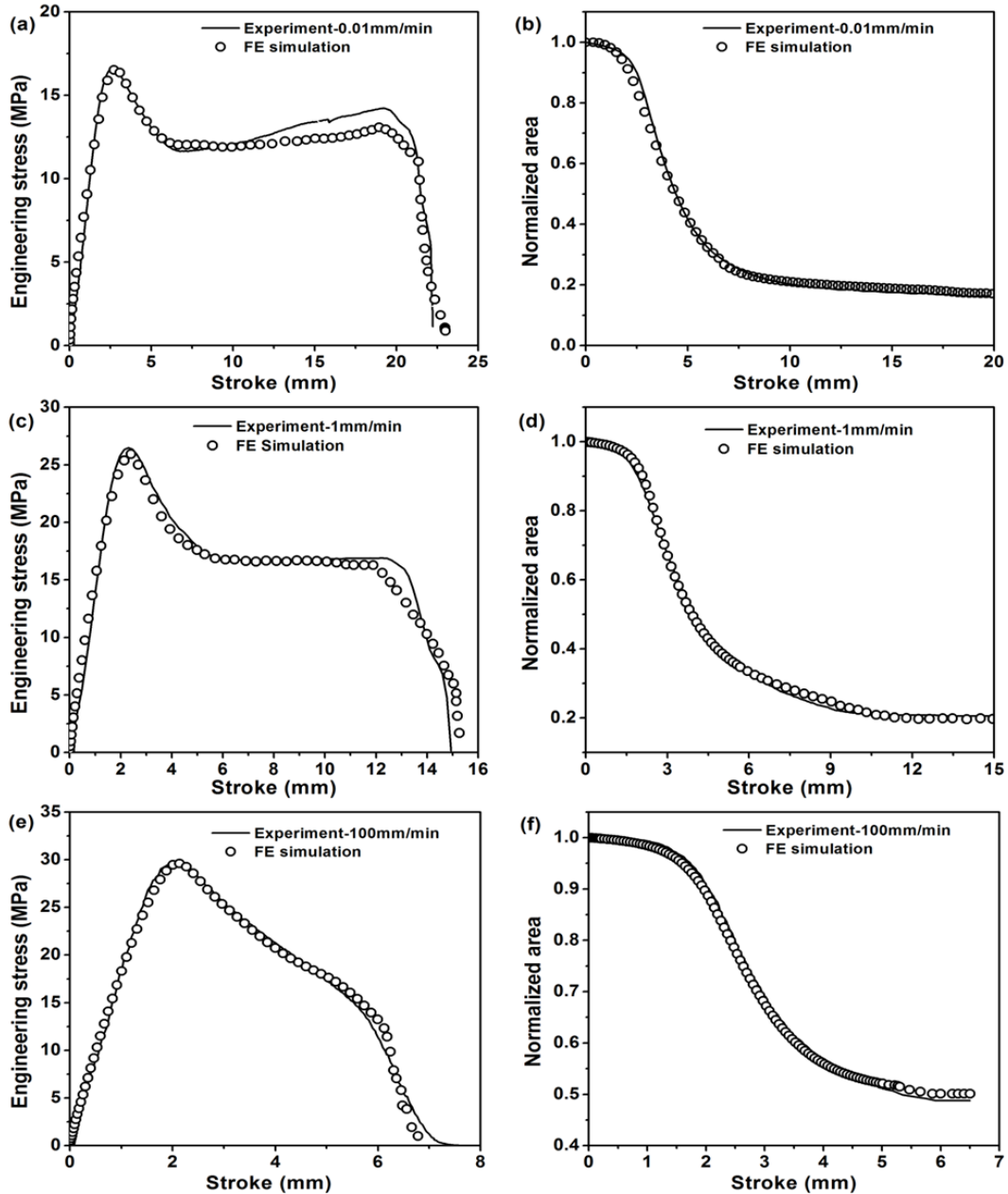


**Fig. 4.6** Comparison of results from the second series of FE simulation with those from the experimental testing: (a) engineering stress at 0.01 mm/min, (b) normalized ligament area at 0.01 mm/min, (c) engineering stress at 1 mm/min, (d) normalized ligament area at 1 mm/min, (e) engineering stress at 100 mm/min, and (f) normalized ligament area at 100 mm/min

The stress-strain relationship and damage evolution determined from the second series of FE simulation are presented in Fig. 4.7(a) and 7(b), respectively, and the corresponding values for

the parameters in Eq. (4.3) listed in Table 4.3, Eq. (4.3) in Table 4.4, and the strain range for Eq. (4.2) in Table 4.5.

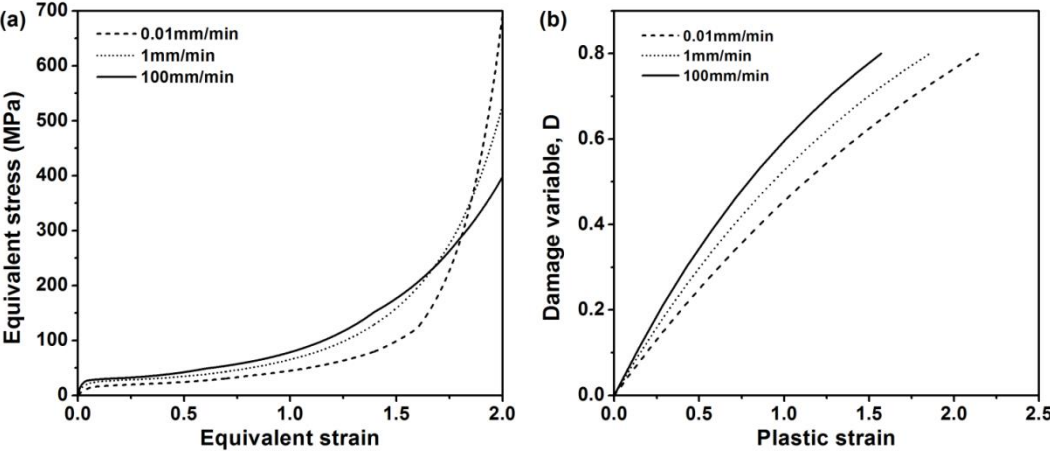


**Fig. 4.7** Input for the second series of FE simulation: (a) equivalent stress versus equivalent strain, and (b) the damage evolution with the increase of the plastic strain

**Table 4.3** Values for parameters in Eq. (4.3) used in the second series of FE simulation

FE model		Notched pipe ring specimen		
Crosshead speed		0.01mm/min	1mm/min	100mm/min
Equation (4.3a)	E	864	880	885
	v	0.35	0.35	0.35
Equation (4.3b)	a	6.3	20	32
	b	0.0889	0.02598	0.01861
	c	0.09	0.141	0.002
	d	-23.8	-23.8	-23.8
	e	15.5	15.5	15.5
	$\alpha k$	25.7	35.8	36.51
Equation (4.3c)	N	0.2	0.16	0.1
Section 1	$K_1$	18.1	26.25	28.92
	$M_1$	1	0.95	1.3
	$\beta_1$	1.8	1.8	1.8
Section 2	$K_2$	22.2	28.41	35.25
	$M_2$	0.7	0.83	0.8
	$\beta_2$	1.8	1.8	1.8
Section 3	$K_3$	16.9	28.36	50.8
	$M_3$	0.85	0.83	0.6
	$\beta_3$	1.8	1.8	1.8
Section 4	$K_4$	3.73	24.6	58.6
	$M_4$	1.5	0.88	0.55
	$\beta_4$	1.8	1.8	1.8
Section 5	$K_5$	64.7	13.11	24.5
	$M_5$	0.8	1.06	0.8
	$\beta_5$	1.8	1.8	1.8

**Table 4.4** Strain ranges used for Eq. (4.3) in the second series of FE simulation

FE model	Notched pipe ring (NPR) specimen			
	Crosshead speed	0.01mm/min	1mm/min	100mm/min
Equation (4.3a)		0-0.0005	0-0.0005	0-0.0005
Equation (4.3b)		0.0005-0.065	0.0005-0.065	0.0005-0.04
Equation (4.3c)		0.065-0.3	0.065-0.2	0.04-0.15
Equation (4.3d)	Section 1	0.3-0.8	0.2-0.8	0.15-0.6
	Section 2	0.8-1.4	0.8-1.4	0.6-1.4
	Section 3	1.4-1.6	1.4-1.8	1.4-1.8
	Section 4	1.6-2.5	1.8-2	1.8-2.0
	Section 5	2.5-3.0	2.0-2.5	2.0-2.5

**Table 4.5** Values for parameters in Eq. (4.2) for the second series of FE simulation

FE model	Notched pipe ring (NPR) specimen			
	Crosshead speed	0.01mm/min	1mm/min	100mm/min
<i>A</i>		1.78709	1.58198	1.58198
<i>B</i>		1.09333	1.53846	1.81818

#### 4.3.4 Rate of damage evolution

Although the second series of FE simulation gives an explicit consideration for the damage evolution during the test and as shown in Fig. 4.7(b), suggests that the rate of damage evolution increases with the increase of the crosshead speed, these results do not show clearly whether the changing rate of damage increase is responsible for the change of the flow stress section shown in Fig. 4.2, that is, from a positive slope for the crosshead speed of 0.01 mm/min to a negative slope for 100 mm/min.

To further investigate the above issue, the FE model with an explicit expression for the damage evolution, based on Eq. (4.2), was used to investigate the influence of the damage increase rate on the change of the flow stress slope. For this part of the FE simulation, the stress-strain relationship is based on the curve for the crosshead speed of 0.01 mm/min in Fig. 4.7(a) and the  $D_C$  value 0.8. Five damage evolution curves, as shown in Fig. 4.8(a), were considered, in which curve #4 is same as that for the crosshead speed of 0.01 mm/min in Fig. 4.7(b) and curve #3 very close to that for 100 mm/min. The curves of engineering stress versus stroke generated from the FE model are presented in Fig. 4.8(b). The number next to each curve indicates the damage evolution law from Fig. 4.8(a) for the FE simulation. Fig. 4.8(b) clearly shows that with the increase of the damage evolution rate, the flow stress after yielding and the maximum stroke before break decrease. The figure also shows that with a sufficiently high damage evolution rate, i.e., #1 in Fig. 4.8(a), specimen with a stress-strain relationship same as that for the crosshead speed of 0.01 mm/min can fracture before the flow stress in the engineering stress-stroke curve is fully developed, similar to the phenomenon shown in Fig. 4.2 for the crosshead speed of 100 mm/min.

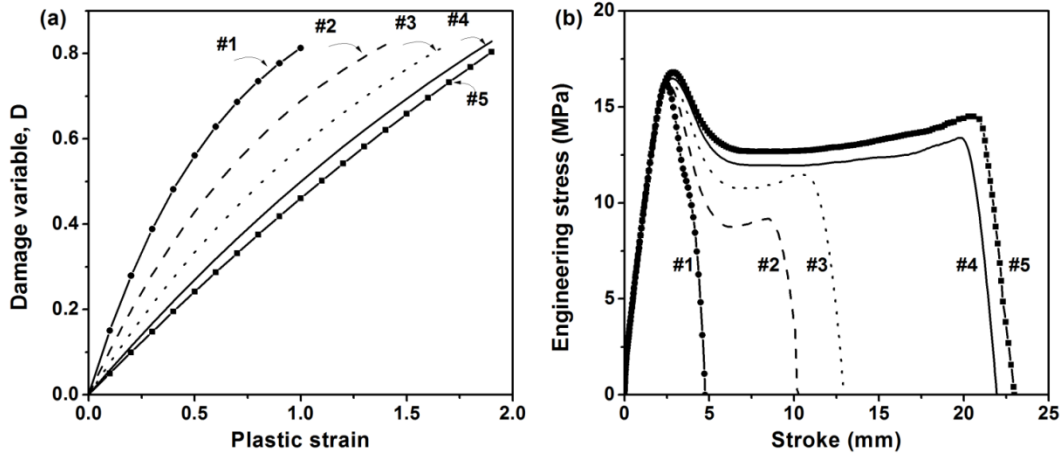


**Fig. 4.8 (a)** Damage evolution laws considered for the FE simulation, and (b) the corresponding curves of engineering stress versus stroke generated from the FE model, based on the stress-strain relationship shown in Fig. 7(a) for 0.01 mm/min

#### 4.4 Conclusions

A phenomenological approach based on experimental testing and FE simulation has been used to investigate large deformation and fracture behavior of modified NPR specimens of HDPE. The results show that through the combination of a phenomenological constitutive equation and an empirical ductile damage model, the FE simulation can successfully regenerate the deformation and fracture behavior observed from the experimental testing. Good agreement between the second series of FE simulation and the experimental testing demonstrates the effectiveness of considering damage evolution for the simulation of large deformation and fracture behavior of HDPE. Results from the FE simulation also indicate that the increase of the damage evolution rate reduces the maximum elongation before fracture. Similarity in the trend of change between Fig. 4.8(b) and Fig. 4.2 suggests that the increase of the crosshead speed has caused the increase of the damage evolution rate, resulting in a significant change of the maximum elongation in the D-split test.

## References

- [1] Krishnaswamy, R. K., 2005, “Analysis of Ductile and Brittle Failures from Creep Rupture Testing of High-Density Polyethylene (HDPE) Pipes,” *Polymer*, **46**(25), pp. 11664–11672.
- [2] Kiass, N., Khelif, R., Boulanouar, L., and Chaoui, K., 2005, “Experimental Approach to Mechanical Property Variability through a High-Density Polyethylene Gas Pipe Wall,” *J. Appl. Polym. Sci.*, **97**(1), pp. 272–281.
- [3] Hasan, F., Iqbal, J., and Ahmed, F., 2007, “Stress Corrosion Failure of High-Pressure Gas Pipeline,” *Engineering Failure Analysis*, **14**(5), pp. 801–809.
- [4] Hernández-Rodríguez, M. A. L., Martínez-Delgado, D., González, R., Pérez Unzueta, A., Mercado-Solís, R. D., and Rodríguez, J., 2007, “Corrosive Wear Failure Analysis in a Natural Gas Pipeline,” *Wear*, **263**(1–6), pp. 567–571.
- [5] Shalaby, H. M., Riad, W. T., Alhazza, A. A., and Behbehani, M. H., 2006, “Failure Analysis of Fuel Supply Pipeline,” *Engineering Failure Analysis*, **13**(5), pp. 789–796.
- [6] Azevedo, C. R. F., 2007, “Failure Analysis of a Crude Oil Pipeline,” *Engineering Failure Analysis*, **14**(6), pp. 978–994.
- [7] Majid, Z. A., Mohsin, R., Yaacob, Z., and Hassan, Z., 2010, “Failure Analysis of Natural Gas Pipes,” *Engineering Failure Analysis*, **17**(4), pp. 818–837.
- [8] Jar, P. B., 2014, “Degradation of Mechanical Properties for Polyethylene by Small-Deformation Damage,” *ASME 2014 Pressure Vessels and Piping Conference*, American Society of Mechanical Engineers, p. V06BT06A040–V06BT06A040.
- [9] Ben Jar, P.-Y., 2014, “Transition of Neck Appearance in Polyethylene and Effect of the Associated Strain Rate on the Damage Generation,” *Polym Eng Sci*, **54**(8), pp. 1871–1878.
- [10] Brown, N., and Crate, J. M., 2012, “Analysis of a Failure in a Polyethylene Gas Pipe Caused by Squeeze off Resulting in an Explosion,” *J Fail. Anal. and Preven.*, **12**(1), pp. 30–36.
- [11] Barker, M. B., Bowman, J., and Bevis, M., 1983, “The Performance and Causes of Failure of Polyethylene Pipes Subjected to Constant and Fluctuating Internal Pressure Loadings,” *J Mater Sci*, **18**(4), pp. 1095–1118.
- [12] Lang, R. W., Stern, A., and Doerner, G., 1997, “Applicability and Limitations of Current Lifetime Prediction Models for Thermoplastics Pipes under Internal Pressure,” *Angewandte Makromolekulare Chemie*, **247**, pp. 131–145.
- [13] Adib, A., Domínguez, C., Rodríguez, J., Martín, C., and García, R. A., 2015, “The Effect of Microstructure on the Slow Crack Growth Resistance in Polyethylene Resins,” *Polymer Engineering & Science*, **55**(5), pp. 1018–1023.
- [14] ISO 9080., 2012, “Plastics Piping and Ducting Systems-Determination of the Long-Term Hydrostatic Strength of Thermoplastics Materials in Pipe Form by Extrapolation.”
- [15] ISO 16770., 2004, “Plastics-Determination of Environmental Stress Cracking (ESC) on Polyethylene (PE) – Full Notch Creep Test (FNCT).”
- [16] Fleissner, M., 1998, “Experience with a Full Notch Creep Test in Determining the Stress Crack Performance of Polyethylenes,” *Polymer Engineering & Science*, **38**(2), pp. 330–340.
- [17] ISO 16241., “Notched Tensile Test to Measure the Resistance to Slow Crack Growth of Polyethylene Materials for Pipe and Fitting Products (PENT).”

- [18] ISO 13479., 2009, “Polyolefin in Pipes for the Conveyance of Fluids-Determination of Resistance to Slow Crack Growth on Notched Pipes.”
- [19] Frank, A., and Pinter, G., 2014, “Evaluation of the Applicability of the Cracked Round Bar Test as Standardized PE-Pipe Ranking Tool,” *Polymer Testing*, **33**, pp. 161–171.
- [20] Drozdov, A. D., and Christiansen, J. deC., 2009, “Creep Failure of Polypropylene: Experiments and Constitutive Modeling,” *Int J Fract*, **159**(1), pp. 63–79.
- [21] Hyde, T. H., Sun, W., and Williams, J. A., 2002, “Life Estimation of Pressurised Pipe Bends Using Steady-State Creep Reference Rupture Stresses,” *International Journal of Pressure Vessels and Piping*, **79**(12), pp. 799–805.
- [22] Rouse, J. P., Sun, W., Hyde, T. H., and Morris, A., 2013, “Comparative Assessment of Several Creep Damage Models for Use in Life Prediction,” *International Journal of Pressure Vessels and Piping*, **108–109**, pp. 81–87.
- [23] Bodner, S. R., and Partom, Y., 1975, “Constitutive Equations for Elastic-Viscoplastic Strain-Hardening Materials,” *Journal of Applied Mechanics*, **42**(2), pp. 385–389.
- [24] Frank, G. J., and Brockman, R. A., 2001, “A Viscoelastic–viscoplastic Constitutive Model for Glassy Polymers,” *International Journal of Solids and Structures*, **38**(30–31), pp. 5149–5164.
- [25] Zairi, F., Woznica, K., Gloaguen, J.-M., and Naït-Abdelaziz, M., 2007, “Elasto-Viscoplastic Constitutive Equations for the Description of Glassy Polymers Behavior at Constant Strain Rate,” *Journal of Engineering Materials and Technology*, **129**(1), pp. 29–35.
- [26] Khan, A. S., and Liang, R., 1999, “Behaviors of Three BCC Metal over a Wide Range of Strain Rates and Temperatures: Experiments and Modeling,” *International Journal of Plasticity*, **15**(10), pp. 1089–1109.
- [27] Khan, A. S., Sung Suh, Y., and Kazmi, R., 2004, “Quasi-Static and Dynamic Loading Responses and Constitutive Modeling of Titanium Alloys,” *International Journal of Plasticity*, **20**(12), pp. 2233–2248.
- [28] Khan, A., and Zhang, H., 2001, “Finite Deformation of a Polymer: Experiments and Modeling,” *International Journal of Plasticity*, **17**(9), pp. 1167–1188.
- [29] Zhang, C., and Moore, I. D., 1997, “Nonlinear Mechanical Response of High Density Polyethylene. Part II: Uniaxial Constitutive Modeling,” *Polym Eng Sci*, **37**(2), pp. 414–420.
- [30] Krempl, E., 1998, “Some General Properties of Solid Polymer Inelastic Deformation Behavior and Their Application to a Class of Clock Models,” *Journal of Rheology* (1978-present), **42**(4), pp. 713–725.
- [31] Colak, O. U., and Krempl, E., 2003, “Modeling of Uniaxial and Biaxial Ratcheting Behavior of 1026 Carbon Steel Using the Simplified Viscoplasticity Theory Based on Overstress (VBO),” *Acta Mechanica*, **160**(1–2), pp. 27–44.
- [32] Colak, O. U., and Dusunceli, N., 2006, “Modeling Viscoelastic and Viscoplastic Behavior of High Density Polyethylene (HDPE),” *Journal of Engineering Materials and Technology*, **128**(4), pp. 572–578.
- [33] Colak, O. U., 2005, “Modeling Deformation Behavior of Polymers with Viscoplasticity Theory Based on Overstress,” *International Journal of Plasticity*, **21**(1), pp. 145–160.
- [34] Ho, K., and Krempl, E., 2002, “Extension of the Viscoplasticity Theory Based on Overstress (VBO) to Capture Non-Standard Rate Dependence in Solids,” *International Journal of Plasticity*, **18**(7), pp. 851–872.

- [35] Haward, R. N., and Thackray, G., 1968, "The Use of a Mathematical Model to Describe Isothermal Stress-Strain Curves in Glassy Thermoplastics," *Proc. R. Soc. Lond. A*, **302**(1471), pp. 453–472.
- [36] DM Parks, AS Argon, and B Bagepalli, 1984, "Large Elastic-Plastic Deformation of Glassy Polymers," *Program in Polymer Science and Technology*.
- [37] Boyce, M. C., Parks, D. M., and Argon, A. S., 1988, "Large Inelastic Deformation of Glassy Polymers. Part I: Rate Dependent Constitutive Model," *Mechanics of Materials*, **7**(1), pp. 15–33.
- [38] Boyce, M. C., Socrate, S., and Llana, P. G., 2000, "Constitutive Model for the Finite Deformation Stress-strain Behavior of Poly(ethylene Terephthalate) above the Glass Transition," *Polymer*, **41**(6), pp. 2183–2201.
- [39] Ahzi, S., Makradi, A., Gregory, R. V., and Edie, D. D., 2003, "Modeling of Deformation Behavior and Strain-Induced Crystallization in Poly(ethylene Terephthalate) above the Glass Transition Temperature," *Mechanics of Materials*, **35**(12), pp. 1139–1148.
- [40] Ayoub, G., Zaïri, F., Naït-Abdelaziz, M., and Gloaguen, J. M., 2010, "Modelling Large Deformation Behaviour under Loading-unloading of Semicrystalline Polymers: Application to a High Density Polyethylene," *International Journal of Plasticity*, **26**(3), pp. 329–347.
- [41] James, H. M., and Guth, E., 1943, "Theory of the Elastic Properties of Rubber," *The Journal of Chemical Physics*, **11**(10), pp. 455–481.
- [42] Flory, P. J., and Jr, J. R., 1943, "Statistical Mechanics of Cross-Linked Polymer Networks I. Rubberlike Elasticity," *The Journal of Chemical Physics*, **11**(11), pp. 512–520.
- [43] Arruda, E. M., and Boyce, M. C., 1993, "A Three-Dimensional Constitutive Model for the Large Stretch Behavior of Rubber Elastic Materials," *Journal of the Mechanics and Physics of Solids*, **41**(2), pp. 389–412.
- [44] Wu, P. D., and Van Der Giessen, E., 1993, "On Improved Network Models for Rubber Elasticity and Their Applications to Orientation Hardening in Glassy Polymers," *Journal of the Mechanics and Physics of Solids*, **41**(3), pp. 427–456.
- [45] McClintock, F. A., 1968, "A Criterion for Ductile Fracture by the Growth of Holes," *J. Appl. Mech.*, **35**(2), pp. 363–371.
- [46] Rice, J. R., and Tracey, D. M., 1969, "On the Ductile Enlargement of Voids in Triaxial Stress Fields," *Journal of the Mechanics and Physics of Solids*, **17**(3), pp. 201–217.
- [47] Kachanov, L. M., 1958, "Time of the Rupture Process under Creep Conditions," *Isv. Akad. Nauk. SSR. Otd Tekh. Nauk*, **8**, pp. 26–31.
- [48] Lemaitre, J., 1985, "A Continuous Damage Mechanics Model for Ductile Fracture," *Journal of Engineering Materials and Technology*, **107**(1), pp. 83–89.
- [49] Alvarado-Contreras, J. A., Polak, M. A., and Penlidis, A., 2010, "Constitutive Modeling of Damage Evolution in Semicrystalline Polyethylene," *Journal of Engineering Materials and Technology*, **132**(4), p. 041009.
- [50] Khelifa, M., Oudjene, M., and Khennane, A., 2007, "Fracture in Sheet Metal Forming: Effect of Ductile Damage Evolution," *Computers & Structures*, **85**(3–4), pp. 205–212.
- [51] Cao, T.-S., Gaillac, A., Montmitonnet, P., and Bouchard, P.-O., 2013, "Identification Methodology and Comparison of Phenomenological Ductile Damage Models via Hybrid Numerical-experimental Analysis of Fracture Experiments Conducted on a Zirconium Alloy," *International Journal of Solids and Structures*, **50**(24), pp. 3984–3999.

- [52] Cao, T.-S., Gachet, J.-M., Montmitonnet, P., and Bouchard, P.-O., 2014, “A Lode-Dependent Enhanced Lemaitre Model for Ductile Fracture Prediction at Low Stress Triaxiality,” *Engineering Fracture Mechanics*, **124–125**, pp. 80–96.
- [53] Mashayekhi, M., and Ziaei-Rad, S., 2006, “Identification and Validation of a Ductile Damage Model for A533 Steel,” *Journal of Materials Processing Technology*, **177(1–3)**, pp. 291–295.
- [54] Xue, L., 2007, “Ductile Fracture Modeling : Theory, Experimental Investigation and Numerical Verification,” Thesis, Massachusetts Institute of Technology.
- [55] Rousselier, G., 1987, “Ductile Fracture Models and Their Potential in Local Approach of Fracture,” *Nuclear Engineering and Design*, **105(1)**, pp. 97–111.
- [56] Belnoue, J. P., and Korsunsky, A. M., 2012, “A Damage Function Formulation for Nonlocal Coupled Damage-Plasticity Model of Ductile Metal Alloys,” *European Journal of Mechanics - A/Solids*, **34**, pp. 63–77.
- [57] Belnoue, J. P., Nguyen, G. D., and Korsunsky, A. M., 2007, “A One-Dimensional Nonlocal Damage-Plasticity Model for Ductile Materials,” *Int J Fract*, **144(1)**, pp. 53–60.
- [58] Belnoue, J. P., Garnham, B., Bache, M., and Korsunsky, A. M., 2010, “The Use of Coupled Nonlocal Damage-Plasticity to Predict Crack Growth in Ductile Metal Plates,” *Engineering Fracture Mechanics*, **77(11)**, pp. 1721–1729.
- [59] Challamel, N., Lanos, C., and Casandjian, C., 2005, “Creep Damage Modelling for Quasi-Brittle Materials,” *European Journal of Mechanics - A/Solids*, **24(4)**, pp. 593–613.
- [60] Hayhurst, D. R., 1972, “Creep Rupture under Multi-Axial States of Stress,” *Journal of the Mechanics and Physics of Solids*, **20(6)**, pp. 381–382.
- [61] Chaboche, J. L., 1984, “Anisotropic Creep Damage in the Framework of Continuum Damage Mechanics,” *Nuclear Engineering and Design*, **79(3)**, pp. 309–319.
- [62] Murakami, S., 1983, “Notion of Continuum Damage Mechanics and Its Application to Anisotropic Creep Damage Theory,” *J. Eng. Mater. Technol.*, **105(2)**, pp. 99–105.
- [63] Betten, J., Sklepus, S., and Zolochovsky, A., 1999, “A Microcrack Description of Creep Damage in Crystalline Solids with Different Behaviour in Tension and Compression,” *International Journal of Damage Mechanics*, **8(3)**, pp. 197–232.
- [64] Chaboche, J. L., and Lesne, P. M., 1988, “A Non-Linear Continuous Fatigue Damage Model,” *Fatigue & Fracture of Engineering Materials & Structures*, **11(1)**, pp. 1–17.
- [65] Dufailly, J., and Lemaitre, J., 1995, “Modeling Very Low Cycle Fatigue,” *International Journal of Damage Mechanics*, **4(2)**, pp. 153–170.
- [66] Lemaitre, J., Sermage, J. P., and Desmorat, R., 1999, “A Two Scale Damage Concept Applied to Fatigue,” *International Journal of Fracture*, **97(1–4)**, pp. 67–81.
- [67] Ladani, L. J., and Dasgupta, A., 2009, “A Meso-Scale Damage Evolution Model for Cyclic Fatigue of Viscoplastic Materials,” *International Journal of Fatigue*, **31(4)**, pp. 703–711.
- [68] Ganczarski, A., and Barwacz, L., 2007, “Low Cycle Fatigue Based on Unilateral Damage Evolution,” *International Journal of Damage Mechanics*, **16(2)**, pp. 159–177.
- [69] Gurson, A. L., 1977, “Continuum Theory of Ductile Rupture by Void Nucleation and Growth: Part I—Yield Criteria and Flow Rules for Porous Ductile Media,” *J. Eng. Mater. Technol.*, **99(1)**, pp. 2–15.
- [70] Needleman, A., and Tvergaard, V., 1984, “An Analysis of Ductile Rupture in Notched Bars,” *Journal of the Mechanics and Physics of Solids*, **32(6)**, pp. 461–490.
- [71] Needleman, A., 1987, “A Continuum Model for Void Nucleation by Inclusion Debonding,” *Journal of applied mechanics*, **54(3)**, pp. 525–531.

- [72] Tvergaard, V., 1982, "On Localization in Ductile Materials Containing Spherical Voids," *Int J Fract*, **18**(4), pp. 237–252.
- [73] Jeong, H.-Y., 2002, "A New Yield Function and a Hydrostatic Stress-Controlled Void Nucleation Model for Porous Solids with Pressure-Sensitive Matrices," *International Journal of Solids and Structures*, **39**(5), pp. 1385–1403.
- [74] Pardoen, T., and Hutchinson, J. W., 2000, "An Extended Model for Void Growth and Coalescence," *Journal of the Mechanics and Physics of Solids*, **48**(12), pp. 2467–2512.
- [75] Cheng, L., and Guo, T. F., 2007, "Void Interaction and Coalescence in Polymeric Materials," *International Journal of Solids and Structures*, **44**(6), pp. 1787–1808.
- [76] Gologanu, M., Leblond, J.-B., and Devaux, J., 1993, "Approximate Models for Ductile Metals Containing Non-Spherical voids—Case of Axisymmetric Prolate Ellipsoidal Cavities," *Journal of the Mechanics and Physics of Solids*, **41**(11), pp. 1723–1754.
- [77] Nahshon, K., and Hutchinson, J. W., 2008, "Modification of the Gurson Model for Shear Failure," *European Journal of Mechanics - A/Solids*, **27**(1), pp. 1–17.
- [78] Benseddiq, N., and Imad, A., 2008, "A Ductile Fracture Analysis Using a Local Damage Model," *International Journal of Pressure Vessels and Piping*, **85**(4), pp. 219–227.
- [79] Nahshon, K., and Xue, Z., 2009, "A Modified Gurson Model and Its Application to Punch-out Experiments," *Engineering Fracture Mechanics*, **76**(8), pp. 997–1009.
- [80] Abbassi, F., Mistou, S., and Zghal, A., 2013, "Failure Analysis Based on Microvoid Growth for Sheet Metal during Uniaxial and Biaxial Tensile Tests," *Materials & Design*, **49**, pp. 638–646.
- [81] Achouri, M., Germain, G., Dal Santo, P., and Saidane, D., 2014, "Experimental and Numerical Analysis of Micromechanical Damage in the Punching Process for High-Strength Low-Alloy Steels," *Materials & Design*, **56**, pp. 657–670.
- [82] Oral, A., Anlas, G., and Lambros, J., 2010, "Determination of Gurson-Tvergaard-Needleman Model Parameters for Failure of a Polymeric Material," *International Journal of Damage Mechanics*, p. 1056789510385261.
- [83] Challier, M., Besson, J., Laiarinandrasana, L., and Piques, R., 2006, "Damage and Fracture of Polyvinylidene Fluoride (PVDF) at 20 °C: Experiments and Modelling," *Engineering Fracture Mechanics*, **73**(1), pp. 79–90.
- [84] Ricard, J., Guigné, F., and Laiarinandrasana, L., 2014, "Damage and Fracture Mechanisms of Polyoxymethylene: Multiscale Experimental Study and Finite Element Modeling," *Engineering Fracture Mechanics*, **115**, pp. 270–283.
- [85] ASTM D2290 - 12, 2012, Test Method for Apparent Hoop Tensile Strength of Plastic or Reinforced Plastic Pipe by Split Disk Method, ASTM International.
- [86] ISO 12162., 2009, "Thermoplastics Materials for Pipes and Fittings for Pressure Applications-Classification, Designation and Design Coefficient."
- [87] Rafiee, R., 2012, "Apparent Hoop Tensile Strength Prediction of Glass Fiber-Reinforced Polyester Pipes," *Journal of Composite Materials*, p. 0021998312447209.
- [88] Shlitsa, R. P., and Novikova, E. A., 1983, "Characteristics of the Use of the Split-Disk Method for Investigating Modern Winding Composites," *Mech Compos Mater*, **18**(4), pp. 502–508.
- [89] Jiang, L., Jonas, J. J., Boyle, K., and Martin, P., 2008, "Deformation Behavior of Two Mg Alloys during Ring Hoop Tension Testing," *Materials Science and Engineering: A*, **492**(1–2), pp. 68–73.

- [90] Chen, J. F., Li, S. Q., Bisby, L. A., and Ai, J., 2011, “FRP Rupture Strains in the Split-Disk Test,” *Composites Part B: Engineering*, **42**(4), pp. 962–972.
- [91] Viana, J. C., 2005, “Structural Interpretation of the Strain-Rate, Temperature and Morphology Dependence of the Yield Stress of Injection Molded Semicrystalline Polymers,” *Polymer*, **46**(25), pp. 11773–11785.
- [92] Celentano, D. J., and Chaboche, J.-L., 2007, “Experimental and Numerical Characterization of Damage Evolution in Steels,” *International Journal of Plasticity*, **23**(10–11), pp. 1739–1762.
- [93] Detrez, F., Cantournet, S., and Seguela, R., 2011, “Plasticity/Damage Coupling in Semicrystalline Polymers prior to Yielding: Micromechanisms and Damage Law Identification,” *Polymer*, **52**(9), pp. 1998–2008.
- [94] Gu, G., Xia, Y., Lin, C., Lin, S., Meng, Y., and Zhou, Q., 2013, “Experimental Study on Characterizing Damage Behavior of Thermoplastics,” *Materials & Design*, **44**, pp. 199–207.
- [95] Hong, K., Rastogi, A., and Strobl, G., 2004, “A Model Treating Tensile Deformation of Semicrystalline Polymers: Quasi-Static Stress–Strain Relationship and Viscous Stress Determined for a Sample of Polyethylene,” *Macromolecules*, **37**(26), pp. 10165–10173.
- [96] Oh, C.-S., Kim, N.-H., Kim, Y.-J., Baek, J.-H., Kim, Y.-P., and Kim, W.-S., 2011, “A Finite Element Ductile Failure Simulation Method Using Stress-Modified Fracture Strain Model,” *Engineering Fracture Mechanics*, **78**(1), pp. 124–137.
- [97] Kwon, H. J., and Jar, P.-Y. B., 2008, “On the Application of FEM to Deformation of High-Density Polyethylene,” *International Journal of Solids and Structures*, **45**(11–12), pp. 3521–3543.
- [98] Muhammad, S., and Jar, P.-Y. B., 2013, “Determining Stress–strain Relationship for Necking in Polymers Based on Macro Deformation Behavior,” *Finite Elements in Analysis and Design*, **70–71**, pp. 36–43.
- [99] Muhammad, S., and Jar, P.-Y. B., 2011, “Effect of Aspect Ratio on Large Deformation and Necking of Polyethylene,” *J Mater Sci*, **46**(4), pp. 1110–1123.
- [100] Humbert, S., Lame, O., Chenal, J. M., Rochas, C., and Vigier, G., 2010, “New Insight on Initiation of Cavitation in Semicrystalline Polymers: In-Situ SAXS Measurements,” *Macromolecules*, **43**(17), pp. 7212–7221.
- [101] Schneider, K., Trabelsi, S., Zafeiropoulos, N. e., Davies, R., Riekkel, C., and Stamm, M., 2006, “The Study of Cavitation in HDPE Using Time Resolved Synchrotron X-Ray Scattering During Tensile Deformation,” *Macromol. Symp.*, **236**(1), pp. 241–248.
- [102] Gu, G., Xia, Y., Lin, C., Lin, S., Meng, Y., and Zhou, Q., 2013, “Experimental Study on Characterizing Damage Behavior of Thermoplastics,” *Materials & Design*, **44**, pp. 199–207.
- [103] Detrez, F., Cantournet, S., and Seguela, R., 2011, “Plasticity/Damage Coupling in Semicrystalline Polymers prior to Yielding: Micromechanisms and Damage Law Identification,” *Polymer*, **52**(9), pp. 1998–2008.

# Chapter 5

## **Effects of squeeze-off on mechanical properties of PE pipe**

Squeeze-off is a common practice in industry to shut off or reduce gas flow in polyethylene (PE) pipe. In this study, influence of squeeze-off on degradation of mechanical properties for PE pipe was examined. Three squeezing speeds of 0.01, 1 and 50mm/min were used to cover the possible scenarios that may be encountered during the pipe repair or maintenance. Results show that squeeze-off of PE pipe causes significant degradation in elastic modulus and yield strength, with the maximum reduction of 82% for elastic modulus and 27% for yield strength. Furthermore, contradictory to the common belief that slower is better, reducing the squeezing speed was found to have no effect on the extent of property degradation. In view of those findings, a study was conducted using mechanical testing and finite element (FE) simulation to elucidate the damage evolution in PE pipe in different loading modes (including tension and compression) and with different loading history (in terms of maximum pre-strain level and loading speed). Results show that both tensile and compressive loading modes can cause severe degradation in elastic modulus and yield strength. The results also show that under a single loading mode, the extent of damage at a given pre-strain level is indeed a function of loading rate. However, in a pipe which has been squeezed to subject the pipe wall to both tensile and compressive stresses, degradation of the “apparent” elastic modulus and yield strength, defined as their equivalent values for a given wall thickness, becomes insensitive to the loading rate.

## 5.1 Introduction

Use of polyethylene (PE) for natural gas transportation has increased rapidly due to its good physical and mechanical properties and outstanding corrosion resistance. Statistics shows that over 90% of the newly installed gas pipeline systems are now made of PE [1]. One main advantage of PE pipe over the metallic counterpart is that a simple and fast procedure, known as squeeze-off process, can be employed to shut off or control gas flow when the pipeline system requires maintenance or repair. However, it is also recognized that several external loading modes, including squeeze-off, rock impingement and pipe bending, can cause mechanical property degradation of the pipe, thus reducing its remaining service life. Evidence has led to suspect that degradation of mechanical properties caused by the squeeze-off process is responsible for some of the unexpected, catastrophic failures of PE pipe [2,3].

A number of experimental studies have been conducted to investigate the influence of squeeze-off process on the mechanical properties of PE pipe [2–9]. Results from the studies suggest that the squeeze-off introduces damage that affects both short- and long-term performance of PE pipe. Parameters in the squeeze-off process that may affect mechanical properties for PE pipe include squeezing speed, release rate, squeeze-off ratio (also known as pipe wall compression ratio), geometry of the squeeze-off tool, PE pipe dimensions, and temperature, just to name a few. Previous work, such as that described in ref. [6], considered the influence of squeezing ratio, pipe diameter and squeeze-off tool geometry on the pipe performance. To our knowledge, not much attention has been paid to the influence of squeezing speed on the mechanical property degradation. It should be noted that although the maximum squeezing speed is specified in standards such as ASTM F1041, no work has been reported which concerns about the effect of squeezing speed on the PE pipe performance.

One of the challenges for quantifying the effect of squeezing speed on the PE pipe performance is the strong time-dependent deformation behaviour of PE. A number of constitutive models, either physically- or phenomenologically-based, have been proposed in the past three decades, to describe elasto-viscoplastic behavior of solid polymers. The physically-based models consider the relationship between macroscopic mechanical properties and microstructure such as orientation of macromolecular chains. A pioneering physically-based model, composed of Eyring dashpot and Langevin spring [10], was proposed to describe the uniaxial stress-strain relationship of glassy thermoplastics. Application of this model was later extended to the assessment of three-dimensional deformation behavior [11]. The approach in [12] was further modified for several applications. One was to investigate the strain-induced crystallization behaviour in poly(ethylene terephthalate) at temperatures above its glass transition [13], another to include the pressure-dependent yield criterion [14], and the third to describe the effect of crystal content on the mechanical behavior of PE [15]. In a similar way, the physically-based models proposed in [11] were modified to simulate large deformation of HDPE under loading-unloading tests [16]. More recently, the model proposed in [14] was used to investigate the mechanical behavior of PVC and HDPE under various levels of stress triaxiality, induced by changing notch radius of the specimens [17].

If the study is only concerned about the macroscopic deformation behavior, the phenomenologically-based models are an attractive alternative to the physically-based models, due to the former's simple process for identifying the model parameters. One of the popular phenomenologically-based models, known as BP model [18], was proposed to assess the elastic-viscoplastic strain hardening behavior of materials, which was later adopted and modified [19] to describe the mechanical behavior of glassy polymers. An empirically-determined constitutive

equation for the stress-strain relationship was proposed [20] and successfully adopted and modified [21–23] to determine neck formation and propagation in polymeric materials. Other phenomenologically-based models, including Khan-Huang-Liang (KHL) model [24–26] and viscoplasticity model based on overstress (VBO) [27–30], are also widely used to represent viscoplastic deformation for both metallic and polymeric materials over a wide range of strain rates and temperatures.

Using some of the above constitutive equations for different stages of the deformation process, a finite element (FE) model has been successfully used to mimic the experimentally observed load-elongation curve and cross sectional reduction of high-density PE (HDPE) in tensile deformation [31,32]. This FE approach is adopted here to determine distribution of stress and strain in PE pipe when subjected to the squeeze-off process.

Work presented in this chapter was initiated from a study that is to quantify the change in mechanical properties of HDPE pipe in terms of squeezing speed in the range recommended in ASTM F1041. As to be shown in the first part of the chapter, the study discovered the unexpected independence of mechanical property change on the squeezing speed. This led to an investigation using experimental testing and FE simulation to understand the influence of loading mode (tension and compression) and loading speed on the mechanical property change of PE. Coupon specimens from the HDPE pipe were used to characterize the mechanical property change, and the concept of damage evolution with the increase of deformation is used to understand the mechanical property change. This chapter uses results from the coupon testing to provide explanations for the influence of squeeze-off on the discovered mechanical property change of HDPE pipe.

## **5.2 Experimental details and test results**

A two-stage scheme was adopted for the mechanical tests, including the following combination of loading modes: squeeze-off-and-tensile, tensile-and-tensile, compressive-and-compressive, and compression-and-tensile tests. These tests were conducted at room temperature using a universal test machine (QUASAR 100). All specimens were prepared from 2-inch HDPE pipe (PE3408, Cell classification 445574C), made of PE80 resin with a minimum required strength (MRS) of 8 MPa.

### **5.2.1 Squeeze-off-and-tensile tests**

Each pipe sample used for the squeeze-off test has length of at least five times of its diameter, following the recommendation given in ASTM F1041. As shown in Fig. 5.1(a), the squeeze-off tool consists of two round bars of 19 mm in radius, as suggested in ASTM F1563. The pipe samples were squeezed to the squeezing ratio of 30% at a constant crosshead speed of 0.01, 1 or 50 mm/min, and then maintained at this squeezing ratio for 10,000 seconds to mimic the onsite maintenance or repair period before being released at a constant crosshead speed of 0.1 mm/min. An example of displacement and force as functions of time applied in the squeeze-off tests are depicted in Fig. 5.1(b).

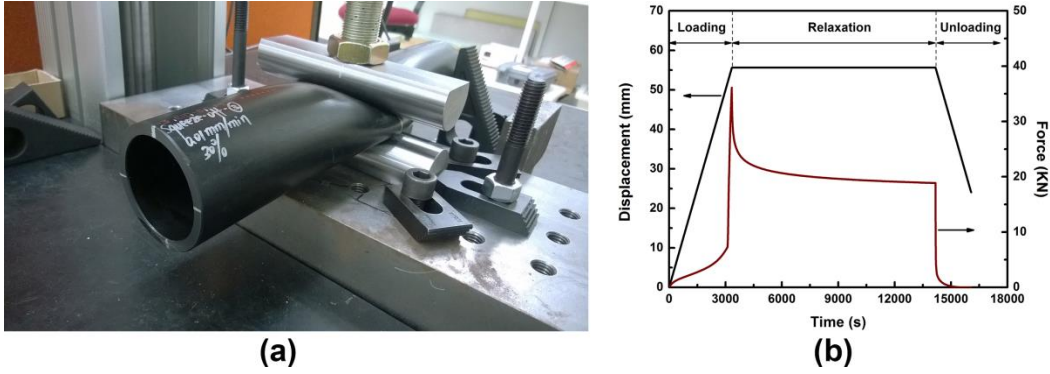


**Fig. 5.1** Squeeze-off test: (a) test setup and specimen and (b) an example of displacement and force as functions of time

In this study, wall compression (WC) and squeezing ratio (SR), as defined in Eq. (5.1) according to ASTM F1734, are kept at 30% and 70%, respectively, for all three squeezing speeds of 0.01, 1 and 50mm/min.

$$WC = \left(1 - \frac{L}{2t}\right) \times 100\% \quad (5.1)$$

$$SR = \frac{L}{2t}$$

where  $L$  and  $t$  are the minimum distance between the squeeze-off bars and the uncompressed pipe wall thickness, respectively.

Fig. 5.2 presents the relationship between force and displacement of the squeeze-off tests at the above three squeezing speeds. It can be seen that the squeeze-off force increases with the increase of the squeezing speed due to the viscous nature of PE pipe.

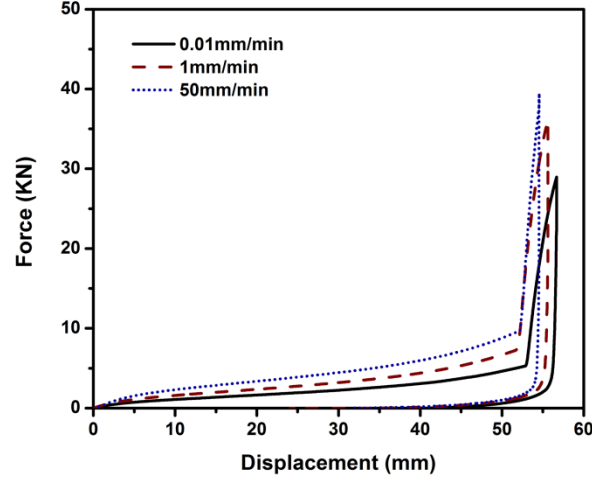


**Fig. 5.2** Variation of squeezing force with displacement at squeezing speeds of 0.01, 1 and 50 mm/min

After two months to allow visco-elastic recovery from the squeeze-off tests, the pipe samples were sliced to make notched pipe ring (NPR) specimens, as shown in Fig. 5.3(a). The NPR specimens were stretched in the D-split tests till fracture occurred in one of the two ligaments at the crosshead speed of 0.01 mm/min, as shown in Fig. 5.3(b), to assess the influence of squeezing speed used in the first test (squeeze-off) on the change in mechanical properties (i.e., yield stress and elastic modulus). Here, yield stress is the engineering stress based on the cross sectional area of the ligament section at the beginning of the test, and the elastic modulus the slope of the curve of true stress versus area strain ( $\epsilon_w$ ) at  $\epsilon_w = 0.5\%$ , where  $\epsilon_w$  is calculated using the following expression under the assumption of volume conservation during the deformation [33].

$$\epsilon_w = 2 \times \ln(w_0/w) \quad (5.2)$$

where  $w_0$  and  $w$  are the original and deformed ligament lengths, respectively. Variation of  $w$  during the test was measured using an extensometer. Dimensions of the NPR specimens used in

the study follow those recommended in ASTM D2290-12, except that the notch profile is flat, instead of round, in order to have a relatively uniform stress distribution in the ligament. Note that ligament length for the NPR specimens was chosen to be close to the pipe wall thickness, of 5.84 mm so that the aspect ratio of width to thickness for the ligament cross section is close to 1. This allows similar contraction in the width and thickness directions during the D-split test.

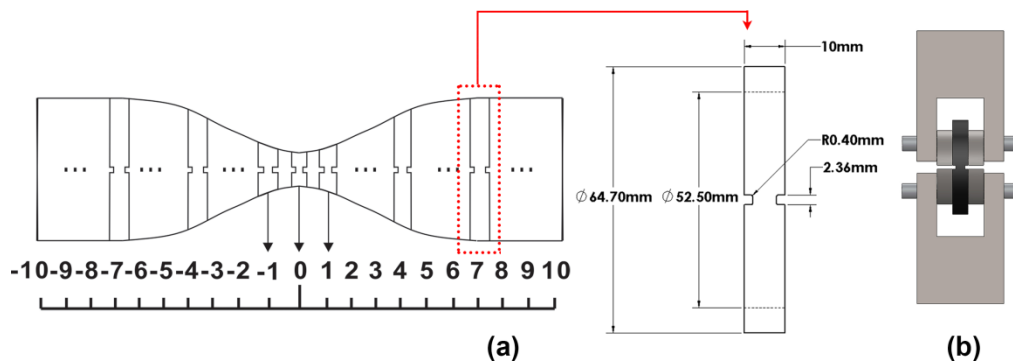


**Fig. 5.3** D-split test and specimen preparation from a squeezed pipe section: (a) schematic description of relative positions (left) and dimensions (right) of NPR specimens, sampled from a squeezed pipe, and (b) D-split test setup

Fig. 5.4 presents yield stress and elastic modulus measured from the D-split test, as functions of distance from the squeeze-off ears of the PE pipe (i.e., the section marked “0” in Fig. 5.3(a), which was directly between the round bars in the squeeze-off test). The elastic modulus is defined as the slope for a straight line that is tangent to the true stress-area strain curve from the second test, at the area strain of 0.5%. Fig. 5.4 suggests that significant degradation for both yield stress and elastic modulus has occurred at the squeeze-off ears. However, at a distance of more than one pipe diameter from the squeeze-off position, i.e. at the relative position bigger than 3 or smaller than -3 in Fig. 5.3(a), both yield stress and elastic modulus were barely affected by the squeeze-off process.

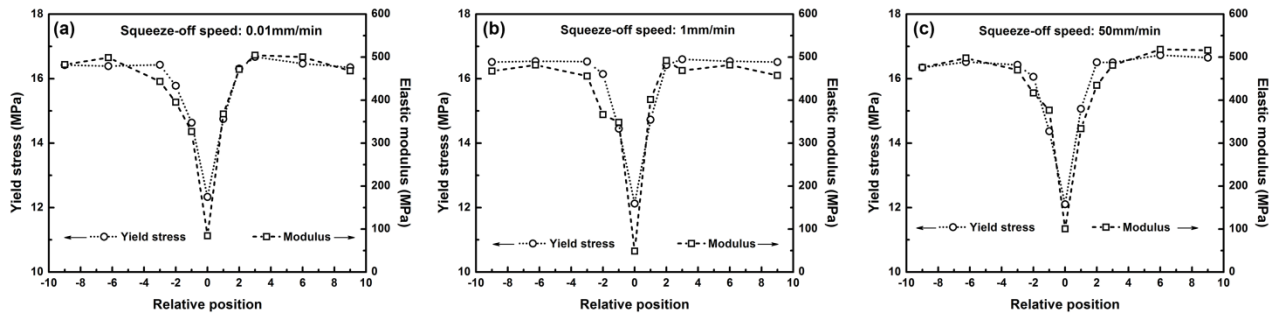


**Fig. 5.4** Effects of the squeeze-off process on mechanical properties of PE pipe at the squeezing speeds of 0.01 mm/min (a), 1 mm/min (b), and 50 mm/min (c) (Note that the relative position is defined in Fig. 5.3(a))

Fig. 5.4 also suggests that the squeezing speeds used in the study, over 3 orders of magnitude in difference, show little effect on the change in mechanical properties for the NPR specimens. This is not consistent with the expectation based on results published previously in which higher the crosshead speed used to apply the tensile loading, more significant the decrease in the measured mechanical properties. Results in Fig. 5.4 are also contradictory to a common belief that a low squeezing speed can prevent damage of the pipe.

To resolve the above contradiction, an investigation was conducted using two-stage tests on three types of coupon specimens, i.e., NPR, stub, and half NPR specimens. As proposed initially in refs. [34,35], first stage of the two-stage tests is to introduce various loading history to the specimens, and after at least two months for the viscoelastic discovery the second stage is conducted to measure the mechanical properties.

### 5.2.2 Tensile-and-tensile tests on NPR specimens

In this part of the study, the first tensile tests were to stretch the NPR specimens to the predetermined area strains of 20%, 40% or 60%, at one of the three crosshead speeds of 0.01, 1 and 50 mm/min. At the end of the stretch in the first tests, the specimens were held at the final

stroke position for 3 hours and then unloaded at the crosshead speed of 0.1 mm/min. To allow post-test recovery of most of the viscoelastic deformation, all specimens were stored for at least two months before the second tests were conducted, in a monotonic tensile mode at the crosshead speed of 0.01 mm/min.

Fig. 5.5 summarizes elastic modulus, the corresponding damage evolution and yield stress for the NPR specimens that have been subjected to the monotonic tensile loading at the crosshead speeds of 0.01, 1 and 50 mm/min in the first tests. Variation of values for the damage parameter, calculated using results in Fig. 5.5(a) based on continuum damage mechanics (CDM), is presented in Fig. 5.5(b) as a function of prestrain introduced in the first tests. Fig. 5.5(b) also includes the fitting curves generated based on an one-term exponential function,  $D = A[1 - \exp(-B\varepsilon)]$ , with values for constants  $A$  and  $B$  adjusted to have the optimum coefficient of determination ( $R^2$ ). Results in Fig. 5.5(b) suggest that at the same prestrain level, damage generated under tension evolves faster at a higher crosshead speed.

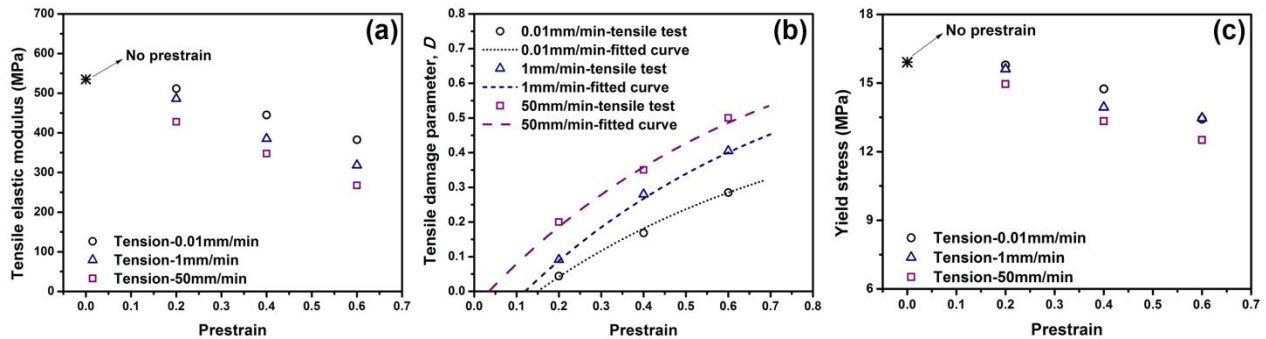


**Fig. 5.5** Variation of the tensile elastic modulus (a), the corresponding damage evolution (b), and yield stress (c) for NPR specimens, as a function of prestrain introduced in the first test

### 5.2.3 Compressive-and-compressive tests on stub specimens

Compressive loading was also considered in the two-stage test to evaluate the influence of compressive prestrain on the change in mechanical properties. Specimens for this type of tests were stubs from PE pipe, with dimensions depicted on the left of Fig. 5.6 and test setup on the right. The first test was to introduce to the stub specimens compressive area strains of up to 45%, at the crosshead speed of 0.01, 1 or 50 mm/min. After a period of at least two months, these specimens were compressed again for the second time to measure the elastic modulus and yield stress. Lubricant was applied between the test fixture and the specimen surface to reduce the effect of interfacial friction on the specimen deformation.

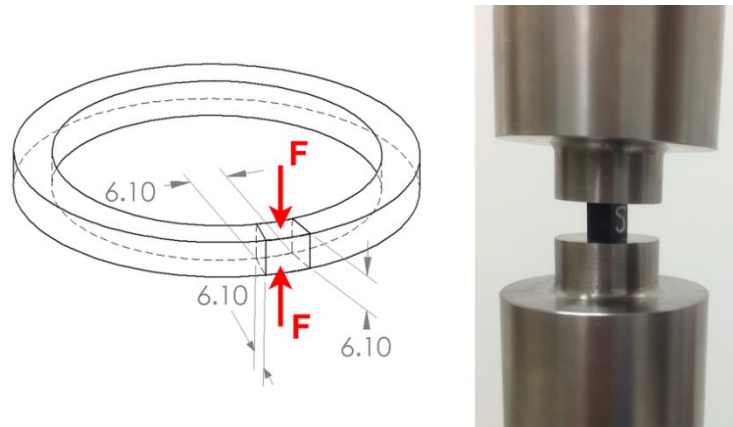


**Fig. 5.6** Dimensions for the stub specimens (left) and compressive test setup (right)

Variation of compressive elastic modulus, the corresponding damage evolution and compressive yield stress for the stub specimens are presented in Fig. 5.7, as functions of prestrain at the crosshead speeds of 0.01, 1 and 50 mm/min. Same as that shown in Fig. 5.5(b), Fig. 5.7(b) includes the fitting curves for the data with the optimum  $R^2$  values. The fitting curves in Figs. 5.5(b) and 5.7(b), named tensile and compressive damage evolution curves, respectively, will be

used later to represent the relationship between damage parameter and prestrain level in order to determine the damage variation across the wall thickness in the squeezed pipe section.

Results presented in Figs. 5.5 and 5.7 suggest that both tensile and compressive loadings introduced in the first tests can cause decrease in elastic modulus and yield stress measured from the second tests. The results support findings from the previous studies which suggest that both tensile [36, 37] and compressive [38, 39] loadings are able to cause decrease in the degree of crystallinity and density of HDPE.

Note that tensile elastic modulus from virgin NPR specimen is 535 MPa, and the compressive counterpart from virgin stub specimen 695 MPa. Although work in the past [40] has suggested that mechanical properties in the axial and hoop directions should almost be identical, difference in the test set-up and loading mode may have caused the difference in the measured elastic modulus values. Furthermore, drop in elastic modulus and yield stress in Fig. 5.5 was measured from tests that applied tensile loading, but that in Fig. 5.7 from tests that applied compressive loading. Therefore, as to be shown in the next section, an additional investigation was conducted to confirm that the phenomenon shown in Fig. 5.7 also exists if tensile loading was applied in the second test.

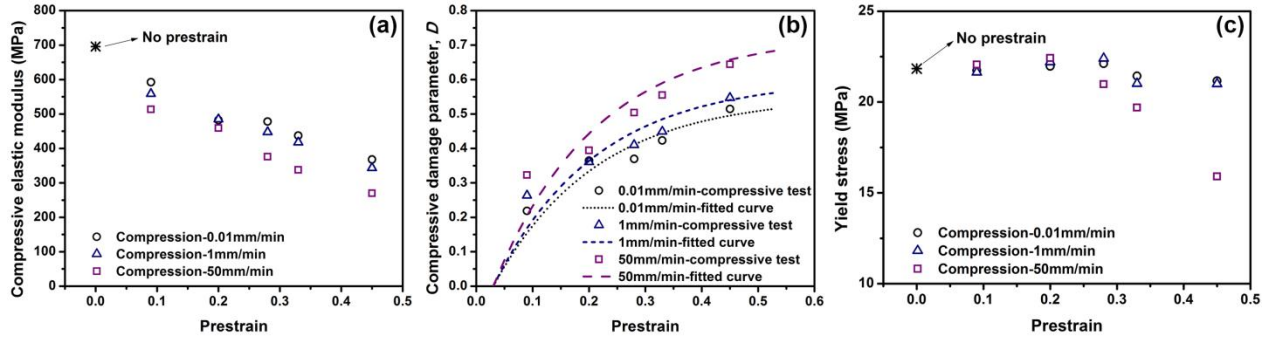


**Fig. 5.7** Variation of the compressive elastic modulus (a), the corresponding damage evolution (b) and compressive yield stress (c) for stub specimens, as a function of compressive prestrain introduced in the first test

#### 5.2.4 Tensile-and-tensile and compressive-and-tensile tests on half NPR specimens

This part of study is to conduct tests on half NPR specimens that have both ends clamped, as shown in Fig. 5.8, so that tensile or compressive prestrains in the hoop direction can be introduced in the first test, and elastic modulus and yield stress under tensile loading can be measured in the second test.

Since purpose of these tests is to confirm that the phenomenon shown in Fig. 5.7 also exists in the hoop direction for elastic modulus and yield stress measured under tensile loading, only one crosshead speed of 50 mm/min was used for the first tests to introduce tensile or compressive prestrains, and a crosshead speed of 0.01 mm/min for the second tests to measure elastic modulus and yield stress under the tensile loading.

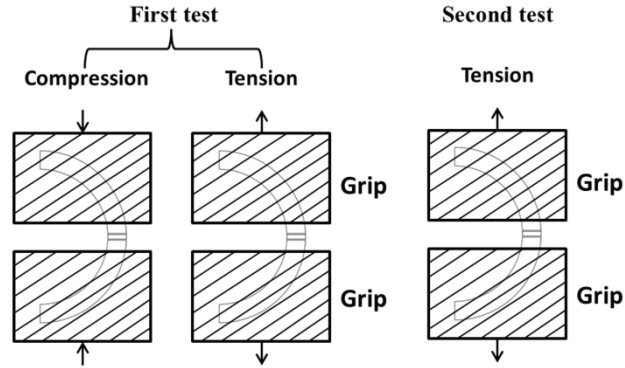
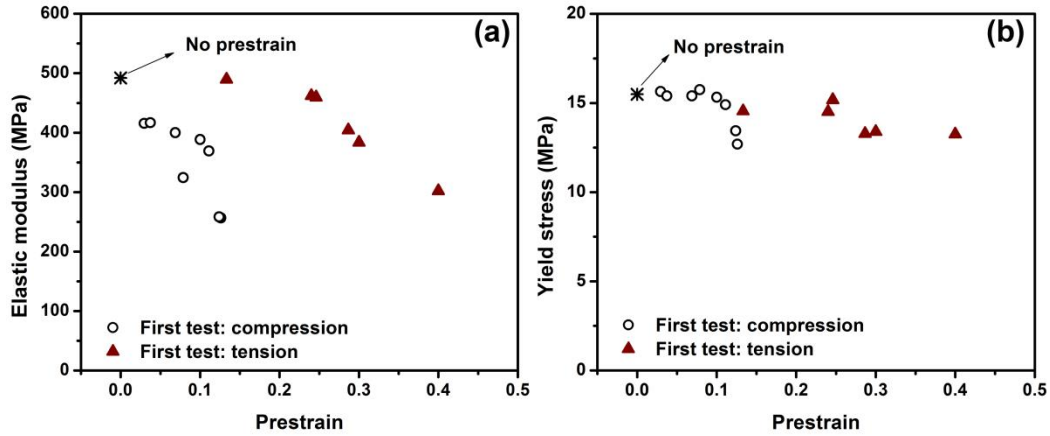


**Fig. 5.8** Schematic description of the two-stage tests on half NPR specimens

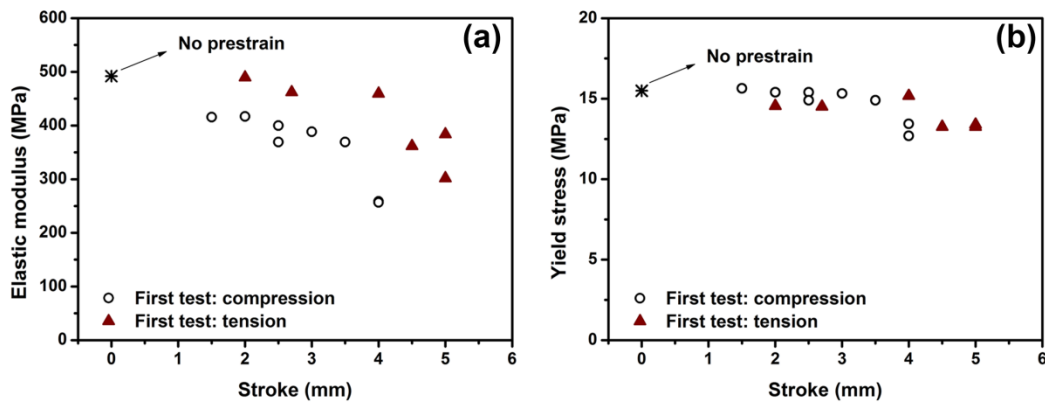
Fig. 5.9 depicts results from the half NPR specimens, expressed as a function of absolute prestrain values introduced in the first test. The figure suggests that both tensile and compressive prestrains can cause decrease of elastic modulus and yield stress, and compressive prestrains have a more significant effect than tensile prestrains on the decrease of the elastic modulus.

Fig. 5.10 presents the same set of data as that for Fig. 5.9 but expressed as a function of stroke used in the first test. Fig. 5.10 is less significant than Fig. 5.9 in the difference of elastic modulus drop caused by the two deformation modes (tension and compression) applied in the first test. On the other hand, the two figures show a similar effect of the two deformation modes used in the first test on the drop of yield stress. Therefore, it can be concluded that the phenomenon shown in Fig. 5.7 also exists in the hoop direction of the PE pipe, for the elastic modulus and yield stress measured under tensile loading. However, Figs. 5.9 and 5.10 do not give a clear indication on how differently the two deformation modes in the first test cause the drop of elastic modulus. This is probably because boundary condition introduced by the grips in Fig. 5.8 is not well defined. Further tests using coupon specimens with firm fixtures are needed. Nevertheless, it is evident that results in Fig. 5.9 support the phenomena shown in Fig. 5.5. Therefore, the

mechanical property change shown in Fig. 5.4 is from a combined effect of tensile and compressive deformation introduced by the squeeze-off process.



**Fig. 5.9** Elastic modulus (a) and yield stress (b) for half NPR specimens, as a function of prestrain applied in the first test



**Fig. 5.10** Elastic modulus (a) and yield stress (b) for half NPR specimens, as a function of stroke applied in the first test

### 5.3 Finite element simulation

Finite element (FE) simulation was carried out using ABAQUS Standard, to quantify the complex strain distribution generated in the PE pipe by the squeeze-off process. The 3-D FE model of which the 2-D view is shown in Fig. 5.11, includes a quarter cross section of a PE pipe

specimen which consists of 18600 C3D8R elements and the upper squeeze-off bar that is modelled as an analytical rigid body. Due to the geometric symmetry only half of the pipe length was constructed in the model. The constitutive equation proposed by Kwon and Jar [31] and later extended by Muhammad and Jar [32] was adopted to simulate the deformation introduced by the squeeze-off process. As shown in Eq. (5.3) below, the constitutive equation is expressed through a series of stress-strain relationships, in which the first four expressions are for different strain ranges of elastic-plastic deformation and the last one for the creep deformation.

$$\sigma(\varepsilon) = \begin{cases} \frac{3}{2(1+\nu)} E\varepsilon & \varepsilon \leq \varepsilon_y \quad (\text{a}) \\ d \left\{ [a(\varepsilon+b)]^{(c-1)} - [a(\varepsilon+b)]^{(-c)} \right\} + e & \varepsilon_y \leq \varepsilon \leq \varepsilon_n \quad (\text{b}) \\ \alpha k \varepsilon^N & \varepsilon_n \leq \varepsilon \leq \varepsilon_t \quad (\text{c}) \\ k \exp(M \varepsilon^\beta) & \varepsilon \geq \varepsilon_t \quad (\text{d}) \\ \dot{\varepsilon}^{cr} = A \sigma^n t^m & (\text{e}) \end{cases} \quad (5.3)$$

where  $\sigma$  and  $\varepsilon$  are equivalent stress and equivalent strain, respectively,  $\varepsilon_y$  the transitional strain from linear to nonlinear deformation,  $\varepsilon_n$  the critical strain for the on-set of necking, and  $\varepsilon_t$  the strain at the beginning of the exponential hardening. The other parameters (a, b, c, d, e,  $\alpha k$ , N, M,  $\beta$ , A, n and m) are user-defined variables for which the values were determined from an iterative process until the time function of force from the FE simulation matched that from the experimental testing.

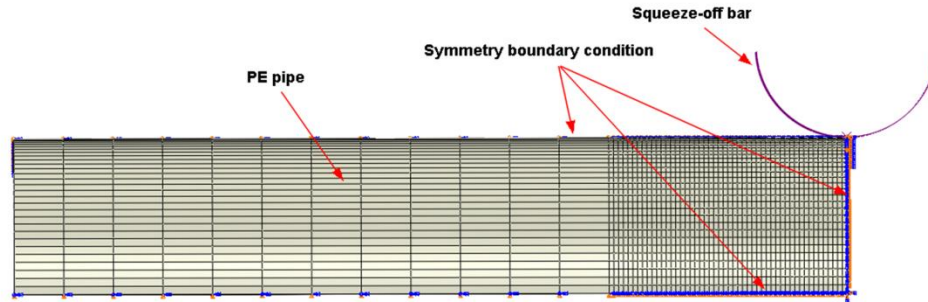


**Fig. 5.11** The 2-D view of a 3-D FE model for the squeeze-off process

Fig. 5.12 compares load-time curves generated from the FE model with those from the experimental testing at squeezing speeds of 0.01, 1 and 50 mm/min. For clarity, zoom-in plots in the time range of 340,000 to 355,000 seconds for the squeezing speed of 0.01 mm/min and 0 to 200 seconds for the squeezing speed of 50 mm/min are also included in the figure. The results suggest that the experimental curves can be reasonably regenerated by the FE model using Eq. (5.3) with values for the parameters and the corresponding strain ranges specified in Table 5.1. Using the FE model, explanation for the drop of elastic modulus being insensitive to the change of squeezing speed, as shown in Fig. 5.4, was searched. Details of the explanation are given in the next section.

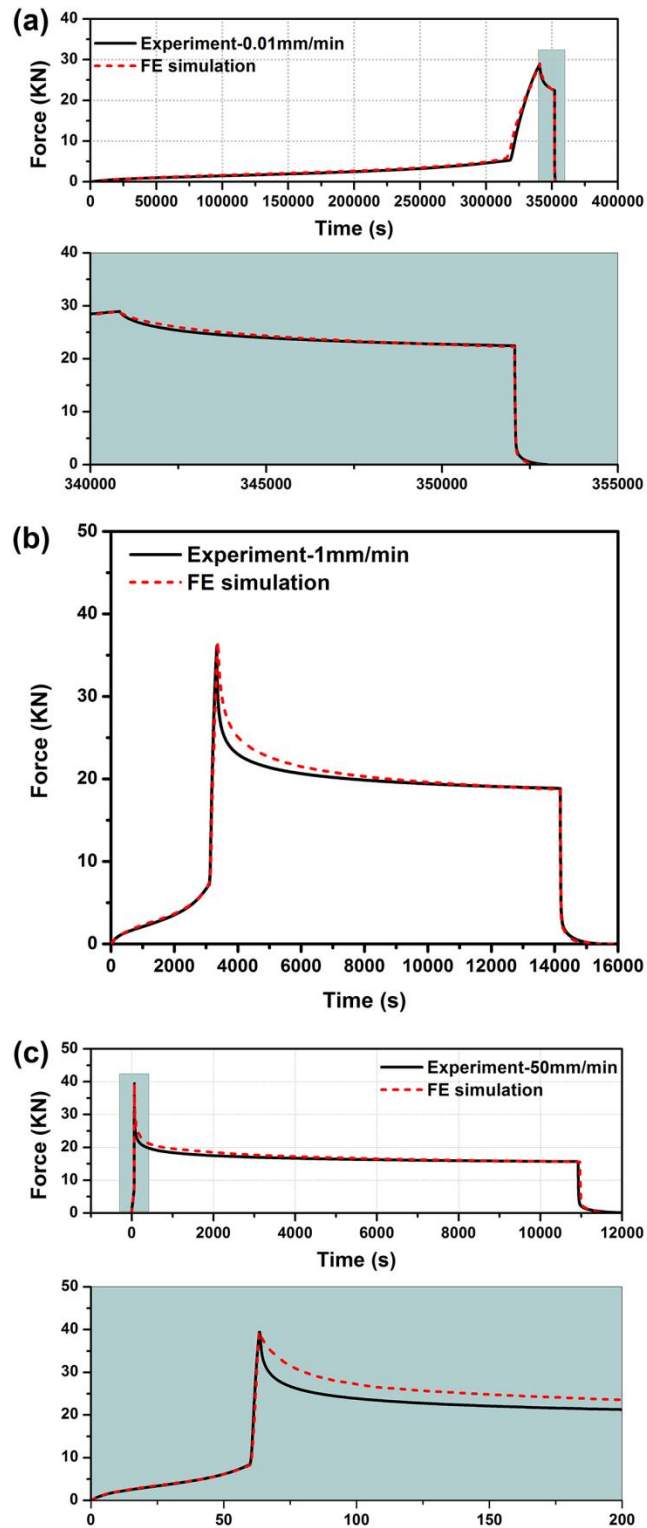


**Fig. 5.12** Comparison between FE simulation and experimental testing at squeezing speeds of 0.01 (a), 1 (b) and 50 mm/min (c)

**Table 5.1** Values for parameters and strain range in Eq. (5.3), determined from the FE simulation

FE model		Squeeze-off process			
Crosshead speed (mm/min)		0.01	1	50	
Equation (3a)	$\varepsilon_y$	0.01	0.005	0.005	
	E (MPa)	900	950	1100	
	$\nu$	0.4	0.4	0.4	
Equation (3b)	$\varepsilon_n$	0.022	0.02	0.02	
	a	9.9	21	31.02	
	b	0.057	0.025	0.018	
	c	0.05	0.05	0.004	
	d	-23.8	-23.8	-23.8	
	e	15.5	15.5	15.5	
Equation (3c)	$\varepsilon_t$	0.3	0.3	0.3	
	$\alpha k$	14.52	18.1	24.1	
	N	0.12	0.07	0.07	
Equation (3d)	Section 1	$\varepsilon_{t1}$	0.6	0.6	0.6
		$K_1$	11.7	15.6	21.06
		$M_1$	0.68	0.59	0.44
		$\beta_1$	1.8	1.8	1.8
	Section 2	$\varepsilon_{t2}$	0.8	0.8	0.8
		$K_2$	11.6	14.6	20.6
		$M_2$	0.72	0.71	0.5
	Section 3	$\beta_2$	1.8	1.8	1.8
		$\varepsilon_{t3}$	1.2	1.2	1.2
		$K_3$	9	13.05	19.13
	Section 4	$M_3$	1.1	0.93	0.61
		$\beta_3$	1.8	1.8	1.8
$\varepsilon_{t4}$		2	2	2	
$K_4$		6.82	9	16.63	
Equation (3e)	$M_4$	1.3	1.2	0.71	
	$\beta_4$	1.8	1.8	1.8	
	$A \times 10^{15}$	6.6	6.6	6.6	
	n	10	10	10	
	m	-0.61	-0.61	-0.61	

#### 5.4 Insensitivity of the drop of elastic modulus to the squeezing speed

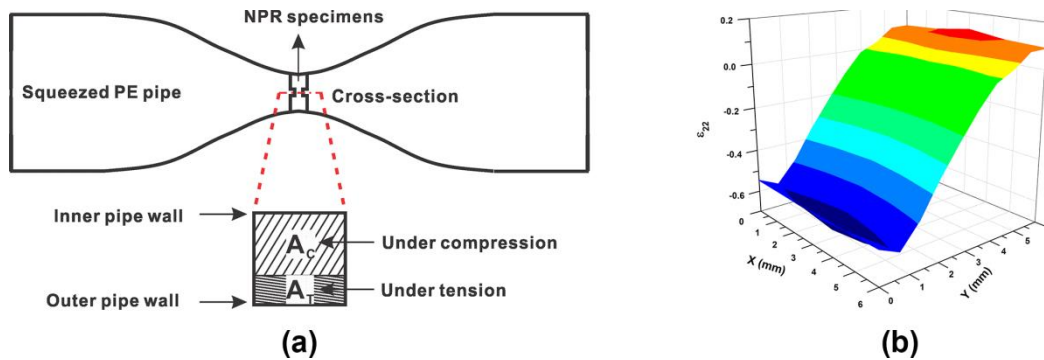
Work in literature [37, 41–44] has suggested that damage development in semi-crystalline polymers depends on strain rate, that is, more damage at a higher strain rate. However, damage

generated in those studies was through tensile, monotonic loading. None of the work considered the damage development under compressive loading.

The finding shown in Fig. 5.4, i.e., little dependence of mechanical property degradation on the squeezing speed, suggests that damage of PE pipe generated by the squeeze-off process may not come only from the tensile loading. Results presented in Figs. 5.7 and 5.9 suggest that compressive loading can also cause damage in PE pipe. Therefore, analysis presented here considers damage generated by both tensile and compressive loading. With the rate sensitivity of the damage evolution and variation of strain rate during the squeeze-off process, even at a constant squeezing speed, the analysis is to seek the possibility of reconciling the difference between the insensitivity of the mechanical property degradation to the loading rate, as shown in Fig. 5.4, and the sensitivity reported in the literature.

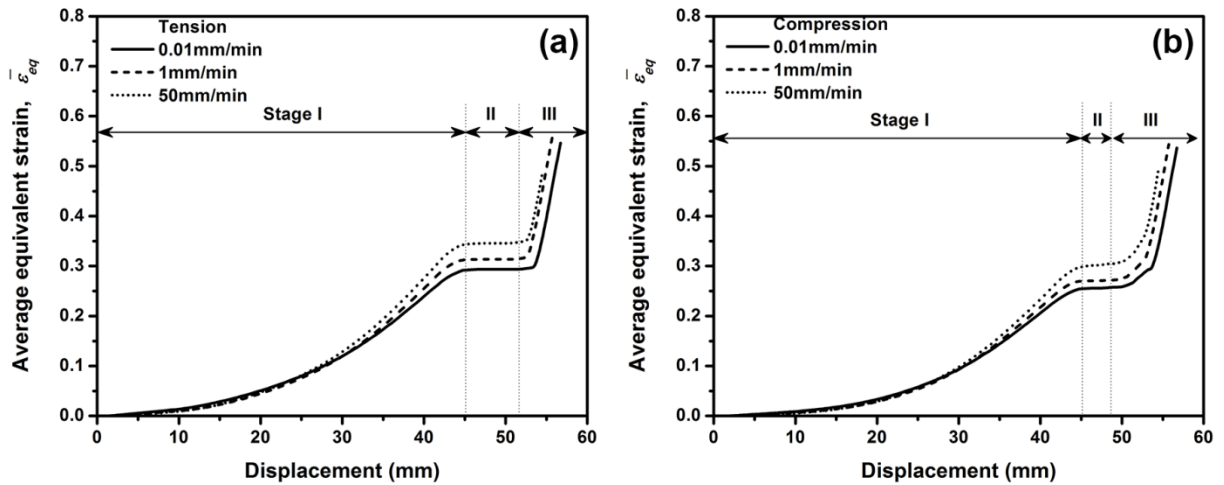
An example of PE pipe deformation generated by the squeeze-off process and the corresponding strain distribution are given in Fig. 5.13. Fig. 5.13(a) depicts the overall deformation of the PE pipe and a schematic presentation of loading mode on the pipe wall cross section between the round bars where a smaller, outer region (denoted  $A_T$  in Fig. 5.13(a)) is under tension and a larger, inner region ( $A_C$ ) under compression. Fig. 5.13(b) depicts variation of the circumferential normal strain ( $\varepsilon_{22}$ ) from the inner pipe wall ( $Y=0$  mm) to the outer pipe wall ( $Y=6$  mm). Based on the FE simulation, it is estimated that approximately 30% of the pipe wall thickness in the section between the round bars is subjected to tensile deformation and the remaining 70% subjected to compressive deformation. Therefore, damage generated by the compressive deformation is expected to play a major role on the mechanical property degradation shown in Fig. 5.4.

Three assumptions are made for the following analysis, as detailed here, in order to simplify the calculation of damage evolution during the squeeze-off process. The first assumption is that the circumferential normal strain ( $\varepsilon_{22}$ ) is uniform for each area of  $A_C$  and  $A_T$  shown in Fig. 5.13(a), and the  $\varepsilon_{22}$  value can be represented by the average equivalent strain ( $\bar{\varepsilon}_{eq}$ ) value for the area, determined from the FE model in Fig. 5.11. The second assumption is that strain rate ( $\dot{\varepsilon}$ ) during the squeeze-off process is uniform in each area of  $A_C$  and  $A_T$ , and the  $\dot{\varepsilon}$  value can be determined from the FE model by averaging the strain rate in the corresponding area. The third assumption is that damage parameter  $D$  is a function of  $\varepsilon_{22}$  only for each of the squeezing speed, and the relationship between  $D$  and  $\varepsilon_{22}$  can be expressed using the fitting curves given in Figs. 5.5(b) and 5.7(b). With the first and third assumptions above, the analysis uses  $\bar{\varepsilon}_{eq}$  value from the FE model for each area of  $A_C$  and  $A_T$  to calculate the corresponding  $D$  value based on the fitting curves provided in Figs. 5.5(b) and 5.7(b).



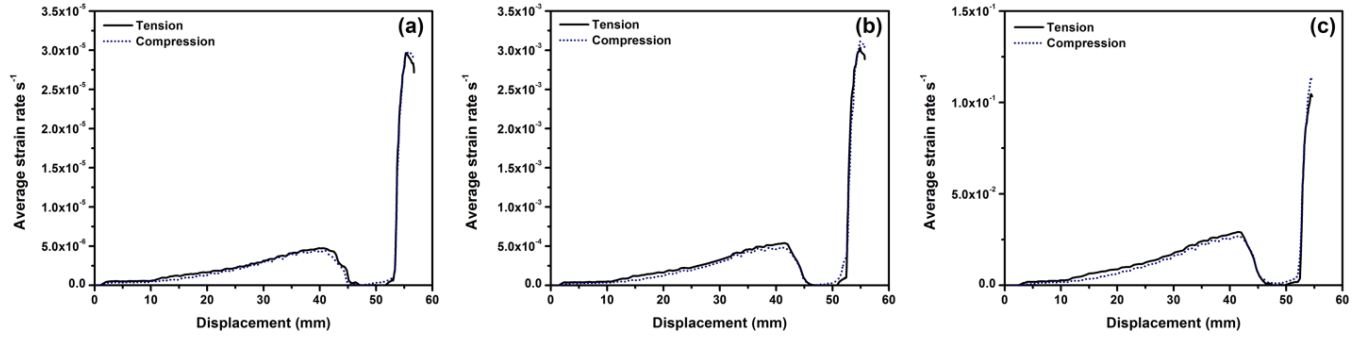
**Fig. 5.13** Strain generated across wall thickness of the PE pipe: (a) schematic description of the cross-section of the PE pipe wall between the squeeze-off bars, and (b) distribution of circumferential normal strain ( $\varepsilon_{22}$ ) on the cross-section of pipe wall directly between the squeeze-off bars

Fig. 5.14 summarizes results from the FE model, showing variation of  $\bar{\varepsilon}_{eq}$  with displacement during the squeeze-off test, in the pipe wall section where the most severe damage is generated. Fig. 5.14(a) is for the cross sectional area  $A_T$  and (b) for  $A_C$ . Each figure shows three stages of strain development: stage I for the initial compression of the pipe, stage II before the top and bottom inner surfaces contact with each other during which  $\bar{\varepsilon}_{eq}$  remains nearly constant, and stage III after the top and bottom inner surfaces meet and are squeezed by the two round bars till the final squeezing ratio is reached.



**Fig. 5.14** Variation of average equivalent strain from the FE simulation as a function of displacement: (a) tension and (b) compression

Using the FE model, strain rate ( $\dot{\varepsilon}$ ) can also be established as a function of displacement with which the average strain rate ( $\bar{\dot{\varepsilon}}$ ) for each cross sectional area of  $A_C$  and  $A_T$  can be established as a function of displacement, which is presented in Fig. 5.15 for each squeezing speed used in the study. Fig. 5.15 shows clearly that for a given squeezing speed and displacement, absolute value of  $\bar{\dot{\varepsilon}}$  for  $A_C$  is very close to that for  $A_T$ .



**Fig. 5.15** Evolution of average strain rate with deformation under tension and compression for squeezing speeds of 0.01 (a), 1 (b) and 50mm/min (c) from the FE simulation

Fig. 5.16 shows two examples of the relationship between  $\bar{\dot{\epsilon}}$  and  $D$  at a given strain level: (a) for tensile strain of 0.56 and (b) for compressive strain of 0.27. Both examples indicate that  $D$  increases with the increase of the strain rate, which is consistent with the results reported in the literature [37, 41–44]. The amount of increase for  $D$  from the lowest squeezing speed to the highest used in this study is about 0.2 in Fig. 5.16(a) and 0.1 in Fig. 5.16(b).

Through curve fitting using the power-law function, variation of  $D$  with the logarithmic value of strain rate is established and also given in Fig. 5.16 for tensile  $\bar{\epsilon}_{eq}$  of 0.56 and compressive  $\bar{\epsilon}_{eq}$  of 0.27.

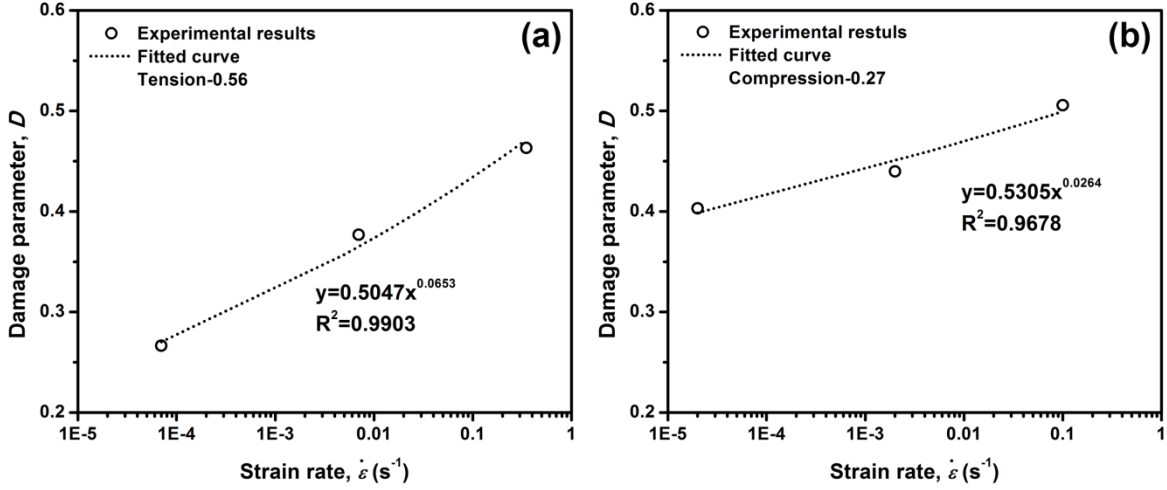


**Fig. 5.16** Relationship between damage parameter ( $D$ ) and strain rate at tensile strain 0.56 (a) and compressive strain 0.27 (b), from Fig. 5.5(b) and 5.7(b), respectively

The accumulative change of  $D$  for each of stages I, II and III in Fig. 5.14, at the squeezing speeds of 0.01, 1 and 50 mm/min, are denoted as  $D_i^{T-j}$  for the damage generated by tensile deformation and  $D_i^{C-j}$  by compressive deformation, in which subscript  $i$  stands for stage I, II or III, and superscript  $j$  crosshead speed of 0.01, 1 or 50 mm/min. The corresponding  $D$  value for the whole squeeze-off process, for a given cross section, is calculated using Eq. (5.4) below for tensile deformation and Eq. (5.5) for compressive deformation.

$$D_{total}^{T-j} = \sum_{i=1}^3 D_i^{T-j} = D_I^{T-j} + D_{II}^{T-j} + D_{III}^{T-j}, j = 0.01, 1 \text{ and } 50 \text{ mm/min} \quad (5.4)$$

$$D_{total}^{C-j} = \sum_{i=1}^3 D_i^{C-j} = D_I^{C-j} + D_{II}^{C-j} + D_{III}^{C-j}, j = 0.01, 1 \text{ and } 50 \text{ mm/min} \quad (5.5)$$

The range for  $\bar{\varepsilon}_{eq}$ ,  $\bar{\varepsilon}$  and change of  $D$  ( $\Delta D$ ) for each stage of Fig. 5.14 and the total damage for the tensile part of the cross-section are summarized in Table 5.2, and the compressive part in Table 5.3. Values in the two tables indicate that change of squeezing speed not only changes

strain rate, but also the strain range covered for each stage. Therefore,  $\Delta D$  for each stage and  $D_{total}$  for a given squeezing speed are not just functions of strain rate generated by the squeezing speed, but also functions of strain range covered in each stage. As a result, difference of  $D_{total}$  between squeezing speeds of 50 and 0.01 mm/min in Table 5.2, is much smaller than that shown in Fig. 5.16(a). Similarly, difference of  $\Delta D_1^C$  between squeezing speeds of 50 and 0.01 mm/min in Table 5.3 is much smaller than that in Fig. 5.16(b), even though the maximum  $\bar{\epsilon}_{eq}$  for stage 1 of compressive deformation at 50 mm/min is larger than that for Fig. 5.16(b), 0.31 and 0.27, respectively. Furthermore, with the consideration of the difference between  $A_C$  and  $A_T$ , that is, 30% of the cross section under tension and 70% under compression, the area-averaged total damage parameter ( $\bar{D}_{total}^j$ ) for the whole cross sectional area with at a given squeezing speeds of 0.01, 1 or 50 mm/min can be calculated using the following equations:

$$\bar{D}_{total}^{0.01} = D_{total}^{T-0.01} \times 30\% + D_{total}^{C-0.01} \times 70\% = 0.48 \quad (5.6)$$

$$\bar{D}_{total}^1 = D_{total}^{T-1} \times 30\% + D_{total}^{C-1} \times 70\% = 0.50 \quad (5.7)$$

$$\bar{D}_{total}^{50} = D_{total}^{T-50} \times 30\% + D_{total}^{C-50} \times 70\% = 0.55 \quad (5.8)$$

Values above indicate that the overall damage among the three squeezing speeds is dominated by compressive deformation and difference of the overall damage caused the change of squeezing speed is less than that would have been expected based on Figs. 5.5(b) or 5.7(b) for the same maximum prestrain level.

**Table 5.2** Damage accumulation data for the part of cross section under tension

	0.01mm/min			1mm/min			50mm/min		
	Stage I	Stage II	Stage III	Stage I	Stage II	Stage III	Stage I	Stage II	Stage III
$\overline{\varepsilon}_{eq}^*$	0-0.29	0.29	0.29-0.55	0-0.31	0.31	0.31-0.56	0-0.34	0.34	0.34-0.49
$\overline{\dot{\varepsilon}}^{**}$	$3.3 \times 10^{-6}$	0	$1.8 \times 10^{-5}$	$2.2 \times 10^{-4}$	0	$1.2 \times 10^{-3}$	$1.1 \times 10^{-2}$	0	$4.1 \times 10^{-2}$
$\Delta D_i^{T***}$	0.13	0	0.28	0.17	0	0.27	0.34	0	0.15
$D_{total}^T$		0.41			0.44			0.49	

Note. \* average equivalent strain; \*\* average strain rate; \*\*\* damage generated during the stage

**Table 5.3** Damage accumulation data for the part of cross section under compression

	0.01mm/min			1mm/min			50mm/min		
	Stage I	Stage II	Stage III	Stage I	Stage II	Stage III	Stage I	Stage II	Stage III
$\overline{\varepsilon}_{eq}^*$	0-0.25	0.25	0.25-0.54	0-0.27	0.27	0.27-0.54	0-0.31	0.31	0.31-0.50
$\overline{\dot{\varepsilon}}^{**}$	$2.5 \times 10^{-6}$	0	$1.7 \times 10^{-5}$	$1.9 \times 10^{-4}$	0	$1.2 \times 10^{-3}$	$9.9 \times 10^{-3}$	0	$5.2 \times 10^{-2}$
$\Delta D_i^C***$	0.39	0	0.12	0.41	0	0.13	0.41	0	0.16
$D_{total}^C$		0.51			0.54			0.57	

Note. \* average equivalent strain; \*\* average strain rate; \*\*\* damage generated in the given stage

## 5.5 Conclusions

The work presented here is to characterize the effects of the squeeze-off process, a popular procedure for pipe maintenance or repair, on PE's mechanical properties, with a special attention to the influence of squeezing speed. The experimental results showed that both elastic modulus and yield stress of the pipe are significantly affected by deformation introduced by the squeeze-

off process. Additionally, the change in mechanical properties showed little dependence on the squeezing speed.

A three-dimensional FE model was developed to facilitate the determination of strain and strain rate in the pipe wall during the squeeze-off process. The FE simulation show that around 70% of the cross section was under compression and 30% under tension. Furthermore, two-stage tests were conducted to confirm the damage development under different loading modes and crosshead speeds. Test results show that both yield stress and elastic modulus decrease with the increase of the deformation. Based on the concept of continuum damage mechanics, value for damage parameter  $D$  was calculated across the pipe wall thickness. The results show that difference of the overall damage among the three squeezing speeds is smaller than that could have been generated in a single loading mode. The study concludes that compressive loading can cause damage in PE pipe, and this damage plays a crucial role in the change of elastic modulus and yield strength of PE pipe. Such an influence of squeeze-off process or any loading scenario that involves compressive deformation should be taken into consideration for evaluation of PE pipe performance.

## References

- [1] Kiass, N., Khelif, R., Boulanouar, L., and Chaoui, K., 2005, "Experimental Approach to Mechanical Property Variability through a High-Density Polyethylene Gas Pipe Wall," *J. Appl. Polym. Sci.*, **97**(1), pp. 272–281.
- [2] Brown, N., and Crate, J. M., 2012, "Analysis of a Failure in a Polyethylene Gas Pipe Caused by Squeeze off Resulting in an Explosion," *Journal of failure analysis and prevention*, **12**(1), pp. 30–36.
- [3] Palermo, G., 2004, "Correlating Aldyl 'A' and Century PE Pipe Rate Process Method Projections with Actual Field Performance," *Plastics Pipes XII Conference. Milan, Italy*.

- [4] Stephens, D. R., Cassady, M. J., and Leis, B. N., 1991, *Progress Report on Preliminary Screening Tests on Squeeze-off of Polyethylene Gas Pipes. Progress Report, January 1987-December 1989*, Battelle, Columbus, OH (United States).
- [5] Stephens, D. R., Leis, B. N., Francini, R. B., and Cassady, M. J., 1992, *Users' Guide on Squeeze-off of Polyethylene Gas Pipes. Plastic Pipes Research Results. Volume 1. Topical Report, August 1989-February 1992*, Battelle, Columbus, OH (United States).
- [6] Yayla, P., and Bilgin, Y., 2007, "Squeeze-off of Polyethylene Pressure Pipes: Experimental Analysis," *Polymer testing*, **26**(1), pp. 132–141.
- [7] Harris, K. E., 2007, "Squeeze-off & Gel Patch Repair Methods for Polyethylene Pipe in Natural Gas Distribution Lines."
- [8] UZELAC, D., BIKIÆ, S., ĐURĐEVIÆ, M., and Bordeasu, I., 2010, "Change of Polyethylene Pipe Wall Thickness after Squeezing Using Squeeze off-Tool," *Materiale Plastice*, **47**(4), pp. 461–466.
- [9] Eugen, A., and Emilia, O. M., 2015, "Determining the Forces in the Polyethylene Pipes after Squeezing Them off with Specific Equipment."
- [10] Haward, R. N., and Thackray, G., 1968, "The Use of a Mathematical Model to Describe Isothermal Stress-Strain Curves in Glassy Thermoplastics," *Proceedings of the Royal Society of London A: Mathematical, Physical and Engineering Sciences*, **302**(1471), pp. 453–472.
- [11] Boyce, M. C., Parks, D. M., and Argon, A. S., 1988, "Large Inelastic Deformation of Glassy Polymers. Part I: Rate Dependent Constitutive Model," *Mechanics of Materials*, **7**(1), pp. 15–33.
- [12] Boyce, M. C., Socrate, S., and Llana, P. G., 2000, "Constitutive Model for the Finite Deformation Stress-strain Behavior of Poly (Ethylene Terephthalate) above the Glass Transition," *Polymer*, **41**(6), pp. 2183–2201.
- [13] Ahzi, S., Makradi, A., Gregory, R. V., and Edie, D. D., 2003, "Modeling of Deformation Behavior and Strain-Induced Crystallization in Poly (Ethylene Terephthalate) above the Glass Transition Temperature," *Mechanics of materials*, **35**(12), pp. 1139–1148.
- [14] Polanco-Loria, M., Clausen, A. H., Berstad, T., and Hopperstad, O. S., 2010, "Constitutive Model for Thermoplastics with Structural Applications," *International Journal of Impact Engineering*, **37**(12), pp. 1207–1219.
- [15] Ayoub, G., Zaïri, F., Frédérix, C., Gloaguen, J.-M., Naït-Abdelaziz, M., Seguela, R., and Lefebvre, J.-M., 2011, "Effects of Crystal Content on the Mechanical Behaviour of Polyethylene under Finite Strains: Experiments and Constitutive Modelling," *International Journal of Plasticity*, **27**(4), pp. 492–511.
- [16] Ayoub, G., Zaïri, F., Naït-Abdelaziz, M., and Gloaguen, J. M., 2010, "Modelling Large Deformation Behaviour under Loading-unloading of Semicrystalline Polymers: Application to a High Density Polyethylene," *International Journal of Plasticity*, **26**(3), pp. 329–347.
- [17] Ognedal, A. S., Clausen, A. H., Dahlen, A., and Hopperstad, O. S., 2014, "Behavior of PVC and HDPE under Highly Triaxial Stress States: An Experimental and Numerical Study," *Mechanics of Materials*, **72**, pp. 94–108.
- [18] Bodner, Sr., and Partom, Y., 1975, "Constitutive Equations for Elastic-Viscoplastic Strain-Hardening Materials," *Journal of Applied Mechanics*, **42**(2), pp. 385–389.

- [19] Frank, G. J., and Brockman, R. A., 2001, "A Viscoelastic–viscoplastic Constitutive Model for Glassy Polymers," *International Journal of Solids and Structures*, **38**(30), pp. 5149–5164.
- [20] G'sell, C., and Jonas, J. J., 1979, "Determination of the Plastic Behaviour of Solid Polymers at Constant True Strain Rate," *Journal of materials science*, **14**(3), pp. 583–591.
- [21] Hutchinson, J. W., and Neale, K. W., 1983, "Neck Propagation," *Journal of the Mechanics and Physics of Solids*, **31**(5), pp. 405–426.
- [22] Fager, L. O., and Bassani, J. L., 1986, "Plane Strain Neck Propagation," *International journal of solids and structures*, **22**(11), pp. 1243–1257.
- [23] Tugcu, P., and Neale, K. W., 1988, "Analysis of Neck Propagation in Polymeric Fibres Including the Effects of Viscoplasticity," *Journal of engineering materials and technology*, **110**(4), pp. 395–400.
- [24] Khan, A. S., and Liang, R., 1999, "Behaviors of Three BCC Metal over a Wide Range of Strain Rates and Temperatures: Experiments and Modeling," *International Journal of Plasticity*, **15**(10), pp. 1089–1109.
- [25] Khan, A., and Zhang, H., 2001, "Finite Deformation of a Polymer: Experiments and Modeling," *International Journal of Plasticity*, **17**(9), pp. 1167–1188.
- [26] Khan, A. S., Suh, Y. S., and Kazmi, R., 2004, "Quasi-Static and Dynamic Loading Responses and Constitutive Modeling of Titanium Alloys," *International Journal of Plasticity*, **20**(12), pp. 2233–2248.
- [27] Krempl, E., McMahon, J. J., and Yao, D., 1986, "Viscoplasticity Based on Overstress with a Differential Growth Law for the Equilibrium Stress," *Mechanics of Materials*, **5**(1), pp. 35–48.
- [28] Ho, K., and Krempl, E., 2002, "Extension of the Viscoplasticity Theory Based on Overstress (VBO) to Capture Non-Standard Rate Dependence in Solids," *International Journal of Plasticity*, **18**(7), pp. 851–872.
- [29] Colak, O. U., 2005, "Modeling Deformation Behavior of Polymers with Viscoplasticity Theory Based on Overstress," *International Journal of Plasticity*, **21**(1), pp. 145–160.
- [30] Colak, O. U., and Dusunceli, N., 2006, "Modeling Viscoelastic and Viscoplastic Behavior of High Density Polyethylene (HDPE)," *Journal of Engineering Materials and Technology*, **128**(4), pp. 572–578.
- [31] Kwon, H. J., and Jar, P.-Y., 2008, "On the Application of FEM to Deformation of High-Density Polyethylene," *International Journal of Solids and Structures*, **45**(11), pp. 3521–3543.
- [32] Muhammad, S., and Jar, P.-Y., 2013, "Determining Stress–strain Relationship for Necking in Polymers Based on Macro Deformation Behavior," *Finite Elements in Analysis and Design*, **70**, pp. 36–43.
- [33] Muhammad, S., and Jar, P.-Y. B., 2011, "Effect of Aspect Ratio on Large Deformation and Necking of Polyethylene," *J Mater Sci*, **46**(4), pp. 1110–1123.
- [34] Ben Jar, P.-Y., 2014, "Transition of Neck Appearance in Polyethylene and Effect of the Associated Strain Rate on the Damage Generation," *Polym Eng Sci*, **54**(8), pp. 1871–1878.
- [35] Jar, P.-Y. B., 2014, "Effect of Tensile Loading History on Mechanical Properties for Polyethylene," *Polym Eng Sci*, p. n/a-n/a.
- [36] Butler, M. F., and Donald, A. M., 1998, "A Real-Time Simultaneous Small-and Wide-Angle X-Ray Scattering Study of in Situ Polyethylene Deformation at Elevated Temperatures," *Macromolecules*, **31**(18), pp. 6234–6249.

- [37] Addiego, F., Dahoun, A., G'Sell, C., and Hiver, J.-M., 2006, "Characterization of Volume Strain at Large Deformation under Uniaxial Tension in High-Density Polyethylene," *Polymer*, **47**(12), pp. 4387–4399.
- [38] Galeski, A., Bartczak, Z., Argon, A. S., and Cohen, R. E., 1992, "Morphological Alterations during Texture-Producing Plastic Plane Strain Compression of High-Density Polyethylene," *Macromolecules*, **25**(21), pp. 5705–5718.
- [39] Bartczak, Z., Cohen, R. E., and Argon, A. S., 1992, "Evolution of the Crystalline Texture of High-Density Polyethylene during Uniaxial Compression," *Macromolecules*, **25**(18), pp. 4692–4704.
- [40] Zhang, C., and Moore, I. D., 1997, "Nonlinear Mechanical Response of High Density Polyethylene. Part I: Experimental Investigation and Model Evaluation," *Polym Eng Sci*, **37**(2), pp. 404–413.
- [41] Pawlak, A., and Galeski, A., 2010, "Cavitation during Tensile Drawing of Annealed High Density Polyethylene," *Polymer*, **51**(24), pp. 5771–5779.
- [42] Pawlak, A., Galeski, A., and Rozanski, A., 2014, "Cavitation during Deformation of Semicrystalline Polymers," *Progress in polymer science*, **39**(5), pp. 921–958.
- [43] Balieu, R., Lauro, F., Bennani, B., Haugou, G., Chaari, F., Matsumoto, T., and Mottola, E., 2015, "Damage at High Strain Rates in Semi-Crystalline Polymers," *International Journal of Impact Engineering*, **76**, pp. 1–8.
- [44] Zhang, Y., and Jar, P.-Y. B., 2015, "Quantitative Assessment of Deformation-Induced Damage in Polyethylene Pressure Pipe," *Polymer Testing*, **47**, pp. 42–50.

# Chapter 6

## **Characterization of ductile damage in polyethylene based on effective stress concept**

In this chapter we introduce a new approach to the characterization of ductile damage in polyethylene (PE) material using the damage variable defined as  $D = 1 - \sigma/\sigma_{eff}$  which is based on the concept of effective stress in continuum damage mechanics (CDM). Quasi-static stress-strain relationship has been established using a spring-damper-plastic element model, calibrated using results from stress relaxation tests. The viscous stress component was then removed from the experimentally measured total stress to determine the quasi-static stress component. The results were used to investigate the influence of crosshead speed and specimen geometry, through varying the ligament width of the PE specimen, on the quasi-static stress-strain curves. Results show that reduction of the crosshead speed leads to larger quasi-static stress due to less damage generated at a lower crosshead speed, while variation of the ligament width has little effect on the quasi-static stress. Using a curve that is fitted to the experimentally determined quasi-static stress as a function of crosshead speed and extrapolated to zero crosshead speed, the effective stress in the undamaged configuration was successfully estimated and used to determine the stress-based damage variable. The damage variable so determined is compared with those measured through the degradation of elastic modulus either based on the hypothesis of strain or energy equivalence. The stress-based damage variable shows good agreement with the damage variable based on the energy-equivalence approach.

## 6.1 Introduction

Semi-crystalline polymers such as polyethylene (PE) and polypropylene (PP) are now widely used in industry as structural materials. Statistics shows that over 90% of the newly installed gas pipeline systems are made of PE [1]. Because of the potentials of pipeline failure for the huge economic losses and threats to the public safety [2-4], it is extremely important to have a tool to characterize the likelihood of pipeline failure. Over the past two decades, continuum damage mechanics (CDM) has played a critical role in modelling material failure behaviour. However, a material-specific damage parameter  $D$  is needed in CDM to quantify degradation in mechanical properties due to various mechanisms such as nucleation, coalescence and growth of microvoids. Accurate quantification of  $D$  relies on proper methodologies to measure the changes in mechanical properties.

Various methods have been proposed to measure and characterize ductile damage in materials. These methods can be categorized into two main approaches, based on (I) mechanics of porous media theory (MPM) and (II) continuum damage mechanics (CDM). The former regards cavitation as the main mechanism for the damage generation, and uses porosity, volume strain or void volume fraction to represent the damage level. In this approach, Gurson damage model [5] is the most popular way to quantify the ductile damage evolution, especially in porous materials, through the use of a porosity term to represent the progressive shrinkage of the yield surface. Later, this model was successfully extended to consideration of voids coalescence and growth [6–8]. Damage quantification based on the porosity measurement has been widely used for semi-crystalline polymers at the macroscopic scale by means of 2D video extensometer [9–

11]. At the microscopic scale, the volume strain or porosity has been characterized by scanning electron microscopy (SEM) [11–14], wide-angle X-ray scattering (WAXS) and small-angle X-ray scattering (SAXS) [15–20]. Although these methods are powerful tools for understanding deformation and cavitation mechanisms from the microscopic point of view, they are difficult to perform, time consuming and subjected to errors due to the lack of objectivity in the definition of the reference volume [21].

The second approach is to characterize the damage state based on a macroscopic damage variable,  $D$ , defined as the ratio of effective area of micro-cracks and cavities to the overall cross-sectional area of the representative volume element (RVE). The concept of effective stress under uniaxial tension, first introduced by Kachanov [22, 23], was later extended to three dimensional stress state by Lemaitre [24, 25]. For the case of isotropic damage, the effective stress is defined by

$$\sigma_{eff} = \frac{\sigma}{1-D} \quad (6.1)$$

where  $\sigma$  is Cauchy stress in the damaged configuration and  $\sigma_{eff}$  the corresponding effective stress in a fictitious state of totally undamaged material. In most cases, hypothesis of either strain equivalence or energy equivalence is needed to convert the above effective-stress-based concept to other experimentally measurable quantities in order to characterize the damage. A number of measurable quantities and the corresponding experimental methods have been proposed to characterize the damage evolution process, such as elastic modulus, stiffness, toughness and hardness. The pioneering work on the damage quantification was conducted by Lemaitre and Dufailly [26] through the application of the effective stress concept to eight

experimental techniques. For example, damage can be quantified directly using the ratio of damaged to total cross-sectional areas,  $D_A = A_D/A_0$ , or the change in material density,  $D_\rho = (1 - \rho_D/\rho_0)^{2/3}$ . In addition to these direct experimental measurements, indirect techniques based on variation in mechanical properties were also proposed, such as the change in elastic modulus,  $D_E = 1 - E_D/E_0$ , micro-hardness,  $D_H = 1 - H_D/H_0$ , or ultrasonic velocity with the assumption of constant density during the damage development,  $D_v \approx 1 - v_D^2/v_0^2$ . More recently, an in-depth comparison of six methodologies was made by Tasan et al. [27] and the results showed that geometry-based damage characterization methodologies introduce significant systematic errors as they probe a very limited damage spectrum, whereas methodologies that measure the degradation of mechanical properties suffer from low precision and high complexity, especially for deformation with large strains and material anisotropy.

Since the damage concept was developed, these CDM-based methodologies have been widely employed for the measurement and characterization of ductile damage in a wide range of engineering materials. For instance, ductile damage in metallic materials was characterized through the degradation of elastic modulus, measured from the unloading phase of loading-unloading tensile test [28–37] or micro-indentation test [38–41]. In addition, potential drop method [42, 43] and ultrasonic technique [44–47] have also been proposed to quantify the ductile damage. Furthermore, influence of external factors, including strain rate, stress triaxiality and temperature, on the evolution of ductile damage has also been investigated. The results show that damage is developed faster at a higher strain rate [35, 36] or a higher level of stress triaxiality [32, 48, 49]. Although significant efforts have been made to evaluate ductile damage

evolution in metallic materials, much less work has been carried out to apply the CDM-based damage characterization methods to semi-crystalline polymers [50–53].

Further to the lack of research work on the damage characterization in semi-crystalline polymers, current approaches to prediction of degradation and failure of engineering structures require a transformation hypothesis such as strain equivalence or energy equivalence to relate stress and strain tensors in the damaged configuration to the corresponding tensors in the undamaged configuration [54–60]. However, constitutive equation for the undamaged configuration of semi-crystalline polymers is not readily available. Without the information, quantifying the damage evolution requires the above hypotheses of strain or energy equivalence. However, deformation in PE is nonlinear and strongly time-dependent, which limits the applicability of the above hypotheses to a very small strain range, thus impractical for common engineering applications. In view of this limitation, an alternative damage parameter is needed to quantify the damage evolution in semi-crystalline polymers. Work presented in this chapter is to develop a stress-based damage characterization approach, by determining the effective stress for a given material and use Eq. (6.1) to quantify the damage.

In this chapter, a procedure to determine the effective stress as a function of strain for the fictitious undamaged state of PE material is described, by removing the viscous stress component and extrapolating the remaining quasi-static stress component to the test condition of zero crosshead speed. Damage introduced to PE under various strain rates is then characterized using the new stress-based damage variable, and compared with the damage variables based on the change of elastic modulus, measured from a two-stage test method [61, 62], under the hypothesis of either strain or energy equivalence.

## 6.2 Experimental details

### 6.2.1 Material and specimens

Notched pipe ring (NPR) specimens, modified from ASTM: D2290-12 [63], were used for the experimental testing, prepared from a commercial PE4710 HDPE pipe with a minimum required strength (MRS) of 10MPa. The inner and outer diameters of all pipes, manufactured by Endot Industries are approximately 52.5 and 64.5mm with a standard dimension ratio of about 11 (average wall thickness of approximately 6mm). For this study, notch tip of the NPR specimens was modified to have a flat profile, instead of round, so that stress distribution in the ligament region is relatively uniform. Since the NPR specimens have a nominal thickness of 6mm, variation of the specimen geometry was through the change of ligament width  $w$  from 6 to 2.5mm, corresponding to the aspect ratio (thickness/width) from 1 to 2.4, as shown in Fig. 6.1(a).

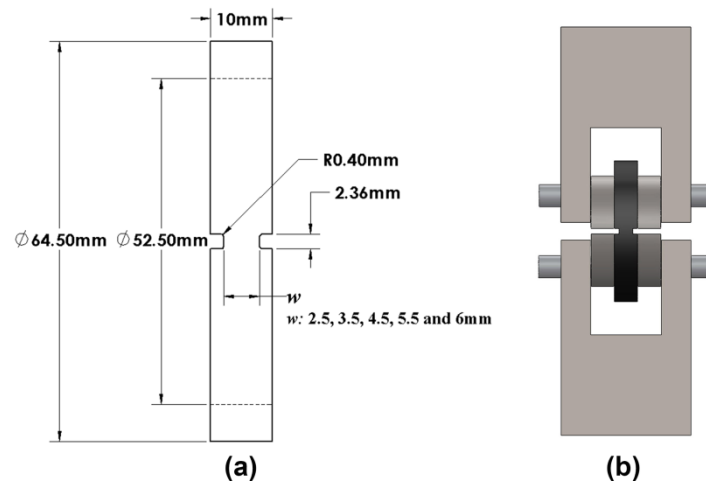


**Fig. 6.1** D-split test: (a) NPR specimen dimensions and (b) test setup

### 6.2.2 Mechanical testing

All tests were conducted using a universal test machine (QUASAR 100) at room temperature. Fig. 6.1(b) presents the D-split tensile test set-up used in this study, which was first proposed for

testing composite materials [8]. Damage development measured from the elastic modulus degradation was characterized using a two-stage test procedure, proposed by Jar [9-11], in which tests at the first stage were to introduce various prestrain levels at crosshead speeds of 0.001, 0.01, 0.1, 1 and 10mm/min, and the second stage tests, conducted at a constant crosshead speed of 0.01mm/min, were to characterize the corresponding change in elastic modulus.

In the first stage tests, stress relaxation was conducted immediately after the NPR specimens were stretched to the preselected strain levels for 3 hours. The prestrain value, which is also equal to relaxation strain ( $\epsilon_{true}$ ) is calculated based on the change of ligament width and thickness, using the following expression:

$$\epsilon_{true} = \ln\left(\frac{w_0 t_0}{w t}\right) \quad (6.2)$$

where  $w_0$ ,  $t_0$ ,  $w$ , and  $t$  are original ligament width, original ligament thickness, deformed ligament width and deformed ligament thickness, respectively. Variation of  $w$  and  $t$  during the test was measured using two separate extensometers. Five crosshead speeds of 0.001, 0.01, 0.1, 1, and 10mm/min, corresponding to the initial strain rates of  $7 \times 10^{-6}$ ,  $7 \times 10^{-5}$ ,  $7 \times 10^{-4}$ ,  $7 \times 10^{-3}$  and  $7 \times 10^{-2} \text{ s}^{-1}$ , respectively, were used in the first stage tests to vary the deformation rate, to examine its influence on the damage development and for the prediction of effective stress in an extrapolation process, as to be shown in Results and Discussion. Unloading for all first tests was kept at the same crosshead speed 0.1mm/min. The prestrain levels were chosen to be 5%, 10%, 20%, 30%, 40% and 50%.

### 6.3 Model for determining the quasi-static stress

A two-component model modified from Strobl's group [24-26] by combining the crystal and network branches into one elasto-plastic branch was used to determine the quasi-static stress-strain relationship of PE materials through removing the viscous stress component from the total true stress measured from uniaxial tensile tests. The proposed two-component model was applied to determine viscous stress component at a given strain level by regenerating results from a stress relaxation test. In addition to the elasto-plastic branch, that contains a spring and a finite plasticity element connected in series, and is responsible for the quasi-static stress  $\sigma_{ep}$ , a viscous branch that contains a spring and a damper connected in series and is responsible for the time-dependent stress component  $\sigma_r$  is included in this model.

Based on the above model, the elastic-plastic stress  $\sigma_{ep}$  at a given strain  $\varepsilon_{true}$  is equivalent to the difference between the total stress and viscous stress  $\sigma_r$  at the beginning of the stress relaxation process at the same strain  $\varepsilon_{true}$ . Value for  $\sigma_r$  at the beginning of the stress relaxation process is denoted as  $\sigma_r(0)$ , and is determined by calibrating the model using the stress relaxation curve obtained experimentally. By determining  $\sigma_{ep}$  values at several strain levels, the quasi-static stress-strain relationship is determined. Details of this procedure are given in [64], and therefore will be briefly described as follows.

The relaxation process in PE can be described using the Eyring's viscosity law using the following expression according to the suggestion made by Hong et al. [25].

$$\frac{d}{dt} \frac{\sigma_r}{\sigma_0} = -\frac{1}{\tau_r} \sinh\left(\frac{\sigma_r}{\sigma_0}\right) \quad (6.3)$$

with

$$\tau_r^{-1} = \frac{\dot{\epsilon}_0 E_r}{\sigma_0} = \frac{E_r}{\eta_0} \quad (6.4)$$

where  $\tau_r$ ,  $E_r$  and  $\sigma_0$  are characteristic relaxation time, relaxation modulus and reference stress, respectively. Solution for Eq. (6.3) can be explicitly obtained and described as

$$\frac{\sigma_r(t)}{\sigma_0} = 2 \operatorname{atanh} \left[ \tanh \left( \frac{\sigma_r(0)}{2\sigma_0} \right) \exp \left( -\frac{t}{\tau_r} \right) \right] \quad (6.5)$$

Using Eq. (6.5), the stress decay ( $\Delta\sigma$ ), defined as

$$\Delta\sigma = \sigma_r(0) - \sigma_r(t) \quad (6.6)$$

can be expressed as

$$\Delta\sigma = \sigma_r(0) - 2\sigma_0 \operatorname{atanh} \left[ \tanh \left( \frac{\sigma_r(0)}{2\sigma_0} \right) \exp \left( -\frac{t}{\tau_r} \right) \right] \quad (6.7)$$

## 6.4 Results and discussion

### 6.4.1 Effects of strain rate

True stress-strain curves from PE specimens at five crosshead speeds of 0.001, 0.01, 0.1, 1 and 10mm/min are presented in Fig. 6.2. It should be pointed out that in view of the high reproducibility of results from this type of tests [53], only one specimen was used for the monotonic tensile test at each crosshead speed, to depict the effects of crosshead speed on the overall stress-strain relationship under the tensile loading. Fig. 6.2 shows the general trend of the

test results, with increase of stress with the increase of crosshead speed, which is consistent with the results reported before [65]. The results suggest that PE used in this study exhibits highly nonlinear and rate-dependent behavior. It has been suggested that the trend of change shown in Fig. 6.2 is attributed to the change in mechanisms involved in the deformation processes. That is, at a low deformation rate, the amorphous region is relatively soft, and therefore the overall stress response is mainly controlled by the stress response to deformation in the amorphous phase. On the other hand, mobility of the amorphous phase is reduced to increase its resistance to deformation at higher strain rate [11, 66], thus increasing the involvement of the crystalline phase in the deformation process.

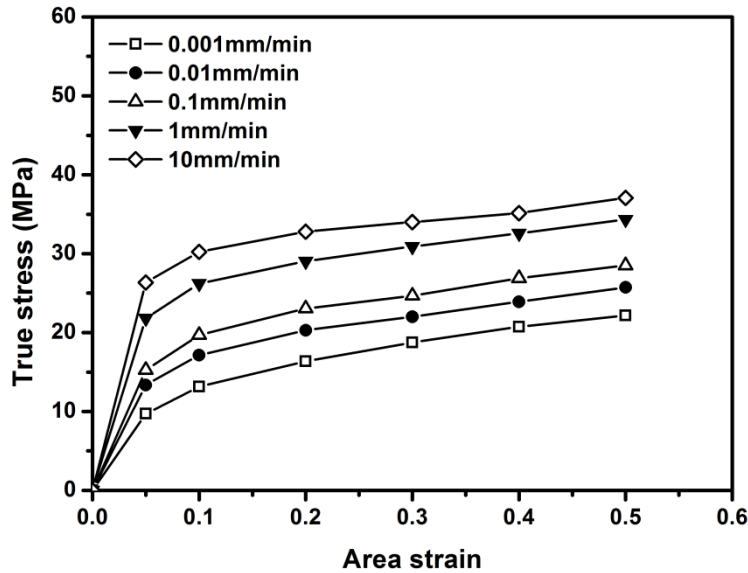


**Fig. 6.2** True stress-strain curves for five crosshead speeds

Curves of stress decay versus relaxation time generated from Eq. (6.7) and those obtained experimentally (lines) at the relaxation strain of 10% and 30% are compared in Fig. 6.3, depicting the excellent agreement. All parameters in Eq. (6.7) used to regenerate the curves in Fig. 6.3 are summarized in Table 6.1.

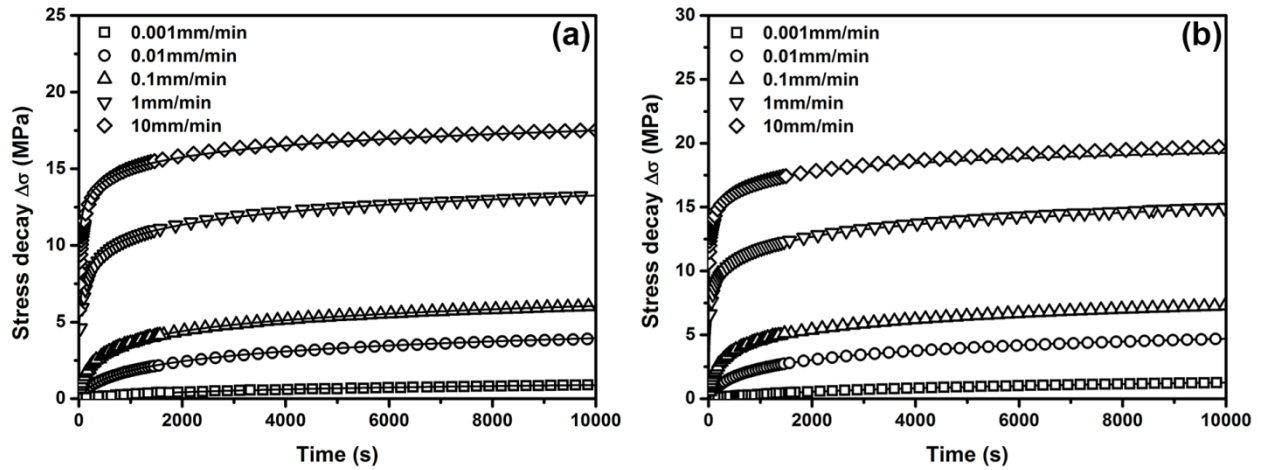


**Fig. 6.3** Curves generated from Eq. (6.7) (open symbols) and obtained from stress relaxation tests (lines) at the relaxation strain of 10% (a) and 30% (b) with the initial stretch introduced at the crosshead speeds of 0.001, 0.01, 0.1, 1 and 10mm/min

**Table 6.1** Summary of values for  $\sigma_r(0)$  and  $\sigma_0$  in Eq. (6.7), with  $\tau_r = 1.6 \times 10^4$

Relaxation strain	0.001mm/min		0.01mm/min		0.1mm/min		1mm/min		10mm/min	
	$\sigma_r(0)$	$\sigma_0$								
5%	1.1	0.32	4.1	0.82	6.1	0.88	12.4	1.03	17.4	1.06
10%	1.3	0.37	5.12	1	7.3	1.05	14.7	1.32	18.8	1.10
20%	1.63	0.52	5.6	1.05	8.55	1.2	16.1	1.35	20.7	1.22
30%	1.9	0.59	5.97	1.08	8.7	1.21	16.7	1.43	21.2	1.24
40%	2.1	0.65	6.01	1.09	9.1	1.22	16.9	1.53	21.5	1.27
50%	2.25	0.72	6.18	1.1	9.3	1.25	17.7	1.55	21.8	1.36

Fig. 6.4 presents results of viscous stress and quasi-static stress determined at crosshead speeds of 0.001, 0.01, 0.1, 1 and 10mm/min for the PE material. As shown in Fig. 6.4(a), viscous stress is larger at a higher deformation rate, which is consistent with the experimental

observation that under monotonic tensile loading condition the measured stress increases with the increase of strain rate. Despite of the widely observed phenomenon that the total stress increases with the increase of strain rate, an opposite trend has been observed after the viscous stress component is removed from the total stress. This is supported by Fig. 6.4(b) in which the quasi-static stress decreases as increase in the crosshead speed. Such an opposite trend of change in stress with the increase of crosshead speed is consistent with the results reported previously [12], and can serve as another evidence to support the effects of deformation rate on the damage growth in PE materials. That is, at a given strain level, damage is larger and grows faster at higher strain rate [8].

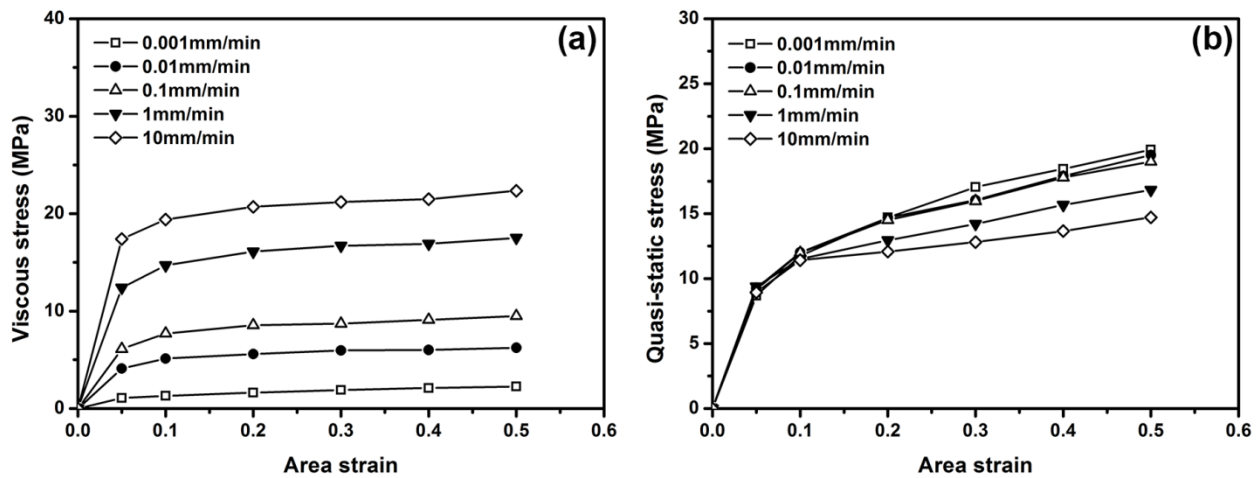


**Fig. 6.4** Viscous stress (a) and quasi-static stress (b) for crosshead speeds of 0.001, 0.01, 0.1, 1 and 10mm/min

To demonstrate clearly the effects of crosshead speed on the quasi-static stress, the results presented in Fig. 6.4(b) are presented in a different way in Fig. 6.5, by plotting the quasi-static stress as a function of logarithmic crosshead speed. In addition to the phenomenon that the quasi-static stress increases with the crosshead speed which is also represented in Fig. 6.4(b), Fig. 6.5 shows a clear trend that reducing the crosshead speed leads to the increase of quasi-static

stress. Taking the damage effects into consideration, the decrease of quasi-static stress with the increase of strain rate is probably caused by the larger damage generated at a higher strain rate. As a result, the quasi-static stress as the strain rate approaches zero should be equivalent to the effective stress at the undamaged configuration (i.e.,  $D = 0$ ). The curves of quasi-static stress versus logarithm crosshead speed, as shown in Fig. 6.5, can be fitted using the following three-parameter arctangent function:

$$y = A - B \operatorname{atan}(Cx) \quad (6.8)$$

where  $x$  and  $y$  are logarithmic crosshead speed and quasi-static stress, respectively,  $A$ ,  $B$  and  $C$  user-defined parameters for which the values are adjusted to fit the experimental data. Choice of the above fitting function is based on the following criteria: (1) the function should fit the experimental results satisfactorily, (2) the function should have a limit when the crosshead speed or strain rate reaches zero, and (3) the function should be monotonic. All values used for parameters in Eq. (6.8) to generate the fitting curves in Fig. 6.5 are summarized in Table 6.2. It should be noted that the zero crosshead speed corresponds to  $x$  value in Eq. (6.8) of negative infinity. The predicted quasi-static stresses at zero crosshead speed (i.e., zero strain rate) are given in the bottom row of Table 6.2.

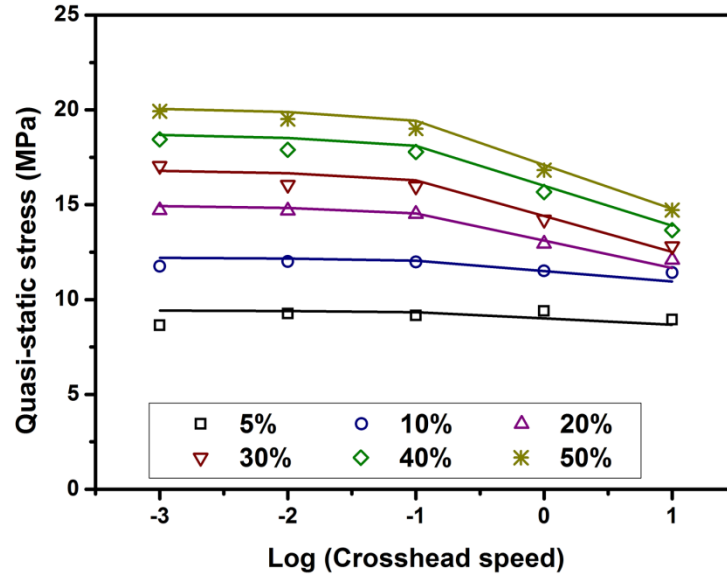


**Fig. 6.5** The relationship between quasi-static stress and crosshead speed for various strains

**Table 6.2** Values for parameters in Eq. (6.8) and quasi-static stress as crosshead speed reaches zero

Prestrain	5%	10%	20%	30%	40%	50%
A	9	11.5	13.1	14.4	16	17.1
B	0.3	0.5	1.3	1.7	1.9	2.1
C	2	2	2	2	2	2
$y @ x \rightarrow -\infty$	9.47	12.29	15.14	17.07	18.98	20.39

#### 6.4.2 Effects of specimen geometry

Typical plots of true stress versus area strain for NPR specimens of different ligament widths, obtained at the crosshead speed of 0.001mm/min, are presented in Fig. 6.6. The figure suggests that change in the ligament width has little effect on the stress-strain curves, which is consistent with the results reported before [67].

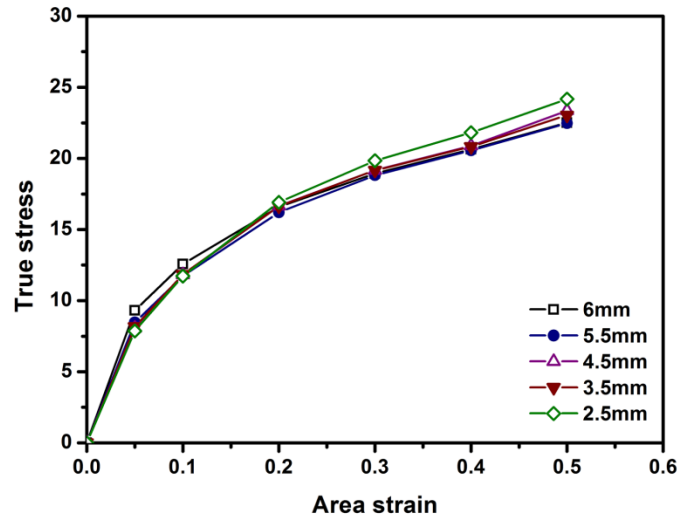


**Fig. 6.6** Experimental curves of true stress versus area strain for PE samples with different ligament widths, at the crosshead speed of 0.001mm/min

Using the model and approach presented in Section 3, the experimentally determined relaxation test results for NPR specimens of different ligament widths, as shown in Fig. 6.6, have been successfully regenerated using Eq. (6.7). Fig. 6.7 presents the results of viscous stress and quasi-static stress components for the data shown in Fig. 6.6. As shown in Fig. 6.7(a), reducing the ligament width leads to increase in the viscous stress. The variation of ligament width, however, does not affect the quasi-static stress-strain curves, as shown in Fig. 6.7(b).

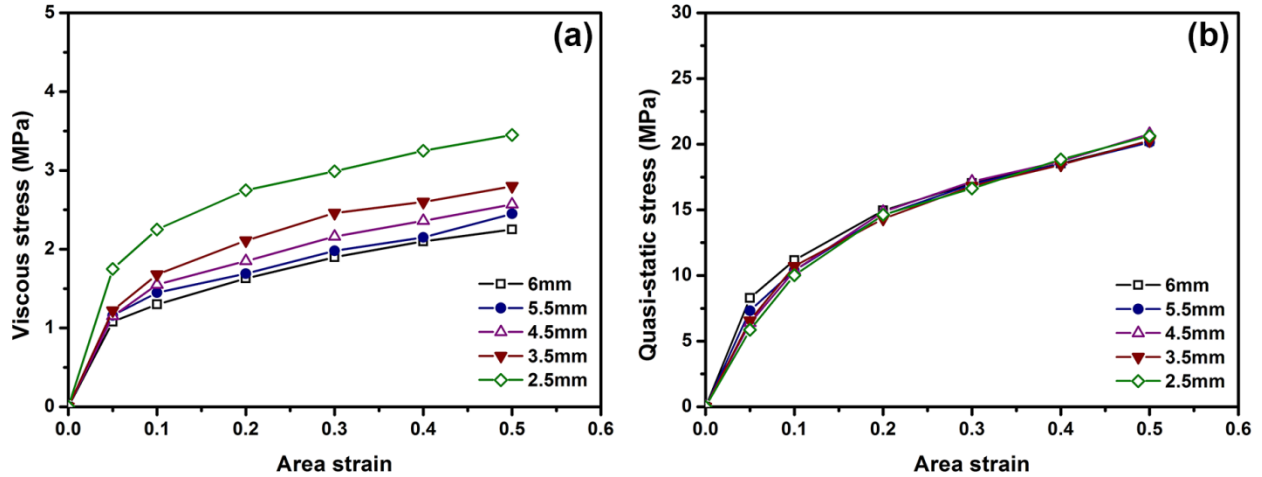


**Fig. 6.7** Viscous stress and quasi-static stress for PE samples with different widths, tested at the crosshead speed of 0.001mm/min

In order to demonstrate clearly the influence of ligament width on the quasi-static stress, data for Fig. 6.7(b) are presented in a different way in Fig. 6.8, by plotting the quasi-static stress as a function of ligament width. Fig. 6.8 suggests that the change in ligament width in the range used in this study does not show a clear influence on the quasi-static stress. As a result, extrapolating the quasi-static stress to zero ligament width was not performed for determining the effective stress values.

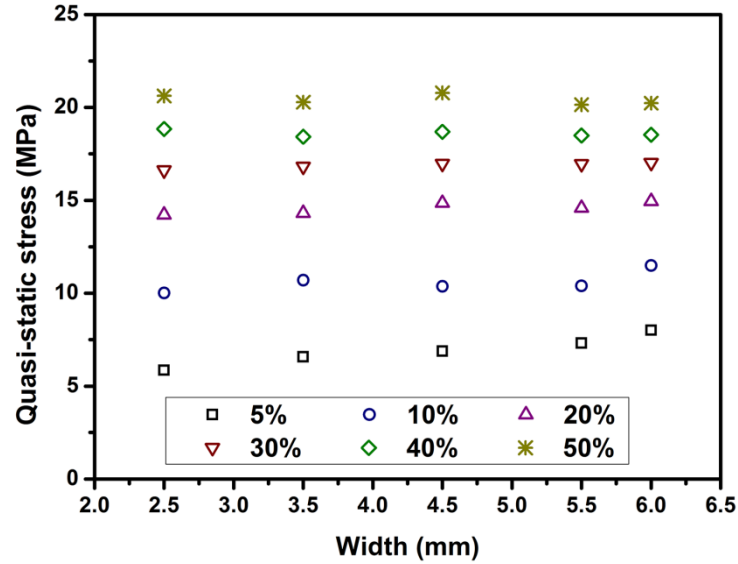


**Fig. 6.8** Variation of quasi-static stress with the ligament width for various strains

### 6.4.3 Damage characterization

The general definition of damage variable  $D$  for isotropic damage is the ratio of damaged area  $S_D$  over the total surface area  $S$ .

$$D = \frac{S_D}{S} \quad (6.9)$$

The relationship between the effective stress  $\sigma_{eff}$  in the fictitious undamaged configuration and the stress  $\sigma$  in the damaged configuration, as shown in Fig. 6.9, is described using the expression in Eq. (6.1).

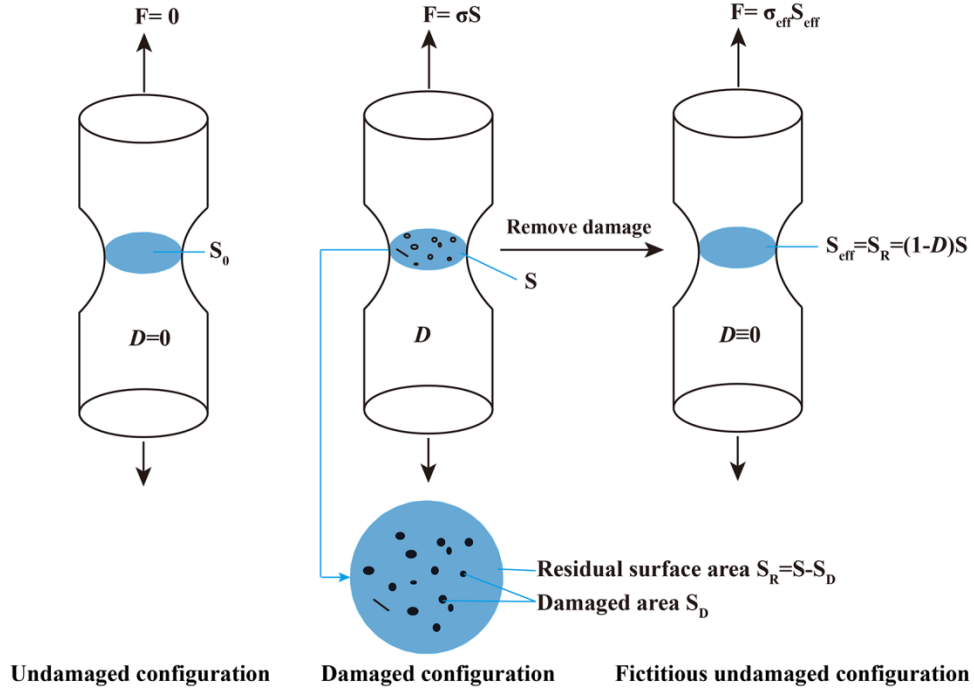


**Fig. 6.9** Schematic depiction of undamaged, damaged and fictitious undamaged configurations

In order to derive the expression for  $D$  based on the degradation of elastic modulus, an assumption needs to be made, which is usually one of the following two hypotheses.

(1) Strain equivalence: Under this assumption, the strain  $\varepsilon$  in the damaged configuration is equal to the effective strain  $\varepsilon_{eff}$  in the fictitious undamaged configuration, that is,

$$\varepsilon = \varepsilon_{eff} \quad (6.10)$$

In the case of elastic deformation, the constitutive equations for damaged and undamaged configurations are given by

$$\sigma = E_D \varepsilon \quad (6.11)$$

$$\sigma_{eff} = E_0 \varepsilon_{eff} \quad (6.12)$$

where  $E_D$  and  $E_0$  are elastic moduli of the damaged and virgin materials, respectively.

The corresponding damage variable  $D_{SE}$ , based on the definition of effective stress given in Eq. (6.1), can be expressed as

$$D_{SE} = 1 - \frac{E_D}{E_0} \quad (6.13)$$

Since this damage variable is based on the hypothesis of strain equivalence, it is named SE method hereafter.

(2) Energy equivalence: Under this assumption, both damaged and fictitious undamaged configurations have the same strain energy,  $\sigma^2/2E$ , that is,

$$\frac{\sigma^2}{2E_D} = \frac{\sigma_{eff}^2}{2E_0} \quad (6.14)$$

Under the hypothesis of energy equivalence and the definition of effective stress given in Eq. (6.1), the damage variable  $D_{EE}$  can be expressed using the following expression.

$$D_{EE} = 1 - \sqrt{\frac{E_D}{E_0}} \quad (6.15)$$

Since this expression is based on the hypothesis of energy equivalence, it is named as EE method hereafter.

Fig. 6.10 presents variation of the damage parameter  $D_{SE}$ , based on Eq. (6.13), as a function of prestrain introduced in the first-stage tests. Fig. 6.10 indicates that damage starts at a critical

prestrain level that is lowered by the increase of crosshead speed used in the first test. In other words, at a given prestrain level damage is more severe by using a higher crosshead speed to generate the prestrain. The figure also indicates that both crosshead speed and prestrain level have a significant effect on the damage generation.

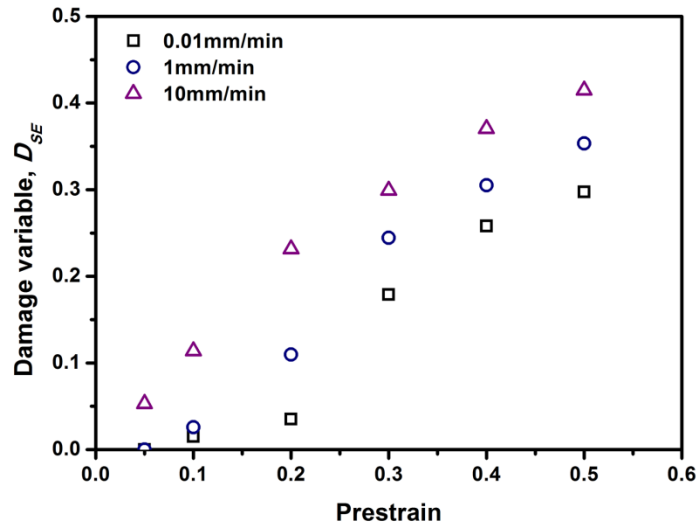


**Fig. 6.10** Damage variable as a function of prestrain, generated at crosshead speeds of 0.01, 1 and 10mm/min

Instead of characterizing damage based on degradation of elastic modulus, damage can be directly expressed in terms of decrease of the stress:

$$D_{eff} = 1 - \frac{\sigma}{\sigma_{eff}} \quad (6.16)$$

where  $\sigma$  and  $\sigma_{eff}$  are stress for the damaged and undamaged material, respectively, at a given strain level. Using the effective stress for fictitious undamaged material, as summarized in Table 6.2, and the stress for the damaged material shown in Fig. 6.2, the damage variables for the crosshead speeds of 0.01, 1 and 10mm/min are presented in Figs. 6.11(a), 6.11(b) and 6.11(c), respectively. For comparison, damage variables calculated using SE and EE methods, according

to Eqs. (6.13) and (6.15), respectively, are also included in Fig. 6.11. Fig. 6.11 suggests that  $D$  values based on the proposed effective stress method and those from the conventional EE method are in close agreement, indicating the feasibility of using the proposed approach to determine the effective stress for polymeric materials that show strong viscous behaviour. Advantage of the proposed effective stress method is that it does not require any hypothesis such as strain or energy equivalence to characterize the damage.

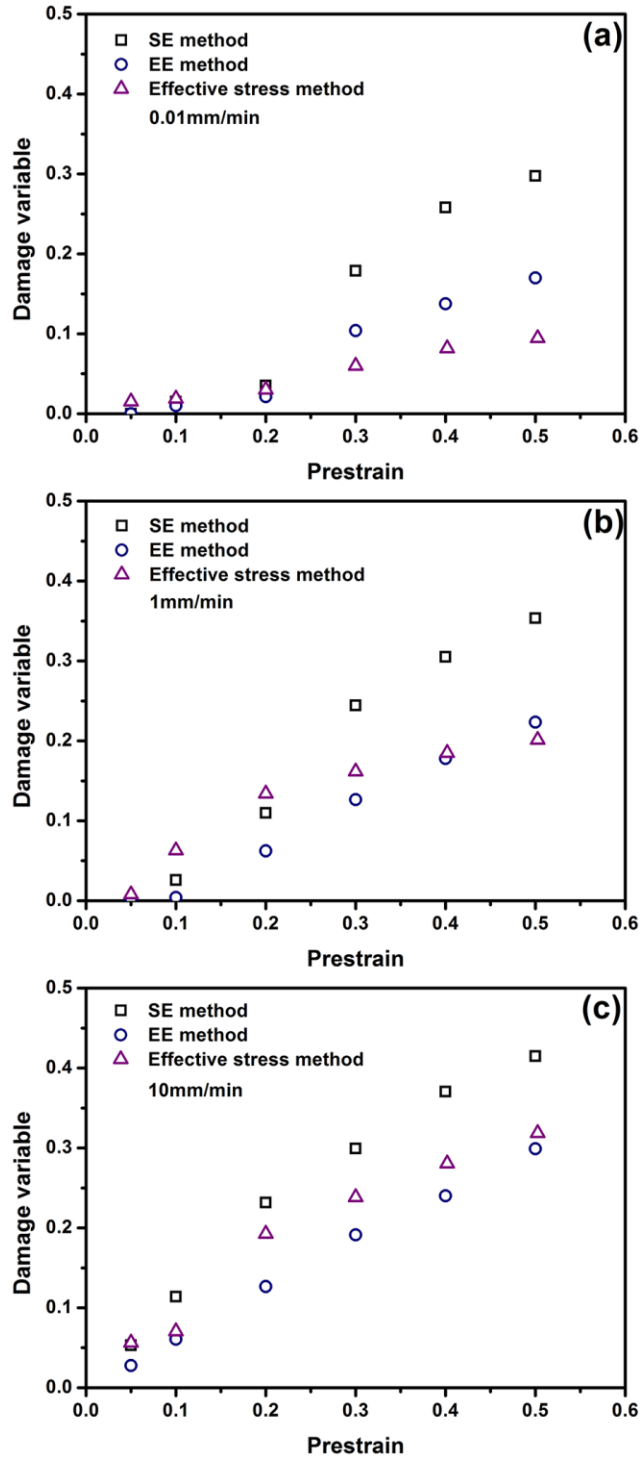


**Fig. 6.11** Comparison of damage variables based on the proposed effective stress method, the SE method and the EE method

## 6.5 Conclusions

An approach for determining the effective stress in the fictitious undamaged state for PE is presented. First, the quasi-static stress-strain relationships for PE deformed at various crosshead speeds were determined by removing the viscous stress component based on a model that consists of spring, damper and finite plasticity elements. The model was calibrated using results from stress relaxation tests. The results show that the quasi-static stress at a given strain level decreases with the increase of crosshead speed, indicating the influence of strain rate on the long-term performance of the PE pipe material (i.e., after viscous stress component is diminished). In addition, influence of aspect ratio of the ligament cross section on the quasi-static stress-strain curves has also been studied by changing ligament width of PE specimens. The results show that the change of ligament width has little effect on the quasi-static stress-strain curve.

By fitting the experimentally-determined curves of quasi-static stress versus logarithm crosshead speed using an arctangent function, the effective stress ( $\sigma_{eff}$ ) at various strain levels is successfully estimated by extrapolating the quasi-static stress to zero crosshead speed. This allows characterization of damage in PE pipe material without any hypothesis such as strain or energy equivalence, by calculating  $D_{EE}$  value directly using the expression  $D_{eff} = 1 - \sigma/\sigma_{eff}$ . Values for  $D$  determined from this approach are compared with those based on the hypotheses of strain and energy equivalence, calculated using degradation of elastic modulus from a two-stage test method. Results show that  $D$  values calculated using the effective stress ( $D_{eff}$ ) and those based on the hypothesis of energy equivalence ( $D_{EE}$ ) are in satisfactory agreement. Therefore, the proposed effective stress method can be used to determine the effective stress and to characterize damage evolution in PE pipe material.

## References

- [1] Kiass, N., Khelif, R., Boulanouar, L., and Chaoui, K., 2005, "Experimental Approach to Mechanical Property Variability through a High-Density Polyethylene Gas Pipe Wall," *J. Appl. Polym. Sci.*, **97**(1), pp. 272–281.
- [2] Shalaby, H. M., Riad, W. T., Alhazza, A. A., and Behbehani, M. H., 2006, "Failure Analysis of Fuel Supply Pipeline," *Eng. Fail. Anal.*, **13**(5), pp. 789–796.
- [3] Azevedo, C. R. F., 2007, "Failure Analysis of a Crude Oil Pipeline," *Eng. Fail. Anal.*, **14**(6), pp. 978–994.
- [4] Majid, Z. A., Mohsin, R., Yaacob, Z., and Hassan, Z., 2010, "Failure Analysis of Natural Gas Pipes," *Eng. Fail. Anal.*, **17**(4), pp. 818–837.
- [5] Gurson, A. L., 1977, "Continuum Theory of Ductile Rupture by Void Nucleation and Growth: Part I—Yield Criteria and Flow Rules for Porous Ductile Media," *J. Eng. Mater. Technol.*, **99**(1), pp. 2–15.
- [6] Needleman, A., and Tvergaard, V., 1984, "An Analysis of Ductile Rupture in Notched Bars," *J. Mech. Phys. Solids*, **32**(6), pp. 461–490.
- [7] Pardoen, T., and Hutchinson, J. W., 2000, "An Extended Model for Void Growth and Coalescence," *J. Mech. Phys. Solids*, **48**(12), pp. 2467–2512.
- [8] Cheng, L., and Guo, T. F., 2007, "Void Interaction and Coalescence in Polymeric Materials," *Int. J. Solids Struct.*, **44**(6), pp. 1787–1808.
- [9] G'Sell, C., Hiver, J. M., and Dahoun, A., 2002, "Experimental Characterization of Deformation Damage in Solid Polymers under Tension, and Its Interrelation with Necking," *Int. J. Solids Struct.*, **39**(13–14), pp. 3857–3872.
- [10] Quatravaux, T., Elkoun, S., G'sell, C., Cangemi, L., and Meimon, Y., 2002, "Experimental Characterization of the Volume Strain of Poly (Vinylidene Fluoride) in the Region of Homogeneous Plastic Deformation," *J. Polym. Sci. Part B Polym. Phys.*, **40**(22), pp. 2516–2522.
- [11] Addiego, F., Dahoun, A., G'Sell, C., and Hiver, J.-M., 2006, "Characterization of Volume Strain at Large Deformation under Uniaxial Tension in High-Density Polyethylene," *Polymer*, **47**(12), pp. 4387–4399.
- [12] Pawlak, A., 2007, "Cavitation during Tensile Deformation of High-Density Polyethylene," *Polymer*, **48**(5), pp. 1397–1409.
- [13] Boisot, G., Laiarinandrasana, L., Besson, J., Fond, C., and Hochstetter, G., 2011, "Experimental Investigations and Modeling of Volume Change Induced by Void Growth in Polyamide 11," *Int. J. Solids Struct.*, **48**(19), pp. 2642–2654.
- [14] Ognedal, A. S., Clausen, A. H., Berstad, T., Seelig, T., and Hopperstad, O. S., 2014, "Void Nucleation and Growth in Mineral-Filled PVC – An Experimental and Numerical Study," *Int. J. Solids Struct.*, **51**(7–8), pp. 1494–1506.
- [15] Butler, M. F., Donald, A. M., Bras, W., Mant, G. R., Derbyshire, G. E., and Ryan, A. J., 1995, "A Real-Time Simultaneous Small- and Wide-Angle X-Ray Scattering Study of In-Situ Deformation of Isotropic Polyethylene," *Macromolecules*, **28**(19), pp. 6383–6393.
- [16] Hughes, D. J., Mahendrasingam, A., Oatway, W. B., Heeley, E. L., Martin, C., and Fuller, W., 1997, "A Simultaneous SAXS/WAXS and Stress-Strain Study of Polyethylene Deformation at High Strain Rates," *Polymer*, **38**(26), pp. 6427–6430.

- [17] Butler, M. F., and Donald, A. M., 1998, “A Real-Time Simultaneous Small-and Wide-Angle X-Ray Scattering Study of in Situ Polyethylene Deformation at Elevated Temperatures,” *Macromolecules*, **31**(18), pp. 6234–6249.
- [18] Castagnet, S., Girault, S., Gacougnolle, J. L., and Dang, P., 2000, “Cavitation in Strained Polyvinylidene Fluoride: Mechanical and X-Ray Experimental Studies,” *Polymer*, **41**(20), pp. 7523–7530.
- [19] Addiego, F., Patlazhan, S., Wang, K., André, S., Bernstorff, S., and Ruch, D., 2015, “Time-Resolved Small-Angle X-Ray Scattering Study of Void Fraction Evolution in High-Density Polyethylene during Stress Unloading and Strain Recovery,” *Polym. Int.*, **64**(11), pp. 1513–1521.
- [20] Yarysheva, A. Y., Rukhlya, E. G., Yarysheva, L. M., Bagrov, D. V., Volynskii, A. L., and Bakeev, N. F., 2015, “The Structural Evolution of High-Density Polyethylene during Crazing in Liquid Medium,” *Eur. Polym. J.*, **66**, pp. 458–469.
- [21] Bonora, N., Ruggiero, A., Gentile, D., and De Meo, S., 2011, “Practical Applicability and Limitations of the Elastic Modulus Degradation Technique for Damage Measurements in Ductile Metals,” *Strain*, **47**(3), pp. 241–254.
- [22] Kachanov, L. M., 1958, “Time of the Rupture Process under Creep Conditions,” *Isv Akad Nauk SSR Otd Tekh Nauk*, **8**, pp. 26–31.
- [23] Kachanov, L., 2013, *Introduction to Continuum Damage Mechanics*, Springer Science & Business Media.
- [24] Lemaitre, J., 1972, “Evaluation of Dissipation and Damage in Metals Submitted to Dynamic Loading,” *Mech. Behav. Mater.*, pp. 540–549.
- [25] Lemaitre, J., 1985, “A Continuous Damage Mechanics Model for Ductile Fracture,” *J. Eng. Mater. Technol.*, **107**(1), pp. 83–89.
- [26] Lemaitre, J., and Dufailly, J., 1987, “Damage Measurements,” *Eng. Fract. Mech.*, **28**(5–6), pp. 643–661.
- [27] Tasan, C. C., Hoefnagels, J. P. M., and Geers, M. G. D., 2012, “Identification of the Continuum Damage Parameter: An Experimental Challenge in Modeling Damage Evolution,” *Acta Mater.*, **60**(8), pp. 3581–3589.
- [28] Chow, C. L., and Wang, J., 1987, “An Anisotropic Theory of Continuum Damage Mechanics for Ductile Fracture,” *Eng. Fract. Mech.*, **27**(5), pp. 547–558.
- [29] Tai, W. H., 1990, “Plastic Damage and Ductile Fracture in Mild Steels,” *Eng. Fract. Mech.*, **37**(4), pp. 853–880.
- [30] Alves, M., Yu, J., and Jones, N., 2000, “On the Elastic Modulus Degradation in Continuum Damage Mechanics,” *Comput. Struct.*, **76**(6), pp. 703–712.
- [31] Straffelini, G., and Molinari, A., 2002, “Evolution of Tensile Damage in Porous Iron,” *Mater. Sci. Eng. A*, **334**(1–2), pp. 96–103.
- [32] Bonora, N., Gentile, D., Pirondi, A., and Newaz, G., 2005, “Ductile Damage Evolution under Triaxial State of Stress: Theory and Experiments,” *Int. J. Plast.*, **21**(5), pp. 981–1007.
- [33] Celentano, D. J., and Chaboche, J.-L., 2007, “Experimental and Numerical Characterization of Damage Evolution in Steels,” *Int. J. Plast.*, **23**(10–11), pp. 1739–1762.
- [34] Wu, T., Coret, M., and Combescure, A., 2011, “Strain Localisation and Damage Measurement by Full 3D Digital Image Correlation: Application to 15-5PH Stainless Steel,” *Strain*, **47**(1), pp. 49–61.

- [35] Abed, F. H., Al-Tamimi, A. K., and Al-Himairee, R. M., 2012, “Characterization and Modeling of Ductile Damage in Structural Steel at Low and Intermediate Strain Rates,” *J. Eng. Mech.*, **138**(9), pp. 1186–1194.
- [36] Darras, B. M., Abed, F. H., Pervaiz, S., and Abdu-Latif, A., 2013, “Analysis of Damage in 5083 Aluminum Alloy Deformed at Different Strainrates,” *Mater. Sci. Eng. A*, **568**, pp. 143–149.
- [37] Chiantoni, G., Comi, C., Mariani, S., and Bonora, N., 2014, “Experimental Assessment of Ductile Damage in P91 Steel at High Temperature,” *Int. J. Damage Mech.*, **23**(4), pp. 567–587.
- [38] Guelorget, B., François, M., and Lu, J., 2007, “Microindentation as a Local Damage Measurement Technique,” *Mater. Lett.*, **61**(1), pp. 34–36.
- [39] Tasan, C. C., Hoefnagels, J. P. M., and Geers, M. G. D., 2009, “A Critical Assessment of Indentation-Based Ductile Damage Quantification,” *Acta Mater.*, **57**(17), pp. 4957–4966.
- [40] Li, J., Li, F., Xue, F., Cai, J., and Chen, B., 2012, “Micromechanical Behavior Study of Forged 7050 Aluminum Alloy by Microindentation,” *Mater. Des.*, **37**, pp. 491–499.
- [41] Li, J., Li, F., Ma, X., Wang, Q., Dong, J., and Yuan, Z., 2015, “A Strain-Dependent Ductile Damage Model and Its Application in the Derivation of Fracture Toughness by Micro-Indentation,” *Mater. Des.*, **67**, pp. 623–630.
- [42] Padma, S., Srivathsa, B., Rao, N. V., and Kumar, V., 2009, “Evolution of Damage in Near IMI-834 Titanium Alloy Under Monotonic Loading Condition: A Continuum Damage Mechanics Approach,” *J. Eng. Mater. Technol.*, **131**, pp. 031012–1.
- [43] Zhang, S. J., Zhou, C., Xia, Q. X., and Chen, S. M., 2015, “Quantification and Characterization of Full Field Ductile Damage Evolution for Sheet Metals Using an Improved Direct Current Potential Drop Method,” *Exp. Mech.*, **55**(3), pp. 611–621.
- [44] Yeh, H.-Y., and Cheng, J.-H., 2003, “NDE of Metal Damage: Ultrasonics with a Damage Mechanics Model,” *Int. J. Solids Struct.*, **40**(26), pp. 7285–7298.
- [45] Kim, J.-Y., Jacobs, L. J., Qu, J., and Littles, J. W., 2006, “Experimental Characterization of Fatigue Damage in a Nickel-Base Superalloy Using Nonlinear Ultrasonic Waves,” *J. Acoust. Soc. Am.*, **120**(3), pp. 1266–1273.
- [46] Antonaci, P., Bruno, C. L. E., Gliozzi, A. S., and Scalerandi, M., 2010, “Monitoring Evolution of Compressive Damage in Concrete with Linear and Nonlinear Ultrasonic Methods,” *Cem. Concr. Res.*, **40**(7), pp. 1106–1113.
- [47] Chen, J., Xu, Z., Yu, Y., and Yao, Y., 2014, “Experimental Characterization of Granite Damage Using Nonlinear Ultrasonic Techniques,” *NDT E Int.*, **67**, pp. 10–16.
- [48] Chandrakanth, S., and Pandey, P. C., 1995, “An Isotropic Damage Model for Ductile Material,” *Eng. Fract. Mech.*, **50**(4), pp. 457–465.
- [49] La Rosa, G., Mirone, G., and Risitano, A., 2001, “Effect of Stress Triaxiality Corrected Plastic Flow on Ductile Damage Evolution in the Framework of Continuum Damage Mechanics,” *Eng. Fract. Mech.*, **68**(4), pp. 417–434.
- [50] Detrez, F., Cantournet, S., and Seguela, R., 2011, “Plasticity/Damage Coupling in Semi-Crystalline Polymers prior to Yielding: Micromechanisms and Damage Law Identification,” *Polymer*, **52**(9), pp. 1998–2008.
- [51] Gu, G., Xia, Y., Lin, C., Lin, S., Meng, Y., and Zhou, Q., 2013, “Experimental Study on Characterizing Damage Behavior of Thermoplastics,” *Mater. Des.*, **44**, pp. 199–207.

- [52] Balieu, R., Lauro, F., Bennani, B., Haugou, G., Chaari, F., Matsumoto, T., and Mottola, E., 2015, "Damage at High Strain Rates in Semi-Crystalline Polymers," *Int. J. Impact Eng.*, **76**, pp. 1–8.
- [53] Zhang, Y., and Jar, P.-Y. B., 2015, "Quantitative Assessment of Deformation-Induced Damage in Polyethylene Pressure Pipe," *Polym. Test.*, **47**, pp. 42–50.
- [54] Al-Rub, R. K. A., and Kim, S.-M., 2010, "Computational Applications of a Coupled Plasticity-Damage Constitutive Model for Simulating Plain Concrete Fracture," *Eng. Fract. Mech.*, **77**(10), pp. 1577–1603.
- [55] Saanouni, K., Forster, C., and Hatira, F. B., 1994, "On the Anelastic Flow with Damage," *Int. J. Damage Mech.*, **3**(2), pp. 140–169.
- [56] Bonora, N., 1997, "A Nonlinear CDM Model for Ductile Failure," *Eng. Fract. Mech.*, **58**(1), pp. 11–28.
- [57] Cicekli, U., Voyiadjis, G. Z., and Al-Rub, R. K. A., 2007, "A Plasticity and Anisotropic Damage Model for Plain Concrete," *Int. J. Plast.*, **23**(10), pp. 1874–1900.
- [58] Voyiadjis, G. Z., Taqieddin, Z. N., and Kattan, P. I., 2008, "Anisotropic Damage–plasticity Model for Concrete," *Int. J. Plast.*, **24**(10), pp. 1946–1965.
- [59] Alvarado-Contreras, J. A., Polak, M. A., and Penlidis, A., 2010, "Constitutive Modeling of Damage Evolution in Semicrystalline Polyethylene," *J. Eng. Mater. Technol.*, **132**(4), p. 041009.
- [60] Cao, T.-S., Gachet, J.-M., Montmitonnet, P., and Bouchard, P.-O., 2014, "A Lode-Dependent Enhanced Lemaitre Model for Ductile Fracture Prediction at Low Stress Triaxiality," *Eng. Fract. Mech.*, **124–125**, pp. 80–96.
- [61] Jar, P.-Y., 2014, "Transition of Neck Appearance in Polyethylene and Effect of the Associated Strain Rate on the Damage Generation," *Polym. Eng. Sci.*, **54**(8), pp. 1871–1878.
- [62] Jar, P.-Y. B., 2014, "Effect of Tensile Loading History on Mechanical Properties for Polyethylene," *Polym. Eng. Sci.*, **55**(9), pp. 2002–2010.
- [63] ASTM D2290 - 12, 2012, *Test Method for Apparent Hoop Tensile Strength of Plastic or Reinforced Plastic Pipe by Split Disk Method*, ASTM International.
- [64] Zhang, Y., and Jar, P.-Y. B., 2016, "Effects of Crosshead Speed on the Quasi-Static Stress-Strain Relationship of Polyethylene (PE) Pipes," *J. Press. Vessel Technol.*
- [65] Ayoub, G., Zaïri, F., Naït-Abdelaziz, M., and Gloaguen, J. M., 2010, "Modelling Large Deformation Behaviour under Loading–unloading of Semicrystalline Polymers: Application to a High Density Polyethylene," *Int. J. Plast.*, **26**(3), pp. 329–347.
- [66] Blaise, A., Baravian, C., André, S., Dillet, J., Michot, L. J., and Mokso, R., 2010, "Investigation of the Mesostructure of a Mechanically Deformed HDPE by Synchrotron Microtomography," *Macromolecules*, **43**(19), pp. 8143–8152.
- [67] Muhammad, S., and Jar, P.-Y. B., 2011, "Effect of Aspect Ratio on Large Deformation and Necking of Polyethylene," *J. Mater. Sci.*, **46**(4), pp. 1110–1123.

# Chapter 7

## **Characterization of ductile damage in polyethylene using ultrasonic technique**

An experimental study was conducted to explore the possibility of using ultrasonic testing to quantify deformation-induced damage in polyethylene (PE) plate. Coupon specimens of two gauge lengths were machined from PE plates with thickness in the range from 1.5 to 10mm. The specimens were first stretched monotonically to various prestrain levels to vary the extent of damage introduced by the stretch. Ultrasonic testing in the through transmission mode was then conducted on the prestrained specimens to determine the time of flight based on which ultrasonic velocity was determined. The results show that the ultrasonic velocity, normalized by the speed in the virgin plate of the same thickness, decreases with the increase of prestrain introduced to the specimens. The study also shows that with the correction of density change by the prestrain, the normalized ultrasonic velocity can be used to determine the dependence of damage level on the prestrain, which for specimens with long gauge length, is consistent with the damage determined from the mechanical testing. The study concludes that ultrasonic testing can be used as a non-destructive means to quantify deformation-induced damage evolution in PE plates.

### **7.1 Introduction**

Semi-crystalline polymers are increasingly used in a wide range of applications, including aerospace, automobiles, nuclear power plants, and pressure tubing for water and natural gas

transportation. In the pressure tubing applications, statistics shows that over 90% of the newly installed gas pipeline systems are now made of PE [1]. Such an extensive usage is attributed to the combination of reliable thermal stability, excellent corrosion resistance, relatively low cost, light weight and good flexibility, to name a few, which provide easy installation and maintenance of PE pipelines. However, unexpected, catastrophic failures of PE pipes were still reported in the last decade [2–4], suggesting that new methodologies are needed to monitor PE's property deterioration in order to predict accurately their remaining service life. Furthermore, in spite of a lot of efforts being devoted to the study of damage and failure mechanisms in PE [5–10], characterization of damage in PE is still a real challenge due to the possibility of damage generation in normal service conditions, such as squeeze-off process for repair and maintenance and variation in service loading histories. The problem is further aggravated by PE's complex deformation behavior.

Over the past decades, thanks to the rapid development of damage mechanics and experimental instrumentation, studies on the behavior of damaged materials have come up with various methods for the damage characterization. These methods can be broadly classified into two approaches based on (i) mechanics of porous media (MPM) and (ii) continuum damage mechanics (CDM). The former uses void volume fraction (i.e., porosity) as the damage indicator to describe property degradation of materials. In this approach, Gurson's damage model [11] is most widely used for quantifying ductile damage evolution, which is through the use of a porosity term to progressively down-scale the yield surface. This model has been successfully extended to account for coalescence and growth of voids [12–14]. Techniques based on this model use volume strain to quantify the porosity, which include scanning electron microscopy

(SEM) [15–18], wide-angle X-ray scattering (WAXS) and small-angle X-ray scattering (SAXS) [19–24].

For the approach based on CDM, a macroscopic damage variable  $D$  is introduced to reflect a progressive deterioration of material properties, and is used to quantify the damage process. Based on the effective stress concept and strain- or energy-equivalent hypotheses, various kinds of methods have been developed to measure degradation of mechanical properties, such as elastic modulus, strength and hardness, based on which damage is quantified. In 1987, eight different experimental methods that use direct or indirect methods for damage characterization were discussed by Lemaitre and Dufailly [25]. The direct methods include digital microscopy to observe areas covered by voids or cracks and measurement of density variation. The indirect methods, on the other hand, are to measure changes in elastic modulus, ultrasonic velocity, micro-hardness or electrical potentials. One of the most widely used methods to characterize damage is to measure degradation of elastic modulus from cyclic loading-unloading tests [26–35]. However, most of the above works are to quantify damage development in metallic materials. Much less attention has been paid to the damage development in semi-crystalline polymers.

Compared to the destructive methods that require preparation of coupon specimens to determine, for example, ratio of damaged area to the total surface area, density, or elastic modulus, non-destructive evaluation (NDE) methods have the advantage of providing in-situ characterization of material properties or inspection of engineering structures such as pipelines. A number of NDE methods, such as acoustic emission methods [36–39], electrical methods [40–42], infrared thermography methods [43–46], vibration-based methods [47–49] and ultrasonic methods [50–54], have been proposed for non-destructive damage characterization. Among

these methods, ultrasonic methods are believed to be one of the most feasible methods for evaluation of the change in mechanical properties because equipment for ultrasonic methods is relatively low in cost, easy in operation, and has the ability to reveal microscopic changes in the inspected materials. Since magnitude of ultrasonic velocity is related to density and stiffness of the material, measurement of the ultrasonic velocity can provide a non-destructive means to assess changes in mechanical properties of the material. Damage state and its evolution can then be determined by comparing the measured mechanical properties with their values for the original materials.

According to the definition of effective stress in continuum damage mechanics, ultrasonic velocity and damage variable  $D$  are suggested to follow the expression of  $D \approx 1 - v_D^2/v_0^2$  [25], where  $v_D$  and  $v_0$  are ultrasonic velocities of longitudinal waves in damaged and virgin materials, respectively. This expression enables people to use ultrasonic methods as an effective tool to characterize various types of damage in materials, such as damages by tensile loading [55, 35], compressive loading [56–58], creep loading [59, 60] and fatigue loading [52, 61]. However, current use of ultrasonic methods for such damage characterization is mainly for concrete and metallic materials. To our knowledge, no work has been reported to use ultrasonic methods to quantitatively characterize damage in semi-crystalline polymers.

Although no work has been reported to use ultrasonic methods to characterize damage in polymers, studies have shown that many factors affect ultrasonic wave propagation in polymers. For example, ultrasonic velocity and attenuation are known to be sensitive to polymer morphology [62–64], and vary markedly with the change of crystallinity and density of polymers. These studies also found that ultrasonic velocity and attenuation vary with frequency

of the ultrasonic transducer used for the measurement. Furthermore, temperature and stress are known to affect ultrasonic velocity of longitudinal waves in polymers [65, 66].

In view that in-service detection and monitoring of damage development is an important means to ensure safe operation of pipeline systems, we have explored the feasibility of using ultrasonic wave propagation as a NDE tool to assess damage development in PE pipes. This chapter summarizes results from a preliminary study that uses ultrasonic wave in the through transmission mode to explore the possibility of developing an ultrasonic method to detect and quantify damage in PE, as a first step to evaluate its applicability to PE pipes.

## **7.2 Experimental details**

### **7.2.1 Material and specimens**

PE plaques, provided by NOVA Chemicals, were used to prepare specimens for the testing. The PE plaques were compression molded from pellets to nominal thickness of 1.5, 3, 6 and 10 mm, of which the material characteristics are shown in Table 7.1. Two types of PE specimens, named “short” and “long” for ligament lengths of 3 and 10 mm, respectively, were used to provide two levels of stress triaxiality at which the damage is generated. The specimen dimensions are shown in Fig 7.1. Because thickness of the specimens ranges from 1.5 to 10 mm, the constant ligament width of 10 mm results in the change in aspect ratio (width/thickness) from 6.7 (for nominally 1.5mm-thick specimens) to 1 (for nominally 10mm-thick specimens). For simplicity, long specimens with nominal thicknesses of 1.5, 3, 6 and 10mm are denoted as L-1.5, L-3, L-6 and L-10, and short specimens S-1.5, S-3, S-6 and S-10.

**Table 7.1** Material characteristics for HDPE used in this study

$M_w$ (g·mol <sup>-1</sup> )	$M_n$ (g·mol <sup>-1</sup> )	$M_z$ (g·mol <sup>-1</sup> )	Density, $\rho$ (g·cm <sup>-3</sup> )	$M_w/M_n$
73,100	30,400	147,000	0.941	2.4

$M_w$ ,  $M_n$  and  $M_z$  stand for weight-average, number-average, and Z-average, respectively, molecular weight

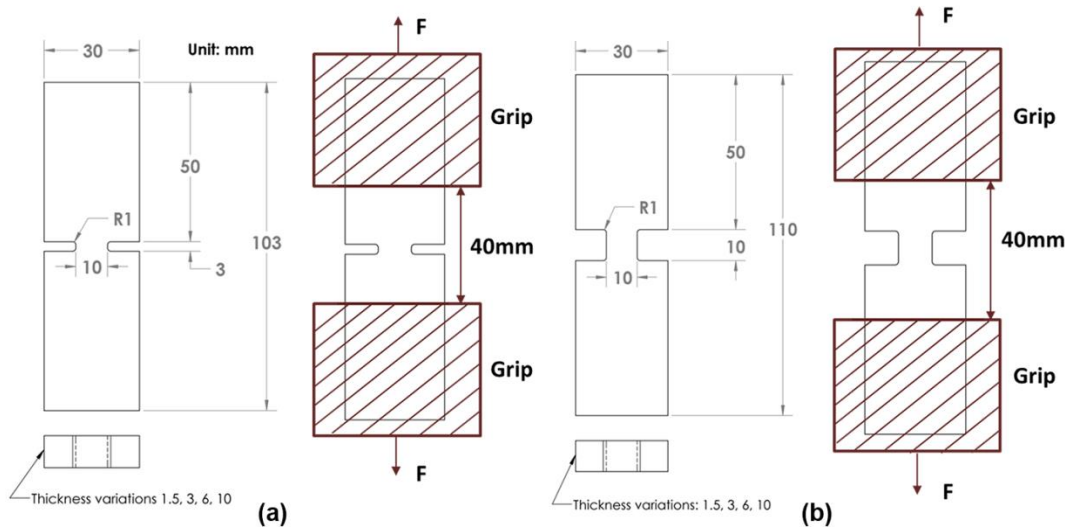


**Fig. 7.1** Dimensions for short (a) and long (b) specimens with nominal thickness ranging from 1.5 to 10mm

### 7.2.2 Mechanical testing

All mechanical tests were conducted using a universal test machine (QUASAR 100) at room temperature. A two-stage test method, initially proposed by Jar [67,68], was adopted to investigate the effect of prestrain on the degradation of elastic modulus. The two-stage test is to use the first stage to introduce prestrain to specimens at a constant crosshead speed of 1mm/min, and two months later the second stage to measure elastic modulus at the crosshead speed of 0.01mm/min. The period of two months is to allow the specimens to recover from the viscoelastic deformation before the second-stage tests.

Procedure for the first-stage tests is similar to that used before [69]. That is, at the end of the loading phase, specimens were held at the displacement for a period of 3 hours for stress relaxation before the unloading. Note that changes in both ligament width and ligament thickness were recorded during the test, the former through a data acquisition portal of the test machine and the latter a digital oscilloscope. Since data recorded using the digital oscilloscope could be converted to thickness only after the test, prestrain introduced in the first-stage test was controlled using the change of ligament width, recorded through the data acquisition portal of the test machine. This provided a similar prestrain range for long specimens of different thickness. For short specimens, however, as to be shown later the prestrain range covered by the same width contraction varies significantly among specimens of different thickness. This is because contraction in the thickness direction shows a strong dependence on the specimen thickness. Nevertheless, results reported here are presented in terms of prestrain values introduced in the first-stage tests, calculated using the following expression.

$$\varepsilon_{true} = \ln\left(\frac{w_0}{w} \frac{t_0}{t}\right) \quad (7.1)$$

where  $w_0$  and  $t_0$  are original ligament width and thickness respectively, and  $w$  and  $t$  the deformed ligament width and thickness. In spite of the difference in the prestrain range among specimens of different gauge length and thickness, the results are sufficient to provide a clear trend of the dependence of damage evolution on the gauge length and ligament aspect ratio, as to be shown in the next section.

Tests at the second stage were conducted at the crosshead speed of 0.01mm/min, to measure elastic modulus at  $\varepsilon_{true}$  of 0.5%. The procedure is identical to that used previously [69], except that both thickness and width changes were recorded to calculate  $\varepsilon_{true}$  values.

### 7.2.3 Ultrasonic testing

Ultrasonic tests were conducted on PE specimens that had been subjected to the first-stage tests to generate prestrains. Fig. 7.2(a) shows the schematic diagram for the ultrasonic test setup. In this study, ultrasonic velocity was measured using two 1-MHz transducers, one as an emitter and the other a receiver (from Olympus) in the through-transmission mode. Ultrasound coupling gel (Aquasonic 100 from Parker Laboratories) was used between the transducers and the specimen. Relative position between the ultrasonic transducers and the specimen was fixed using a specimen holder shown in Fig. 7.2(b), in order to avoid pressure variation and to ensure good alignment during the test. Signals collected from the tests were analyzed and displayed on a two-channel digital oscilloscope (LeCroy 422 WaveSurfer). Ultrasonic measurement was conducted at three locations on each specimen, labelled 1, 2 and 3 in Fig. 7.2(c). Material at locations 1 and 3 was assumed to be undamaged and confirmed by comparing the ultrasonic velocity measured there with that from a virgin specimen.

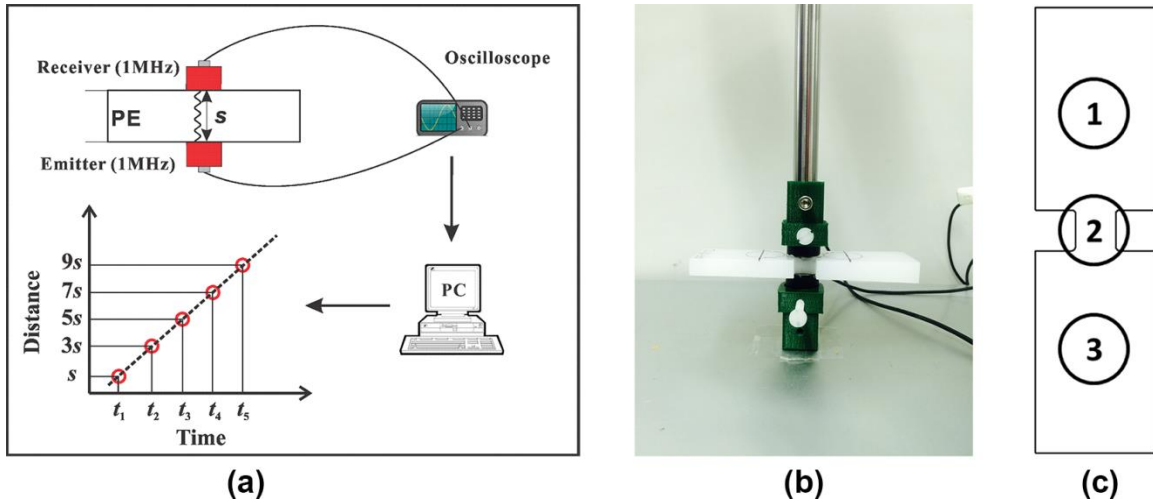


**Fig. 7.2** Ultrasonic test: (a) schematic diagram of the test setup, (b) transducers and PE specimen used in the ultrasonic tests, and (c) three measurement locations on the specimen

Ultrasound velocities in the PE specimens were measured in the thickness direction using the time-of-flight method [64]. A tone burst signal was generated from a function generator and injected into the specimen through the transmitting transducer. The transmitted signal, received by a transducer on the other side of the specimen, is recorded and averaged 256 times by the oscilloscope and sent to a personal computer for post processing. Multiple echoes in the ecogram were originated from the back and forth reflections of ultrasonic wave between the two transducers. The travelling time and distance for the first signal were denoted as  $t_1$  and  $s_1$ , respectively. In general, the  $i^{\text{th}}$  signal travels for a distance of  $(2i-1)$  times of the specimen thickness, and the corresponding time is  $t_i$  which does not include the time for travelling in the coupling gel. To reduce the influence from the ultrasonic noise, only the first five sets of signals that show well defined first valley position were used to calculate the ultrasonic velocity. Data for the five sets of signals were fitted using a straight line of which the slope represents the ultrasonic velocity, as illustrated in the bottom left figure in Fig. 7.2(a). The linear relationship between travelling distance and time for specimens L-6 and S-3, as shown in Fig. 7.3(a) and (b),

respectively, suggests that there is little effect of attenuation on the detection of valley positions. Each of the measured ultrasonic velocity values was the average of three repeated measurements.

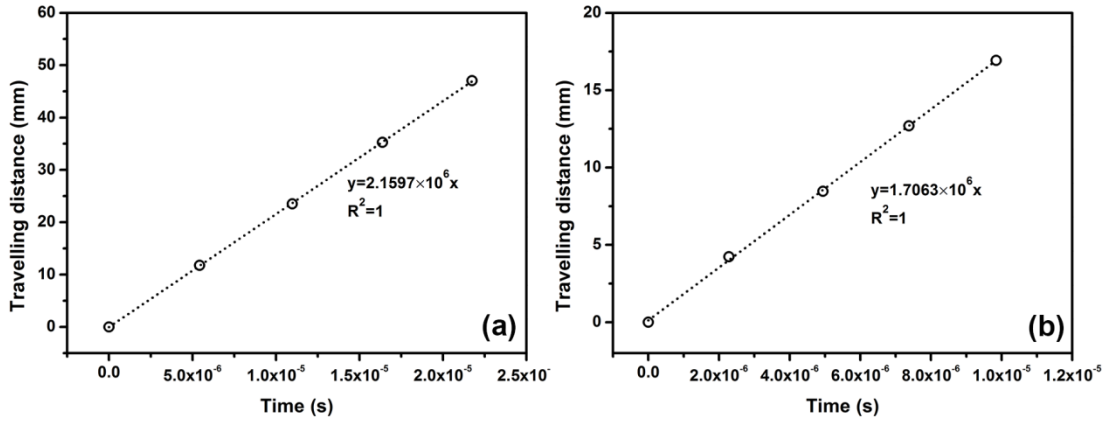
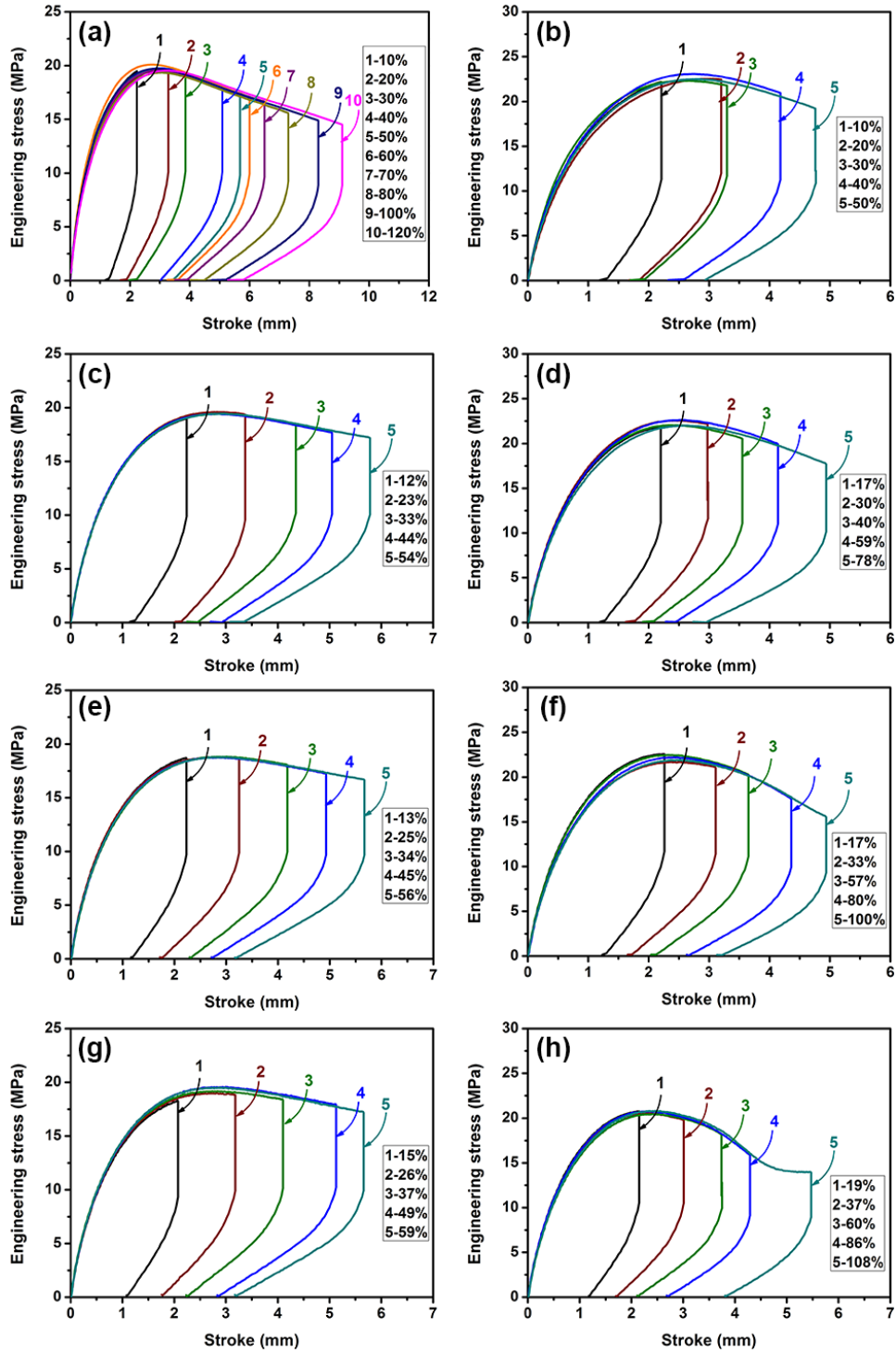


Fig. 7.3 Relationship between travelling distance and time for specimens L-6 (a) and S-3 (b)

### 7.3 Results and discussion

Fig. 7.3 summaries the plots of engineering stress versus stroke from the first-stage tests. For example, Figs. 7.3(a) and 3(b) present curves from long and short specimens of 10mm thick, respectively. As shown in the figure, at least five prestrain levels were used for each specimen thickness. For the long specimens of 10mm thick, additional five pre-strain levels were used, to have the prestrain range similar to that for the short specimens. Note that test results show excellent reproducibility. Therefore, only one specimen was used for each combination of prestrain, specimen type and specimen thickness. Occasionally, the curve did not fall into the trend shown by the rest of the curves for the same specimen type and thickness. In that case, the test was repeated using another specimen, to ensure that all curves of the same specimen type and thickness overlap with each other reasonably well. Such a repeated test only occurred twice for long specimens and four times for short specimens, for totally 51 specimens used in the entire test program.



**Fig. 7.4** Summary of curves of engineering stress versus stroke: (a) L-10, (b) S-10, (c) L-6, (d) S-6, (e) L-3, (f) S-3, (g) L-1.5, and (h) S-1.5. Prestrain for each curve, as indicated by the legend, is calculated using Eq. (7.1).

Table 7.2 summarizes ultrasonic velocities for undamaged PE specimens ( $v_{L0}$ ), which were measured from locations 1 and 3 in Fig. 7.2(c). Values listed on Table 7.2 show dependence of the  $v_{L0}$  on the specimen thickness, especially for specimens of 1.5 and 3mm thick. A similar phenomenon was also reported before [70]. Although it is not quite clear about the cause for the phenomenon, both cases are for specimen thickness that is close to the ultrasonic wave length. In our case, wavelength used is around 2.2mm, which travels through the thickness of PE specimens at a speed of approximately 2200m/s, i.e., at the frequency of 1MHz.

**Table 7.2** Measurements of the longitudinal wave velocity for undamaged material

Thickness (mm)	Long specimen	Short Specimen
1.5	2023±5.1	2035±13.2
3	2102±6.8	2066±7.5
6	2251±5.7	2252±5.6
10	2249±2.5	2250±3.1

According to continuum damage mechanics (CDM) [25], damage can be determined based on degradation of ultrasonic velocity using the following expression, with the assumption that the density change is negligible.

$$D_v \approx 1 - \frac{v_{LD}^2}{v_{L0}^2} \quad (7.2)$$

where  $v_{LD}$  and  $v_{L0}$  are ultrasonic velocities for damaged and undamaged materials, respectively.

In our case, since the wave velocity varies with the specimen thickness used for the testing,  $v_{L0}$  in the above expression should be for the specimen that has the same thickness as the specimen

that has been subjected to a prestrain in the first-stage test. In order to establish the relationship between the ultrasonic velocity  $v_{L0}$  and thickness of a virgin specimen, a test block that contains ten different thicknesses was manufactured from the same PE material, of which the geometry and dimensions are shown in Fig. 7.4.

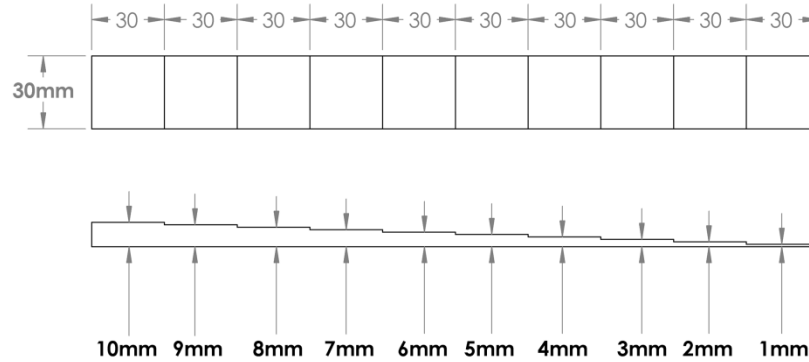


**Fig. 7.5** Top and front views of a test block used to establish the relationship between ultrasonic velocity and specimen thickness

Ultrasonic velocities determined using the test block are presented in Fig. 7.5 as a function of test block thickness, which confirms the dependence of the measured ultrasonic velocity on the test block thickness till the thickness is greater than 8mm. In general, it is believed that ultrasonic velocity is affected by constraint imposed on the wave front. For a sufficiently thick specimen that provides constraint for ultrasonic wave propagation in all directions, the ultrasonic wave can be considered as a bulk wave of which the velocity is determined using Eq. (7.3):

$$C_p = \sqrt{\frac{E(1-\nu)}{\rho(1+\nu)(1-2\nu)}} \quad (7.3)$$

where  $E$ ,  $\nu$  and  $\rho$  are elastic modulus, Poisson's ratio and density of the measured material. However, with less constraint, such as a longitudinal wave traveling along a bar of sufficient length, the wave velocity is determined using Eq. (7.4):

$$C_{bar} = \sqrt{\frac{E}{\rho}} \quad (7.4)$$

Therefore, we believe that a thin plate does not provide sufficient constraint for the ultrasonic wave traveling in the thickness direction, resulting in the dependence of the wave velocity on the test block thickness, as depicted in Fig. 7.5.

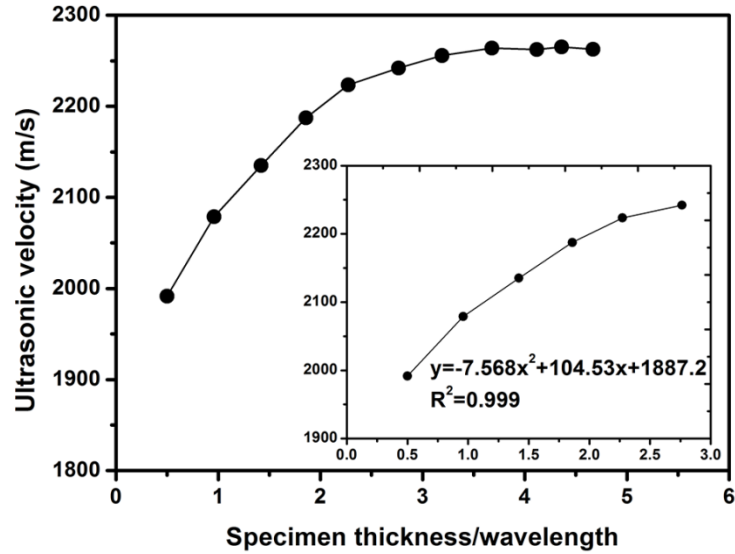
The dependence of ultrasonic velocity on the specimen thickness is determined using a second order polynomial function, which is also included in Fig. 7.5, to fit data for thickness below 6mm. The polynomial function is then used to calculate ultrasonic velocity in a virgin specimen of any thickness. By having the ultrasonic velocity for prestrained and virgin specimens of the same thickness, the damage parameter  $D_v$  can then be determined using Eq. (7.2).

Using Eq. (7.3) and based on the damage concept, that is, change in elastic modulus is due to the presence of damage, the ultrasonic velocities for the undamaged and damaged specimens can be expressed in Eqs. (7.5) and (7.6), respectively.

$$v_{L0} = \sqrt{\frac{E_0(1-\nu)}{\rho_0(1+\nu)(1-2\nu)}} \quad (7.5)$$

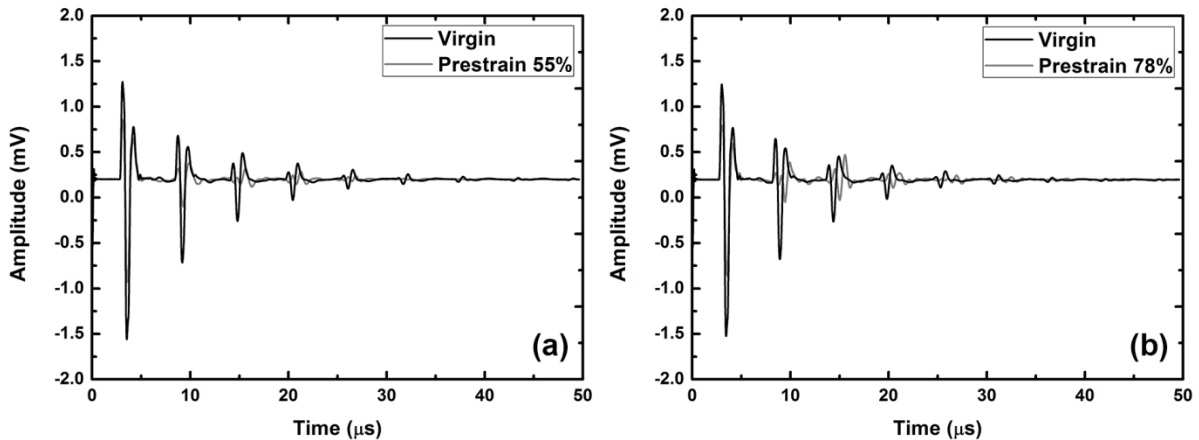
$$v_{LD} = \sqrt{\frac{E_D(1-\nu)}{\rho_D(1+\nu)(1-2\nu)}} \quad (7.6)$$

where  $E$  and  $\rho$  with subscript 0 are for virgin specimens, and those with subscript  $D$  which stands for “damage” are for prestrained specimens.



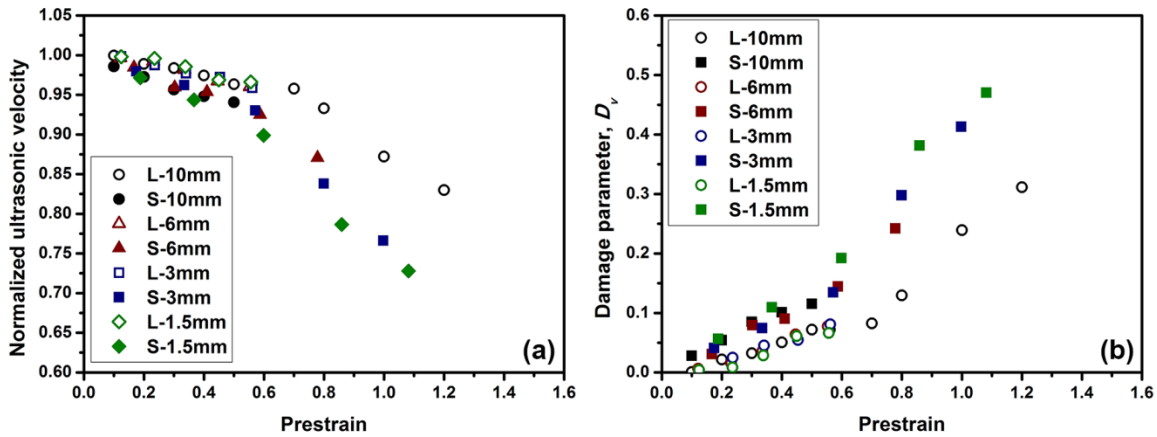
**Fig. 7.6** Dependence of ultrasonic velocity on specimen thickness that is normalized by the wavelength

Fig. 7.6 shows two examples of typical time domain waveforms for both virgin and damaged specimens using 1MHz transducers. As shown in Fig. 7.6, amplitude in both prestrained specimens is slightly lower than that in the corresponding virgin specimens, possibly due to the presence of cavities or voids in the prestrained specimens which disperse and scatter the transmitted wave to increase the energy loss.



**Fig. 7.7** Examples of longitudinal wave traces from virgin and prestrained specimens: (a) L-6 and (b) S-6

The ultrasonic velocities in prestrained specimens, normalized by the ultrasonic velocity in virgin specimens of the same thickness (i.e.,  $v_{LD}/v_{L0}$ ), for both long and short specimens are summarized in Fig. 7.7(a). The figure suggests that ultrasonic velocity decreases with the increase of prestrain introduced in the first-stage test. The corresponding value for damage parameter  $D_v$ , calculated using Eq. (7.2), is presented in Fig. 7.7(b) as a function of prestrain, which suggests that damage develops faster in short specimens than in long specimens, possibly because a higher level of stress triaxiality was generated in the former in the first-stage tests [30,70,71].



**Fig. 7.8** Ultrasonic test results: (a) normalized ultrasonic velocity versus prestrain and (b) damage parameter  $D_v$  based on the decrease of ultrasonic velocity, Eq. (7.2)

Damage evolution in the PE specimens was also established using degradation of elastic modulus, and compared with that obtained from the ultrasonic method. The elastic modulus was measured in the second-stage tests on both virgin and prestrained specimens after the measurement of ultrasonic velocity, based on the hypothesis of strain equivalence (SE). Value for damage parameter so determined, denoted  $D_{SE}$ , can be expressed in terms of the ratio of

elastic modulus for the prestrain specimen to that for the virgin specimen of the same specimen type and nominal thickness, as shown in the expression below.

$$D_{SE} = 1 - \frac{E_D}{E_0} \quad (7.7)$$

Damage parameters  $D_v$  and  $D_{SE}$ , calculated using Eqs. (7.2) and (7.7), respectively, are compared in Fig. 7.8. The figure shows that at a small prestrain level values for  $D_v$ , based on the degradation of ultrasonic velocity, shows a good agreement with that for  $D_{SE}$ , based on the degradation of elastic modulus. However, discrepancy between  $D_v$  and  $D_{SE}$  increases with the increase of prestrain introduced in the first-stage tests. The discrepancy is believed to be caused by the assumption of constant density in Eq. (7.2). If density change is taken into consideration, the damage parameter based on the degradation of ultrasonic velocity should be expressed as

$$D_{v\rho} = 1 - \frac{v_{LD}^2}{v_{L0}^2} \cdot \frac{\rho_D}{\rho_0} \quad (7.8)$$

where  $\rho_D$  and  $\rho_0$  represent densities for damaged (i.e., prestrained) and undamaged (i.e., virgin) specimens, respectively. It is obvious that because density is decreased by the deformation process,  $D_v$  value should be smaller than  $D_{v\rho}$  value for the same specimen.

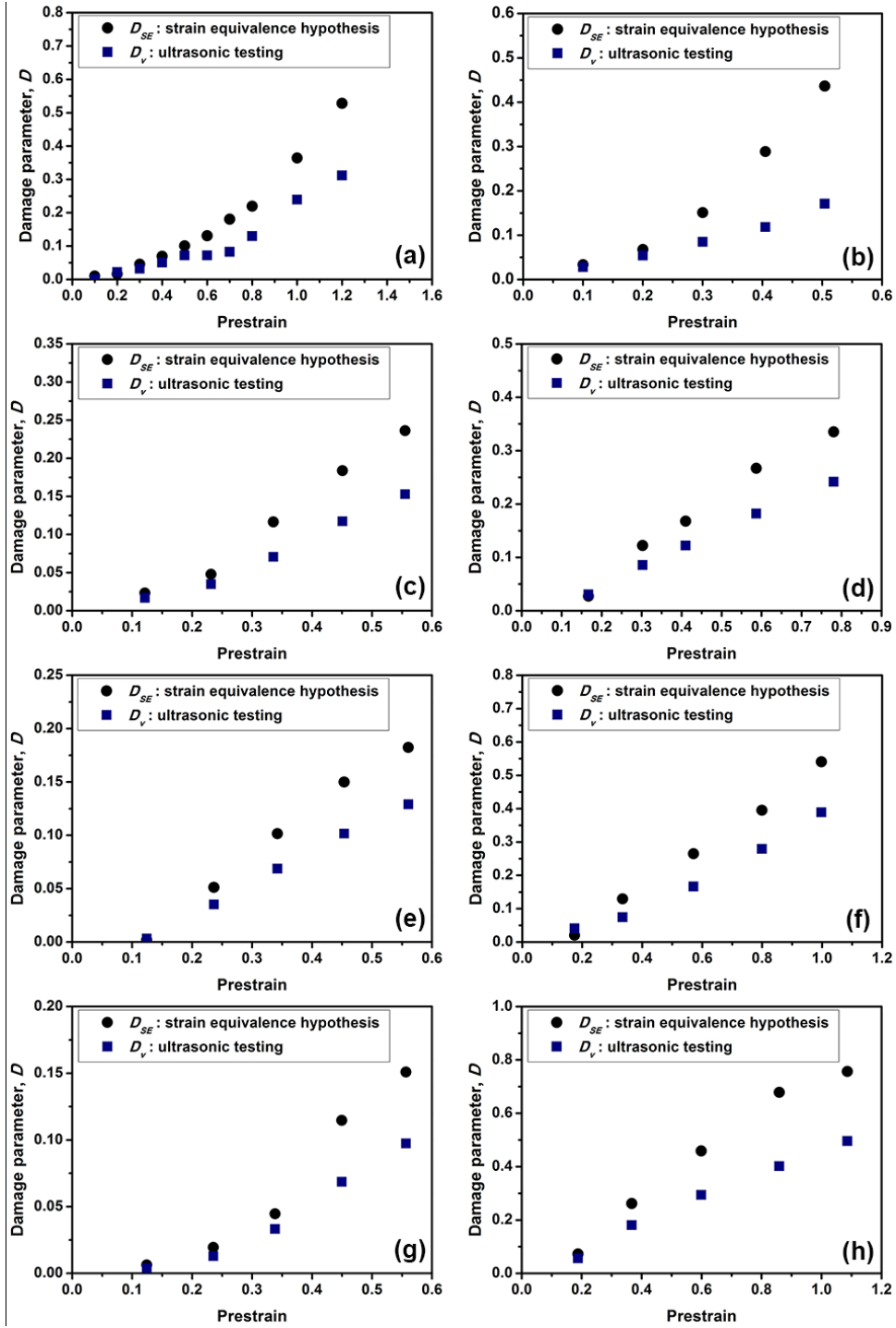


**Fig. 7.9** Comparison of damage parameter  $D_v$  based on degradation of ultrasonic velocity without considering the density change, with damage parameter  $D_{SE}$  based on degradation of elastic modulus under the hypothesis of strain equivalence: (a) L-10, (b) S-10, (c) L-6, (d) S-6, (e) L-3, (f) S-3, (g) L-1.5 and (h) S-1.5.

To confirm that difference between  $D_v$  and  $D_{SE}$  in Fig. 7.8 is due to the change in density of PE caused by the deformation introduced in the first-stage tests,  $D_{v\rho}$  from Eq. (7.8) should show dependence on prestrain similar to that for  $D_{SE}$  from Eq. (7.7). This idea was explored by adopting the experimentally established relationship between plastic volume strain and the applied strain (prestrain) for PE in ref. [15], with the plastic volume strain defined by Eq. (7.9) below. Eq. (7.9) also includes the relationship between the plastic volume strain and the density ratio of virgin to prestrained specimens,  $\rho_0$  and  $\rho_D$ , respectively.

$$\varepsilon_v = \frac{\Delta V}{V_0} = \frac{V_D - V_0}{V_0} = \frac{V_D}{V_0} - 1 = \frac{\rho_0}{\rho_D} - 1 \quad (7.9)$$

where  $V_D$  is the deformed volume after the recovery of elastic deformation and  $V_0$  the original volume before the deformation. The density ratio as a function of prestrain, based on data given ref. [15], is presented in Fig. 7.9(a).

With the assumption that the curve shown in Fig. 7.9(a) also represents the density change for our long specimens of 10mm thick (L-10), results in Fig. 7.9(a) can then be used to determine the evolution of  $D_{v\rho}$  based on the ultrasonic test results. Fig. 7.9(b) presents the variation of  $D_{v\rho}$  with prestrain for L-10, along with  $D_{SE}$  and  $D_v$  that have been presented in Fig. 7.8(a). Fig. 7.9(b) suggests that evolution of  $D_{v\rho}$  shows better agreement with  $D_{SE}$  than  $D_v$  does, thus confirming that density change by deformation introduced in the first-stage test does play an important role for quantifying the damage evolution using degradation of ultrasonic velocity, and that the ultrasonic method can serve as a non-destructive means for damage characterization of PE. However, at this stage similar correction for the damage parameter  $D_v$  for short specimens cannot be made, as

literature has shown that volume strain rate is highly sensitive to the change of stress triaxiality [72] and no data are available for the volume strain evolution at the stress triaxiality level that is similar to that in the short specimens. Another problem for the correction of ultrasonic-based damage parameter for short specimens is the size of the ultrasonic transducer probe. In the current study, the ultrasonic transducer probe has a diameter of 27.5mm which is much larger than the ligament length for short specimen (3mm). Therefore, signals collected by the ultrasonic transducer, which reflect the average property degradation of the area covered by the probe, may underestimate the damage level introduced to the ligament region in the first-stage tests. In other words, even with the density correction for short specimens, the corresponding  $D_{v\rho}$  evolution determined may still be slower than that shown by  $D_{SE}$  in Fig. 7.8 unless a much smaller probe is used which has a size similar to the ligament dimension of the short specimens.

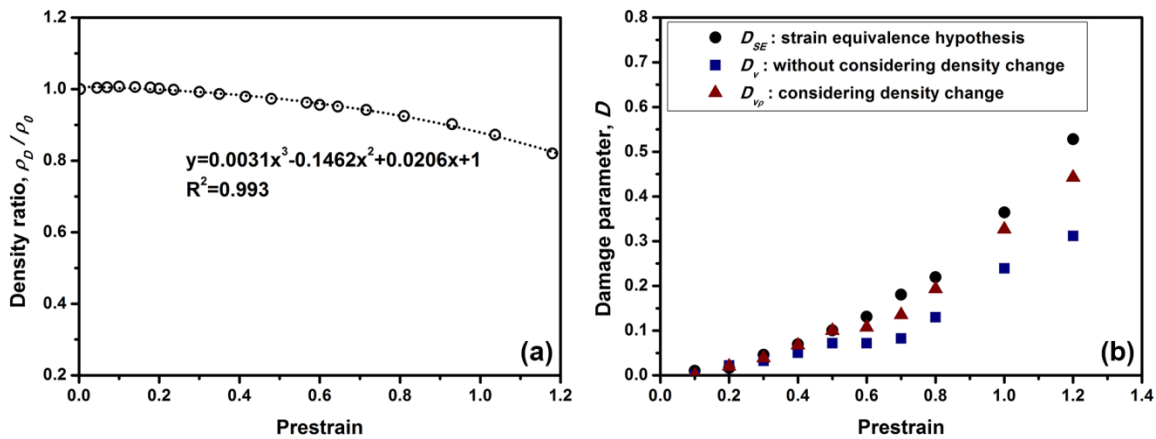


**Fig. 7.10** (a) Change of the density ratio ( $\rho_D/\rho_0$ ) as a function of prestrain based on experimental data given in ref. [15], and (b) variation of damage parameters  $D_{SE}$ ,  $D_v$  and  $D_{v\rho}$  as functions of prestrain for L-10.

## 7.4 Conclusions

Damage evolution in polyethylene materials was characterized using ultrasonic velocity in the through-transmission mode and elastic modulus from mechanical testing. Both long and short specimens show increase in degradation of ultrasonic velocity and elastic modulus with the increase of prestrain levels. Results from the ultrasonic tests also show that even without any prestrain, the ultrasonic velocity decreases with the decrease of specimen thickness below 8mm. By establishing the relationship between ultrasonic velocity and thickness of virgin specimens, damage parameter based on the degradation of ultrasonic velocity ( $D_v$ ) gives a trend of change similar to that based on the degradation of elastic modulus ( $D_{SE}$ ). Values for  $D_{SE}$  also suggest that damage evolution in short specimens is faster than that in long specimens, possibly because the former generates a higher level of stress triaxiality at a given prestrain level. The study found that disparity between  $D_{SE}$  and  $D_v$ , especially for specimens with large prestrains, can be reduced by considering density change introduced by the prestrain. Using experimental data in literature, the study demonstrates the possibility of matching the damage parameter values from the ultrasonic method with  $D_{SE}$  by considering the density change in determining the damage parameter ( $D_{v\rho}$ ). The study concludes that ultrasonic method can also be used as a non-destructive means to characterize damage evolution in PE. However, due to the high signal attenuation in PE and its significant density change with deformation, further studies are required before developing a non-destructive ultrasonic technique for in-situ inspection of PE pipe for its damage development.

## References

- [1] Kiass, N., Khelif, R., Boulanouar, L., and Chaoui, K., 2005, “Experimental Approach to Mechanical Property Variability through a High-Density Polyethylene Gas Pipe Wall,” *J. Appl. Polym. Sci.*, **97**(1), pp. 272–281.
- [2] Majid, Z. A., Mohsin, R., Yaacob, Z., and Hassan, Z., 2010, “Failure Analysis of Natural Gas Pipes,” *Eng. Fail. Anal.*, **17**(4), pp. 818–837.
- [3] Brown, N., and Crate, J. M., 2012, “Analysis of a Failure in a Polyethylene Gas Pipe Caused by Squeeze off Resulting in an Explosion,” *J. Fail. Anal. Prev.*, **12**(1), pp. 30–36.
- [4] American Gas Association, 2016, “Plastic Piping Data Collection Initiative Status Report” [Online]. Available: [https://www.aga.org/sites/default/files/ppdc\\_august\\_2016\\_status\\_report.pdf](https://www.aga.org/sites/default/files/ppdc_august_2016_status_report.pdf). [Accessed: 16-Feb-2017].
- [5] G’sell, C., and Dahoun, A., 1994, “Evolution of Microstructure in Semi-Crystalline Polymers under Large Plastic Deformation,” *Mater. Sci. Eng. A*, **175**(1–2), pp. 183–199.
- [6] Plummer, C. J. G., Goldberg, A., and Ghanem, A., 2001, “Micromechanisms of Slow Crack Growth in Polyethylene under Constant Tensile Loading,” *Polymer*, **42**(23), pp. 9551–9564.
- [7] Hamouda, H. B. H., Simoes-betbeder, M., Grillon, F., Blouet, P., Billon, N., and Piques, R., 2001, “Creep Damage Mechanisms in Polyethylene Gas Pipes,” *Polymer*, **42**(12), pp. 5425–5437.
- [8] Bartczak, Z., 2005, “Effect of Chain Entanglements on Plastic Deformation Behavior of Linear Polyethylene,” *Macromolecules*, **38**(18), pp. 7702–7713.
- [9] Deblieck, R. A. C., van Beek, D. J. M., Remerie, K., and Ward, I. M., 2011, “Failure Mechanisms in Polyolefines: The Role of Crazing, Shear Yielding and the Entanglement Network,” *Polymer*, **52**(14), pp. 2979–2990.
- [10] Detrez, F., Cantournet, S., and Seguela, R., 2011, “Plasticity/Damage Coupling in Semi-Crystalline Polymers prior to Yielding: Micromechanisms and Damage Law Identification,” *Polymer*, **52**(9), pp. 1998–2008.
- [11] Gurson, A. L., 1977, “Continuum Theory of Ductile Rupture by Void Nucleation and Growth: Part I—Yield Criteria and Flow Rules for Porous Ductile Media,” *J. Eng. Mater. Technol.*, **99**(1), pp. 2–15.
- [12] Needleman, A., and Tvergaard, V., 1984, “An Analysis of Ductile Rupture in Notched Bars,” *J. Mech. Phys. Solids*, **32**(6), pp. 461–490.
- [13] Pardoen, T., and Hutchinson, J. W., 2000, “An Extended Model for Void Growth and Coalescence,” *J. Mech. Phys. Solids*, **48**(12), pp. 2467–2512.
- [14] Cheng, L., and Guo, T. F., 2007, “Void Interaction and Coalescence in Polymeric Materials,” *Int. J. Solids Struct.*, **44**(6), pp. 1787–1808.
- [15] Addiego, F., Dahoun, A., G’sell, C., and Hiver, J.-M., 2006, “Characterization of Volume Strain at Large Deformation under Uniaxial Tension in High-Density Polyethylene,” *Polymer*, **47**(12), pp. 4387–4399.
- [16] Pawlak, A., 2007, “Cavitation during Tensile Deformation of High-Density Polyethylene,” *Polymer*, **48**(5), pp. 1397–1409.
- [17] Boisot, G., Laiarinandrasana, L., Besson, J., Fond, C., and Hochstetter, G., 2011, “Experimental Investigations and Modeling of Volume Change Induced by Void Growth in Polyamide 11,” *Int. J. Solids Struct.*, **48**(19), pp. 2642–2654.

- [18] Ognedal, A. S., Clausen, A. H., Berstad, T., Seelig, T., and Hopperstad, O. S., 2014, “Void Nucleation and Growth in Mineral-Filled PVC – An Experimental and Numerical Study,” *Int. J. Solids Struct.*, **51**(7–8), pp. 1494–1506.
- [19] Butler, M. F., Donald, A. M., Bras, W., Mant, G. R., Derbyshire, G. E., and Ryan, A. J., 1995, “A Real-Time Simultaneous Small- and Wide-Angle X-Ray Scattering Study of In-Situ Deformation of Isotropic Polyethylene,” *Macromolecules*, **28**(19), pp. 6383–6393.
- [20] Hughes, D. J., Mahendrasingam, A., Oatway, W. B., Heeley, E. L., Martin, C., and Fuller, W., 1997, “A Simultaneous SAXS/WAXS and Stress-Strain Study of Polyethylene Deformation at High Strain Rates,” *Polymer*, **38**(26), pp. 6427–6430.
- [21] Butler, M. F., and Donald, A. M., 1998, “A Real-Time Simultaneous Small-and Wide-Angle X-Ray Scattering Study of in Situ Polyethylene Deformation at Elevated Temperatures,” *Macromolecules*, **31**(18), pp. 6234–6249.
- [22] Castagnet, S., Girault, S., Gacougnolle, J. L., and Dang, P., 2000, “Cavitation in Strained Polyvinylidene Fluoride: Mechanical and X-Ray Experimental Studies,” *Polymer*, **41**(20), pp. 7523–7530.
- [23] Addiego, F., Patlazhan, S., Wang, K., André, S., Bernstorff, S., and Ruch, D., 2015, “Time-Resolved Small-Angle X-Ray Scattering Study of Void Fraction Evolution in High-Density Polyethylene during Stress Unloading and Strain Recovery,” *Polym. Int.*, **64**(11), pp. 1513–1521.
- [24] Yarysheva, A. Y., Rukhlya, E. G., Yarysheva, L. M., Bagrov, D. V., Volynskii, A. L., and Bakeev, N. F., 2015, “The Structural Evolution of High-Density Polyethylene during Crazeing in Liquid Medium,” *Eur. Polym. J.*, **66**, pp. 458–469.
- [25] Lemaitre, J., and Dufailly, J., 1987, “Damage Measurements,” *Eng. Fract. Mech.*, **28**(5–6), pp. 643–661.
- [26] Chow, C. L., and Wang, J., 1987, “An Anisotropic Theory of Continuum Damage Mechanics for Ductile Fracture,” *Eng. Fract. Mech.*, **27**(5), pp. 547–558.
- [27] Tai, W. H., 1990, “Plastic Damage and Ductile Fracture in Mild Steels,” *Eng. Fract. Mech.*, **37**(4), pp. 853–880.
- [28] Alves, M., Yu, J., and Jones, N., 2000, “On the Elastic Modulus Degradation in Continuum Damage Mechanics,” *Comput. Struct.*, **76**(6), pp. 703–712.
- [29] Straffelini, G., and Molinari, A., 2002, “Evolution of Tensile Damage in Porous Iron,” *Mater. Sci. Eng. A*, **334**(1–2), pp. 96–103.
- [30] Bonora, N., Gentile, D., Pironi, A., and Newaz, G., 2005, “Ductile Damage Evolution under Triaxial State of Stress: Theory and Experiments,” *Int. J. Plast.*, **21**(5), pp. 981–1007.
- [31] Celentano, D. J., and Chaboche, J.-L., 2007, “Experimental and Numerical Characterization of Damage Evolution in Steels,” *Int. J. Plast.*, **23**(10–11), pp. 1739–1762.
- [32] Wu, T., Coret, M., and Combescure, A., 2011, “Strain Localisation and Damage Measurement by Full 3D Digital Image Correlation: Application to 15-5PH Stainless Steel,” *Strain*, **47**(1), pp. 49–61.
- [33] Abed, F. H., Al-Tamimi, A. K., and Al-Himairee, R. M., 2012, “Characterization and Modeling of Ductile Damage in Structural Steel at Low and Intermediate Strain Rates,” *J. Eng. Mech.*, **138**(9), pp. 1186–1194.
- [34] Darras, B. M., Abed, F. H., Pervaiz, S., and Abdu-Latif, A., 2013, “Analysis of Damage in 5083 Aluminum Alloy Deformed at Different Strainrates,” *Mater. Sci. Eng. A*, **568**, pp. 143–149.

- [35] Chiantoni, G., Comi, C., Mariani, S., and Bonora, N., 2014, “Experimental Assessment of Ductile Damage in P91 Steel at High Temperature,” *Int. J. Damage Mech.*, **23**(4), pp. 567–587.
- [36] Bohse, J., 2000, “Acoustic Emission Characteristics of Micro-Failure Processes in Polymer Blends and Composites,” *Compos. Sci. Technol.*, **60**(8), pp. 1213–1226.
- [37] Fregonese, M., Idrissi, H., Mazille, H., Renaud, L., and Cetre, Y., 2001, “Monitoring Pitting Corrosion of AISI 316L Austenitic Stainless Steel by Acoustic Emission Technique: Choice of Representative Acoustic Parameters,” *J. Mater. Sci.*, **36**(3), pp. 557–563.
- [38] Casiez, N., Deschanel, S., Monnier, T., and Lame, O., 2014, “Acoustic Emission from the Initiation of Plastic Deformation of Polyethylenes during Tensile Tests,” *Polymer*, **55**(25), pp. 6561–6568.
- [39] Pacheco-Salazar, O. F., Wakayama, S., Sakai, T., Ríos-Soberanis, C. R., Cauch-Rodríguez, J. V., and Cervantes-Uc, J. M., 2016, “Damage Accumulation Studied by Acoustic Emission in Bone Cement Prepared with Core-shell Nanoparticles under Fatigue,” *J. Mater. Sci.*, **51**(12), pp. 5635–5645.
- [40] Wang, D., Wang, S., Chung, D. D. L., and Chung, J. H., 2006, “Sensitivity of the Two-Dimensional Electric Potential/Resistance Method for Damage Monitoring in Carbon Fiber Polymer-Matrix Composite,” *J. Mater. Sci.*, **41**(15), pp. 4839–4846.
- [41] Sposito, G., Cawley, P., and Nagy, P. B., 2010, “Potential Drop Mapping for the Monitoring of Corrosion or Erosion,” *Ndt E Int.*, **43**(5), pp. 394–402.
- [42] Xie, S., Chen, Z., Takagi, T., and Uchimoto, T., 2012, “Development of a Very Fast Simulator for Pulsed Eddy Current Testing Signals of Local Wall Thinning,” *NDT E Int.*, **51**, pp. 45–50.
- [43] Meola, C., and Carlomagno, G. M., 2004, “Recent Advances in the Use of Infrared Thermography,” *Meas. Sci. Technol.*, **15**(9), p. R27.
- [44] Meola, C., Carlomagno, G. M., and Giorleo, L., 2004, “The Use of Infrared Thermography for Materials Characterization,” *J. Mater. Process. Technol.*, **155–156**, pp. 1132–1137.
- [45] Ummenhofer, T., and Medgenberg, J., 2009, “On the Use of Infrared Thermography for the Analysis of Fatigue Damage Processes in Welded Joints,” *Int. J. Fatigue*, **31**(1), pp. 130–137.
- [46] Lisle, T., Bouvet, C., Pastor, M.-L., Rouault, T., and Margueres, P., 2015, “Damage of Woven Composite under Tensile and Shear Stress Using Infrared Thermography and Micrographic Cuts,” *J. Mater. Sci.*, **50**(18), pp. 6154–6170.
- [47] Cawley, P., and Adams, R. D., 1979, “The Location of Defects in Structures from Measurements of Natural Frequencies,” *J. Strain Anal. Eng. Des.*, **14**(2), pp. 49–57.
- [48] Salawu, O. S., 1997, “Detection of Structural Damage through Changes in Frequency: A Review,” *Eng. Struct.*, **19**(9), pp. 718–723.
- [49] Alvandi, A., and Cremona, C., 2006, “Assessment of Vibration-Based Damage Identification Techniques,” *J. Sound Vib.*, **292**(1), pp. 179–202.
- [50] Reynolds, W. N., Scudder, L. P., and Pressman, H., 1986, “The Use of Ultrasonic Wave Attenuation to Monitor Polymer and Composite Quality,” *Polym. Test.*, **6**(5), pp. 325–336.
- [51] Furushima, R., Matsuo, Y., Shiota, T., and Yasuda, K., 2007, “Damage Evaluation of Refractories under Cyclic Loading-unloading Processes Using Ultrasonic Method,” *J. Mater. Sci.*, **42**(20), pp. 8652–8661.

- [52] Kim, J.-Y., Jacobs, L. J., Qu, J., and Littles, J. W., 2006, "Experimental Characterization of Fatigue Damage in a Nickel-Base Superalloy Using Nonlinear Ultrasonic Waves," *J. Acoust. Soc. Am.*, **120**(3), pp. 1266–1273.
- [53] Shui, G. S., and Wang, Y. S., 2012, "Nondestructive Evaluation of Material Damage Using Nonlinear Rayleigh Waves Approach," *Adv. Mater. Res.*, **463–464**, pp. 1522–1526.
- [54] Ju, T., Achenbach, J. D., Jacobs, L. J., Guimaraes, M., and Qu, J., 2017, "Ultrasonic Nondestructive Evaluation of Alkali–silica Reaction Damage in Concrete Prism Samples," *Mater. Struct.*, **50**(1), p. 60.
- [55] Pruell, C., Kim, J.-Y., Qu, J., and Jacobs, L. J., 2007, "Evaluation of Plasticity Driven Material Damage Using Lamb Waves," *Appl. Phys. Lett.*, **91**(23), p. 231911.
- [56] Berthaud, Y., 1991, "Damage Measurements in Concrete via an Ultrasonic Technique. Part I Experiment," *Cem. Concr. Res.*, **21**(1), pp. 73–82.
- [57] Nogueira, C. L., and Willam, K. J., 2001, "Ultrasonic Testing of Damage in Concrete under Uniaxial Compression," *Mater. J.*, **98**(3), pp. 265–275.
- [58] Shah, A. A., and Ribakov, Y., 2009, "Non-Linear Ultrasonic Evaluation of Damaged Concrete Based on Higher Order Harmonic Generation," *Mater. Des.*, **30**(10), pp. 4095–4102.
- [59] Balasubramaniam, K., Valluri, J. S., and Prakash, R. V., 2011, "Creep Damage Characterization Using a Low Amplitude Nonlinear Ultrasonic Technique," *Mater. Charact.*, **62**(3), pp. 275–286.
- [60] Xiang, Y., Zhu, W., Liu, C.-J., Xuan, F.-Z., Wang, Y.-N., and Kuang, W.-C., 2015, "Creep Degradation Characterization of Titanium Alloy Using Nonlinear Ultrasonic Technique," *NDT E Int.*, **72**, pp. 41–49.
- [61] Liu, J. H., Li, G. L., Hao, X. Y., Zeng, D. B., and Sun, Z. H., 2001, "Ultrasonic Measurement of Fatigue Damage of Nodular Cast Iron," *Mater. Lett.*, **50**(4), pp. 194–198.
- [62] Piche, L., 1984, "Ultrasonic Velocity Measurement for the Determination of Density in Polyethylene," *Polym. Eng. Sci.*, **24**(17), pp. 1354–1358.
- [63] Mažeika, L., Šlitteris, R., and Vladišauskas, A., 2016, "Measurement of Velocity and Attenuation for Ultrasonic Longitudinal Waves in the Polyethylene Samples," *Ultragarsas Ultrasound*, **65**(4), pp. 12–15.
- [64] Rae, P. J., and Brown, E. N., 2015, "Some Observations on Measuring Sound Speeds in Polymers Using Time-of-Flight," *Exp. Tech.*
- [65] Bray, D. E., Vela, J., and Al-Zubi, R. S., 2005, "Stress and Temperature Effects on Ultrasonic Properties in Cross-Linked and High Density Polyethylene," *J. Press. Vessel Technol.*, **127**(3), pp. 220–225.
- [66] Jia, D., Bourse, G., Chaki, S., Lacrampe, M. F., Robin, C., and Demouveau, H., 2014, "Investigation of Stress and Temperature Effect on the Longitudinal Ultrasonic Waves in Polymers," *Res. Nondestruct. Eval.*, **25**(1), pp. 20–29.
- [67] Jar, P.-Y., 2014, "Transition of Neck Appearance in Polyethylene and Effect of the Associated Strain Rate on the Damage Generation," *Polym. Eng. Sci.*, **54**(8), pp. 1871–1878.
- [68] Ben Jar, P.-Y., 2014, "Transition of Neck Appearance in Polyethylene and Effect of the Associated Strain Rate on the Damage Generation," *Polym. Eng. Sci.*, **54**(8), pp. 1871–1878.
- [69] Zhang, Y., and Jar, P.-Y. B., 2015, "Quantitative Assessment of Deformation-Induced Damage in Polyethylene Pressure Pipe," *Polym. Test.*, **47**, pp. 42–50.

- [70] Castagnet, S., and Deburck, Y., 2007, “Relative Influence of Microstructure and Macroscopic Triaxiality on Cavitation Damage in a Semi-Crystalline Polymer,” *Mater. Sci. Eng. A*, **448**(1–2), pp. 56–66.
- [71] Clausen, A. H., Børvik, T., Hopperstad, O. S., and Benallal, A., 2004, “Flow and Fracture Characteristics of Aluminium Alloy AA5083–H116 as Function of Strain Rate, Temperature and Triaxiality,” *Mater. Sci. Eng. A*, **364**(1), pp. 260–272.
- [72] Ognedal, A. S., Clausen, A. H., Dahlen, A., and Hopperstad, O. S., 2014, “Behavior of PVC and HDPE under Highly Triaxial Stress States: An Experimental and Numerical Study,” *Mech. Mater.*, **72**, pp. 94–108.

# Chapter 8

## Summary and future work

This chapter summarizes the main contributions of this research work and suggests possible work for future investigation.

### 8.1 Summary of contributions

Polyethylene (PE) pipe are being increasingly used for natural gas and water transportation. The damage generated during installation or maintenance process such as dig-in, squeeze-off and bending causes mechanical property degradation of the pipe, thus reducing its remaining service life. Because of the potentials of pipeline failure for the huge economic losses and threats to the public safety, it is extremely important to have a tool to characterize the likelihood of pipeline failure. On the other hand, a material-specific damage parameter  $D$  is required in continuum damage models to model material failure behaviour. Accurate quantification of  $D$  relies on proper methodologies to measure the changes in mechanical properties. However, few experimental studies have been conducted on the characterization of damage behavior in PE pipes. Therefore, this dissertation focuses on the characterization and detection of damage in PE pipes. The pertinent research work presented in this dissertation is summarized below.

#### (1) Characterization of deformation damage in PE pipe

The study of damage evolution in PE pipe is important not only from an academic viewpoint, but also for prediction of service life for pipeline components. A two-stage test method has been developed to quantitatively evaluate effects of deformation-induced damage (or loading history) on mechanical properties of PE pipe. The damage development in PE pipe is characterized and quantified by measurement of elastic modulus degradation. In particular, the influence of strain rate and microstructure on damage development in PE pipe is investigated. The results show that damage is larger and grows faster at a higher deformation rate. Mechanical properties, including yield stress, relaxation behaviour, and moduli (elastic modulus at a strain of 5% and strain hardening modulus at strains above 70%), are compared between two widely used PE pipes that are made of PE80 and PE100 resins. In addition, a phenomenological approach based on experimental testing and FE simulation has been used to investigate large deformation and fracture behaviour of PE pipe. The results show that through the combination of a phenomenological constitutive equation and an empirical ductile damage model, the FE simulation can successfully regenerate the deformation and fracture behaviour observed from the experimental testing.

## **(2) Effects of Squeeze-off on Mechanical Properties of Polyethylene Pipes**

Influence of the squeeze-off process, a popular procedure for pipe maintenance or repair, on PE's mechanical properties has been investigated, with a special attention to the effect of squeezing speed. The experimental results show that both elastic modulus and yield stress of the pipe are significantly affected by deformation introduced by the squeeze-off process. Additionally, the change in mechanical properties showed little dependence on the squeezing speed. A three-dimensional FE model was developed to facilitate the determination of strain and strain rate in the pipe wall during the squeeze-off process. The FE simulation show that around

70% of the cross section was under compression and 30% under tension. Furthermore, the above mentioned two-stage test methods are applied to confirm the damage development under different loading modes and crosshead speeds. The results show that difference of the overall damage among the three squeezing speeds is smaller than that could have been generated in a single loading mode. The study concludes that compressive loading can cause damage in PE pipe, and this damage plays a crucial role on the change of elastic modulus and yield strength of PE pipe. Such an influence of squeeze-off process or any loading scenario that involves compressive deformation should be considered for evaluation of PE pipe performance.

### **(3) Characterization of Ductile Damage in Polyethylene Based on Effective Stress Concept**

A novel approach for determining the effective stress in the fictitious undamaged state for PE is proposed. First, the quasi-static stress-strain relationships for PE deformation at various crosshead speeds were determined by removing the viscous stress component based on a model that consists of spring, damper and finite plasticity elements. The model was calibrated using results from stress relaxation tests. The results show that the quasi-static stress at a given strain level decreases with the increase of crosshead speed, indicating the influence of strain rate on the long-term performance of the PE pipe material. In addition, influence of aspect ratio of the ligament cross section on the quasi-static stress-strain curves has also been studied by changing ligament width of PE specimens. The results show that the change of ligament width has little effect on the quasi-static stress-strain curve. By fitting the experimentally-determined curves of quasi-static stress versus logarithm crosshead speed using an arctangent function, the effective stress at various strain levels is successfully estimated by extrapolating the quasi-static stress to zero crosshead speed. This allows characterization of damage in PE pipe material without any hypothesis such as strain or energy equivalence, by calculating damage value directly using the

expression  $D_{eff} = 1 - \sigma/\sigma_{eff}$  . Damage values determined from this approach are compared with those based on the hypotheses of strain and energy equivalence, calculated using degradation of elastic modulus from a two-stage test method. Results show that damage values calculated using the effective stress and those based on the hypothesis of energy equivalence are in satisfactory agreement. Therefore, the proposed effective stress method can be used to determine the effective stress and to characterize damage evolution in PE pipe material.

#### **(4) Characterization of Ductile Damage in Polyethylene Using Ultrasonic Technique**

Damage evolution in polyethylene (PE) materials was measured using ultrasonic and two-stage test methods. In the first stage test, various prestrain values were first introduced to two types of PE specimens, named as long and short specimens with different thicknesses through a monotonic tensile test at the crosshead speed of 1mm/min. Before the second stage test, damage in the PE specimens was characterized through the measurement of time-of-flight of ultrasonic velocity in the through transmission mode. Results show that ultrasonic velocity decreases with the increase of prestrain generated in the first stage test. In addition, it was observed that the longitudinal wave speed was dependent on the thickness of PE sample. The relationship between the ultrasonic velocity and specimen thickness was obtained and used to determine damage parameter based on the degradation of ultrasonic velocity. Damage develops faster in short specimen, of which stress triaxiality is higher than that in long specimen. After taking density change into consideration, damage parameter measured from the degradation of ultrasonic velocity shows good agreement with that measured from the elastic modulus degradation. Therefore, ultrasonic method can also be used for non-destructive damage characterization for PE materials.

## **8.2 Future work**

The research work presented in this dissertation is a step toward developing a reliable instrumentation system for early detection of damage and estimation of remaining service life in PE pipes. However, further research is needed before its application is realized in industry.

### **(1) Characterization of damage development under different loading conditions**

The proposed two-stage test method has been successfully used to determine damage evolution under tensile and compressive loading conditions in this thesis. In order to obtain the damage evolution under the loading condition which is the same as that in the real situation, this method can be extended in the future to study damage behavior under fatigue or creep loading. In addition, the experimentally measured damage evolution law can be further implemented in FE models to study fracture behaviors of PE pipe.

### **(2) Effects of temperature on damage behavior in PE pipe**

The influence of strain rate on damage development in PE pipe has been quantitatively investigated in this dissertation. However, according to the experimental results reported in ref. [1] that volume strain in poly(vinylidene fluoride) (PVDF) materials evolves faster as the temperature decreases, it is believed that temperature may also play an important role in the damage growth in PE pipes, which needs to be further studied. Furthermore, in order to determine long-term hydrostatic strength for PE pipe, hydrostatic pressure tests are conducted based on standard ASTM D 2837 or ISO 9080. However, performing such tests takes an extremely long time (at least one year) by just using temperature as accelerating factor. In Chapter 3, time-strain rate superposition principle has been proposed, in which strain rate,

instead of temperature, is used as an accelerating factor to construct the relaxation master curves. In the future, I plan to extend this principle to time-temperature-strain rate superposition principle (TTSrSP) to predict long-term relaxation and creep behaviors for PE pipe. By applying the TTSrSP to the current test method, the time-to-failure of plastic pipe should be greatly reduced.

### **(3) Development of in-situ damage detection methodologies**

Although several studies [2–4] have been carried out to evaluate the quality of PE joint through developing non-destructive ultrasonic techniques, to my best knowledge, there is no in-situ damage detection method available for PE pipe inspection. The traditional damage characterization method, such as through the measurement of the degradation of elastic modulus, is destructive, thus not applicable for in-situ detection and inspection of damage state in PE pipe. The proposed damage characterization methods based on the degradation of stress and ultrasonic velocity in Chapters 6 and 7, respectively, show good agreement with the damage measured from elastic modulus degradation, indicating their potential use for the in-situ damage detection for PE pipe. However, further studies are needed to develop the details of the test methodology. For example, nonlinear ultrasonic method may be developed to improve its sensitivity to the degradation of PE pipe's mechanical properties.

## **References**

- [1] Quatravaux, T., Elkoun, S., G'sell, C., Cangemi, L., and Meimon, Y., 2002, "Experimental Characterization of the Volume Strain of Poly (Vinylidene Fluoride) in the Region of Homogeneous Plastic Deformation," *J. Polym. Sci. Part B Polym. Phys.*, **40**(22), pp. 2516–2522.

- [2] Caravaca, D. S., Bird, C., and Kleiner, D., 2007, "Ultrasonic Phased Array Inspection of Electrofusion Joints in Polyethylene Pipes," *Insight-Non-Destr. Test. Cond. Monit.*, **49**(2), pp. 83–86.
- [3] Troughton, M., Spicer, M., and Hagglund, F., 2012, "Development of Ultrasonic Phased Array Inspection of Polyethylene Pipe Joints," *ASME 2012 Pressure Vessels and Piping Conference*, American Society of Mechanical Engineers, pp. 285–293.
- [4] Spicer, M., Troughton, M., and Hagglund, F., 2013, "Development and Assessment of Ultrasonic Inspection System for Polyethylene Pipes," *ASME 2013 Pressure Vessels and Piping Conference*, American Society of Mechanical Engineers, p. V06BT06A042–V06BT06A042.

## Bibliography

- Abbassi F, Mistou S, Zghal A (2013) Failure analysis based on microvoid growth for sheet metal during uniaxial and biaxial tensile tests. *Mater. Des.* 49:638–646.
- Abed FH, Al-Tamimi AK, Al-Himairee RM (2012) Characterization and modeling of ductile damage in structural steel at low and intermediate strain rates. *J. Eng. Mech.* 138(9):1186–1194.
- Acharyya S, Dhar S (2008) A complete GTN model for prediction of ductile failure of pipe. *J. Mater. Sci.* 43(6):1897–1909.
- Achouri M, Germain G, Dal Santo P, Saidane D (2014) Experimental and numerical analysis of micromechanical damage in the punching process for High-Strength Low-Alloy steels. *Mater. Des.* 56:657–670.
- Addiego F, Dahoun A, G'Sell C, Hiver JM (2006) Characterization of volume strain at large deformation under uniaxial tension in high-density polyethylene. *Polymer* 47(12):4387–4399.
- Addiego F, Patlazhan S, Wang K, André S, Bernstorff S, Ruch D (2015) Time-resolved small-angle X-ray scattering study of void fraction evolution in high-density polyethylene during stress unloading and strain recovery. *Polym. Int.* 64(11):1513–1521.
- Adib A, Domínguez C, Rodríguez J, Martín C, García RA (2014) The effect of microstructure on the slow crack growth resistance in polyethylene resins. *Polym. Eng. Sci.* 55(5):1018–1023.
- Ahzi S, Makradi A, Gregory RV, Edie DD (2003) Modeling of deformation behavior and strain-induced crystallization in poly(ethylene terephthalate) above the glass transition temperature. *Mech. Mater.* 35(12):1139–1148.
- Al-Rub RKA, Kim SM (2010) Computational applications of a coupled plasticity-damage constitutive model for simulating plain concrete fracture. *Eng. Fract. Mech.* 77(10):1577–1603.
- Alvandi A, Cremona C (2006) Assessment of vibration-based damage identification techniques. *J. Sound Vib.* 292(1):179–202.
- Alvarado-Contreras J, Polak MA, Penlidis A (2007) Micromechanical approach to modeling damage in crystalline polyethylene. *Polym. Eng. Sci.* 47(4):410–420.
- Alvarado-Contreras JA, Polak MA, Penlidis A (2010) Constitutive modeling of damage evolution in semicrystalline polyethylene. *J. Eng. Mater. Technol.* 132(4):041009.
- Alves M, Yu J, Jones N (2000) On the elastic modulus degradation in continuum damage mechanics. *Comput. Struct.* 76(6):703–712.
- Andrews JM, Ward IM (1970) The cold-drawing of high density polyethylene. *J. Mater. Sci.* 5(5):411–417.
- ASTM D5262 Standard Test Method for Evaluating the Unconfined Tension Creep and Creep Rupture Behavior of Geosynthetics* (ASTM International).

- ASTM D6048 Standard Practice for Stress Relaxation Testing of Raw Rubber, Unvulcanized Rubber Compounds, and Thermoplastic Elastomers* (ASTM International).
- ASTM F1473 Standard Test Method for Notch Tensile Test to Measure the Resistance to Slow Crack Growth of Polyethylene Pipes and Resins* (ASTM International).
- Antonaci P, Bruno CLE, Gliozzi AS, Scalerandi M (2010) Monitoring evolution of compressive damage in concrete with linear and nonlinear ultrasonic methods. *Cem. Concr. Res.* 40(7):1106–1113.
- Arruda EM, Boyce MC (1993) A three-dimensional constitutive model for the large stretch behavior of rubber elastic materials. *J. Mech. Phys. Solids* 41(2):389–412.
- Ayoub G, Zaïri F, Frédérix C, Gloaguen JM, Naït-Abdelaziz M, Seguela R, Lefebvre JM (2011) Effects of crystal content on the mechanical behaviour of polyethylene under finite strains: Experiments and constitutive modelling. *Int. J. Plast.* 27(4):492–511.
- Ayoub G, Zaïri F, Naït-Abdelaziz M, Gloaguen JM (2010) Modelling large deformation behaviour under loading–unloading of semicrystalline polymers: Application to a high density polyethylene. *Int. J. Plast.* 26(3):329–347.
- Azevedo CRF (2007) Failure analysis of a crude oil pipeline. *Eng. Fail. Anal.* 14(6):978–994.
- Balasubramaniam K, Valluri JS, Prakash RV (2011) Creep damage characterization using a low amplitude nonlinear ultrasonic technique. *Mater. Character.* 62(3):275–286.
- Balieu R, Lauro F, Bennani B, Haugou G, Chaari F, Matsumoto T, Mottola E (2015) Damage at high strain rates in semi-crystalline polymers. *Int. J. Impact Eng.* 76:1–8.
- Barham PJ, Keller A (1976) A study on the achievement of high-modulus polyethylene fibres by drawing. *J. Mater. Sci.* 11(1):27–35.
- Barker MB, Bowman J, Bevis M (1983) The performance and causes of failure of polyethylene pipes subjected to constant and fluctuating internal pressure loadings. *J. Mater. Sci.* 18(4):1095–1118.
- Bartczak Z (2005) Effect of chain entanglements on plastic deformation behavior of linear polyethylene. *Macromolecules* 38(18):7702–7713.
- Bartczak Z, Cohen RE, Argon AS (1992) Evolution of the crystalline texture of high-density polyethylene during uniaxial compression. *Macromolecules* 25(18):4692–4704.
- Belnoue JP, Garnham B, Bache M, Korsunsky AM (2010) The use of coupled nonlocal damage-plasticity to predict crack growth in ductile metal plates. *Eng. Fract. Mech.* 77(11):1721–1729.
- Belnoue JP, Korsunsky AM (2012) A damage function formulation for nonlocal coupled damage-plasticity model of ductile metal alloys. *Eur. J. Mech. - ASolids* 34:63–77.
- Belnoue JP, Nguyen GD, Korsunsky AM (2007) A One-Dimensional Nonlocal Damage-Plasticity Model for Ductile Materials. *Int. J. Fract.* 144(1):53–60.
- Ben Jar PY (2014) Transition of neck appearance in polyethylene and effect of the associated strain rate on the damage generation. *Polym. Eng. Sci.* 54(8):1871–1878.

- Benseddiq N, Imad A (2008) A ductile fracture analysis using a local damage model. *Int. J. Press. Vessels Pip.* 85(4):219–227.
- Berthaud Y (1991) Damage measurements in concrete via an ultrasonic technique. Part I experiment. *Cem. Concr. Res.* 21(1):73–82.
- Betten J, Sklepus S, Zolochovsky A (1999) A Microcrack Description of Creep Damage in Crystalline Solids with Different Behaviour in Tension and Compression. *Int. J. Damage Mech.* 8(3):197–232.
- Bigg DM (1976) A review of techniques for processing ultra-high modulus polymers. *Polym. Eng. Sci.* 16(11):725–734.
- Blaise A, Baravian C, André S, Dillet J, Michot LJ, Mokso R (2010) Investigation of the Mesostructure of a Mechanically Deformed HDPE by Synchrotron Microtomography. *Macromolecules* 43(19):8143–8152.
- Bodner SR, Partom Y (1975) Constitutive equations for elastic-viscoplastic strain-hardening materials. *J. Appl. Mech.* 42(2):385–389.
- Bohse J (2000) Acoustic emission characteristics of micro-failure processes in polymer blends and composites. *Compos. Sci. Technol.* 60(8):1213–1226.
- Boisot G, Laiarinandrasana L, Besson J, Fond C, Hochstetter G (2011) Experimental investigations and modeling of volume change induced by void growth in polyamide 11. *Int. J. Solids Struct.* 48(19):2642–2654.
- Bonora N (1997) A nonlinear CDM model for ductile failure. *Eng. Fract. Mech.* 58(1):11–28.
- Bonora N, Gentile D, Pironi A, Newaz G (2005) Ductile damage evolution under triaxial state of stress: theory and experiments. *Int. J. Plast.* 21(5):981–1007.
- Bonora N, Ruggiero A, Gentile D, De Meo S (2011) Practical applicability and limitations of the elastic modulus degradation technique for damage measurements in ductile metals. *Strain* 47(3):241–254.
- Boyce MC, Parks DM, Argon AS (1988) Large inelastic deformation of glassy polymers. part I: rate dependent constitutive model. *Mech. Mater.* 7(1):15–33.
- Boyce MC, Socrate S, Llana PG (2000) Constitutive model for the finite deformation stress–strain behavior of poly(ethylene terephthalate) above the glass transition. *Polymer* 41(6):2183–2201.
- Bozorg-Haddad A, Iskander M (2008) Compressive Creep Behavior of HDPE Using Time Temperature Superposition. *GeoCongress 2008 SGeosustainability Geohazard Mitig.* (ASCE), 915–922.
- Bozorg-Haddad A, Iskander M (2011) Comparison of accelerated compressive creep behavior of virgin HDPE using thermal and energy approaches. *J. Mater. Eng. Perform.* 20(7):1219–1229.
- Bray DE, Vela J, Al-Zubi RS (2005) Stress and temperature effects on ultrasonic properties in cross-linked and high density polyethylene. *J. Press. Vessel Technol.* 127(3):220–225.
- Brooks NWJ, Duckett RA, Ward IM (1999) Effects of crystallinity and stress state on the yield strain of polyethylene. *Polymer* 40(26):7367–7372.

- Brown N, Crate JM (2012) Analysis of a Failure in a Polyethylene Gas Pipe Caused by Squeeze off Resulting in an Explosion. *J. Fail. Anal. Prev.* 12(1):30–36.
- Butler MF, Donald AM (1998) A real-time simultaneous small-and wide-angle X-ray scattering study of in situ polyethylene deformation at elevated temperatures. *Macromolecules* 31(18):6234–6249.
- Butler MF, Donald AM, Bras W, Mant GR, Derbyshire GE, Ryan AJ (1995) A Real-Time Simultaneous Small- and Wide-Angle X-ray Scattering Study of In-Situ Deformation of Isotropic Polyethylene. *Macromolecules* 28(19):6383–6393.
- Butler MF, Donald AM, Ryan AJ (1998) Time resolved simultaneous small-and wide-angle X-ray scattering during polyethylene deformation—II. Cold drawing of linear polyethylene. *Polymer* 39(1):39–52.
- Cao TS, Gachet JM, Montmitonnet P, Bouchard PO (2014) A Lode-dependent enhanced Lemaitre model for ductile fracture prediction at low stress triaxiality. *Eng. Fract. Mech.* 124–125:80–96.
- Cao TS, Gaillac A, Montmitonnet P, Bouchard PO (2013) Identification methodology and comparison of phenomenological ductile damage models via hybrid numerical–experimental analysis of fracture experiments conducted on a zirconium alloy. *Int. J. Solids Struct.* 50(24):3984–3999.
- Capaccio G, Ward I (1973) Properties of Ultrahigh Modulus Linear Polyethylenes. *Nat.-Phys. Sci.* 243(130):143–143.
- Capaccio G, Ward IM (1974) Preparation of ultra-high modulus linear polyethylenes; effect of molecular weight and molecular weight distribution on drawing behaviour and mechanical properties. *Polymer* 15(4):233–238.
- Capiati N, Porter R (1975) Tensile Properties of Ultradrawn Polyethylene. *J. Polym. Sci. Part B-Polym. Phys.* 13(6):1177–1186.
- Caravaca DS, Bird C, Kleiner D (2007) Ultrasonic phased array inspection of electrofusion joints in polyethylene pipes. *Insight-Non-Destr. Test. Cond. Monit.* 49(2):83–86.
- Casiez N, Deschanel S, Monnier T, Lame O (2014) Acoustic emission from the initiation of plastic deformation of Polyethylenes during tensile tests. *Polymer* 55(25):6561–6568.
- Castagnet S, Deburck Y (2007) Relative influence of microstructure and macroscopic triaxiality on cavitation damage in a semi-crystalline polymer. *Mater. Sci. Eng. A* 448(1–2):56–66.
- Castagnet S, Girault S, Gacougnolle JL, Dang P (2000) Cavitation in strained polyvinylidene fluoride: mechanical and X-ray experimental studies. *Polymer* 41(20):7523–7530.
- Cawley P, Adams RD (1979) The location of defects in structures from measurements of natural frequencies. *J. Strain Anal. Eng. Des.* 14(2):49–57.
- Celentano DJ, Chaboche JL (2007) Experimental and numerical characterization of damage evolution in steels. *Int. J. Plast.* 23(10–11):1739–1762.
- Chaboche JL (1984) Anisotropic creep damage in the framework of continuum damage mechanics. *Nucl. Eng. Des.* 79(3):309–319.

- Chaboche JL (1988) Continuum Damage Mechanics: Part II—Damage Growth, Crack Initiation, and Crack Growth. *J. Appl. Mech.* 55(1):65–72.
- Chaboche JL, Lesne PM (1988) A Non-Linear Continuous Fatigue Damage Model. *Fatigue Fract. Eng. Mater. Struct.* 11(1):1–17.
- Challamel N, Lanos C, Casandjian C (2005) Creep damage modelling for quasi-brittle materials. *Eur. J. Mech. - ASolids* 24(4):593–613.
- Challier M, Besson J, Laiarinandrasana L, Piques R (2006) Damage and fracture of polyvinylidene fluoride (PVDF) at 20 °C: Experiments and modelling. *Eng. Fract. Mech.* 73(1):79–90.
- Chandrakanth S, Pandey PC (1995) An isotropic damage model for ductile material. *Eng. Fract. Mech.* 50(4):457–465.
- Chen J, Xu Z, Yu Y, Yao Y (2014) Experimental characterization of granite damage using nonlinear ultrasonic techniques. *NDT E Int.* 67:10–16.
- Chen JF, Li SQ, Bisby LA, Ai J (2011) FRP rupture strains in the split-disk test. *Compos. Part B Eng.* 42(4):962–972.
- Cheng L, Guo TF (2007) Void interaction and coalescence in polymeric materials. *Int. J. Solids Struct.* 44(6):1787–1808.
- Chiantoni G, Comi C, Mariani S, Bonora N (2014) Experimental assessment of ductile damage in P91 steel at high temperature. *Int. J. Damage Mech.* 23(4):567–587.
- Chow CL, Wang J (1987) An anisotropic theory of continuum damage mechanics for ductile fracture. *Eng. Fract. Mech.* 27(5):547–558.
- Cicekli U, Voyiadjis GZ, Al-Rub RKA (2007) A plasticity and anisotropic damage model for plain concrete. *Int. J. Plast.* 23(10):1874–1900.
- Colak OU (2005) Modeling deformation behavior of polymers with viscoplasticity theory based on overstress. *Int. J. Plast.* 21(1):145–160.
- Colak OU, Dusunceli N (2006) Modeling viscoelastic and viscoplastic behavior of high density polyethylene (HDPE). *J. Eng. Mater. Technol.* 128(4):572–578.
- Colak OU, Krempl E (2003) Modeling of uniaxial and biaxial ratcheting behavior of 1026 Carbon steel using the simplified Viscoplasticity Theory Based on Overstress (VBO). *Acta Mech.* 160(1–2):27–44.
- Darras BM, Abed FH, Pervaiz S, Abdu-Latif A (2013) Analysis of damage in 5083 aluminum alloy deformed at different strainrates. *Mater. Sci. Eng. A* 568:143–149.
- Dasari A, Misra RDK (2003) On the strain rate sensitivity of high density polyethylene and polypropylenes. *Mater. Sci. Eng. A* 358(1–2):356–371.
- Deblieck RAC, van Beek DJM, Remerie K, Ward IM (2011) Failure mechanisms in polyolefines: The role of crazing, shear yielding and the entanglement network. *Polymer* 52(14):2979–2990.

- Detrez F, Cantournet S, Seguela R (2011) Plasticity/damage coupling in semi-crystalline polymers prior to yielding: Micromechanisms and damage law identification. *Polymer* 52(9):1998–2008.
- Djoković V, Kostoski D, Dramićanin MD (2000) Viscoelastic behavior of semicrystalline polymers at elevated temperatures on the basis of a two-process model for stress relaxation. *J. Polym. Sci. Part B Polym. Phys.* 38(24):3239–3246.
- DM Parks, AS Argon, B Bagepalli (1984) Large elastic-plastic deformation of glassy polymers. *Program Polym. Sci. Technol.*
- Drozдов AD, Christiansen J deC (2009) Creep failure of polypropylene: experiments and constitutive modeling. *Int. J. Fract.* 159(1):63–79.
- Drozдов AD, Yuan Q (2003) The viscoelastic and viscoplastic behavior of low-density polyethylene. *Int. J. Solids Struct.* 40(10):2321–2342.
- Dufailly J, Lemaitre J (1995) Modeling Very Low Cycle Fatigue. *Int. J. Damage Mech.* 4(2):153–170.
- Dusunceli N, Aydemir B (2011) The Effects of Loading History and Manufacturing Methods on the Mechanical Behavior of High-Density Polyethylene. *J. Elastomers Plast.* 43(5):451–468.
- Dusunceli N, Colak OU (2006) High density polyethylene (HDPE): Experiments and modeling. *Mech. Time-Depend. Mater.* 10(4):331–345.
- Dusunceli N, Colak OU (2008) The effects of manufacturing techniques on viscoelastic and viscoplastic behavior of high density polyethylene (HDPE). *Mater. Des.* 29(6):1117–1124.
- Eugen A, Emilia OM (2015) Determining the Forces in the Polyethylene Pipes after Squeezing them off with Specific Equipment.
- Fager LO, Bassani JL (1986) Plane strain neck propagation. *Int. J. Solids Struct.* 22(11):1243–1257.
- Ferry JD (1980) *Viscoelastic properties of polymers* (John Wiley & Sons).
- Fleissner M (1998) Experience with a full notch creep test in determining the stress crack performance of polyethylenes. *Polym. Eng. Sci.* 38(2):330–340.
- Flory PJ, Jr JR (1943) Statistical Mechanics of Cross-Linked Polymer Networks I. Rubberlike Elasticity. *J. Chem. Phys.* 11(11):512–520.
- Frank A, Hutař P, Pinter G (2012) Numerical Assessment of PE 80 and PE 100 Pipe Lifetime Based on Paris-Erdogan Equation. *Macromol. Symp.* (Wiley Online Library), 112–121.
- Frank A, Pinter G (2014) Evaluation of the applicability of the cracked round bar test as standardized PE-pipe ranking tool. *Polym. Test.* 33:161–171.
- Frank A, Pinter G, Lang RW (2010) Fracture mechanics lifetime prediction of PE 80 and PE 100 pipes under complex loading conditions. *Proc. Pipes XV Vanc. Can.*
- Frank GJ, Brockman RA (2001) A viscoelastic–viscoplastic constitutive model for glassy polymers. *Int. J. Solids Struct.* 38(30–31):5149–5164.

- Fregonese M, Idrissi H, Mazille H, Renaud L, Cetre Y (2001) Monitoring pitting corrosion of AISI 316L austenitic stainless steel by acoustic emission technique: choice of representative acoustic parameters. *J. Mater. Sci.* 36(3):557–563.
- Furushima R, Matsuo Y, Shiota T, Yasuda K (2007) Damage evaluation of refractories under cyclic loading–unloading processes using ultrasonic method. *J. Mater. Sci.* 42(20):8652–8661.
- Galeski A, Bartczak Z, Argon AS, Cohen RE (1992) Morphological alterations during texture-producing plastic plane strain compression of high-density polyethylene. *Macromolecules* 25(21):5705–5718.
- Ganczarski A, Barwacz L (2007) Low Cycle Fatigue Based on Unilateral Damage Evolution. *Int. J. Damage Mech.* 16(2):159–177.
- Gibson AG, Ward IM, Cole BN, Parsons B (1974) Hydrostatic extrusion of linear polyethylene. *J. Mater. Sci.* 9(7):1193–1196.
- Gologanu M, Leblond JB, Devaux J (1993) Approximate models for ductile metals containing non-spherical voids—Case of axisymmetric prolate ellipsoidal cavities. *J. Mech. Phys. Solids* 41(11):1723–1754.
- Graice LM, Younan MYA, Naga SAR (2004) Experimental investigation into the fracture toughness of polyethylene pipe material. *J. Press. Vessel Technol.* 127(1):70–75.
- G’sell C, Dahoun A (1994) Evolution of microstructure in semi-crystalline polymers under large plastic deformation. *Mater. Sci. Eng. A* 175(1–2):183–199.
- G’Sell C, Hiver JM, Dahoun A (2002) Experimental characterization of deformation damage in solid polymers under tension, and its interrelation with necking. *Int. J. Solids Struct.* 39(13–14):3857–3872.
- G’Sell C, Hiver JM, Dahoun A, Souahi A (1992) Video-controlled tensile testing of polymers and metals beyond the necking point. *J. Mater. Sci.* 27(18):5031–5039.
- G’sell C, Jonas JJ (1979) Determination of the plastic behaviour of solid polymers at constant true strain rate. *J. Mater. Sci.* 14(3):583–591.
- Gu G, Xia Y, Lin C hsu, Lin S, Meng Y, Zhou Q (2013) Experimental study on characterizing damage behavior of thermoplastics. *Mater. Des.* 44:199–207.
- Guelorget B, François M, Lu J (2007) Microindentation as a local damage measurement technique. *Mater. Lett.* 61(1):34–36.
- Gurson AL (1977) Continuum Theory of Ductile Rupture by Void Nucleation and Growth: Part I—Yield Criteria and Flow Rules for Porous Ductile Media. *J. Eng. Mater. Technol.* 99(1):2–15.
- Hamouda HBH, Simoes-betbeder M, Grillon F, Blouet P, Billon N, Piques R (2001) Creep damage mechanisms in polyethylene gas pipes. *Polymer* 42(12):5425–5437.
- Harris KE (2007) *Squeeze-off & gel patch repair methods for polyethylene pipe in natural gas distribution lines.*
- Hasan F, Iqbal J, Ahmed F (2007) Stress corrosion failure of high-pressure gas pipeline. *Eng. Fail. Anal.* 14(5):801–809.

- Haward RN (1993) Strain hardening of thermoplastics. *Macromolecules* 26(22):5860–5869.
- Haward RN (2007) Strain hardening of high density polyethylene. *J. Polym. Sci. Part B Polym. Phys.* 45(9):1090–1099.
- Haward RN, Thackray G (1968) The Use of a Mathematical Model to Describe Isothermal Stress-Strain Curves in Glassy Thermoplastics. *Proc. R. Soc. Lond. Ser. Math. Phys. Sci.* 302(1471):453–472.
- Hayhurst DR (1972) Creep rupture under multi-axial states of stress. *J. Mech. Phys. Solids* 20(6):381–382.
- Hernández-Rodríguez MAL, Martínez-Delgado D, González R, Pérez Unzueta A, Mercado-Solís RD, Rodríguez J (2007) Corrosive wear failure analysis in a natural gas pipeline. *Wear* 263(1–6):567–571.
- Ho K, Krempl E (2002) Extension of the viscoplasticity theory based on overstress (VBO) to capture non-standard rate dependence in solids. *Int. J. Plast.* 18(7):851–872.
- Hobeika S, Men Y, Strobl G (2000) Temperature and Strain Rate Independence of Critical Strains in Polyethylene and Poly(ethylene-co-vinyl acetate). *Macromolecules* 33(5):1827–1833.
- Hong K, Rastogi A, Strobl G (2004) A Model Treating Tensile Deformation of Semicrystalline Polymers: Quasi-Static Stress–Strain Relationship and Viscous Stress Determined for a Sample of Polyethylene. *Macromolecules* 37(26):10165–10173.
- Hughes DJ, Mahendrasingam A, Oatway WB, Heeley EL, Martin C, Fuller W (1997) A simultaneous SAXS/WAXS and stress-strain study of polyethylene deformation at high strain rates. *Polymer* 38(26):6427–6430.
- Humbert S, Lame O, Chenal JM, Rochas C, Vigier G (2010) New Insight on Initiation of Cavitation in Semicrystalline Polymers: In-Situ SAXS Measurements. *Macromolecules* 43(17):7212–7221.
- Humbert S, Lame O, Vigier G (2009) Polyethylene yielding behaviour: What is behind the correlation between yield stress and crystallinity? *Polymer* 50(15):3755–3761.
- Hutchinson JW, Neale KW (1983) Neck propagation. *J. Mech. Phys. Solids* 31(5):405–426.
- Hyde TH, Sun W, Williams JA (2002) Life estimation of pressurised pipe bends using steady-state creep reference rupture stresses. *Int. J. Press. Vessels Pip.* 79(12):799–805.
- Imada K, Yamamoto T, Shigematsu K, Takayanagi M (1971) Crystal orientation and some properties of solid-state extrudate of linear polyethylene. *J. Mater. Sci.* 6(6):537–546.
- ISO 9080. (2012) Plastics piping and ducting systems-Determination of the long-term hydrostatic strength of thermoplastics materials in pipe form by extrapolation.
- ISO 13479. (2009) Polyolefin in pipes for the conveyance of fluids-Determination of resistance to slow crack growth on notched pipes.
- ISO 16241. (2005) Notched tensile test to measure the resistance to slow crack growth of polyethylene materials for pipe and fitting products (PENT).

- ISO 16770. (2004) Plastics-Determination of environmental stress cracking (ESC) on polyethylene (PE) – full notch creep test (FNCT).
- James HM, Guth E (1943) Theory of the Elastic Properties of Rubber. *J. Chem. Phys.* 11(10):455–481.
- Jar PB (2013) Assessment of damage and long-term strength of polyethylene. *ICF13*.
- Jar PB (2014) Degradation of Mechanical Properties for Polyethylene by Small-Deformation Damage. *ASME 2014 Press. Vessels Pip. Conf.* (American Society of Mechanical Engineers), V06BT06A040–V06BT06A040.
- Jar PY (2014) Transition of neck appearance in polyethylene and effect of the associated strain rate on the damage generation. *Polym. Eng. Sci.* 54(8):1871–1878.
- Jar PYB (2014) Effect of tensile loading history on mechanical properties for polyethylene. *Polym. Eng. Sci.* 55(9):2002–2010.
- Jar P.-Y. Ben (2015) Effect of Loading History on Elastic Modulus of HDPE. *ASME 2015 Press. Vessels Pip. Conf.* (American Society of Mechanical Engineers), V06BT06A045–V06BT06A045.
- Jar P.-Y. B (2015) Deformation-Induced Change in Long-Term Mechanical Properties of Polyethylene (PE). (Lille, France).
- Jeong HY (2002) A new yield function and a hydrostatic stress-controlled void nucleation model for porous solids with pressure-sensitive matrices. *Int. J. Solids Struct.* 39(5):1385–1403.
- Jia D, Bourse G, Chaki S, Lacrampe MF, Robin C, Demouveau H (2014) Investigation of Stress and Temperature Effect on the Longitudinal Ultrasonic Waves in Polymers. *Res. Nondestruct. Eval.* 25(1):20–29.
- Jiang L, Jonas JJ, Boyle K, Martin P (2008) Deformation behavior of two Mg alloys during ring hoop tension testing. *Mater. Sci. Eng. A* 492(1–2):68–73.
- Jiang Z, Tang Y, Rieger J, Enderle HF, Lilge D, Roth SV, Gehrke R, Heckmann W, Men Y (2010) Two Lamellar to Fibrillar Transitions in the Tensile Deformation of High-Density Polyethylene. *Macromolecules* 43(10):4727–4732.
- Ju T, Achenbach JD, Jacobs LJ, Guimaraes M, Qu J (2017) Ultrasonic nondestructive evaluation of alkali–silica reaction damage in concrete prism samples. *Mater. Struct.* 50(1):60.
- Kachanov L (2013) *Introduction to continuum damage mechanics* (Springer Science & Business Media).
- Kachanov LM (1958) Time of the rupture process under creep conditions. *Isv Akad Nauk SSR Otd Tekh Nauk* 8:26–31.
- Khan A, Zhang H (2001) Finite deformation of a polymer: experiments and modeling. *Int. J. Plast.* 17(9):1167–1188.
- Khan AS, Liang R (1999) Behaviors of three BCC metal over a wide range of strain rates and temperatures: experiments and modeling. *Int. J. Plast.* 15(10):1089–1109.
- Khan AS, Sung Suh Y, Kazmi R (2004) Quasi-static and dynamic loading responses and constitutive modeling of titanium alloys. *Int. J. Plast.* 20(12):2233–2248.

- Khan F (2006) Loading history effects on the creep and relaxation behavior of thermoplastics. *J. Eng. Mater. Technol.* 128(4):564–571.
- Khelifa M, Oudjene M, Khennane A (2007) Fracture in sheet metal forming: Effect of ductile damage evolution. *Comput. Struct.* 85(3–4):205–212.
- Kiass N, Khelif R, Boulanouar L, Chaoui K (2005) Experimental approach to mechanical property variability through a high-density polyethylene gas pipe wall. *J. Appl. Polym. Sci.* 97(1):272–281.
- Kikuchi S, Ilschner B (1986) Effects of a small prestrain at high temperatures on the creep behaviour of AISI 304 stainless steel. *Scr. Metall.* 20(2):159–162.
- Kim JH, Park WS, Chun MS, Kim JJ, Bae JH, Kim MH, Lee JM (2012) Effect of pre-straining on low-temperature mechanical behavior of AISI 304L. *Mater. Sci. Eng. A* 543:50–57.
- Kim JY, Jacobs LJ, Qu J, Littles JW (2006) Experimental characterization of fatigue damage in a nickel-base superalloy using nonlinear ultrasonic waves. *J. Acoust. Soc. Am.* 120(3):1266–1273.
- Krempf E (1998) Some general properties of solid polymer inelastic deformation behavior and their application to a class of clock models. *J. Rheol. 1978-Present* 42(4):713–725.
- Krempf E, McMahon JJ, Yao D (1986) Viscoplasticity based on overstress with a differential growth law for the equilibrium stress. *Mech. Mater.* 5(1):35–48.
- Krishnaswamy RK (2005) Analysis of ductile and brittle failures from creep rupture testing of high-density polyethylene (HDPE) pipes. *Polymer* 46(25):11664–11672.
- Kwon HJ, Jar PYB (2008) On the application of FEM to deformation of high-density polyethylene. *Int. J. Solids Struct.* 45(11–12):3521–3543.
- La Rosa G, Mirone G, Risitano A (2001) Effect of stress triaxiality corrected plastic flow on ductile damage evolution in the framework of continuum damage mechanics. *Eng. Fract. Mech.* 68(4):417–434.
- Ladani LJ, Dasgupta A (2009) A meso-scale damage evolution model for cyclic fatigue of viscoplastic materials. *Int. J. Fatigue* 31(4):703–711.
- Lai J, Bakker A (1995a) An integral constitutive equation for nonlinear plasto-viscoelastic behavior of high-density polyethylene. *Polym. Eng. Sci.* 35(17):1339–1347.
- Lai J, Bakker A (1995b) Analysis of the non-linear creep of high-density polyethylene. *Polymer* 36(1):93–99.
- Laiarinandrasana L, Besson J, Lafarge M, Hochstetter G (2009) Temperature dependent mechanical behaviour of PVDF: Experiments and numerical modelling. *Int. J. Plast.* 25(7):1301–1324.
- Laiarinandrasana L, Morgenev TF, Proudhon H, N'guyen F, Maire E (2012) Effect of multiaxial stress state on morphology and spatial distribution of voids in deformed semicrystalline polymer assessed by x-ray tomography. *Macromolecules* 45(11):4658–4668.

- Lang RW, Stern A, Doerner G (1997) Applicability and limitations of current lifetime prediction models for thermoplastics pipes under internal pressure. *Angew. Makromol. Chem.* 247(1):131–145.
- Lemaitre J (1972) Evaluation of dissipation and damage in metals submitted to dynamic loading. *Mech. Behav. Mater.:*540–549.
- Lemaitre J (1985) A continuous damage mechanics model for ductile fracture. *J. Eng. Mater. Technol.* 107(1):83–89.
- Lemaitre J (2012) *A course on damage mechanics* (Springer Science & Business Media).
- Lemaitre J, Dufailly J (1987) Damage measurements. *Eng. Fract. Mech.* 28(5–6):643–661.
- Lemaitre J, Sermage JP, Desmorat R (1999) A two scale damage concept applied to fatigue. *Int. J. Fract.* 97(1–4):67–81.
- Li J, Li F, Ma X, Wang Q, Dong J, Yuan Z (2015) A strain-dependent ductile damage model and its application in the derivation of fracture toughness by micro-indentation. *Mater. Des.* 67:623–630.
- Li J, Li F, Xue F, Cai J, Chen B (2012) Micromechanical behavior study of forged 7050 aluminum alloy by microindentation. *Mater. Des.* 37:491–499.
- Lisle T, Bouvet C, Pastor ML, Rouault T, Margueres P (2015) Damage of woven composite under tensile and shear stress using infrared thermography and micrographic cuts. *J. Mater. Sci.* 50(18):6154–6170.
- Liu JH, Li GL, Hao XY, Zeng DB, Sun ZH (2001) Ultrasonic measurement of fatigue damage of nodular cast iron. *Mater. Lett.* 50(4):194–198.
- Lu X, Qian R, Brown N (1995) The effect of crystallinity on fracture and yielding of polyethylenes. *Polymer* 36(22):4239–4244.
- Lu Y, Yang W, Zhang K, Yang M bo (2010) Stress relaxation behavior of high density polyethylene (HDPE) articles molded by gas-assisted injection molding. *Polym. Test.* 29(7):866–871.
- Majid ZA, Mohsin R, Yaacob Z, Hassan Z (2010) Failure analysis of natural gas pipes. *Eng. Fail. Anal.* 17(4):818–837.
- Mashayekhi M, Ziaei-Rad S (2006) Identification and validation of a ductile damage model for A533 steel. *J. Mater. Process. Technol.* 177(1–3):291–295.
- Mažeika L, Šlīteris R, Vladišauskas A (2016) Measurement of velocity and attenuation for ultrasonic longitudinal waves in the polyethylene samples. *Ultragarsas Ultrasound* 65(4):12–15.
- McClintock FA (1968) A Criterion for Ductile Fracture by the Growth of Holes. *J. Appl. Mech.* 35(2):363–371.
- Meola C, Carlomagno GM (2004) Recent advances in the use of infrared thermography. *Meas. Sci. Technol.* 15(9):R27.
- Meola C, Carlomagno GM, Giorleo L (2004) The use of infrared thermography for materials characterization. *J. Mater. Process. Technol.* 155–156:1132–1137.

- Mohanraj J, Barton DC, Ward IM, Dahoun A, Hiver JM, G'Sell C (2006) Plastic deformation and damage of polyoxymethylene in the large strain range at elevated temperatures. *Polymer* 47(16):5852–5861.
- Muhammad S (2014) *Deformation and Fracture of Polymers with Work Hardening Behavior*. Ph.D. (University of Alberta, Canada).
- Muhammad S, Jar PYB (2011) Effect of aspect ratio on large deformation and necking of polyethylene. *J. Mater. Sci.* 46(4):1110–1123.
- Muhammad S, Jar PYB (2013) Determining stress–strain relationship for necking in polymers based on macro deformation behavior. *Finite Elem. Anal. Des.* 70–71:36–43.
- Murakami S (1983) Notion of Continuum Damage Mechanics and its Application to Anisotropic Creep Damage Theory. *J. Eng. Mater. Technol.* 105(2):99–105.
- Nahshon K, Hutchinson JW (2008) Modification of the Gurson Model for shear failure. *Eur. J. Mech. - ASolids* 27(1):1–17.
- Nahshon K, Xue Z (2009) A modified Gurson model and its application to punch-out experiments. *Eng. Fract. Mech.* 76(8):997–1009.
- Nakajima M, Akita M, Uematsu Y, Tokaji K (2010) Effect of strain-induced martensitic transformation on fatigue behavior of type 304 stainless steel. *Procedia Eng.* 2(1):323–330.
- Needleman A (1972) A numerical study of necking in circular cylindrical bar. *J. Mech. Phys. Solids* 20(2):111–127.
- Needleman A (1987) A continuum model for void nucleation by inclusion debonding. *J. Appl. Mech.* 54(3):525–531.
- Needleman A, Tvergaard V (1984) An analysis of ductile rupture in notched bars. *J. Mech. Phys. Solids* 32(6):461–490.
- Nitta K hei, Maeda H (2010) Creep behavior of high density polyethylene under a constant true stress. *Polym. Test.* 29(1):60–65.
- Njeh CF, Hans D, Wu C, Kantorovich E, Sister M, Fuerst T, Genant HK (1999) An in vitro investigation of the dependence on sample thickness of the speed of sound along the specimen. *Med. Eng. Phys.* 21(9):651–659.
- Nogueira CL, Willam KJ (2001) Ultrasonic testing of damage in concrete under uniaxial compression. *Mater. J.* 98(3):265–275.
- Ognedal AS, Clausen AH, Berstad T, Seelig T, Hopperstad OS (2014) Void nucleation and growth in mineral-filled PVC – An experimental and numerical study. *Int. J. Solids Struct.* 51(7–8):1494–1506.
- Ognedal AS, Clausen AH, Dahlen A, Hopperstad OS (2014) Behavior of PVC and HDPE under highly triaxial stress states: An experimental and numerical study. *Mech. Mater.* 72:94–108.
- Oh CK, Kim YJ, Baek JH, Kim YP, Kim W (2007) A phenomenological model of ductile fracture for API X65 steel. *Int. J. Mech. Sci.* 49(12):1399–1412.

- Oh CS, Kim NH, Kim YJ, Baek JH, Kim YP, Kim WS (2011) A finite element ductile failure simulation method using stress-modified fracture strain model. *Eng. Fract. Mech.* 78(1):124–137.
- Oral A, Anlas G, Lambros J (2012) Determination of Gurson–Tvergaard–Needleman Model Parameters for Failure of a Polymeric Material. *Int. J. Damage Mech.* 21(1):3–25.
- Pacheco-Salazar OF, Wakayama S, Sakai T, Ríos-Soberanis CR, Cauch-Rodríguez JV, Cervantes-Uc JM (2016) Damage accumulation studied by acoustic emission in bone cement prepared with core–shell nanoparticles under fatigue. *J. Mater. Sci.* 51(12):5635–5645.
- Padma S, Srivathsa B, Rao NV, Kumar V (2009) Evolution of Damage in Near IMI-834 Titanium Alloy Under Monotonic Loading Condition: A Continuum Damage Mechanics Approach. *J. Eng. Mater. Technol.* 131:031012–1.
- Palermo G (2004) Correlating Aldyl “A” and Century PE Pipe Rate Process Method Projections with Actual Field Performance. *Plast. Pipes XII Conf. Milan Italy.*
- Pardoën T, Hutchinson JW (2000) An extended model for void growth and coalescence. *J. Mech. Phys. Solids* 48(12):2467–2512.
- Patlazhan S, Remond Y (2012) Structural mechanics of semicrystalline polymers prior to the yield point: a review. *J. Mater. Sci.* 47(19):6749–6767.
- Pawlak A (2007) Cavitation during tensile deformation of high-density polyethylene. *Polymer* 48(5):1397–1409.
- Pawlak A, Galeski A (2008) Cavitation during tensile deformation of polypropylene. *Macromolecules* 41(8):2839–2851.
- Pawlak A, Galeski A (2010a) Cavitation and morphological changes in polypropylene deformed at elevated temperatures. *J. Polym. Sci. Part B Polym. Phys.* 48(12):1271–1280.
- Pawlak A, Galeski A (2010b) Cavitation during tensile drawing of annealed high density polyethylene. *Polymer* 51(24):5771–5779.
- Pawlak A, Galeski A, Rozanski A (2014) Cavitation during deformation of semicrystalline polymers. *Prog. Polym. Sci.* 39(5):921–958.
- Piche L (1984) Ultrasonic velocity measurement for the determination of density in polyethylene. *Polym. Eng. Sci.* 24(17):1354–1358.
- Plummer CJG, Goldberg A, Ghanem A (2001) Micromechanisms of slow crack growth in polyethylene under constant tensile loading. *Polymer* 42(23):9551–9564.
- Polanco-Loria M, Clausen AH, Berstad T, Hopperstad OS (2010) Constitutive model for thermoplastics with structural applications. *Int. J. Impact Eng.* 37(12):1207–1219.
- Popelar CF, Popelar CH, Kenner VH (1990) Viscoelastic material characterization and modeling for polyethylene. *Polym. Eng. Sci.* 30(10):577–586.
- Popelar CH, Kenner VH, Wooster JP (1991) An accelerated method for establishing the long term performance of polyethylene gas pipe materials. *Polym. Eng. Sci.* 31(24):1693–1700.

- Popli R, Mandelkern L (1987) Influence of structural and morphological factors on the mechanical properties of the polyethylenes. *J. Polym. Sci. Part B Polym. Phys.* 25(3):441–483.
- Pruell C, Kim JY, Qu J, Jacobs LJ (2007) Evaluation of plasticity driven material damage using Lamb waves. *Appl. Phys. Lett.* 91(23):231911.
- Quatravaux T, Elkoun S, G'sell C, Cangemi L, Meimon Y (2002) Experimental characterization of the volume strain of poly (vinylidene fluoride) in the region of homogeneous plastic deformation. *J. Polym. Sci. Part B Polym. Phys.* 40(22):2516–2522.
- Rae PJ, Brown EN (2015) Some Observations on Measuring Sound Speeds in Polymers Using Time-of-Flight. *Exp. Tech.*
- Rafiee R (2012) Apparent hoop tensile strength prediction of glass fiber-reinforced polyester pipes. *J. Compos. Mater.*:0021998312447209.
- Reis JML, Pacheco LJ, da Costa Mattos HS (2013a) Influence of the temperature and strain rate on the tensile behavior of post-consumer recycled high-density polyethylene. *Polym. Test.* 32(8):1576–1581.
- Reis JML, Pacheco LJ, da Costa Mattos HS (2013b) Tensile behavior of post-consumer recycled high-density polyethylene at different strain rates. *Polym. Test.* 32(2):338–342.
- Reis JML, Pacheco LJ, da Costa Mattos HS (2014) Temperature and variable strain rate sensitivity in recycled HDPE. *Polym. Test.* 39:30–35.
- Reynolds WN, Scudder LP, Pressman H (1986) The use of ultrasonic wave attenuation to monitor polymer and composite quality. *Polym. Test.* 6(5):325–336.
- Ricard J, Guigné F, Laiarinandrasana L (2014) Damage and fracture mechanisms of polyoxymethylene: Multiscale experimental study and finite element modeling. *Eng. Fract. Mech.* 115:270–283.
- Rice JR, Tracey DM (1969) On the ductile enlargement of voids in triaxial stress fields. *J. Mech. Phys. Solids* 17(3):201–217.
- Rosenberg E, Brusselle-Dupend N, Epsztein T (2011) A mesoscale quantification method of cavitation in semicrystalline polymers using X-ray microtomography. *Mater. Sci. Eng. A* 528(21):6535–6544.
- Rouse JP, Sun W, Hyde TH, Morris A (2013) Comparative assessment of several creep damage models for use in life prediction. *Int. J. Press. Vessels Pip.* 108–109:81–87.
- Rousselier G (1987) Ductile fracture models and their potential in local approach of fracture. *Nucl. Eng. Des.* 105(1):97–111.
- Rozanski A, Galeski A, Debowska M (2011) Initiation of Cavitation of Polypropylene during Tensile Drawing. *Macromolecules* 44(1):20–28.
- Saanouni K, Forster C, Hatira FB (1994) On the anelastic flow with damage. *Int. J. Damage Mech.* 3(2):140–169.
- Salawu OS (1997) Detection of structural damage through changes in frequency: a review. *Eng. Struct.* 19(9):718–723.

- Schneider K, Trabelsi S, Zafeiropoulos N e., Davies R, Riekkel C, Stamm M (2006) The Study of Cavitation in HDPE Using Time Resolved Synchrotron X-ray Scattering During Tensile Deformation. *Macromol. Symp.* 236(1):241–248.
- Shah AA, Ribakov Y (2009) Non-linear ultrasonic evaluation of damaged concrete based on higher order harmonic generation. *Mater. Des.* 30(10):4095–4102.
- Shalaby HM, Riad WT, Alhazza AA, Behbehani MH (2006) Failure analysis of fuel supply pipeline. *Eng. Fail. Anal.* 13(5):789–796.
- Shlitsa RP, Novikova EA (1983) Characteristics of the use of the split-disk method for investigating modern winding composites. *Mech. Compos. Mater.* 18(4):502–508.
- Shui GS, Wang YS (2012) Nondestructive Evaluation of Material Damage Using Nonlinear Rayleigh Waves Approach. *Adv. Mater. Res.* 463–464:1522–1526.
- Spicer M, Troughton M, Hagglund F (2013) Development and assessment of ultrasonic inspection system for polyethylene pipes. *ASME 2013 Press. Vessels Pip. Conf.* (American Society of Mechanical Engineers), V06BT06A042–V06BT06A042.
- Sposito G, Cawley P, Nagy PB (2010) Potential drop mapping for the monitoring of corrosion or erosion. *Ndt E Int.* 43(5):394–402.
- Stephens DR, Cassady MJ, Leis BN (1991) *Progress report on preliminary screening tests on squeeze-off of polyethylene gas pipes. Progress report, January 1987-December 1989* (Battelle, Columbus, OH (United States)).
- Stephens DR, Leis BN, Francini RB, Cassady MJ (1992) *Users' guide on squeeze-off of polyethylene gas pipes. Plastic pipes research results. Volume 1. Topical report, August 1989-February 1992* (Battelle, Columbus, OH (United States)).
- Straffelini G, Molinari A (2002) Evolution of tensile damage in porous iron. *Mater. Sci. Eng. A* 334(1–2):96–103.
- Struik LCE (1989) Mechanical behaviour and physical ageing of semi-crystalline polymers: 3. Prediction of long term creep from short time tests. *Polymer* 30(5):799–814.
- Tai WH (1990) Plastic damage and ductile fracture in mild steels. *Eng. Fract. Mech.* 37(4):853–880.
- Tasan CC, Hoefnagels JPM, Geers MGD (2009) A critical assessment of indentation-based ductile damage quantification. *Acta Mater.* 57(17):4957–4966.
- Tasan CC, Hoefnagels JPM, Geers MGD (2012) Identification of the continuum damage parameter: An experimental challenge in modeling damage evolution. *Acta Mater.* 60(8):3581–3589.
- Troughton M, Spicer M, Hagglund F (2012) Development of Ultrasonic Phased Array Inspection of Polyethylene Pipe Joints. *ASME 2012 Press. Vessels Pip. Conf.* (American Society of Mechanical Engineers), 285–293.
- Tuǧcu P, Neale KW (1988) Analysis of Neck Propagation in Polymeric Fibres Including the Effects of Viscoplasticity. *J. Eng. Mater. Technol.* 110(4):395–400.
- Tvergaard V (1982) On localization in ductile materials containing spherical voids. *Int. J. Fract.* 18(4):237–252.

- Ummenhofer T, Medgenberg J (2009) On the use of infrared thermography for the analysis of fatigue damage processes in welded joints. *Int. J. Fatigue* 31(1):130–137.
- UZELAC D, BIKLÆ S, ĐURĐEVIÆ M, Bordeasu I (2010) Change of Polyethylene Pipe Wall Thickness after Squeezing Using Squeeze off-Tool. *Mater. Plast.* 47(4):461–466.
- Viana JC (2005) Structural interpretation of the strain-rate, temperature and morphology dependence of the yield stress of injection molded semicrystalline polymers. *Polymer* 46(25):11773–11785.
- Voyiadjis GZ, Taqieddin ZN, Kattan PI (2008) Anisotropic damage–plasticity model for concrete. *Int. J. Plast.* 24(10):1946–1965.
- Wang D, Wang S, Chung DDL, Chung JH (2006) Sensitivity of the two-dimensional electric potential/resistance method for damage monitoring in carbon fiber polymer-matrix composite. *J. Mater. Sci.* 41(15):4839–4846.
- Wang LL, Zhou FH, Sun ZJ, Wang YZ, Shi SQ (2010) Studies on Rate-dependent Macro-damage Evolution of Materials at High Strain Rates. *Int. J. Damage Mech.* 19(7):805–820.
- Weeks N, Porter R (1974) Mechanical-Properties of Ultra-Oriented Polyethylene. *J. Polym. Sci. Part B-Polym. Phys.* 12(4):635–643.
- Wu PD, Van Der Giessen E (1993) On improved network models for rubber elasticity and their applications to orientation hardening in glassy polymers. *J. Mech. Phys. Solids* 41(3):427–456.
- Wu T, Coret M, Combescure A (2011) Strain Localisation and Damage Measurement by Full 3D Digital Image Correlation: Application to 15-5PH Stainless Steel. *Strain* 47(1):49–61.
- Xiang Y, Zhu W, Liu CJ, Xuan FZ, Wang YN, Kuang WC (2015) Creep degradation characterization of titanium alloy using nonlinear ultrasonic technique. *NDT E Int.* 72:41–49.
- Xie S, Chen Z, Takagi T, Uchimoto T (2012) Development of a very fast simulator for pulsed eddy current testing signals of local wall thinning. *NDT E Int.* 51:45–50.
- Xiong B, Lame O, Chenal JM, Rochas C, Seguela R, Vigier G (2013) In-situ SAXS study and modeling of the cavitation/crystal-shear competition in semi-crystalline polymers: Influence of temperature and microstructure in polyethylene. *Polymer* 54(20):5408–5418.
- Xu M, Wang L (2006) A new method for studying the dynamic response and damage evolution of polymers at high strain rates. *Mech. Mater.* 38(1–2):68–75.
- Xue L (2007) *Ductile fracture modeling : theory, experimental investigation and numerical verification*. Thesis. (Massachusetts Institute of Technology).
- Yarysheva AY, Rukhlya EG, Yarysheva LM, Bagrov DV, Volynskii AL, Bakeev NF (2015) The structural evolution of high-density polyethylene during crazing in liquid medium. *Eur. Polym. J.* 66:458–469.
- Yayla P, Bilgin Y (2007) Squeeze-off of polyethylene pressure pipes: Experimental analysis. *Polym. Test.* 26(1):132–141.
- Yeh HY, Cheng JH (2003) NDE of metal damage: ultrasonics with a damage mechanics model. *Int. J. Solids Struct.* 40(26):7285–7298.

- Zaïri F, Woznica K, Gloaguen JM, Naït-Abdelaziz M (2007) Elasto-viscoplastic constitutive equations for the description of glassy polymers behavior at constant strain rate. *J. Eng. Mater. Technol.* 129(1):29–35.
- Zhang C, Liu G, Song Y, Zhao Y, Wang D (2014) Structural evolution of  $\beta$ -iPP during uniaxial stretching studied by in-situ WAXS and SAXS. *Polymer* 55(26):6915–6923.
- Zhang C, Moore ID (1997a) Nonlinear mechanical response of high density polyethylene. Part I: Experimental investigation and model evaluation. *Polym. Eng. Sci.* 37(2):404–413.
- Zhang C, Moore ID (1997b) Nonlinear mechanical response of high density polyethylene. Part II: Uniaxial constitutive modeling. *Polym. Eng. Sci.* 37(2):414–420.
- Zhang SJ, Zhou C, Xia QX, Chen SM (2015) Quantification and Characterization of Full Field Ductile Damage Evolution for Sheet Metals Using an Improved Direct Current Potential Drop Method. *Exp. Mech.* 55(3):611–621.
- Zhang X, Schneider K, Liu G, Chen J, Brüning K, Wang D, Stamm M (2012) Deformation-mediated superstructures and cavitation of poly (L-lactide): In-situ small-angle X-ray scattering study. *Polymer* 53(2):648–656.
- Zhang Y, Ben Jar PY (2015) Quantitative assessment of deformation-induced damage in polyethylene pressure pipe. *Polym. Test.* 47:42–50.
- Zhang Y, Jar PYB (2015) Phenomenological modelling of tensile fracture in PE pipe by considering damage evolution. *Mater. Des.* 77:72–82.